NUMERICAL MODELING OF SOIL FLOW AND PRESSURE DISTRIBUTION ON A SIMPLE TILLAGE TOOL USING COMPUTATIONAL FLUID DYNAMICS

A Thesis

Submitted to the Faculty of Graduate Studies and Research
in Partial Fulfilment of the Requirement
for the Degree of

Doctor of Philosophy

In the Department of Agricultural and Bioresource Engineering,
University of Saskatchewan

By

Subrata Karmakar

Saskatoon, Saskatchewan

Permission to Use

In presenting this thesis in partial fulfilment of the requirements for a Postgraduate degree from the University of Saskatchewan, I agree that the Libraries of this University may make it freely available for inspection. I further agree that permission for copying of this thesis in any manner, in whole or in part, for scholarly purposes may be granted by the professor or professors who supervised my thesis work or, in their absence, by the Head of the Department or the Dean of the College in which my thesis work was done. It is understood that any copying or publication or use of this thesis or parts thereof for financial gain shall not be allowed without my written permission. It is also understood that due recognition shall be given to me and to the University of Saskatchewan in any scholarly use which may be made of any material in my thesis. Requests for permission to copy or to make other use of material in this thesis in whole or part should be addressed to:

Head of the Department of Agricultural and Bioresource Engineering
University of Saskatchewan
Saskatoon, Saskatchewan S7N 5A9

Abstract

Soils, in general, undergo both elastic and plastic deformations upon loading. Strain dependant anisotropic elasto-plastic models are required for realistic modeling for soil-tool mechanics that will address issues like stress history and soil anisotropy. Although several such models have been proposed, the science of coupled poro-mechanical analysis of an unsaturated soil has not been fully addressed.

Tillage tool modeling is primarily concerned with the analysis of soil deformation patterns and development of force prediction models for design optimization. Most of the models are based on quasi-static soil failure patterns that cause difficulty in accurately predicting soil-tool behaviour and soil forces for high speed operation. In recent years efforts have been made to improve the conventional analytical and experimental models by numerical approaches. Numerical simulations of soil-tool interactions using finite element modeling (FEM) and discrete element method (DEM) were mostly based on a solid mechanics approach. Due to limitations of constitutive relations, predictions of these numerical models have not been able to address tillage dynamics with high shear rates. The contribution of this research was to study the dynamics of soil-tool interaction using computational fluid dynamics (CFD) from the perspective of soil visco-plastic behavior.

A motorised soil rheometer was developed for evaluating soil visco-plastic parameters for CFD simulations. The apparatus was used to determine soil yield stress and viscosity at different soil moisture and compaction levels.

Three-dimensional CFD analyses were carried out using a commercial software CFX 4.4 to observe soil failure patterns around a tool and the pressure distribution on and around the tool. Duct flow as well as free-surface flow simulations of visco-plastic soil as a non-Newtonian Bingham material indicated soil deformation comprising of '*plastic flow*' and '*plug flow*' patterns. The soil failure front advancement demonstrated a critical speed range of 4 to 6.5 ms^{-1} where advancement of the failure front did not increase with speed. Soil pressure on the tool surface increased with the tool operating speed. Pressure distribution on the tool surface and draft requirement agreed well with the published literature based on experimental results and FEM analysis. The CFD approach, in its first attempt to tillage process, demonstrated its greater potential for dynamic modeling of soil-tool interaction.

Acknowledgement

My sincere appreciation and gratitude to my supervisor, Professor Radhey Lal Kushwaha for his inspiration, guidance and support during this adventure. Critical thinking and reflections of Profs. V. Meda, C. Laguë, O. D. Baik, R. Fotouhi, J. Sharma and G. Watson, members of my advisory committee in different stages of the project is gratefully acknowledged. Professor K. C. Watts from Dalhousie University, Halifax is sincerely acknowledged for his comprehensive review as the External Examiner, which brought the thesis to a higher level.

Special thanks to my wife Anindita for her exceptional encouragement, moral support and sacrifice. My whole hearted gratitude to my sisters, Jaya and Jaba (who wanted me to be a doctor besides being an engineer ☺) and their family for their love and encouragement.

Study leave granted by Bidhan Chandra Agricultural (*Krishi*) University (*Viswavidyalaya*), India with full pay during my doctoral program is highly appreciated. I take the opportunity to thank my teachers and, undergrad and masters' supervisors, Profs. P. K. Singh and V. K. Tewari for their encouragement, love and blessings.

Staff of the Department of Agricultural and Bioresource Engineering of the University of Saskatchewan, especially Mr. Louis Roth, Wayne Morley, Mike Miller and Randy Lorenz is thankfully acknowledged for their technical help.

Thanks are due to my friends in Saskatoon who made me feel it home away from home. I cannot go without mentioning the names of Sushmita, Victoria, Sujata, Satyada and Sumith. Thanks to everyone else not mentioned, but not forgotten.

The financial support received from the Natural Science and Engineering Research Council of Canada, Department of National Defence, Canada and University of Saskatchewan Partnership Research Program is also acknowledged.

Thank You Almighty GOD for everything.

Dedication

This work is dedicated to my parents (Srinibash Karmakar and Rama Karmakar)
and my little hearts Soumya (*Deep*) and Stuti (*Diya*).

Table of Contents

List of Figures

List of Symbols

Chapter 1

ϕ	angle of internal friction [deg]
τ	shear stress at failure [Pa]
δ	external frictional angle at soil-tool interface [deg]
σ_n	normal stress on the failure plane [Pa]
γ	specific weight of soil [N m^{-3}]
P	force [N]
a	adhesion at soil tool interface [Pa]
c	soil cohesion [Pa]
q	surcharge pressure [N]
z	depth of tine or tool [m]
N_γ	soil reaction component due to gravity [--]
N_c	soil component reaction due to soil cohesion [--]
N_a	soil reaction component due to soil-metal adhesion [--]
N_q	soil reaction component tool due to surcharge [--]

Chapter 2

q_C	deviatoric stress in compression [Pa]
p'	mean normal effective stress [Pa]
q_E	deviatoric stress in extension [Pa]
ε_q	deviatoric strain [--]
p_o'	stress at yield surface [Pa]
K_o	coefficient of lateral earth pressure at-rest [--]
q	deviatoric stress [Pa]
α	angle of soil dilation [deg]

ϕ'_{cs}	critical state angle of internal friction [deg]

Chapter 3

$\dot{\gamma}$	shear rate [s^{-1}]
τ	shear stress [Pa]
τ_y^*	Dimensionless yield stress [--]
v_x	directional velocity [m s^{-1}]
μ	Newtonian viscosity [Pa.s]
μ	viscosity coefficient or plastic viscosity [Pa.s]
τ_{xy}	shear stress [Pa]
ε_c	total compressive strain [--]
η_c	flow constant governing the rate of flow of soil under load [Pa.s]
$\dot{\varepsilon}_{cy}$	rate of strain at yield point [s^{-1}]
τ_y	yield stress [Pa]
B_i	Bingham number [--]
c	cohesion [Pa]
d	diameter of shear-vane [m]
D	vane blade diameter [m]
H	half width of flow channel [m]
h	length of vanes [m]
K_d	modulus of delayed elasticity in compression [Pa]
K_e	modulus of instantaneous elasticity in compression [Pa]
K_f	modulus of instantaneous fracture in compression [Pa]
K_p	modulus of instantaneous plasticity [Pa]
M	maximum torque [N.m]
m, n	exponent [--]
S_c	compressive stress [Pa]
S_c	compressive stress [Pa]

S_{cy}	yield stress [Pa]
S_y	compressive stress at yield point [Pa]
T	time elapsed since the application of load [s]
V_N	average fluid velocity [m s^{-1}]
y	depth of flow [m]

Chapter 4

$\dot{\gamma}$	shear rate [s^{-1}]
ρ	density of the fluid [kg m^{-3}]
U_i	directional velocity of the fluid [m s^{-1}]
μ	plastic viscosity [Pa.s]
τ_{ij}	shear stress tensor [Pa]
τ_y	yield stress [Pa]
g	acceleration due to gravity [m s^{-2}]
p	hydrostatic pressure [Pa]
t	time [s]
x_i	directional displacement of the fluid element [m]
C_D	drag coefficient [--]
V	fluid velocity [m s^{-1}]
A	characteristic area [m^2]

Chapter 5

D	implement draft [N]
F	dimensionless soil texture adjustment parameter [--]
S	operating speed [km h^{-1}]
T	tillage depth [cm]
W	machine width [m]

Chapter 1

Introduction and Objectives of the Thesis

1.1 Preamble

"When Egyptians introduced the plow 7,000 years ago, they provided mankind with the single technological innovation which has had the most profound and lasting influence on the surface of the earth"

- René Dubos (1972) commented in his book "A God Within".

Tool interaction with agricultural soil basically deals with soil cutting, compaction and traction. Tillage is the mechanical manipulation of the soil by disturbing its original structure in the plow layer in order to promote tilth i.e. desired soil physical condition in relation to plant growth. Soil cutting, the prime objective of tillage, is associated with large soil deformation and soil translocation. The extent of soil disturbance and pulverization depends on the soil properties, tool configuration and system parameters. Soil disturbance is a quality measuring parameter for tillage. Performance efficiency of tillage is measured in terms of draft or input energy (Gill and Vanden Berg, 1967). Optimization in tillage tool design necessitates minimization of the input energy with a desired soil disturbance.

Stress is a philosophical concept – deformation is the physical reality (Burland, 1967). This is very pragmatic in the field of agricultural soil mechanics, where the crucial factor is the effect of the tool on soil deformation and it is the strain, which is of much importance. The first doctoral thesis in Agricultural Engineering in the United States was written by E. A. White at Cornell University in 1918, which was entitled "A Study of the Plow Bottom and its Action Upon the Furrow Slice". This research is considered as a landmark in the theoretical studies of soil-tool interaction (Gill and Vanden Berg, 1967).

1.2 Tillage and Soil Mechanics

Agricultural soils generally refer to the cultivable region of land. Soil-tool interaction is of much concern for these top soil strata. Methods of classical soil mechanics are often applied to agricultural soil mechanics with little modification for studying soil deformation (Koolen, 1983). Soil mechanics dealing with agricultural soils has the distinction from those of civil engineering problems in the context of the soil behavior. Civil engineering problems are concerned with stability of structures and foundations for soil settlement with a concern to prevent failure of soil under heavy loads generally for large depths. Agricultural soil mechanics mostly deals with soil failure at shallow depth with the interaction of relatively low load. Classical soil mechanics deals with mainly on the response of soil to small displacements due to loading and its behavior up to failure, whereas, tillage mechanics is concerned with the soil condition after failure. A substantial soil deformation is associated with the generation of nonlinearity in stress-strain relations in agricultural soil failure with tillage tool interaction (Kushwaha and Shen, 1994).

1.2.1 Earth pressure theories

Earth pressure is the lateral force exerted by the soil on a structure. Active and passive earth pressures are the two stages of stress in soils which are of particular interest in the analysis of soil-structure interactions (Anonymous, 2001). Active pressure is the condition in which the earth exerts a force on the retaining system and the members tend to move towards the excavation. Passive pressure is a condition in which the retaining system exerts a force on the soil. Since soils have greater passive resistance, the earth pressures are not the same for active and passive conditions.

There are two commonly accepted methods for calculating simple earth pressures, Coulomb and Rankine theories (Lambe and Whitman, 1969). The Coulomb theory was developed in the 1776 and the Rankine theory was developed in the 1857 and both remain the basis for present day earth pressure calculation. The general equations developed for both theories are based on the fundamental assumptions that the soil is

cohesionless (no clay component), homogeneous (not a varying mixture of materials), isotropic (similar stress-strain properties in all directions or in practical terms, not reinforced), semi-infinite (wall is very long and soil goes back a long distance without bends or other boundary conditions), and well drained to avoid consideration of pore pressures. The Rankine theory assumes that there is no wall friction, the ground and the failure surfaces are straight planes and the resultant force acts parallel to the backfill slope. This theory is not intended to be used for determining earth pressures directly against a wall; it is intended for determining earth pressures on a vertical plane within a mass of soil. The Coulomb theory provides a method of analysis that gives the resultant horizontal force on a retaining system for any slope of wall, wall friction, and slope of backfill, provided the slope is less than or equal to the soil internal angle of friction. This theory is based on the assumption that soil shear resistance develops along the wall and failure plane.

A log-spiral theory was developed because of the unrealistic values of earth pressures that are obtained by theories which assume a straight line failure plane (Anonymous, 2001). Rankine is conservative relative to the other methods. Except for the passive condition when the wall friction angle is greater than one third of the soil friction angle (ϕ), Coulomb is conservative relative to the log-spiral. These methods developed as refinements to one another; each in its turn accounting for more variables and thereby requiring increasing levels of analytical complexity. Basic theories based on the soil pressures have been depicted in Figure 1.1.

1.2.2 Classical soil mechanics and soil cutting

Soil cutting involves the mechanical failure of soil, which usually occurs in the shear mode along internal rupture surfaces in the soil, and often at the boundary between the soil and cutting tool surface (McKyes, 1985).

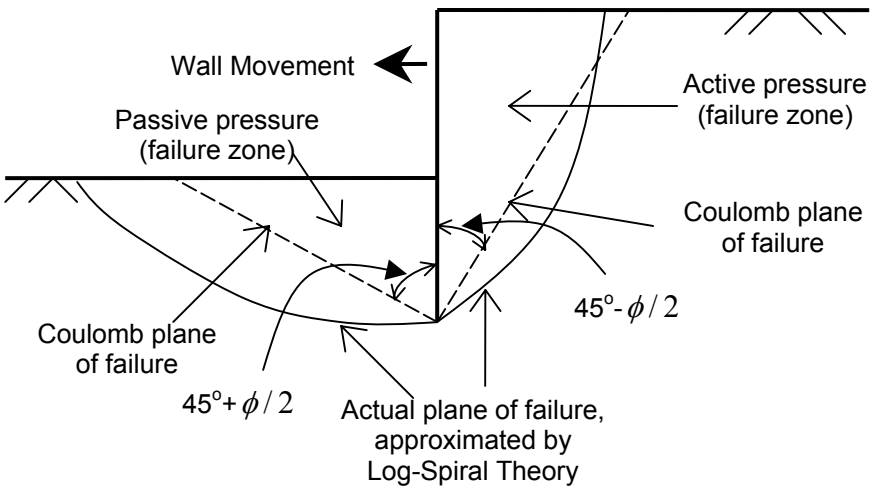

Figure 1.1 Schematic of earth pressure theories

The Mohr-Coulomb equation and the method of stress characteristics are the most widely used for representing the state of stress or strain at a point in a soil body which is failing in shear. Coulomb's equation (Coulomb, 1776) states that

$$\tau = c + \sigma_n \tan\phi \tag{1.1}$$

where:

τ = shear stress at failure on the failure plane (Pa),

c = soil cohesion (Pa),

σ_n = normal stress on the failure plane (Pa),

ϕ = angle of internal friction (degree).

Angle of internal friction is also termed as 'angle of contact friction' (Vyalov, 1986). The forces interacting on a tool-soil interface are determined by

$$\tau = a + \sigma_n \tan\delta \tag{1.2}$$

where:

a = adhesion at soil tool interface (Pa),

δ = external frictional angle at soil-tool interface (deg.).

Different types of failure features were considered by researchers towards analyzing the power requirement for a tillage tool during the last four decades. Analytical models are

mostly based on logarithmic spiral method of passive earth pressure theory for calculating soil resistance. Passive shear failure has been considered with respect to passive earth pressure theory, progressive shear type of failure was assumed as formation of soil blocks at uniform intervals. Rigid-brittle type of failure was considered for soils below plastic range and flow type - above the plastic range (Stafford, 1984). Reece (1965) described the process of soil cutting by a tillage tool with the following expression based on the universal earthmoving equation (Terzaghi, 1943) and incorporating an additional parameter considering the soil-tool interface:

$$P = \gamma z^2 N_\gamma + czN_c + c_a zN_a + qzN_q \qquad (1.3)$$

where:

P = force required to cut the soil per unit width of the tool (N),

γ = specific weight of soil (Nm^{-3}),

z = depth of tine or tool (m),

c = soil cohesion (Pa),

$c_{a=}$ soil-metal adhesion (Pa),

q = surcharge pressure (Pa).

The 'N' terms (dimensionless numbers) represent gravitational, cohesive, adhesive, and surcharge components of soil reaction per unit width of interface, respectively.

From visual observations of tillage processes, Ibarra et al. (2005) stated that soil cutting and fracturing process consisted of the following three distinct steps:

1. The compressive force applied by the tillage blade to the semi-infinite soil medium causes the development of compressive stresses in a radial manner and vertically due to soil weight. The compressive pressure increases from a minimum at the surface of the soil with depth.

2. Subsequently, the shear failure plane starts at the bottom of the blade when the shear strength of the soil is reached. The soil fails in shear according to the Rankine passive theory in a log spiral shape from the edge of the blade and

approximately semi-circular plan shape from the edge of the blade. The sheared segment becomes a finite mass, acted upon by the external stresses from the blade and the rest of the soil.

3. The continuous action of the forces produces reaction stresses around the border of the soil segment. Then, there is the development of tensile stresses within the soil segment producing breaking of soil in a radial manner from the centre of the cross-section.

1.2.3 Soil mechanics and tillage tool modeling

During tillage, soil particles move ahead and around the tool as they fail in shear. As the tool engages soil, high stiffness of the undisturbed soil is sustained by the tool up to its elastic limit, and then it fails in shear. The soil failure front, an indicator of soil disturbance is directly associated with slip surfaces generated by yielding and plastic deformation. The advancement of the soil failure front, influenced by the tool action, depends on the operating speed, tool shape and size, tool orientation, and the soil conditions.

During the last four decades, much research has been conducted on parametric studies for soil-tool interaction for modeling energy requirement of a tillage tool using analytical and numerical methods (Payne, 1956; Reece, 1965; Hettiaratchi et al., 1966; Godwin and Spoor, 1977; McKyes and Ali, 1977; Yong and Hanna, 1977; Perumpral et al., 1983; Liu and Hou, 1985; Chi and Kushwaha, 1989; Plouffe et al. 1999). These parameters have primarily been studied in a quasi-static condition considering the equilibrium of the soil-tool system. The models developed are accurate for predicting soil mechanical behavior and energy requirement for a very low speed of operation. However, little information is available on the physical and mechanical soil deformation pattern due to soil-tool interaction. High speed operation, practiced in conservation or reduced tillage, necessitates optimization of soil disturbance coupled with energy

efficiency. Recently a few studies have been conducted taking the dynamic feature of soil-tool interface due to machine interaction by numerical modeling (Swick and Perumpral, 1988; Zeng and Yao, 1992; Shen and Kushwaha, 1995). These studies, in contrast to the conventional assumption of passive earth pressure theory (quasi-static), considered velocity and acceleration of the tool during the soil-tool interaction. Numerical simulations of soil-tool interactions using finite element modeling were mostly based on solid mechanics approach. Due to the limitations of constitutive relations, predictions of these analyses have not been able to address tillage dynamics with high shear rates. The large-scale deformation of soil is still an area in which little research has been conducted. Research on the movement of soil around and ahead of the tool is not complete for predicting the soil mechanical behavior. A better understanding of the soil-tool interface mechanism can be obtained by correlating soil rheological behavior with its dynamic characteristics from fluid flow perspective.

The inter-particulate contact zones within the soil mass can be viscous in nature leading to a non linear rate dependent response (Keedwell, 1984). Soil deformation under steady state stress can be described by a simple linear model of visco-plasticity, the Bingham rheological model (Vyalov, 1986). In contrast to classical elasto-plastic materials, the soil medium can experience significant volume changes. Soil is usually highly nonlinear and needs characterization as nonlinear plastic or visco-plastic material (Desai and Phan, 1980).

Tillage is primarily a dynamic operation. Though the analytical models serve the purpose to a certain extent, one of the weaknesses is that they do not adequately define the influence of tool speed on soil failure pattern (Shen and Kushwaha, 1998). With a dynamic process, two possible effects, which are an inertia effect and a rate-effect, might need to be considered in an analysis. The tillage energy requirement, tool wear, and the final soil conditions are rate-dependent, which necessitates optimization of parameters for tillage operations to take account of the effects of soil-tool dynamics on tillage performance.

In design and development, computational fluid dynamics (CFD) programs are now considered to be standard numerical tools for predicting not only fluid flow behavior, but also the transfer of heat and mass, phase change, chemical reaction, mechanical movement and stress or deformation of structures (Sethian, 1993). The programs provide a detailed description of flow distributions, making it possible to evaluate geometric changes with much less time and cost than would be involved in laboratory testing. Study of soil mechanical behavior as a visco-plastic fluid flow and its interaction with a tool using computational fluid dynamics (CFD) would represent the dynamics of soil tillage.

1.3 Objectives of the Thesis

A project was undertaken with an overall goal to study the flow behavior of soil around a tillage tool using computational fluid dynamics. The specific objectives of the thesis are:

1. to study the soil mechanical behavior and different aspects of soil-tool modeling,
2. to determine soil rheological properties towards model development,
3. to simulate and predict soil deformation due to tillage tool interaction using CFD modeling,
4. to predict pressure distribution on a tool surface using CFD modeling and validate the simulation results by comparing with published data.

The thesis is structured into six chapters and is presented in a paper format i.e., as a series of manuscripts written suitable for publication in scientific journals. The first chapter is an introduction that presents the context and the objectives of the research work. Objective 1 is associated with Chapter 2, which has been presented as a case study on soil crack propagation and general literature review. Objective 2 is associated with Chapter 3, which is a paper on the experimental determination of visco-plastic parameters for soil. Objectives 3 and 4 are associated with the numerical modeling (computational fluid dynamics) of soil-tool interactions which are presented in Chapters 4 and 5, respectively. Chapter 6 presents the general conclusions of the research work as well as recommendations arising from this work.

1.4 References

Anonymous, 2001. Earth pressure theory and applications. Chapter 4, Trenching and Shoring Manual. Sacramento, California: California Department of Transportation.

Burland, J. B. 1967. Deformation of soft clay. PhD thesis, University of Cambridge.

Chi, L. and R. L. Kushwaha. 1989. Finite element analysis of forces on a plane soil blade. Canadian Agriculture Engineering 31(2):135-140.

Coulomb, C. A. 1776. Essai sur une application des regles des maximis et minimis a quelues problemes de statique relatifs a l'architecture. Mem. Acad. Roy. des Sciences, Paris, 3, p.38.

Desai, C. S. and H. V. Phan. 1980. Computational Methods in Nonlinear Mechanics. Ed. J. T. Oden. 205-224. New York: North Holland Publishing Company.

Dubos, R. J. 1972. A God Within. New York: Scribner Publishing Company.

Gill, W. R. and G. E Vanden Berg. 1967. Soil Dynamics in Tillage and Traction. Agriculture Handbook No. 316. United States Department of Agriculture.

Godwin, R. J. and G. Spoor. 1977. Soil failure with narrow tines. J Agric Eng Res 22: 213 -228.

Hettiaratchi, D. R. P., B. D. Witney and A. R. Reece. 1966. The calculation of passive pressure in two-dimensional soil failure. J Agric Eng Res 11(2): 89-107.

Ibarra, S. Y., E. McKyes and R. S. Broughton. 2005. A model of stress distribution and cracking in cohesive soils produced by simple tillage implements. J Terramech 42: 115-139.

Keedwell, M. J. 1984. Rheology and Soil Mechanics. 1 ed.: Elsevier applied science publishers, pp. 323.

Koolen, A. J. 1983. Agricultural Soil Mechanics. Advanced series in agricultural sciences. Springer- Verlag, Berlin.

Kushwaha, R. L. and J. Shen. 1994. The application of plasticity in soil constitutive modeling. ASAE Paper No. 941072, St Joseph, MI:ASAE.

Lambe, T. W. and R. V. Whitman. 1969. Soil Mechanics. New York: John Wiley & Sons, Inc.

Liu, Y. and Z. M. Hou. 1985. Three-dimensional nonlinear finite element analysis of soil cutting by narrow blades. Proc Int Conf Soil Dyn. Auburn, AL 2: 338-347.

McKyes, E. 1985. Soil Cutting and Tillage. New York: Elsevier Science Publishing Company.

McKyes, E. and O. S. Ali. 1977. The cutting of soil by narrow blades. J Terramech 14(2): 43-58.

Payne, P. C. J. 1956. The relationship between the mechanical properties of soil and the performance of simple cultivation implements. J Agric Eng Res 1(1): 23-50.

Perumpral, J. V., R. D. Grisso and C. S. Desai. 1983. A soil-tool model based on limit equilibrium analysis. Trans ASAE 26(4): 991-995.

Plouffe, C., C. Laguë, S. Tessier, M. J. Richard and N. B. McLaughlin. 1999. Mouldboard plow performance in a clay soil: Simulations and experiment. Trans ASAE 42(6): 1531-1539.

Reece, A. R. 1965. The fundamental equations of earth-moving mechanics. Proc Symp Earth Moving Machinery. Institute of Mechanical Engineering 179(3F): 8-14.

Sethian, J. A. 1993. Computational fluid dynamics. From Desktop to Teraflop: Exploiting the US Lead in High Performance Computing. Washington DC, USA: NSF Publications.

Shen, J. and R. L. Kushwaha. 1995. Investigation of an algorithm for nonlinear and dynamic problems in soil-machine systems. Comp Electronics Agric 13: 51-66.

Shen, J. and R. L. Kushwaha. 1998. Soil-Machine Interactions – A Finite Element Perspective. New York: Marcel Dekker Inc. Publishers.

Stafford, J. V. 1984. Force prediction models for brittle and flow failure of soil by draught tillage tools. J Agric Eng Res 29: 51-60.

Swick, W. C. and J. V. Perumpral. 1988. A model for predicting soil-tool interaction. J Terramech 25(1): 43-56.

Terzaghi, K. 1943. Theoretical soil mechanics. New York: John Wiley and Sons Inc.

Vyalov, S. S. 1986. Rheological Fundamentals of Soil Mechanics. Amsterdam, The Netherlands: Elsevier Science Publishing Co. Inc.

Yong, R. N. and A.W. Hanna. 1977. Finite element analysis of plane soil cutting. J Terramech 15(1): 43-63.

Zeng, D. and Y. Yao. 1992. A dynamic model for soil cutting by blade and tine. J Terramech 29(3): 317-327.

Chapter 2

Soil Crack Propagation- A Case Study, and General Literature Review

2.1 Significance

The brief review of soil mechanics and different approaches for soil-tool modeling in Chapter 1 revealed a necessity to investigate the dynamics of soil-tool interaction. The specific objectives of this chapter were to investigate the soil crack propagation due to tool interaction as a case study, review the details of agricultural soil mechanics and soil-tool modeling approaches with their pros- and- cons, and review on the features of large soil deformation with respect to soil rheology.

Soil failure pattern can be analysed based on the mechanics of soil cracks developed due to tool interaction. A case study was undertaken to understand the features of crack propagation leading to the soil failure front at different operating conditions. The content of this research was accepted for publication (*S. Karmakar, R. L. Kushwaha and D. S. Stilling. 2005. Soil failure associated with crack propagation for an agricultural tillage tool. Soil & Tillage Research 84(2):119-126*). The manuscript in its published format is included in Appendix E.

In order to describe the behavior of soil subjected to a complex loading path, the model should also account for the dependency of certain material properties on the stress history of the soil. Attempt has been made to review some of these critical state elasto-

plastic models with reference to their application in soil-tool interactions. Strain dependant anisotropic elasto-plastic models are required for realistic modeling for agricultural soil-tool mechanics. Based on this study, a paper was published (*S. Karmakar, J. Sharma and R. L. Kushwaha. 2004. Critical state elasto-plastic constitutive models for soil failure in tillage – A Review. Canadian Biosystems Engineering 46: 2.19-2.23*). The published format of this review study has been included in the thesis as Appendix F.

A better understanding of the soil-tool interface mechanism can be obtained by correlating soil rheological behavior with its dynamic characteristics. A preliminary study was conducted to explore application of the computational fluid dynamics (CFD) modeling to large and irrecoverable soil deformations due to tool interaction. Based on this study a paper (Appendix G) was accepted for publication (*S. Karmakar and R. L. Kushwaha. 2005. Dynamic modeling of soil-tool interaction: An overview from a fluid flow perspective. Journal of Terramechanics, accepted on April 20, 2005).*

2.2 Crack propagation due to soil-tool interaction: A case study

2.2.1 Introduction

Soils, in general, undergo both elastic and plastic deformations upon loading. A realistic constitutive model of soil behavior must be able to distinguish between the elastic and plastic deformations. A large number of isotropic elasto-plastic constitutive models have been developed for sand, clay and rock during the last four decades. Tillage is concerned with the top soil strata (up to about 100 cm depth). Thus the matrix suction and pore pressures, which are significant in geotechnical engineering problems like stability of slope, foundation of structures, etc, do not contribute much to the constitutive modeling for tillage. Failure of soil front advancement is related to the soil crack propagation due to tool interaction. The furthermost boundary of the propagated cracks forms the soil failure front.

Tillage loosens soil to depths of 75 to 150 mm. As the soil is tilled, the failure path precedes the motion of the tillage tool. Previous studies have examined soil forces

acting on a tine by predicting different soil failure patterns. A study was conducted to analyse the soil crack propagation due to the interaction of sweep, a commonly used tillage tool in North America. This study investigated the rate and the path of the cracks associated with soil failure front. This research examined both qualitatively and quantitatively the soil crack propagation and failure patterns for a commonly used cultivating tool. In contrary to the previous studies on soil cleavage formation due to the vertical flat blade in a vertical plane, this study focused mainly on the process of crack propagation due to soil-sweep interaction in the horizontal plane. The propagation of the soil failure path by observing the temporal profile of the leading edge of the failure crack with respect to the tool motion was examined. Crack propagations were analyzed for sweep operating at 4 km h^{-1} speed and two operating depths of 75 and 100 mm using high speed digital videography. Higher depth of operation showed distinct phases for crack development and propagation. Short and intermittent soil crack propagation with lower propagation growth rates were observed for shallow depths of operation. Crack growth rate has been observed to have a sinusoidal relation with time.

2.2.2 Soil failure phases: A brief review

Considering soil deformations that occur when a load is applied to the soil by a flat vertical plate, two modes of ruptures are predicted in 'shallow' and 'deep' regimes depending on the depth/width ratio of the tine (O'Callaghan and Farrelly, 1964; Godwin and Spoor, 1977). O'Callaghan and Farrelly attributed this aspect ratio as the sole parameter determining the mechanism of cleavage from the perspective of slip surfaces in a vertical plane. A vertical tine acted as a 'retaining wall' with less than 0.6 aspect ratio and as a 'footing' with an aspect ratio more than 0.6. At shallow depth, the tine displaced a chip of soil, slightly wider than the tine face width, immediately in front of it; while for deep operations, a fissure was developed in the soil some distance in front of the tine face and across the path of the tine. The fissure curved backwards on both sides of the tine forming a triangular wedge. The process of soil cleavage or cracks was considered.

Elijah and Weber (1971) studied the soil failure pattern in the vertical plane perpendicular to the direction of travel for an inclined flat blade of full scale and $1/8^{th}$ scale in a soil bin using film. They observed and defined four distinct types of soil failure; namely, shear-plane, flow, bending and tensile. The study revealed that 'shear-failure' and 'flow' occurred in granular-brittle material at relatively slow tool speeds. 'Bending' was evident in relatively high-moisture clays, which had enough toughness to prevent failure planes, yet sufficient plasticity to allow considerable strain with the formation of a minimum number of tension cracks occurred.

Godwin and Spoor (1977) observed that a change in soil failure mechanism occurred with depth for narrow tines. Above a certain 'critical depth' (small aspect ratio), the soil was displaced forwards, sideways and upwards creating a 'crescent failure', and below this depth (high aspect ratio), the displaced soil had components only in forward and sideways direction with no formation of distinct shear plane from the tine base creating a 'lateral failure'.

The study of soil failure and corresponding force-distance behavior for flat tines in clay soil under quasi-static conditions with varying soil moisture, tine width and constant working depth revealed that the nature of failure depended on the soil moisture level (Rajaram and Gee-Clough, 1988). They also observed four mechanisms of soil failure; namely, collapsing, fracturing, chip forming and flow failure. When the tine interacted with the virgin soil, the stress conditions were different from those during subsequent passes. During the tine's initial movement, soil was continuously displaced upwards and part of the displaced mass fell into the trench cut by the tine. After a few failures, the rate of upward flow became equal to the rate of sideways flow into the trench and, therefore, the volume of the surcharging soil mass reached a stable value. The number of failures after which the surcharge stabilized depended on the width of the tine. They also observed, for given moisture content and tine width, a sinusoidal time relation of the force on the tine existed. Rajaram (1990) found the soil failure pattern caused due to collapsing of soil in front of the tine is periodic, the frequency and magnitude of which depended on tine width.

Failure surface propagation of landslides has been studied in the context of stability of slopes, where progressive failure was the key focus. Kamai (1993) conducted a similar study using an experimental approach with the Ring Shear Creep test following the 'Sohmen method' on a landslide clay. Four stages of the soil failure process in the context of creep test were proposed. The 'preceding stage' is characterized by small a displacement rate and corresponds to the second stage of creep with no failure surface yet developed. The second is a 'seeding stage' when several failure zones are formed arbitrarily and are disconnected from each other with an accelerated displacement rate. Next, the 'propagation stage', where the failure zones formed in the previous stage propagates to each area completing the failure surface. Fourth, the 'post-failure stage', sliding occurs along the failure surface that has been formed completely.

2.2.3 Methodology

Experiments were conducted in the soil bin facilities of the Department of Agricultural and Bioresource Engineering of the University of Saskatchewan. The sweep (12″-1/4″) used for the experiment has 50^{o} nose angle and 50^{o} stem angle (Fig. 2.1). Tool operating speed was slightly above 1m s^{-1} for operating depths of 75 and 100 mm. The soil was a clay loam (sand 47%, silt 24%, and clay 29%). Soil preparation involved a roto tiller, a flat surface packing roller, a sheep foot roller, a soil leveller, and a water spray boom for maintaining a constant soil moisture content. The soil bed was prepared to have a moisture content of 12.4% (d.b) and an average compaction level with cone index of 492 kPa. The soil compaction levels were measured using a cone penetrometer.

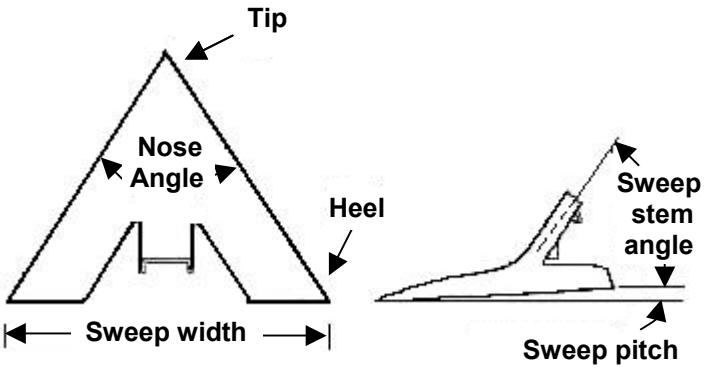

Figure 2.1 Details of sweep.

A high-speed video camera was mounted to the carriage frame where the tillage tool was mounted. Therefore, the recorded field of view had the tillage tool in the same location (the camera and the tool moved in unison). The digital film was transferred to standard video allowing the soil failure pattern to be observed conveniently. In addition, the film was converted to Audio Video Interleave (AVI) format to allow for subsequent video processing.

Visual interpretations were made from segments of the video clips, their still images, and soil crack propagations were analyzed by digitizing the data using commercial software. For qualitative assessment, video clips (moving pictures) have been converted to still pictures using a commercial MPEG (Moving Picture Experts Group) Encoder TMPGEnc with a video encoding speed of three frames per second. For the quantitative assessment, a commercial software package for Automatic Motion Analysis, 'WINanalyze' was used to digitize the crack tip (x-y coordinates) frame-by-frame. The program calibrated the distance based on the known grid and calculated crack tip growth (velocity) and rate of growth (acceleration) using finite differences in the respective directions. The analysis involved determining resultant displacement, velocity and acceleration for the soil failure crack.

2.2.4 Results and discussions

2.2.4.1 Visual interpretation

Analysis of the still images obtained by encoding the moving pictures revealed sequential soil crack development and propagation associated with soil deformation. For the sweep, operating at a depth of 100 mm in a soil of 12.4% (d.b) moisture content and 492 kPa cone index, the following visual interpretation were observed (Fig. 2.2).

As the tool started tilling undisturbed soil, the elevated nose of the sweep pushed the soil sideways (clear from the shifting of chalk marks sideways) and cracks developed from the base of the sweep stem along the direction of motion and at about 45^{o} to both

the sides (Fig.2.2a). Then, the crack following the sweep tip widened and propagated after splitting again at 45^{o} to both sides of sweep nose (Fig. 2.2b). With further widening of

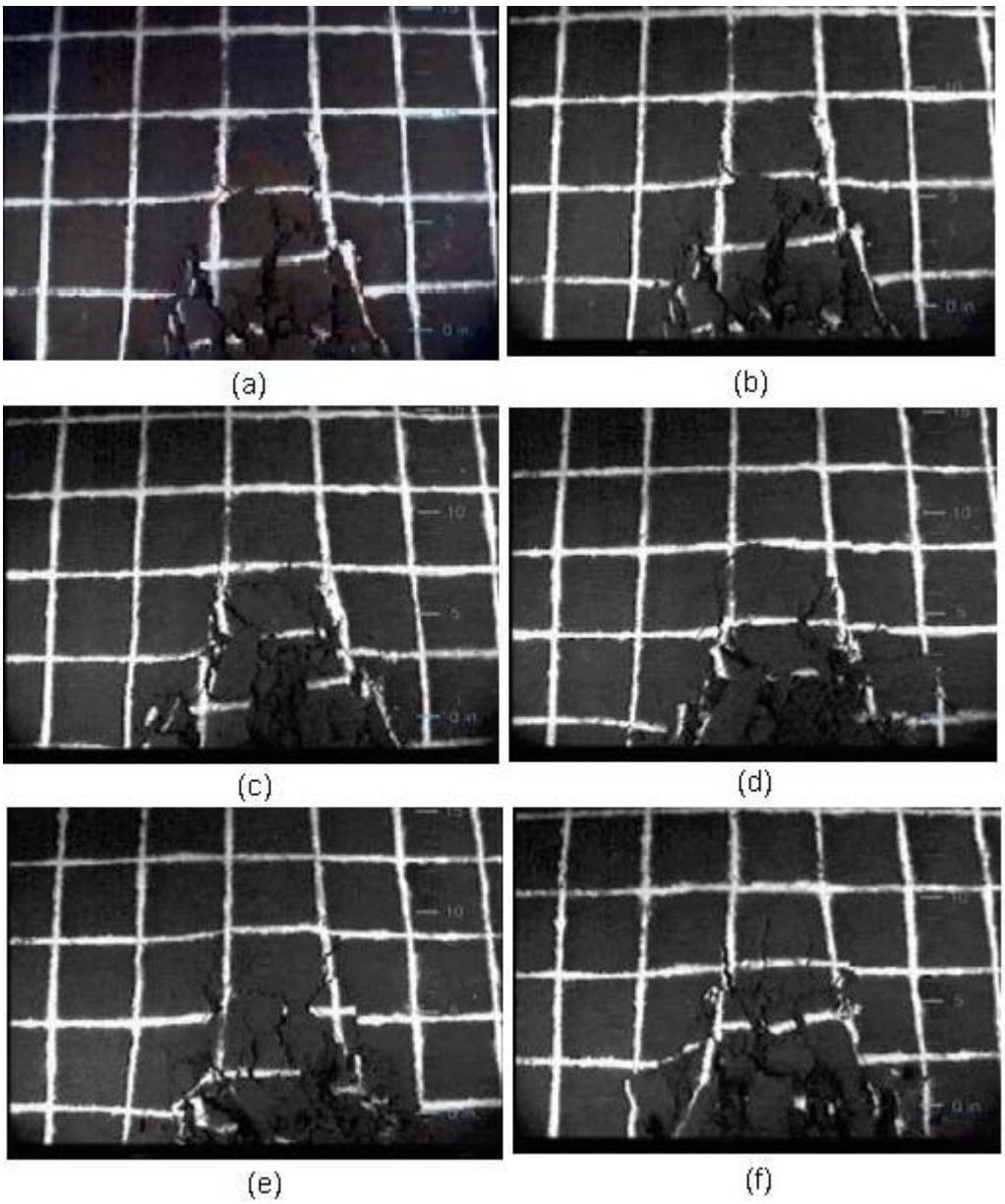

Figure 2.2 Crack propagation with 100 mm depth of operation.

the central crack, the cracks developed from sideways also widened and propagated (Fig. 2.2c). In this way, the soil around the stem base completely deformed (Fig. 2.2d) into small chips and was pushed sideways (clear from the disappearance of the chalk

marks near the stem base). At the same time, the crack development region extended from the sweep stem base and new cracks developed from the whole plan area of the tool and propagated to the direction of motion and at angles ranging 30-60^{o}. With the tool forward motion, new cracks developed from stem base and earlier developed cracks propagate and widen (Fig. 2.2e) as a part of the cyclic process. Due to the stabilised soil deformation process, the propagation seemed to be faster with simultaneous crack development (Fig. 2.2f).

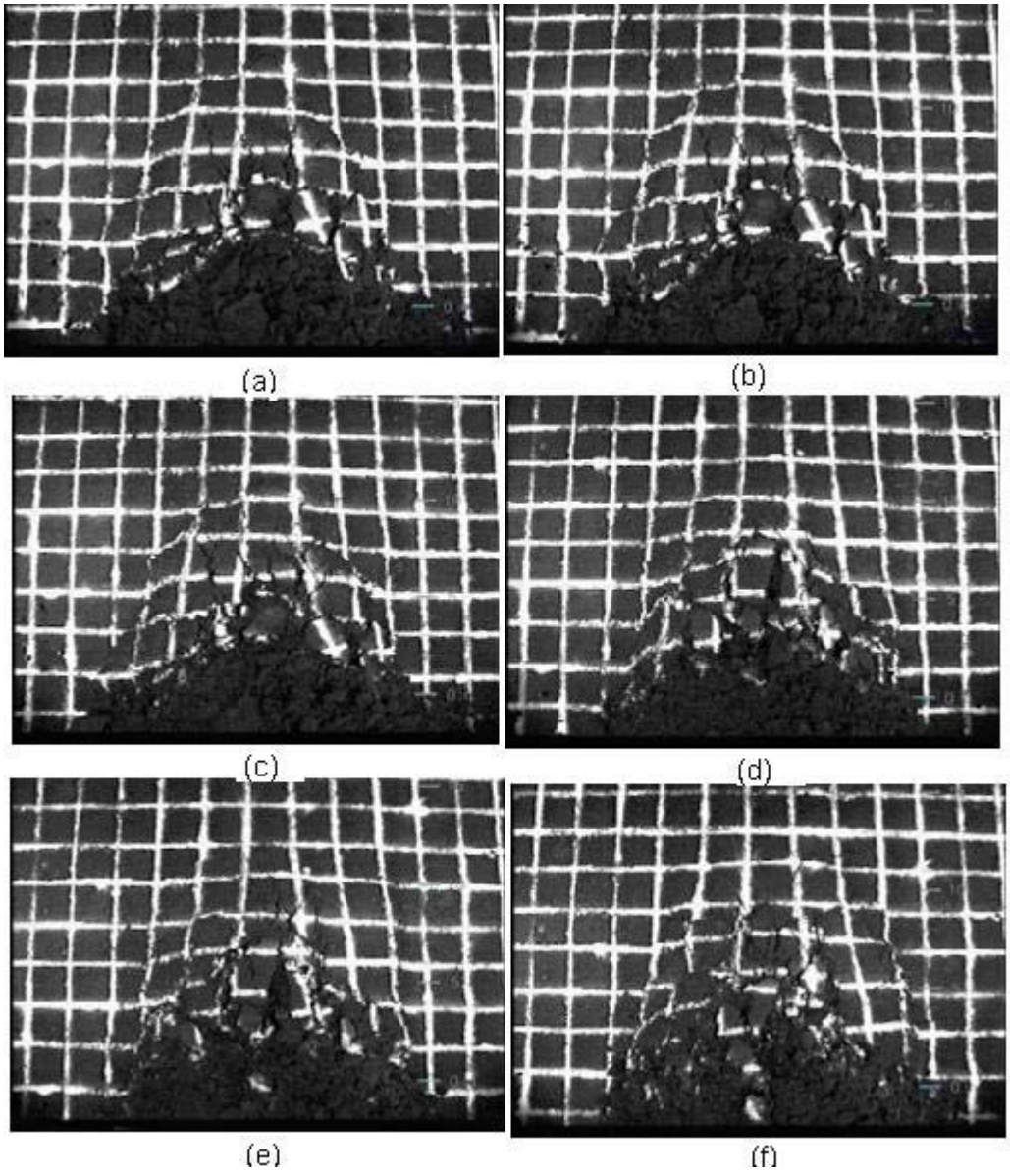

Figure 2.3 Crack propagation with 75 mm depth of operation.

Significant still images obtained by encoding the video clips for 75 mm depth of operation are shown in Fig. 2.3 for visual interpretation. As soon as the tool engaged the soil, cracks developed from the stem base and propagated in different directions. The number of cracks developed was very high in comparison to that of 100 mm depth. Crack initiation, development and subsequent processes were not as distinct as that for 100 mm depth of operation. Soil displacement to the sideways was also higher in this case.

The differential feature of soil crack development and propagation with the sweep in respect of the operating depth was similar to the observation by O'Callaghan and Farrelly (1964) for a flat vertical plate. However, experiments with more operating depths would be required for specifying two and three dimensional soil failure patterns with a well defined critical depth for sweep based on its shape.

The generalized feature of the observed soil failure cracks and their propagation can be illustrated as in Fig. 2.4. Since the camera was mounted on the tool carrier, the observed soil failure propagation is the relative soil failure advancement. Thus, failure advancement rate of soil relative to the tool can be written as

$$V_s = \frac{d}{dt}(\overline{x_s} - \overline{x_t}) \tag{2.1}$$

where, V_s = rate of soil failure advancement,

$\overline{x_t}$ = the average tool displacement,

$\overline{x_s}$ = the average resulting soil failure propagation.

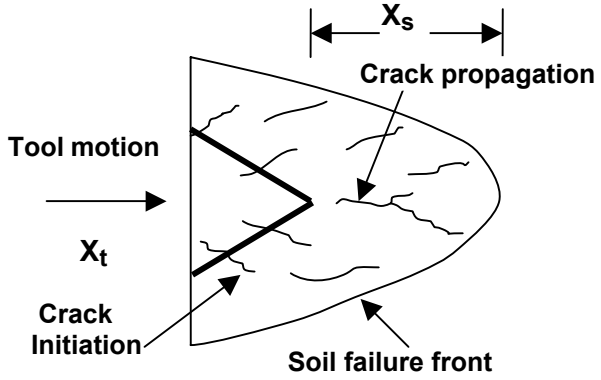

Figure 2.4 Schematics of crack propagation and failure front advancement.

2.2.4.2 Analytical interpretation

Image analysis of the soil failure pattern allowed the crack propagation to be quantified. The observation of soil movement with respect to the advancing tool revealed a process of crack initiation and its development. Cracks developed from the stem base of the sweep were considered for analysis.

Figure 2.5 shows the process of crack propagation of a particular crack with respect to its lateral and longitudinal components. After a crack was initiated, for a little duration it sustained the compressive force without any displacement and then propagated suddenly until it deformed completely. For this particular crack which completes the whole process in less than 15 ms, the longitudinal component is seen to have higher displacement of about 50 mm than the lateral component of about 25 mm before complete deformation.

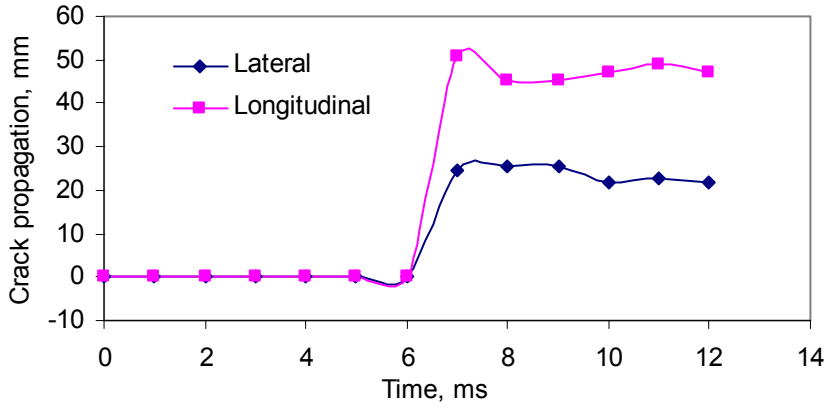

Figure 2.5 Directional crack development and soil deformation.

For 75 mm depth of operation a maximum of about 8 mm s^{-1} crack velocity occurred during the crack propagation (Fig. 2.6). The acceleration of the crack propagation followed a sinusoidal type of response (Fig. 2.7) with a higher growth rate in longitudinal direction than in lateral direction. For this particular soil crack, developed with 75 mm depth of operation, the maximum accelerations in longitudinal and lateral direction were found to be 0.28 and 0.15 mm s^{-2} respectively.

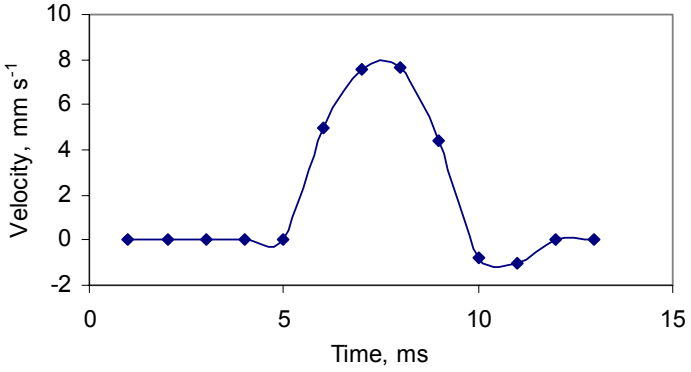

Figure 2.6 Velocity of soil crack propagation.

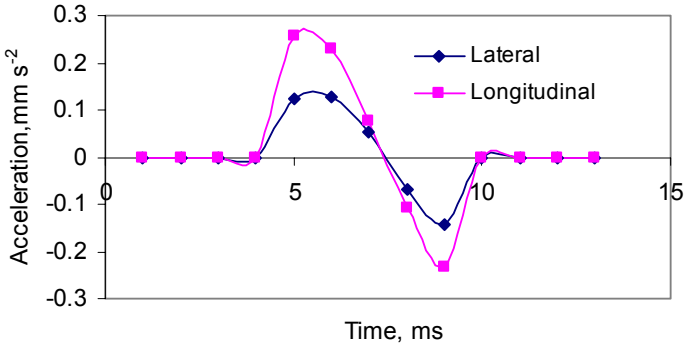

Figure 2.7 Growth rate of soil crack.

The process of soil crack propagation and soil deformation due to soil-tool interaction can be explained in a general form as shown in Fig. 2.8. The growth rate (acceleration) of a crack showed sinusoidal response after it was initiated. In the next phase of propagation, it decelerated and finally came to rest. Simultaneously, other cracks initiated and continued with the same process. For the 100 mm depth of operation, the longitudinal component of acceleration was found to be maximum of about 2.0 mm s^{-2} and that of lateral component was about 1.5 mm s^{-2}.

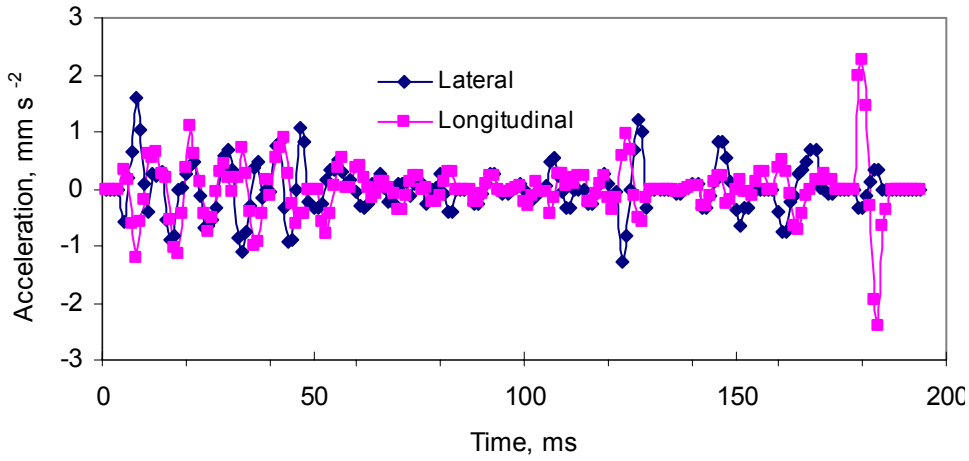

Figure 2.8 Phases of soil failure for 100 mm depth of operation.

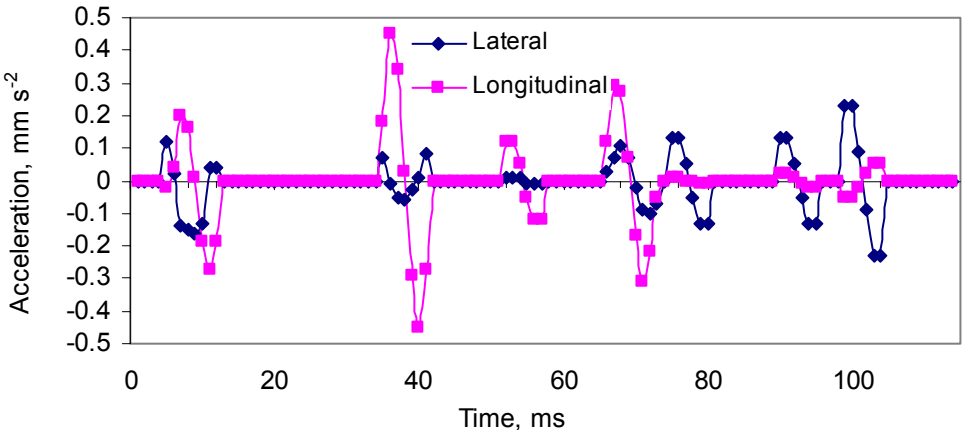

Figure 2.9 Phases of soil failure for 75 mm depth of operation.

The features of crack propagation for a shallower depth are shown in Fig. 2.9. The crack development and propagation process is found to last for a very small period for each individual crack. This supports the visual interpretation for 75 mm depth of operation. The process is not distinct as that of the 100 mm depth of operation. In this case, the maximum longitudinal and lateral components of crack growth rate were found to be about 0.5 and 0.3 mm s^{-2} respectively.

Various stages of soil failure during a landslide (Kamai, 1993) do not correspond to the soil failure pattern by a tillage tool, since soil-tool interaction is very quick with an external loading. As the tillage tool advances, the soil gets compressed (elastic deformation) and the crack is initiated. The crack grows rapidly and then the growth

rate (propagation) is reduced considerably. This is followed by soil plastic failure and soil particles come to a rest (post-tilling phase). Thus, the soil failure feature in the case of tillage tool may be divided into the phases of soil compression and elastic deformation, crack initiation, crack propagation or crack growth and plastic failure or post-tilling phase.

2.2.5 Conclusions

Following conclusions were drawn from the above experimental study, and visual and analytical observations of soil crack propagation for a sweep operating at two different depths in clay loam soil:

1. Features of soil crack development and propagation indicated the nonlinear characteristics of soil.
2. Shallower depth of operation caused short and intermittent soil crack propagation with lower growth rate.
3. The growth rate or the acceleration of the crack propagation followed a sinusoidal response.
4. The longitudinal component of a crack had a higher displacement and growth rate than the lateral component during the deformation process.
5. With a fluid flow approach, the soil crack propagation may not be depicted as observed from the digitised video graphs. However, the soil failure front advancement, which is associated to the crack propagation, is expected to be analysed from a fluid flow approach based on a particular fluid model. For example, Bingham visco-plastic model would help analyse the extent of yield surfaces developed for a particular soil and tool operating conditions.

2.3 Critical state soil mechanics

Elastic and plastic models, primarily based on the assumption of soil isotropy, have been used to model tillage tool interaction with soil. The force experienced by a tillage tool is influenced by both the stiffness and the strength of the soil. This is also affected by the stress history of soil with an anisotropic behavior. The modeling of soil-tool interaction using numerical methods can be improved further by incorporating strain-dependent stiffness and strength of soil associated with soil anisotropy.

The basic requirement for integrated analyses of movements and failure of a soil mass is a constitutive relationship capable of modeling stress-strain behavior of soil up to and beyond failure. Development of such a relationship generally involves separating the elastic and plastic behavior. This is achieved using a well-defined curve known as the yield locus located in a shear stress – normal stress space (Wood, 1990). If the stress state of a soil plots inside the yield locus, it is considered to be elastic and undergoes recoverable deformation. On the other hand, if a particular stress path puts the stress state of the soil on or outside the yield locus, plastic or irrecoverable deformation of soil occurs. Elasto-plastic constitutive models help distinguish between the recoverable and irrecoverable deformations for understanding the stress strain behavior of soil during loading and unloading.

2.3.1 Elasto-plastic soil constitutive models

A soil is said to be in critical state when it undergoes large shear deformations at constant volume and constant shear and normal effective stress (Schofield and Wroth, 1968). A locus of critical states of all shear tests on a soil is called a Critical State Line (CSL). The CSL is plotted in a three-dimensional space consisting of deviatoric stress, mean-normal effective stress and void ratio. Where a particular soil sample will end up on the CSL depends on its initial void ratio, initial mean normal effective stress and the stress path. All the elasto-plastic models based on the critical state concept have a well-defined yield locus that can be either isotropic or anisotropic. These models are not based on the Mohr-Coulomb failure criterion although the slope of the CSL can be

readily correlated with the critical state angle of internal friction. However, some of these models (e.g. Cam Clay) gives a unique strain response to an increment of stress but does not give a unique stress response to an applied strain increment and therefore, these models cannot be used for finite element computations without some modifications (Simpson, 1973).

2.3.1.1 Effect of stress history

The stress-strain response of soil not only depends on the current stress state but also on the recent stress history of the soil (Stallebrass, 1990). Problems involving unidirectional stress path may be described by a relatively simple nonlinear elasto-plastic model. However, for situations where the stress path directions may vary either because of the stress history or because of loading, a strain dependent nonlinear elasto-plastic model is desirable. The magnitude of the effect of recent stress history (Fig. 2.10) is determined largely by the difference in direction of loading between the current and previous stress path (Atkinson et al. 1990).

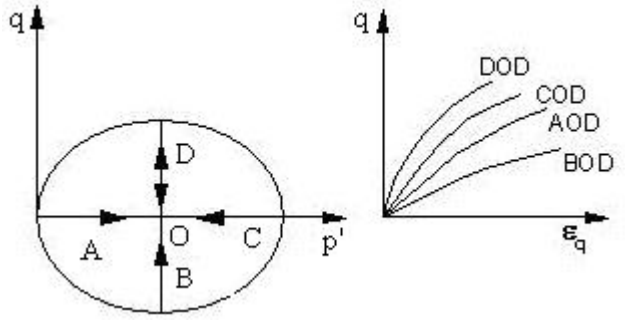

Figure 2.10 Effect of stress history on the strength and stiffness of soil (Atkinson et al. 1990).

The stress-strain behavior for a common stress path OD is shown after various histories. The DOD stress path is stiffest as the stress path changes its direction by 180^o followed by COD and AOD where stress path changes its direction by 90^o in deviatoric stress (q) vs. mean normal effective stress (p') space. The stress path BOD is the softest as it continues its previous direction. Soil offers resistance to change in direction of loading which implies stress-strain behavior of current stress path depends on the stress history of soil.

2.3.1.2 Isotropic models – Cam Clay and Modified Cam Clay

Cam Clay (Roscoe et al. 1958) and Modified Cam Clay (Roscoe and Burland, 1968) were developed by the Geotechnical Group at Cambridge University in the UK. These models were proposed on the basis of experimental evidence obtained from axisymmetric shear tests (the so-called triaxial tests) on remoulded soil samples of clay that were isotropically consolidated. For this reason, these models cannot be applied to conditions other than axisymmetric without attempting a generalization based on certain assumptions. The most important assumption made in this regard is that of isotropy. An isotropic soil constitutive model gives the same value of stiffness and strength irrespective of the direction of principal stresses. For such a model, there is no "preferred" direction that the stresses in soil can choose in order to mobilize minimum stiffness and strength and the yield curve is symmetric about the space diagonal – a line in principal stress space on which the three principal stresses are equal.

The yield locus for the Cam Clay model (Roscoe et al. 1958) is defined using a logarithmic spiral as shown in Fig. 2.11(a). The position of the yield surface is defined by $p_o^{'}$. The point C represents the point of the yield curve with horizontal slope. At this point plastic volumetric strain is zero and the yield surface becomes stationary. A point like C is the final state for a soil taken to failure, independently of initial conditions. This state is called critical state. If a soil element yields at a point to the right of C ('wet' or subcritical side), plastic volumetric strains are positive and hardening is ensured. If yielding takes place to the left of C ('dry' or supercritical side), plastic volumetric strains are negative and softening is resulted. The Cam Clay model assumes that the elastic shear strain is zero and the soil dissipates the applied energy by undergoing plastic shear strains. On the other hand, the Modified Cam Clay (MCC) model developed by Roscoe and Burland (1968) assumes that the dissipation of energy is due to both the elastic and plastic shear strains and thus the yield curve is elliptical as shown in Fig. 2.11(b).

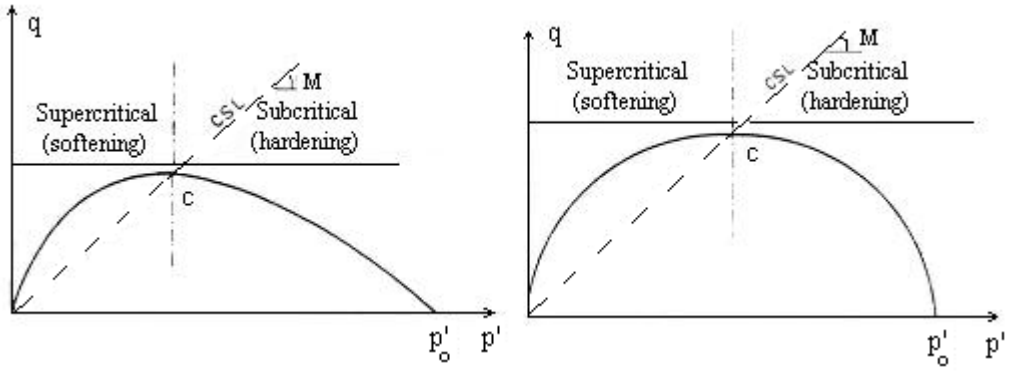

Figure 2.11 (a) The Cam Clay Model (Roscoe et al., 1958);
(b) The Modified Cam Clay Model (Roscoe and Burland , 1968).

2.3.1.3 Anisotropic models

Soil is a natural body comprised of solids (minerals and organic matter), liquid, and gases that occurs on the land surface, occupies space, and is characterized by one or both of the following: horizons, or layers, that are distinguishable from the initial material as a result of additions, losses, transfers, and transformations of energy and matter or the ability to support rooted plants in a natural environment (USDA, 2005). Naturally occurring soil is essentially a cross-anisotropic material. The main reason for the anisotropy is that most natural soils have been subjected to one-dimensional consolidation with a horizontal effective stress that is smaller than the vertical effective stress (coefficient of lateral earth pressure at-rest, K_o, is around 0.5 to 0.75 for most soils). The main implication of such a formation process is that the yield locus is no longer symmetrical about the mean normal effective stress (p′) axis. An asymmetric yield curve implies that the stiffness and strength of a soil in the vertical direction is significantly different than that in the horizontal direction. For a cross-anisotropic material, it is important to know the direction of the principal stresses because it influences the magnitude of the mobilized shear strength. A cross-anisotropic soil undergoing pure vertical compression (vertical major principal stress) would mobilize higher shear strength compared to that undergoing pure shear (major principal stress at 45°) or pure vertical expansion (horizontal major principal stress). This effect is

illustrated in Fig. 2.12 that shows that a cross-anisotropic soil will yield at a much lower value of deviatoric stress in extension (q_E) than that in compression (q_C).

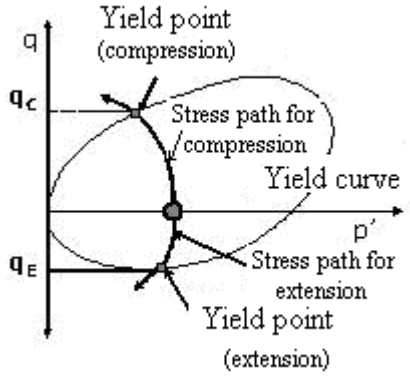

Figure 2.12 Yielding of a cross-anisotropic soil (Simpson et al., 1979).

2.3.1.4 Strain dependent models

Simpson et al. (1979) developed a London Clay (LC) model to predict the effect of stiffness variation with elastic, intermediate and plastic strain. The model also takes into account the variation of stiffness with mean normal stress and of plastic flow at large strains by relating increments of effective stress to increments of strain, given the current stress state. For this model, a kinematic yield surface (KYS), which depicts a small zone in the stress or strain space representing a higher stiffness at small strain, was defined in terms of strain. Straining within the KYS is purely elastic, though nonlinear. The dependency of soil stiffness on the level of soil strain is modeled in a stepwise manner (Fig. 2.13). At very small strain, the soil is completely elastic and very stiff. As straining proceeds, plastic strain develops and there is a drop in the overall stiffness of soil.

2.3.2 Application of Critical State Models to Tillage

Elastic and plastic models have been used to model soil-tool interactions, taking into account the formation of two and three dimensional soil failure patterns. A nonlinear hyperbolic elastic model developed by Kondner and Zelasko (1963) and later modified

by Duncan and Chang (1970) has been extensively used in tillage tool modeling (Chi and Kushwaha, 1989; Pollock et al., 1986; Bailey et al., 1984; Yong and Hanna, 1977). Chi et al. (1993) developed an elasto-plastic model using the incremental Lade and Nelson (1984) model and applied it to finite element analysis of soil tillage. The soil-tool interaction modeling using numerical methods can be improved further by incorporating a strain-dependent stiffness and the strength of soil.

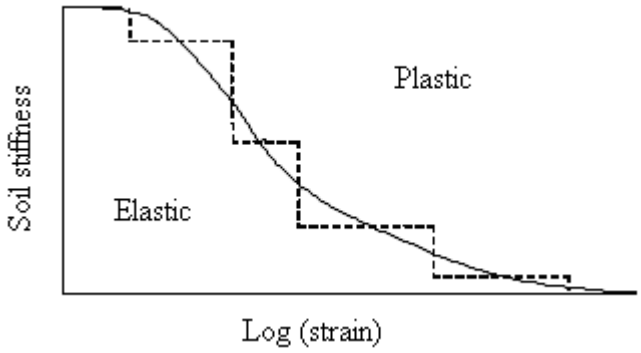

Figure 2.13 Stepwise simulation of the stiffness vs. strain curve (Simpson, 1992).

The force experienced by a tillage tool is influenced by both the stiffness and the strength of the soil as shown in Fig. 2.14(a). At the beginning of the tilling activity, most of the soil is elastic and offers significant resistance. Therefore, the force required to till soil is quite high. As the tool moves, more and more soil begins to yield and fail, resulting in the propagation of failure planes or cracks from the tip of the tillage tool to the surface (Fig. 2.14(b)). Once the soil begins to yield, the magnitude of the required force drops and reaches a residual level as the soil in front of the tool reaches a steady state in terms of crack propagation.

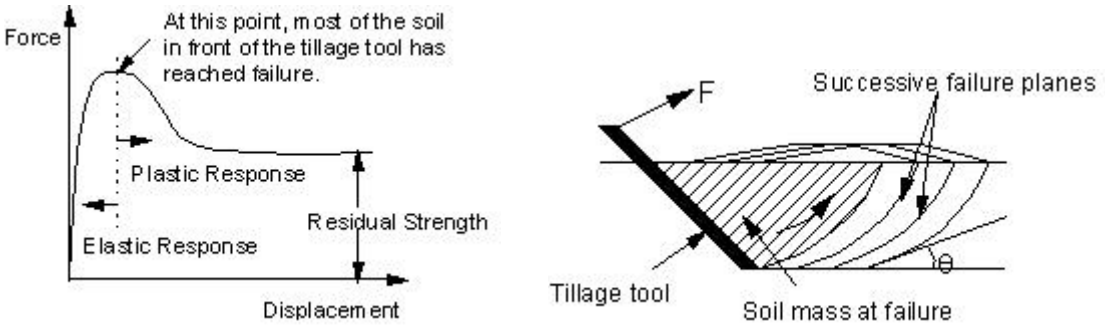

Figure 2.14 (a) Force required for tillage; (b) Successive failure planes in front of the tool (Karmakar et al., 2004).

As the tillage tool is dragged further, new failure planes are initiated in the soil in front of the tool and this cycle of peak and residual force repeats itself as shown in Fig. 2.15. The frequency of the cycle and the magnitude of the peak tillage force are influenced by the speed at which tilling is carried out. Zhang and Kushwaha (1998) reported a similar repeated soil failure pattern as demonstrated by shank vibrations.

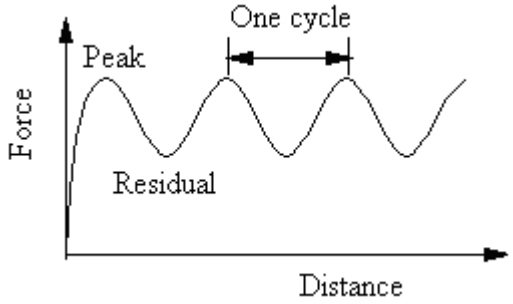

Figure 2.15 Fluctuations in the tillage force due to formation of failure planes in the soil.

The inclination of successive failure planes with respect to the horizontal (θ in Fig. 2.13(b)) is a function of the critical state angle of internal friction (ϕ'_{cs}) as well as the angle of dilation (α) of the soil. The angle of dilation (α) increases as the effective confining stress decreases (Wood, 1990). The peak tillage force is a function of both the stiffness and the strength of the soil whereas the residual tillage force depends primarily on the strength of the soil. As shown in the previous sections of this paper, both the stiffness and the strength of the soil are influenced significantly by the past stress (or strain) history of the soil. Therefore, in order to predict the magnitude of the tillage force, it is crucial to choose a strain dependent elasto-plastic constitutive model for the soil.

In addition to strain dependency, the change in the direction of the strain path is also a crucial factor in the analysis of soil-tool interaction during tillage. Before the tilling activity, the soil has experienced a strain path that is primarily vertical due to one-dimensional compaction or consolidation of the ground. During tillage, the soil experiences a strain path inclined at an angle of 30° to 90° with respect to the horizontal

depending on the type of the tillage tool being used (Fig. 2.16). This change in the strain path reversal means that the soil is likely to have a higher stiffness as demonstrated experimentally by Atkinson et al. (1990). The increased stiffness of the soil will influence mainly the peak required tillage force.

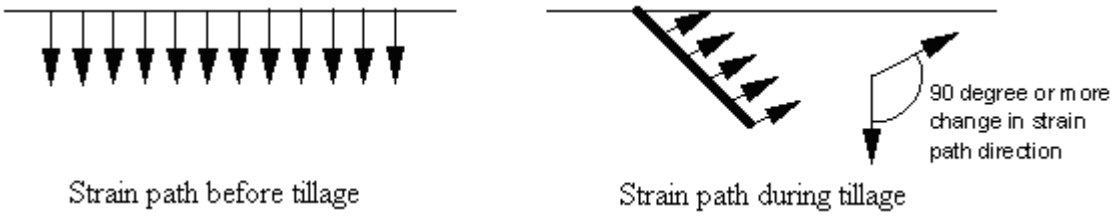

Figure 2.16 Change in strain path direction due to tillage (Karmakar et al., 2004).

As mentioned above, most soils are formed anisotropically by the process of deposition and subsequent consolidation in horizontal layers. Therefore, the magnitude of mobilized shear strength for these soils will be affected by the rotation of principal stresses experienced during tillage. Before the tillage activity, the major principal stress direction is vertical and the minor principal stress direction is horizontal (Fig. 2.17). During tillage, the soil in front of the tillage tool undergoes shear and passive failure. Therefore, the major principal stress direction changes from vertical to nearly horizontal close to the ground surface as shown in Fig. 2.17 and the soil is deemed to have failed in extension (negative deviatoric stress q as shown in Fig. 2.12). An anisotropic soil mobilizes shear strength in extension that is only about 50 to 60% of its shear strength in compression (Kulhawy and Mayne, 1990). If the strength parameters are specified on the basis of, for example, triaxial compression test, an analysis using isotropic elasto-plastic soil model will result in an over prediction of the required tillage force. Therefore, it may be necessary to use an anisotropic elasto-plastic soil model for achieving accurate simulation of soil tillage.

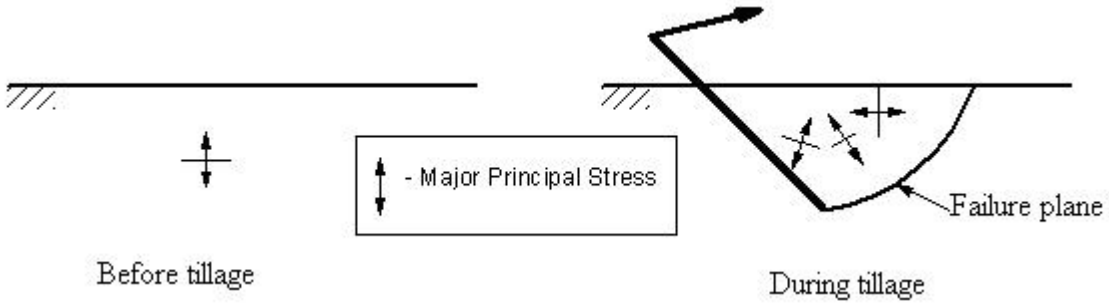

Figure 2.17 Rotation of principal stresses in the ground due to tillage (Karmakar et al., 2004).

It is also important to recognize that most of the agricultural topsoil is unsaturated and therefore, a strain-dependent elasto-plastic model incorporating essential aspects of unsaturated soil behavior may be necessary for numerical modeling of soil-tool interaction during tillage. Although several such models have been proposed (e.g. Wheeler and Sivakumar, 1992; Fredlund and Rahardjo, 1993), the science of coupled poro-mechanical analysis of an unsaturated soil is in a fairly nebulous stage. Therefore, special attention has to be taken for application of such models in machine-tool interactions.

An attempt has been made to review several elasto-plastic soil constitutive models for possible use in the soil-tool interaction analysis during tillage. A wide range of such models is available from rather simple isotropic models requiring a few parameters to fairly complex models requiring 15 or more parameters. It is recognized that soil is an anisotropic material and its strength and stiffness are influenced by the past stress history as well as rotation of the direction of principal stresses. It is a daunting task to model all aspects of soil behavior when analyzing tillage. However, certain key aspects such as strain-dependent stiffness and strength as well as anisotropy should be considered in order to obtain significant results from such analyses.

2.4 Soil-tool Modeling: A General Review

2.4.1 Different modeling approaches

Studies of soil-tool interaction have been carried out mostly for the development of force prediction models using different soils, tools, and operating conditions (speed and depth of operation, tool orientation, etc.). The formation of two- and three-dimensional soil failure patterns have been taken into account. So far, five major methods, namely empirical and semi-empirical, dimensional analysis, finite element method (FEM), discrete or distinct element method (DEM) and artificial neural network (ANN), have been used as approaches to solve problems in the area of soil-tool interaction and failure mechanism.

Mathematical solutions based on empirical and semi-empirical models have been developed to describe soil-tool interaction that helps designers and researchers develop an understanding through parametric studies. These analytical models are based on the physics of soil and system parameters, tool configuration and simple assumptions. Experimental models are cost and time effective. The relation between the variables is expressed by a suitable curve that fits best to the observed data and an appropriate model is developed. Similitude or dimensional analysis techniques involve representing different parameters of a tillage system by 'PI' terms and developing relations between dependent and independent variables. Effectiveness of a similitude model depends on the completeness of the list of parameters (Luth and Wismer, 1971). Here, scaling of parameters is a complicating factor, which results in distorted models. Improper scaling may lead to errors in two- and three-dimensional problems. High-speed computers and commercial software have allowed numerical models to be developed to take care of complex tool geometry and other parameters that are difficult to consider in analytical modeling.

Relationships have been established between draft force and operating speed. The soil worked by tines has been assumed to obey the Mohr-Coulomb failure criterion of classical soil mechanics in most of the models. The Cambridge theory of critical state

soil mechanics, which deals with the saturated soil and postulates the effect of stress on pore pressure, has also been adopted for soil tillage study (Hettiaratchi and O'Callaghan, 1980). Following the methods of fracture mechanics for partially saturated soil, Hettiaratchi (1987) developed a critical state soil mechanics model for agricultural soils.

Analytical models are primarily based on the logarithmic spiral method and passive earth pressure theory for calculating soil resistance. Osman (1964) initiated a study on the mechanics of simple two-dimensional soil cutting blades based on the theories concerning the passive pressure on large retaining walls. Based on Reece's equation, models (Reece, 1965; Hettiaratchi et al., 1966) have been developed for two-dimensional soil failures. Improvement in prediction models was achieved by three-dimensional soil failure models (Hettiaratchi and Reece, 1967; Godwin and Spoor, 1977; McKyes and Ali, 1977; Perumpral et al., 1983). Two-dimensional failures may be in a vertical plane with tools operating at shallow depths or in a horizontal plane for tools operating at deeper depths and are applicable to wider tools. A three-dimensional failure (Payne, 1956) involves a failure pattern in both planes and is generally considered for narrow tools. Models have been developed by calculating the total force on a tillage tool due to forward (*crescent*) and side failures, soil-metal and soil internal frictional forces with some modification from one to the other. Some of the models have also considered a critical depth with respect to describing a failure pattern in two and three dimensions for precise calculation of the draft. Godwin and Spoor (1977) considered three-dimensional crescent failure above critical depth and two-dimensional lateral failure below critical depth for narrow tillage tools. Models developed with the limit equilibrium method (McKyes and Ali, 1977; Perumpral et al., 1983) of analytical approach assume that the failure surface emanates from the tool tip and intersects the soil surface at a failure angle. These methods can only be used to obtain information of the maximum forces that are generated inside the soil because of soil-tool interaction, without providing much information about how the soil body deforms (Shen and Kushwaha, 1998).

The above stated types of models are not based on actual soil failure patterns that vary with rake angle, moisture content, soil density, etc. The soil failure profile varies with tool shape, operating speed, and soil physical properties. Therefore, the use of the analytical models, based on passive earth pressure theory and assumptions of a preliminary soil failure pattern, is limited for optimum design of a tillage tool (Kushwaha et al., 1993). Numerical methods help analyse the soil-tool interaction of complex shaped machines with the development of a suitable constitutive relation for a specific working condition with a proper algorithm. Several models (Yong and Hanna, 1977; Liu and Hou, 1985; Chi and Kushwaha, 1990; Wang and Gee-Clough, 1991; Plouffe et al. 1999) have been developed based on finite element analysis. For agricultural soils, which are usually unsaturated, a hyperbolic stress-strain model developed by Duncan and Chang (1970) was adopted by many researchers in their FEM applications. FEM can partly overcome the shortcomings of analytical methods in supplying more information about the progressive soil failure zone, field of stress, displacement, velocity, and acceleration of soil-tool interaction (Kushwaha and Zhang, 1998).

Studies using distinct element method (DEM) are based on mechanical behaviors of granular assemblies. If the soil model by the DEM is constructed with high accuracy, it could be applied to many mechanical and dynamic problems between soil and machines in the field of Terramechanics (Tanaka et al., 2000). A technique based upon the DEM has been developed to model the dynamic interaction of an implement (a typical dozer blade) with cohesively bonded particles by simulating cohesive soils (Hofstetter, 2002). Comparisons with test data showed good correlation for cutting forces, but poor correlation for penetration forces. A generalized flow-chart has been drawn (Fig. 2.18) based on the researches conducted on soil-tool modeling.

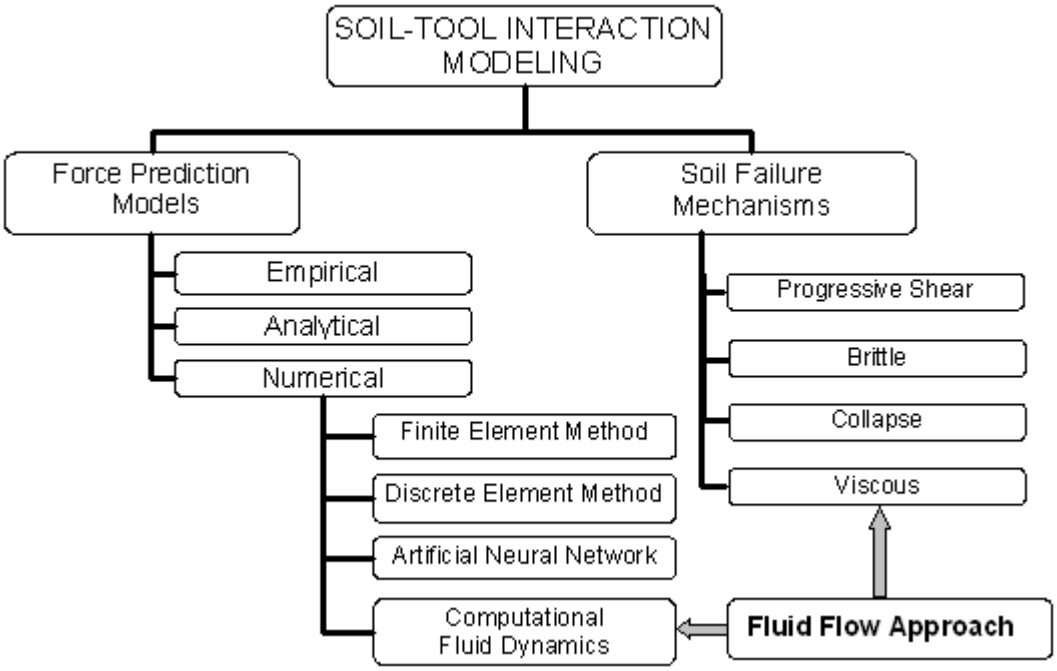

Figure 2.18 Schematics of soil-tool modeling approaches.

2.4.2 Problem areas in tillage-tool modeling

The following aspects can be highlighted as problem areas in tillage-tool design.

2.4.2.1 Tool geometry

Analytical models are good for simple geometries. Design of tillage tools with complex shape cannot be handled with this conventional and lengthy method for varying soil-tool parameters. Numerical methods are capable of analyzing the physics of a problem with complex tool geometry using computer-aided design (CAD). The CAD files are loaded in the respective computer program and parametric studies are carried out by sensitivity analysis in a very short time.

2.4.2.2 Dynamic modeling

During the last four decades, much research has been conducted on parametric studies for soil-tool interaction with different approaches. These parameters have primarily been studied in a quasi-static condition considering the equilibrium of the soil-tool system. Recently few studies have been conducted taking the dynamic feature of soil-

tool interface due to machine interaction by numerical modeling. These studies, in contrast to the conventional assumption of passive earth pressure theory (quasi-static), considered velocity and acceleration of the tool during the soil-tool interaction. However, the large-scale deformation of soil is still an area in which little research has been conducted. Force prediction models for tillage tools have been relying on the classical soil failure theory for quasi-static conditions.

The engineering soil mechanics approach is based on equilibrium state stress-strain relationships for the study of soil deformation, while deformations in agricultural soils rarely reach equilibrium (Or, 1996). In soil tillage, the soil is lifted and accelerated and thereby given potential and kinetic energies, and it is manipulated such that a change of state occurs. These processes occur under non-equilibrium conditions (Fornstrom et al., 1970). Also, soil tillage is carried on the unsaturated soil zone, where it is difficult to achieve the critical state condition (no volume change due to external loading). Thus, tillage is a non-equilibrium process.

The experimental results clearly showed a significant effect of strain rate on the stress-strain behavior of the soil (Yamamuro, 2004). While the peak stress increased only slightly with greater strain rate, the stiffness of the soil appeared much more significantly affected. Moreover, the mode of failure changed with increasing strain rate. It was also observed that at high strain rates the soil was much stiffer and reached a peak at much lower axial strains, whereupon it rapidly decreased. Shear band formation appears to be the cause of failure at high strain rates. Thus, the mode of failure appears to change from a type characterized by the development of uniform strains to that typified by the development of shear bands with increasing strain rate.

Most of the assumptions involved with the models based on earth pressure theory neglect the inertial forces and are suitable only for predicting the forces on a narrow tine moving at very slow speed. Though the application of existing numerical techniques like FEM and ANN have been found to predict the soil-tool system in a better approximation to the exact solution, soils have been considered for static analysis and

the mass soil deformations have been ignored. Recently a few studies (Swick and Perumpral, 1988; Zeng and Yao, 1992; Shen and Kushwaha, 1995) based on numerical methods have been conducted using FEM with the dynamic perspective of tillage. However, in this case, prior knowledge of shear strain at failure for determining the position of a shear failure boundary is required. With a few exceptions, the finite element method, the boundary element method, and the finite difference method require the fabric to be continuous in nature, not allowing for separation, rotation, large scale deformation and displacement (Nordell, 1997). For dynamic modeling, the conventional DEM model for calculation of contact forces between elements has some problems; for example, the movement of elements is too discrete to simulate real soil particle movement (Momozu et al., 2003). The distinct element method has been shown to predict the horizontal force on implements, such as dozer blades, with reasonable accuracy. The vertical force predictions on the dozer blade, however, do not correlate well with measured data. It appeared, in general, that more capable computational methods are required to effectively simulate the dynamic response characteristics of cohesive earthen materials and their interaction with components of off-road machines. The challenge is daunting, but the need is great (Hofstetter, 2002).

Simulations were performed using FEM (Plouffe et al., 1999) to evaluate the effects of mouldboard settings and operating speed on plow performance in a clay soil. They have suggested that other numerical tools should be combined with FEM to enable evaluation of overall behaviors of tillage implements. This is because the current formulation of FEM alone cannot solve such a complex behavior and field experiments may not allow clear depiction of the effect of changing a single part.

Soil shear rate with respect to the tool operational speed plays a very important role in analyzing and optimizing high speed tillage. The size of the furrow formed behind the tool is a function of the operating speed. Photographic and video camera analysis indicated increasing soil crumbling with increasing tool speed. While trying to estimate the furrow profile using a soil profilometer, difficulties arose and quantification could not be addressed (Rosa, 1997).

2.4.2.3 Material complexity and stress path variation

Most soils are formed anisotropically by the process of deposition and subsequent consolidation in horizontal layers. Soil complexity is compounded by the influences of moisture content, structural disturbance, stress history, time, and environmental conditions. Different soil formation phases and previous activities cause agricultural soil to be basically an anisotropic material. An anisotropic soil tends to fail due to shear strength in extension that is only about 50 to 60 % of its shear strength in compression (Kulhawy and Mayne, 1990). Modeling of soil-tool interaction using FEM, soil strength parameters have been based in triaxial compression tests. Before the tillage activity, the major principal stress direction is vertical and the minor principal stress direction is horizontal. During tillage, the soil undergoes shear and passive failure. Therefore the major principal stress direction changes from vertical to nearly horizontal close to the ground surface and soil is deemed to fail in extension. Thus, analyses that use isotropic elastic-plastic soil models result in an over prediction of the required tillage forces (Karmakar et al., 2004).

2.4.2.4 Limitations of existing constitutive models

The peak tillage force is a function of both stiffness and strength of the soil, whereas the residual tillage force depends primarily on the strength of soil. Both the stiffness and the strength of soil are influenced significantly by the past stress (or strain) history of the soil. Therefore, in order to predict the magnitude of the tillage force, it is crucial to choose a strain-dependent elastoplastic model for the soil (Karmakar et al., 2004). Thus, analysis of soil-tool interaction taking the dynamic feature into consideration remains unsatisfied.

2.4.3 Large soil deformation: Flow perspective

The rheology of soil is very complex. In the case of Newtonian fluids, like air and water, the shear stress versus shear rate relationship is linear and the fluids have a constant viscosity at a particular temperature. However, high molecular suspensions of fine particles, pastes and slurries are usually non-Newtonian (Skelland, 1967). Soils,

like most real bodies, deform at a variable rate. Only at the certain stage of the process is the rate of deformation constant (Vyalov, 1986).

Upon close examination of experimental stress-strain rate relationships of several soils, Vyalov (1986) concluded that a simple linear model of visco-plasticity, the Bingham rheological model, can describe soil deformation under steady-state stress. Soil visco-plastic behavior has been reported in several studies (Day and Holmgren, 1952; McMurdie and Day, 1958; Ghavami et al., 1974). The relation between the stress and rate of flow is nonlinear in soil, and the flow is induced by the difference between total stress and the yield stress. The generalized observation was that flow of soil is initiated only when the stress acting upon the inter-aggregate contact exceeds a '*critical yield point'* (threshold stress value). This threshold stress is termed as yield stress. Beyond this stress, soil aggregates flow in a manner similar to viscous material at a rate proportional to the stress in excess of the yield stress. Visco-plastic fluids behave like solids when the applied shear stress is less than the yield stress; once it exceeds the yield stress, it will flow just like a fluid (Bird et al., 1983).

2.4.3.1 Soil flow phenomena

Goryachkin (1968) explained the soil flow phenomena over an inclined tillage tool surface using a trihedral wedge and three theories. The crushing theory considered the absolute soil motion normal to the tool surface, lifting theory considered the relative position of the soil aggregates within a soil slice to remain the same; and, the shearing theory considered soil motion parallel to the planes of soil shear failure.

Fornstrom et al. (1970) proposed non-equilibrium process concepts for tillage with emphasis on the notion of change of state. The theory considers the energy balance taking into account a stress tensor to represent internal mechanical effects involving kinetics and kinematics. The externally applied force was related to the changes in internal energy and specific volume (dilation) and to viscous flow. Since soil flow is not always a continuous process, '*scale of motion'*, represented by '*integral or macro scale'*

and '*micro scale*' was recommended for consideration. Macro scale is a measure of the average longest distance over which the motion of a particle or group of particles persists in a given direction. Micro scale is some measure of the average shortest distance travelled by a particle or group of particles before a change of direction occurs.

The feature of large deformation of soil due to tillage tool interaction can be viewed as soil flow around the tillage tool. By definition, a fluid is a material continuum that is unable to withstand a static shear stress. Unlike an elastic solid which responds to a shear stress with a recoverable deformation, a fluid responds with an irrecoverable flow (White, 1999). Fluid flow can generally be of either an internal flow or an external flow type. Examples of internal flow are pipe flow of air or water or any other fluids. Flow of air over an aircraft is a perfect example of external flow. When a tool is operated for soil cutting, this dynamic process can be viewed as an external flow over a bluff body; soil flow over the tool. Desai and Phan (1980) presented the general case of the three-dimensional soil tool interaction in which the tool is moving relative to the soil as shown in Fig. 2.19. Thus the soil shear failure due to the translation of the tool is analogous to the fluid flow over a blunt body. The velocity vectors of the soil particles as they encounter with the tool and soil failure front propagation can be derived from a fluid mechanistic approach. Since the structure and soil move relative to each other, there is shear transfer through relative slip. This is postulated in the current research through computational fluid dynamics simulations.

2.4.3.2 Soil flow pattern

Soil flow around the tool can be categorized and analyzed from the perspective of fluid and flow parameters. Fluid parameters are concerned with the physical properties of the fluid while flow parameters represent the feature of the flow with respect to the system as a whole. Though both air flow over an aircraft and soil flow over a tillage tool are external flows, much difference exists in the fluid characteristics. A fluid flow could be laminar or turbulent depending on several factors, including flow velocity, fluid viscosity and length scale, etc. The general demarcation of the two types of flow is specified by the Reynolds number, which is the ratio of inertia and viscous forces. Even

in high speed tillage, due to the high molecular weight of soil and high viscosity, the unsaturated soil flow pattern will be more like a cripping flow as the Reynolds number would be very low (less than 1).

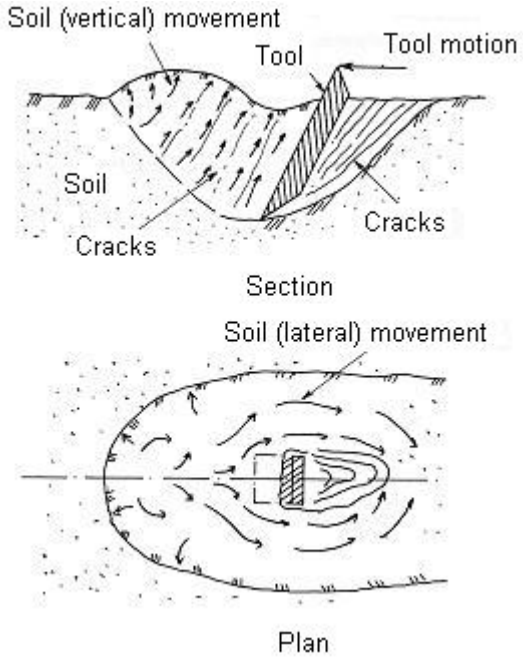

Figure 2.19 Soil tool idealization (Desai and Phan, 1980).

Davison *et al.* (2002) investigated the validity of using CFD for simulation of soil flow over augers and reasonable evidence has been produced in the positive sense. It was also shown that for loose soils with low internal angle of internal friction, such as liquefied sand, Newtonian viscosity was an acceptable assumption.

Large soil mass deformation during tilling can be correlated to a flow pattern and can be expressed in terms of constitutive modeling by incorporating some non-Newtonian parameter in the basic Navier-Stokes equation. The variables are subject to the laws of conservation of mass and momentum and two other constitutive laws like the yield criteria. Constitutive relations can be formed in respect of soil rheological behavior and soil-tool interacting parameters. Stress distribution over the tool section and velocity profile can be calculated by solving these equations with pertinent boundary conditions. Because of nonlinearity in the material derivative term, numerical solution becomes a

necessity. Thus, any commercial package for computational fluid dynamics can be used for determining the soil flow pattern with tillage tool interaction.

2.4.4 Application of CFD to Tillage

Movies have shown the fundamental behavior of an artificial soil failure to change from shear to plastic flow as the tool velocity was increased (Schimming et al., 1965). Olson and Weber (1966) also observed that an increase in the speed of a blade could cause a transition between the shear-plane and flow failures. As the speed was increased, there was more general shear and less sliding of one soil block on another, until the shear failure plane no longer formed and only a flow failure occurred. At high speed, soil underwent plastic failure when both dry and wet soils were used (Stafford, 1979). It was believed that the soil strength parameters, cohesion and angle of internal friction, were dependant on strain rate. Successive studies by Stafford and Tanner (1983) on sandy and clay soils revealed that deformation (shear) rate had a very significant effect on the shear strength over a wide range of moisture content.

In design and development, computational fluid dynamics (CFD) programs are now considered to be standard numerical tools for predicting not only fluid flow behavior, but also the transfer of heat and mass, phase change, chemical reaction, mechanical movement and stress or deformation of structures (Sethian, 1993). The programs provide a detailed description of flow distributions, making it possible to evaluate geometric changes with much less time and cost than would be involved in laboratory testing.

2.4.5 Soil flow hypothesis

Changes in void ratio due to soil loading by interaction with a tillage tool, and hence density change which causes the rheological behavior to be altered can be neglected. Thus, soil can be considered as a single-phase continuous medium and its rheological properties can be analyzed and used to simulate the soil deformation process associated

with tillage. The approach could be to consider the tool as stationary and visco-plastic soil flow over the tool. The flow domain could be decided based on the tool influence zone. Thus the influence of the tool in a fully developed flow could be utilized to calculate the soil disturbance and force imposed on the tool.

2.4.6 Conclusions

Predicting the changes of complex soil mechanical behaviour with different texture and structures at different places is either intractable or very costly. Taking the soil stress history and anisotropy into account for modeling soil-tool interaction is also a daunting task. There are limitations of the presently used constitutive models used in FEM. Soil-tool modeling using fluid flow approach is also not expected to incorporate the complex phenomena of stress history and soil anisotropy.

Scale of motion as explained by Fornstorm et al. (1970) may not be applicable for unsaturated agricultural soil as the fluid flow approach to analyse this soil needs the soil to be considered as a laminar flow or more likely as a pressure driven cripping flow. However, the scale of motion, regarding turbulent fluid flow, which accounts for the energy dissipation due to motion as the production, separation and dissipation of eddies as a function of length scale (White, 1999), can be applied for puddle soil and its interaction with rotary tines used for paddy cultivation.

For many interactive applications, realistic appearance is more important than accuracy. Hence, for simulation purposes, initially, soil could be considered to be homogeneous and incompressible. Soil could also be modeled as a compressible material in this fluid flow approach. In this case, a multiphase fluid flow would have to be considered. The specific volume fraction of solid, water, and air with their mechanical characteristics would be analyzed using a volume of fluid approach. However, since this was the first attempt, for simplification, the soil could be considered to be incompressible.

2.5 References

Atkinson, J. H., D. Richardson and S. E. Stallebrass. 1990. Effect of recent stress history on the stiffness of over-consolidated soil. Géotechnique 40(4): 531-541.

Bailey, A. C., C.E. Johnson, and R.L. Schafer. 1984. Hydrostatic compaction of agricultural soils. Trans ASAE 27(4): 925-955.

Bird, R. B., G. C. Dai and B. J. Yarusso. 1983. The rheology and flow of visco-plastic materials. Rev Chem Eng 1: 1–70.

Chi, L. and R. L. Kushwaha. 1989. Finite element analysis of forces on a plane soil blade. Canadian Agric Eng 31(2): 135-140.

Chi, L. and R. L. Kushwaha. 1990. A nonlinear 3-D finite element analysis of soil failure with tillage tools. J Terramech 27(4): 343-366.

Chi, L., R. L. Kushwaha and J. Shen. 1993. An elasto-plastic constitutive model for agricultural cohesive soil. Canadian Agric Eng 35(4): 245-251.

Davison, J., R. K. Calay, T. Sands and M. England. 2002. CFD simulation of soil flow over augers. Proc ASME PVP Conf, August 4-8, Vancouver, Canada.

Day, P. R. and G. G. Holmgren. 1952. Microscopic change in soil structure during compression. Soil Sci Soc Am Proc 16: 73-77.

Desai, C. S. and H. V. Phan. 1980. Computational Methods in Nonlinear Mechanics. Ed. J. T. Oden. New York: North Holland Publishing Company.

Duncan, J. M. and C. Y. Chang. 1970. Nonlinear analysis of stress and strain in soil. Journal of the Soil Mechanics and Foundations Division, ASCE 96(SM5): 1629-1653.

Elijah, D. L. and J. A. Weber. 1971. Soil failure and pressure patterns for flat cutting blades. Trans ASAE 14(4): 781-785.

Fornstrom, K. J., R. D. Brazee and W. H. Johnson. 1970. Tillage-tool Interaction with a bounded, artificial soil. Trans ASAE 13(4): 409-416, 418.

Fredlund, D. G. and H. Rahardjo. 1993. Soil Mechanics for Unsaturated Soils. New York: John Wiley.

Ghavami, M., J. Keller and I. S. Dunn. 1974. Predicting soil density following irrigation. Trans ASAE 17: 166-171.

Godwin, R. J. and G. Spoor. 1977. Soil failure with narrow tines. J Agric Eng Res 22: 213 -228.

Goryachkin, V. P. 1968. Collected works in three volumes. N. D. Luchinski, eds. Translated 1972. Jerusalem, Israel: Ketter Press.

Hettiaratchi, D. R. P. 1987. A critical state soil mechanics model for agricultural soils. J Soil Use Management 3: 94-105.

Hettiaratchi, D. R. P. and A. R. Reece. 1967. Symmetrical three-dimensional soil failure. J Terramech 4(3): 45-52.

Hettiaratchi, D. R. P. and J. R. O'Callaghan. 1980. Mechanical behavior of Agricultural soils. J Agric Eng Res 25: 239-259.

Hettiaratchi, D. R. P., B. D. Witney and A. R. Reece. 1966. The calculation of passive pressure in two-dimensional soil failure. J Agric Eng Res 11(2): 89-107.

Hofstetter, K. 2002. Analytic Method to Predict the Dynamic Interaction of a Dozer Blade with Earthen Material. Proc 14th Int Conf ISTVS Vicksburg, MS USA on CD-ROM.

Kamai, T. 1993. Failure propagation process in landslide clay. In Proc. 7th Int. Conf. and Field Workshop on Landslides, 243-248. Brastislava, Slovakia.

Karmakar, S., J. Sharma and R. L. Kushwaha. 2004. Critical state elasto-plastic constitutive models for soil failure in tillage – A Review. Canadian Biosystems Engineering 46: 2.19-2.23.

Kondner, R. L. and J. S. Zelasko. 1963. A hyperbolic stress-strain response: cohesive soil. Journal of the Soil Mechanics and Foundations Division, ASCE 89(SM1): 115-143.

Kulhawy, F. H. and P. W. Mayne. 1990. Manual on estimating soil properties. Report EL-6800, Electric Power Research Institute, Davis, California, USA.

Kushwaha, R. L. and Z. X. Zhang. 1998. Evaluation of factors and current approaches related to computerized design of tillage tools: A review. J Terramech 35(2): 69-86.

Kushwaha, R. L., L. Chi and J. Shen. 1993. Analytical and numerical models for predicting soil forces on narrow tillage tools – A review. Canadian Agric Eng 35(3): 183-190.

Lade, P.V. and R.B. Nelson. 1984. Incrementalization procedure for elasto-plastic constitutive model with multiple, intersecting yield surface. Intl J Num Anal Meth Geomech 8: 311-323.

Liu, Y. and Z. M. Hou. 1985. Three-dimensional nonlinear finite element analysis of soil cutting by narrow blades. Proc Int Conf Soil Dyn. Auburn, AL 2: 338-347.

Luth, H. J. and R. D. Wismer. 1971. Performance of plane soil cutting blades in sand. Trans ASAE 14: 255-259.

McKyes, E. and O. S. Ali. 1977. The cutting of soil by narrow blades. J Terramech 14(2): 43-58.

McMurdie, J. L. and P. R. Day. 1958. Compression of soil by isotropic stress. Soil Sci Soc Am Proc 22: 18-22.

Momozu, M., A. Oida, M. Yamazaki and A. J. Koolen. 2003. Simulation of a soil loosening process by means of the modified distinct element method. J Terramech 39: 207-220.

Nordell, L. K. 1997. Particle flow modeling: Transfer chutes & other applications. Chute Design Conf BELTCON, Republic of South Africa.

O'Calleghan, J. R. and K. M. Farrely. 1964. Cleavage of soil by tined implements. J Agric Eng Res 9(3): 259-270.

Olson, D. J. and J. A. Weber. 1966. Effect of speed on soil failure patterns in front of model tillage tools. Trans SAE 74(4): 298-310.

Or, D. 1996. 1996. Wetting induces soil structural changes: the theory of liquid phase sintering. Water Resour Res 32: 3041-3049.

Osman, M. S. 1964. The mechanics of soil cutting blades. J Agric Eng Res 9(4): 313-328.

Payne, P. C. J. 1956. The relationship between the mechanical properties of soil and the performance of simple cultivation implements. J Agric Eng Res 1(1): 23-50.

Perumpral, J. V., R. D. Grisso and C. S. Desai. 1983. A soil-tool model based on limit equilibrium analysis. Trans ASAE 26(4): 991-995.

Plouffe, C., C. Laguë, S. Tessier, M. J. Richard and N. B. McLaughlin. 1999. Mouldboard plow performance in a clay soil: Simultaneous and experiment. Trans ASAE 42(6): 1531-1539.

Pollock, D. Jr., J. V. Perumpral and T. Kuppusamy. 1986. Finite element analysis of multipass effects of vehicles on soil compaction. Trans ASAE 29(1):45-50.

Rajaram, G. 1990. Collapse failure in dry clay soils caused by implements. J Terramech 27(2): 69-78.

Rajaram, G. and D. Gee-Clough. 1988. Force distance behavior of tine implements. J Agric Eng Res 41: 81-98.

Reece, A. R. 1965. The fundamental equations of earth-moving mechanics. Proc Symp Earth Moving Machinery. Institute of Mechanical Engineering 179(3F): 8-14.

Rosa, U. A. 1997. Performance of narrow tillage tools with inertial and strain rate effects. Unpublished PhD thesis. Saskatoon, Saskatchewan: University of Saskatchewan.

Roscoe, K. H. and J. B. Burland. 1968. On the generalized stress-strain behavior of wet clay. In Engineering Plasticity, eds. J. Heyman and F.A. Leckie, 535-609. Cambridge, England: Cambridge University Press.

Roscoe, K. H., A. N. Schofield and C.P. Wroth. 1958. On the yielding of soils. Géotechnique 8: 22-53.

Schimming, B. B., H. J. Hass and H. C. Saxe. 1965. A comparison of the dynamic and static shear strengths of cohesion less, cohesive, and combined soils. Tech Report No. AFWL TR-65-48, Department of Civil Engineering, University of Notre Dame.

Sethian, J. A. 1993. Computational fluid dynamics. From Desktop to Teraflop: Exploiting the US Lead in High Performance Computing. Washington DC, USA: National Science Foundation Publications.

Shen, J. and R. L. Kushwaha. 1995. Investigation of an algorithm for nonlinear and dynamic problems in soil-machine systems. Comp Electronics Agric 13: 51-66.

Shen, J. and R. L. Kushwaha. 1998. Soil-Machine Interactions – A Finite Element Perspective: Marcel Dekker Inc. Publishers.

Simpson, B. 1973. Finite elements applied to earth pressure problems. Unpublished Ph.D. thesis, Cambridge, UK: Department of Engineering, University of Cambridge.

Simpson, B. N. J. O'Riordon and D.D. Croft. 1979. A computer model for the analysis of ground movements in London Clay. Géotechnique 29(2): 149-175.

Skelland, A. H. P. 1967. Non-Newtonian Flow and Heat Transfer. New York: John Wiley and Sons Inc.

Stafford, J. V. 1979. The performance of rigid tine in relation to soil properties and speed. J Agric Eng Res 24(1): 41-56.

Stafford, S. V. and D. W. Tanner. 1983. Effect of rate on soil shear strength and soil-metal friction. Soil Tillage Res 3: 245-260.

Stallebrass, S.E. 1990. Modelling the effect of recent stress history on the deformation of over-consolidated soils. Unpublished Ph.D. thesis, London, UK: Department of Geotechnical Engineering, City University.

Swick, W. C. and J. V. Perumpral. 1988. A model for predicting soil-tool interaction. J Terramech 25(1): 43-56.

Tanaka, H., M. Momozu, A. Oida and M. Yamazaki. 2000. Simulation of soil deformation and resistance at bar penetration by the distinct element method. J Terramech 37(1): 41–56.

USDA (Unites States Department of Agriculture), 2005. Soil Science Glossary (Soil Science Society of America). Accessed from http://soils.usda.gov/education/facts/soil.html.

Vyalov, S. S. 1986. Rheological fundamentals of soil mechanics. Amsterdam, The Netherlands: Elsevier.

Wang, J. and D. Gee-Clough. 1991. Deformation and failure in wet clay soil. II. Simulation of tine soil cutting. Proc IAMC Conf Beijing, China, Session 2: 219-226.

Wheeler, S. J. and V. Sivakumar. 1992. Critical state concepts for unsaturated soil. Proc Seventh Intl Conf on Expansive Soils, 167-172. Dallas, TX. August 3-5.

White, F. M. 1999. Fluid Mechanics. 4th ed. New York: WCB McGraw Hill.

Wood, D. M. 1990. Soil behavior and critical state soil mechanics. Cambridge, England: Cambridge University Press.

Yamamuro. 2004. Department of Civil and Environmental Engineering University of Delaware, Newark, DE19716-3120. Available at www.ce.udel.edu/directories/profiles/yamamuro.html. Accessed on 6 November, 2004.

Yong, R. N. and A. W. Hanna. 1977. Finite element analysis of plane soil cutting. J Terramech 14(3): 103-125.

Zeng, D. and Y. Yao. 1992. A dynamic model for soil cutting by blade and tine. J Terramech 29(3): 317-327.

Zhang, J. and R. L. Kushwaha. 1998. Dynamic analysis of a tillage tool: Part I – Finite element method. Canadian Agric Eng 40(4): 287-292.

Chapter 3

Determination of Soil Visco-plastic Parameters

3.1 Significance

The case study in Chapter 2 re-confirmed the soil non linearity and variation of soil failure front with the tool operating conditions. Review of the critical state soil mechanics for tillage tool modeling revealed the limitations with the constitutive relations related to soil anisotropy and stress path variation during tillage. From the discussion of soil rheology and fluid flow features, the soil can be considered as a visco-plastic material and its mechanical behavior during tillage can be studied from a fluid flow perspective with non-Newtonian flow behavior.

Estimation of soil parameters is important for analysing the dynamic soil-tool interaction. Most of the studies on tillage for soil-tool modeling were based on quasi-static assumptions and the corresponding parameters were also estimated by quasi-static test conditions, where the strain rate is very low. Considering visco-plastic behaviour of soil, dynamic parameters like viscosity and yield stress are of prime importance. The objectives of the research presented in this chapter are to develop and test a soil rheometer for investigating soil visco-plastic parameters for model development using computational fluid dynamics.

3.2 Introduction

Soil parameters contributing to the performance of a tillage tool can be categorized broadly as physical and mechanical properties. Soil mechanical behavior is also influenced by the physical conditions. Soil texture and structure, bulk density, pore space and void ratio, consistency limits, specific gravity are considered as physical properties. Shear strength in drained and undrained conditions, penetration resistance have been considered as important soil mechanical parameters in modeling soil-tool interaction using analytical and numerical methods.

Soil mechanical behavior is very complex due to its non homogeneity and discontinuousness in the structure. The dynamic properties are often expressed in terms of shear wave velocity, dynamic shear modulus and material damping ratio in shear (Stokoe, 1999). These properties are influenced by various soil parameters like soil type, plasticity index, mean effective confining pressure, and system parameters like, excitation frequency, shearing strain amplitude and number of loading cycles. However, the dynamic properties required for analysis of soil-tool interaction with fluid dynamics approach are the dynamic viscosity and the yield strength. These parameters are the variables of the Bingham model. Commercial software packages for modeling non-Newtonian flow are designed to obtain user defined values for these variables. These parameters are related to soil physical and mechanical properties, like, soil compaction, moisture content, shear strength etc. Variation of soil compaction, which is also a function of bulk density, would be related to yield stress and soil viscosity. Soil characteristics related to particle size could be related to computational fluid dynamics modeling when a multiphase fluid flow would be taken into account in advanced stage of modeling.

3.3 Literature Review

The following sections are focused on the soil mechanical behavior with the perspective of visco-plastic parameters.

3.3.1 Material Characteristics

Soil is a very complex material and its behavior is not completely understood. The complexity grows further when soils of different places with different agro-climatic conditions are taken into considerations. For the purpose of developing prediction models, soil mechanical behavior has been descried in different ways represented by combination of elastic spring, dashpot and slider in the perspective of elasticity, plasticity and viscosity.

3.3.1.1 Non-Newtonian Rheology

General theory of rheology assumes that similar processes of deformation can be produced in different materials by varying the intensity of loading; its character; its rate of application, and the temperature and shape and dimensions of the loaded body (Gupta and Pandya, 1966). In the case of Newtonian fluids, like air and water, the shear stress versus shear rate relationship is linear and the fluids have a constant viscosity at a particular temperature. For structurally simple Newtonian fluids (gases and liquids of low molecular weight) the relation between shear stress and velocity gradient in a shear flow is expressed as,

$$\tau_{xy} = \mu \frac{dv_x}{dy} \tag{3.1}$$

where:

τ_{xy} = shear stress (Pa),

μ = Newtonian viscosity (Pa.s),

v_x = directional velocity (m s^{-1}),

y = depth of flow (m).

Any fluid that does not obey the Newtonian relationship between the shear stress and shear rate is called non-Newtonian (Skelland, 1967). High molecular weight liquids, which include polymer melts and solutions of polymers, as well as liquids in which fine particles are suspended (slurries and pastes), are usually non-Newtonian. Non-Newtonian materials are conveniently grouped into three general classes, time

independent or purely viscous or inelastic or Generalized Newtonian fluids, time-dependent fluids and visco-elastic fluids (Chhabra and Richardson, 1999). Based on relation between the shear rate and shear stress, time-independent fluids are further classified into three types as shear thinning, visco-plastic and shear thickening. When the viscosity decreases with increasing shear rate, the fluid is shear-thinning. In the opposite case where the viscosity increases as the fluid is subjected to a higher shear rate, the fluid is called shear-thickening. Shear-thinning behavior is more common than shear-thickening. Shear-thinning fluids also are called pseudoplastic fluids.

Visco-plastic fluid behavior is characterised by the existence of a critical shear stress. Many non-Newtonian materials have a 'yield stress', a critical value of stress below which they do not flow; they are sometimes called visco-plastic materials (Bird et al. 1983). Yield stress is generally explained in terms of physical behavior associated with an internal structure in three dimensions, which is capable of preventing movement for values of shear stress less than the yield value. A few definitions of yield stress have been cited below:

- The stress at which a substantial amount of plastic deformation takes place under constant load. This sudden yielding is characteristic of iron and annealed steel. In other material deformation begins gradually (Collocott, 1971).
- The minimum stress for creep to take place. Below this value any deformation produced by an external force will be purely elastic (Illigworth, 1991).
- The level of stress at which substantial sudden deformation takes place (Robinson, 1996)

For shear stress greater than yield stress, the internal structure collapses completely, allowing shearing movement to occur (Zisis and Mitsoulis, 2002). Thus, visco-plastic fluids behave like solids when the applied shear stress is less than the yield stress. When the shear stress falls below the yield stress, a solid structure (unyielded) is formed. Once it exceeds the yield stress, the visco-plastic fluid will flow just like a fluid. Bird et al.

(1983) cited extensive examples of visco-plastic materials. A few of them include clay with water, drilling mud, nuclear fuel slurries, mayonnaise, toothpaste, cement-clay-water mixture, carbon black in oil, grease, inorganic solid with polymer solvent, meat extract, butter, sauces, blood etc.

Three commonly used models for visco-plastic fluids are Bingham plastic model, Herschel-Bulkley fluid model and Casson fluid model. Bingham plastics exhibit a linear behavior of shear stress against shear rate. The most elementary constitutive equation in common use that describes a material that yields is the Bingham fluid (Lipscomb and Denn, 1984). Bingham visco-plastic fluids combine the behavior of rigid solids and non-Newtonian viscous liquids by differentiating between physical regions where these descriptions hold according to criteria based on the level of stress in the material. Here regions of rigid solid and plastic fluid behavior are separated by von Mises' yield criteria (Beris et. al., 1985). This two-parameter Bingham model in simple shear flow takes the form,

$$\tau = \tau_y + \mu \dot{\gamma}, \text{ for } |\tau| > \tau_y \tag{3.2}$$

$$\dot{\gamma} = 0, \text{ for } |\tau| \leq \tau_y \tag{3.3}$$

where:

τ = shear stress (Pa),

$\dot{\gamma}$ = shear rate (s^{-1}),

τ_y = yield stress (Pa), and

μ = viscosity coefficient or plastic viscosity (Pa.s).

Several dimensionless groups have been introduced (Bird et al, 1983). The most common ones are:

- Bingham number, $B_i = \dfrac{\tau_y D}{\mu V}$ (3.4)

  where:

  D = characteristic length (m),

  V = characteristic velocity (m s^{-1}).

- Dimensionless yield stress, $\tau_y^* = \frac{\tau_y H}{\mu V_N}$ (3.5)

where:

H = half width of flow channel (m),

V_N = average fluid velocity (m s^{-1}).

3.3.1.2 Soil Rheology

As the soil is a deformable body whose behavior falls between a linear elastic solid and ideal viscous liquid, its behavior is governed by general theory of rheology (Gupta and Pandya, 1966). The rheology of soil is very complex. Soils, like most real bodies, deform at a variable rate. Only at the certain stage of the process the rate of deformation is constant. Upon close examination of experimental stress-strain rate relationships of several soils, Vyalov (1986) concluded that a simple linear model of visco-plasticity, the Bingham rheological model, can describe soil deformation under steady-state stress. Soil visco-plastic behavior has been reported in several studies (Day and Holmgren, 1952; McMurdie and Day, 1958; Ghavami et al., 1974; Ghazehei and Or, 2001). The relation between the stress and rate of flow is nonlinear in soil, and the flow is induced by the difference between total stress and the yield stress. The generalized observation was that flow of soil is initiated only when the stress acting upon the inter-aggregate contact exceeds a '*critical yield point'* (threshold stress value). This threshold stress is termed as yield stress. Beyond this stress, soil aggregates flow in a manner similar to viscous material at a rate proportional to the stress in excess of the yield stress. Visco-plastic fluids behave like solids when the applied shear stress is less than the yield stress; once it exceeds the yield stress, it will flow just like a fluid (Bird et al. 1983).

The available experimental data on soil viscosity have a spread varying between 10^5 to 10^{16} Pa.s (Vyalov, 1986). Plastic viscosity of different types of clay as was observed by Ermolaeva et al. (1968) is given as,

- Remoulded Cambrain clay (w = 24-27%): 1.5 x 10^8 to 8 x 10^{11} Pa.s,
- Remoulded Khvalynsk clay (w = 38%): 1.5 x 10^6 to 1.8 x 10^9 Pa.s.

Maslov (1968) recommended the use of the following averaged viscosities for clay soils:

- Soft clay: $10^9 – 10^{10}$ Pa.s,
- Firm clay: $10^{11} – 10^{12}$ Pa.s,
- Stiff clay: 10^{13}- 10^{14} Pa.s,
- Hard clay: 10^{14}- 10^{16} Pa.s.

Gupta and Pandya (1966) from their study of soil rheological behavior under static loading, concluded that soil was a nonlinear visco-elastic solid and it exhibited resistance to shearing strain that varies with the rate at which shearing strain occurs. Soil behavior was characterized by moduli of instantaneous elasticity, plasticity and fracture; delayed elasticity and retardation time, the flow constant and yield stress, as well as rate of strain at the yield point. Knowing the stress-strain-time relationship of soil in compression and shear, soil behavior can be predicted under any system of stresses. The proposed relationship was as follows:

$$\varepsilon_c = \frac{S_c}{K_e} + \frac{S_c}{K_p} + \frac{S_c}{K_f} + \frac{S_c}{K_d}(1 - e^{-t/\tau}) + \dot{\varepsilon}_{cy}.t.\exp(\frac{S_c - S_{cy}}{\eta_c}) \qquad (3.6)$$

where,

ε_c = total compressive strain,

S_c = compressive stress (Pa),

K_e = modulus of instantaneous elasticity in compression (Pa),

K_p = modulus of instantaneous plasticity (Pa),

K_f = modulus of instantaneous fracture in compression (Pa),

K_d = modulus of delayed elasticity in compression (Pa),

T = time elapsed since the application of load (s),

τ = retardation time (s),

$\dot{\varepsilon}_{cy}$ = rate of strain at yield point (s^{-1}),

S_{cy} = yield stress (Pa),

η_c = flow constant governing the rate of flow of soil under load (Pa.s).

Ram and Gupta (1972) established the relationship between different rheological coefficients and soil parameters by a mechanical model with the combinations of different rheological elements like elastic spring, dashpot and slider. They expressed the total strain as a combination of three parts of strain: instantaneous strain (ε_i), delayed strain (ε_d) and creep strain (ε_{cs}) as:

$$\varepsilon_c = \frac{S_c^m}{K_e} + \frac{S_c^n}{K_d}(1 - e^{t/\tau}) + \dot{\varepsilon}_{cy}.t.\exp(\frac{S_c - S_y}{\eta_c}) \qquad (3.7)$$

where,

S_c = compressive stress (Pa),

S_y = compressive stress at yield point (Pa),

m & n = exponent.

Oida (1992) developed a five element rheological model for analyzing stress relaxation behavior of silt-clay-loam soil and analyzed it with the Finite Element Method for obtaining a good agreement with the experiment data. The rheological constants, Young's modulus and viscosity coefficient were linearly correlated to the specimen density. The value of rheological constants decreased with increased in soil moisture content. The viscosity coefficient decreased with an increased in elapsed time.

Rheological properties of soil have shown that wet soils have visco-plastic behavior with well-defined yield stress and nearly constant plastic viscosity (Ghezzehei and Or, 2001). Results showed that for low moisture content and high tractor speed, the elastic component of deformation increased, whereas with higher moisture contents, viscosity and shear modulus decreased. Under steady stress, wet soils and clay minerals exhibited visco-plastic properties characterized by a well defined yield stress and constant coefficient of plastic viscosity, both of which increased with decreasing viscosity.

3.3.2 Measurement of soil rheological properties

In some non-Newtonian systems, such as concentrated suspensions, rheological measurements may be complicated by nonlinear, dispersive and thixotropic mechanical properties. The rheometrical challenges posed by these features may be compounded by an apparent yield stress (Chhabra and Richardson, 1999). Rotational viscometers are important for characterisation of non-Newtonian fluid behavior (Walters, 1975). These are of two main types, namely; the controlled shear rate instruments (also known as controlled rate devices) and controlled stress instruments. These are classified as concentric cylinder, cone and plate and parallel plate systems.

3.3.2.1 Rheometers

Viscosity could be measured by any of the following rotational rheometers (Chhabra and Richardson, 1999):

- Concentric cylinder type
- Cone and plate type and
- Parallel plate type

Direct measurement of shear stress can only be made if the shear rate is constant (or very close to constant) throughout the shearing gap. Coaxial instruments do not comply with this. To obtain this phenomenon, the shearing gap has to be very small. This is a problem with most of the non Newtonian materials as it is suggested that the shearing gap should vary 10-100 times the particle size of the materials to be measured for maintaining bulk material properties. Thus a concentric cylinder, which may be used for soil slurry, is not a good choice for unsaturated soil viscosity measurement.

Cone and plate type is useful for the time dependent (history dependant) materials. The small cone angle takes care of the same shear history to all the elements of the material. But the small gap restricts it to the use of materials with very fine particles. In contrast to the cone and plate geometry, as seen in a parallel plate viscometer, the shear strain is

proportional to the gap height and may be varied to adjust the sensitivity of the shear rate, a factor which facilitates testing for wall slip effects. In a study of rheological properties of unsaturated soil, Ghezzehei and Or (2001) used a rotational (torsional) rheometer with parallel plate sensor system. Davison et al. (2002) obtained viscosity and other dynamic soil properties of cohesive soil using a parallel plate rheometer for their CFD simulation of soil flow over augers.

3.3.2.2 Vane shear test

The field vane is the most widely used method for the in-situ determination of the undrained shear strength. In vane shear test, it is usually assumed that the torque originates from the shear stresses mobilized on the right cylindrical surface whose shape coincides with the dimensions of the vane blades (Karube et al., 1988). The vane shear has for many years been regarded as a device for measuring strength properties of soils in-situ (Gill and Vanden Berg, 1968) because of the ease and convenience of such measurements. Since it is assumed that the final form of the soil failure surface is that of a cylinder with the length and diameter of the vane, and no normal forces are applied to these surfaces, torsional resistance is caused by cohesion acting on all surfaces of the cylinder (Hillel, 1980). Thus the torque applied to cause soil failure is given as:

$$T = c\pi\left(\frac{1}{2}d^2h + \frac{1}{6}d^3\right) \tag{3.8}$$

where:

c = cohesion (Pa),

d = diameter of shear-vane (m),

h = length of vanes (m).

3.4 Development of soil rheometer

3.4.1 Objectives and Requirements

The goal of this research was to use the values obtained from this test for computational fluid dynamics (CFD) simulations. Rheological measurements were carried out to find the effects of soil moisture content and cone index on soil viscosity and yield strength. A motorised soil rheometer has been developed at the Department of Agricultural and Bioresource Engineering, University of Saskatchewan to evaluate the dynamic soil parameters. The apparatus is capable of measuring yield stress and soil viscosity. The device works on the principle of torsional shear applied to a standard vane with controlled strain rate.

Strain rate effects are important in the vane test, and since these effects vary with the vane diameter, having one particular size of the vane would be convenient for use. The vane test was standardized by the ASTM (D2573-01, 2004). The usual 'rest- period' following the vane insertion would be 5 min, and the rate of rotation is generally specified as either 6^o or 12^o per minute. In practice this typically results in failure occurring at about 1 minute, as these two factors significantly influence the measured undrained strength. The distribution of shear stress around the vane may be assumed to be uniform on the vertical edges of the vane blades but are probably highly non-uniform on the top and the bottom surfaces. As a consequence the conventional interpretation of the test, given by the following expression is more conservative:

$$\text{Shear stress (Pa)}, \ \tau = \frac{0.86M}{\pi D^3} \tag{3.9}$$

where:

M = maximum torque (N.m),

D = vane blade diameter (m).

3.4.2 Description of the apparatus

The torsional soil rheometer (Fig. 3.1) consists of the following components:

a. Main frame

b. Shearing vane and vane spindle
c. Driveline
d. Torque sensor
e. Soil box
f. Data Acquisition system

The working parts of the apparatus were based on the mechanical design of a Drill Press. Motor assembly and the power transmission system (belt/pulley) were removed from the body of the drill press. Head assembly, mounted on the column that is supported on a base, was modified to act as a part of the power transmission system for the shearing vane.

3.4.2.1 Main frame

The base (0.61x 0.91 m) of the main frame was build out of square steel bars (50x50 mm). Supports were fabricated on this rectangular frame for the column base and the speed reducers.

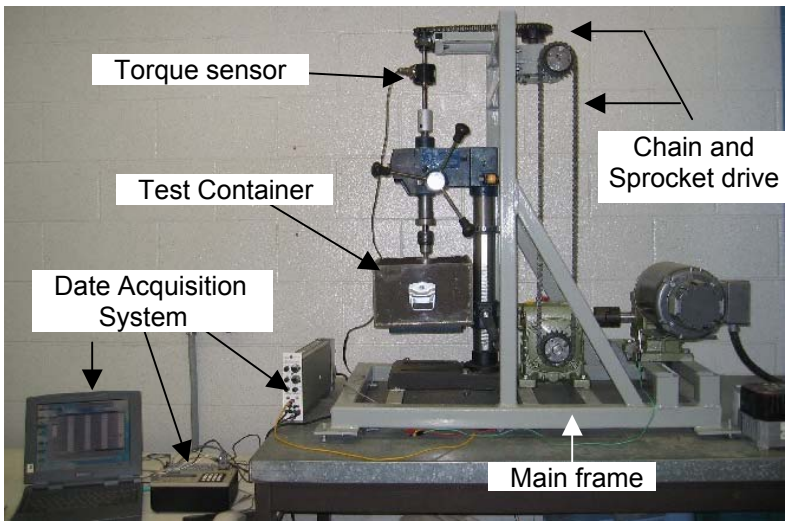

Figure 3.1 Experimental set up of the soil rheometer.

3.4.2.2 Shearing vane and spindle

The vane was made of a standard size specified by the ASTM standards (ASTM 2005). The dimensions of the vane are as follows:

Vane length = 101.6 mm.

Diameter = 50.86 mm.

Blade thickness = 2 mm.

Figure 3.2 Soil shearing device.

The shearing vane and the spindle were designed (Figures 3.3 and 3.4) using commercial computer aided design (CAD) software Solidworks2003. The diameter of the spindle was 12.5 mm and length of 114.3 mm. The vane holding end of the spindle was protruded to hold the vanes in the slots. The vane spindle was tested for the torsional strength.

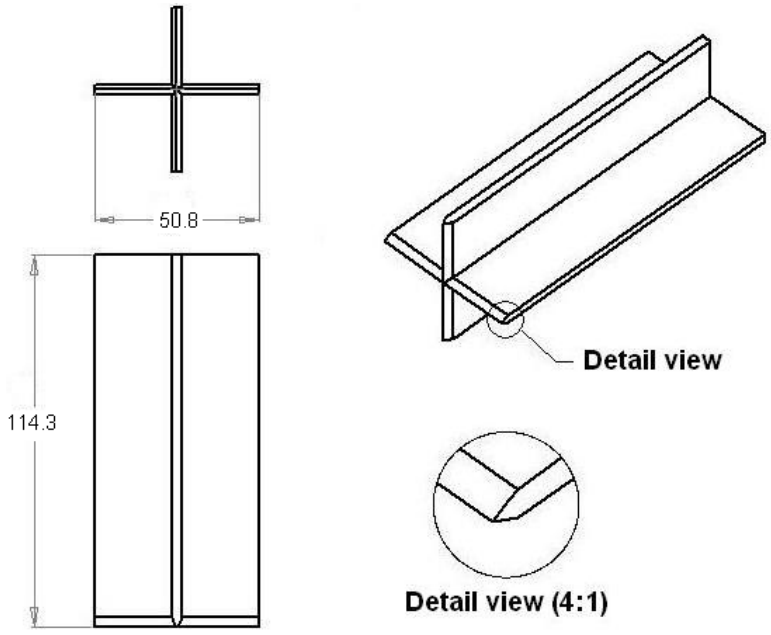

Figure 3.3 Schematics of the shear vane.

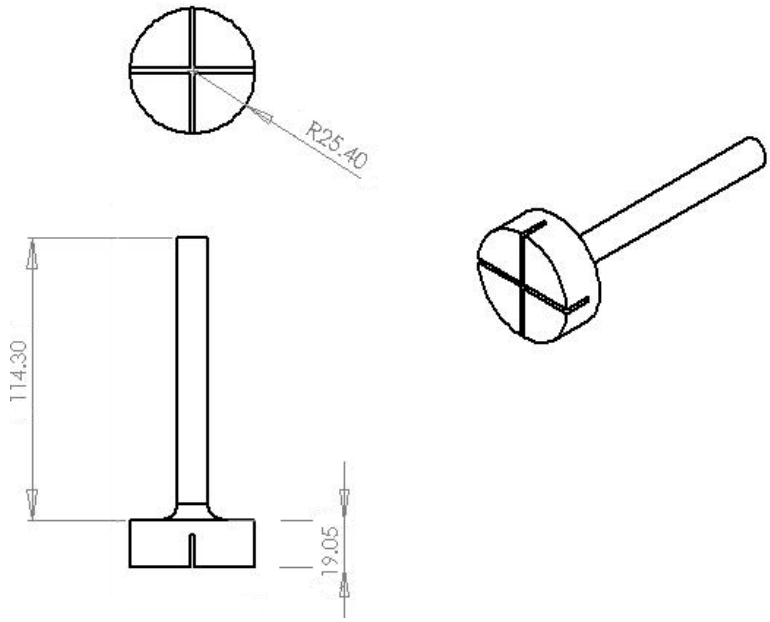

Figure 3.4 Schematics of the vane spindle.

3.4.2.3 Driveline

A three-phase motor with the help of chain and sprocket power transmission system imparted rotary motion to the shearing vane. The driveline consists of a 3-Phase motor, three speed reducers, torque sensor shaft, adapter and spindle of the vane. An inverter was used to control speed of the motor (1/2 HP, 1725 RPM at 60 Hz) for driving the vane at different shear rates. Reducer 1 (Regal Mfg. Co. Ltd., Model 70) had a speed ratio of 60:1 and, Reducers 2 and 3 had speed ratio 15:1.

The motor was connected directly to the input shaft of 70W Reducer 1. Reducer1 and Reducer2 were connected by a Composite Jaw Coupler (Series FS 052). Output shaft of the Reducer2 was connected to a 22-tooth sprocket. This was connected with the 22-tooth sprocket of the input shaft of the Reducer 3 (15:1) by a 40-size chain. A sprocket of 22 teeth was mounted on the output shaft of the reducer3. This is connected to a 12-tooth sprocket mounted on the slip ring shaft via a 40-size chain. Thus, the speed reduction from the motor to the vane was as follows:

Vane speed (RPM) = $\frac{1}{60} x \frac{1}{15} x \frac{1}{15} x \frac{22}{12}$ = (136×10^{-6}) Motor speed (RPM).

For the recommended range of vane rotation of 6^o or 12^o per minute, number of revolutions per minute of the vanes should be approximately 1/50 or 1/33. Thus, for a motor speed of 150 RPM, the revolutions of the vane obtained in the designed driveline was $= 150x0.000136 = 0.0204$ or 1/50 RPM.

Figure 3.5 Adapter for connecting the slip ring shaft and head assemble spindle.

The shaft at the other end of the slip ring was connected to the head spindle on the head assembly through a custom designed adapter (Figure 3.5). The vane spindle was connected to the integrated head spindle using a chuck. The torque sensor was mounted between speed reducer2 and the vane spindle. It was connected to the speed reducer by a chain and sprocket and was stable vertically in its position with a bearing mounted on the auxiliary frame of the apparatus. The other end of the torque sensor spindle was connected to the vane by an adaptor. Figure 3.6 shows the design of the adapter (Solidworks2003).

3.4.2.4 Torque sensor

The torque required to shear the soil by the vanes was measured using a torque sensor. Figure 3.7 shows the rotating-shaft slip-ring type torque transducer (Lebow Products, Inc. MI; Model 6118-4) with four rings. The rings were molded on a hollow steel shaft. The brush assembly was supported through shielded ball bearings by the slip ring housing. Figure 3.8 shows the sectional view of the slip ring. The overall diameter and length of the torque sensor were 60.3 and 54.0 mm respectively, with a bore diameter of 12.7 mm.

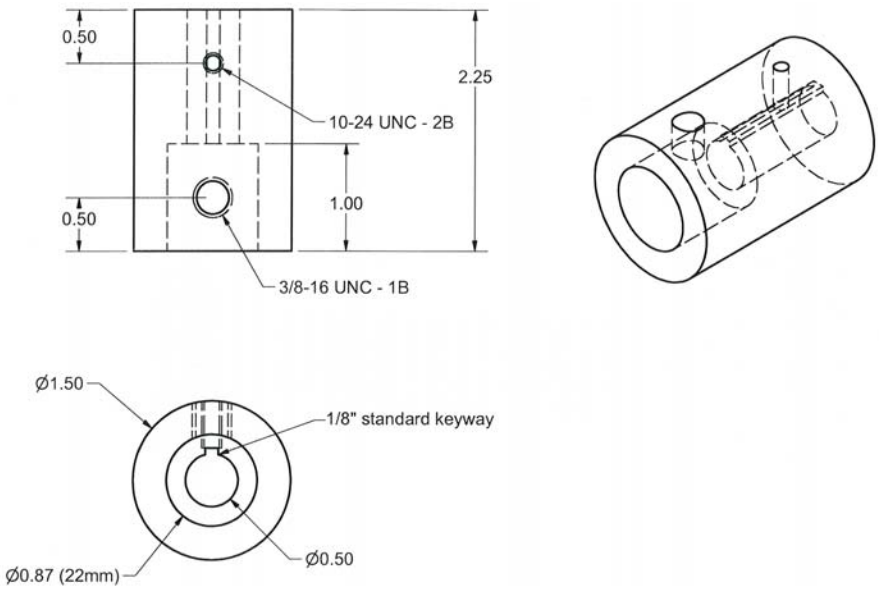

Figure 3.6 Sectional view of the adapter.

Figure 3.7 Torque sensors (Lebow Products, Inc. MI).

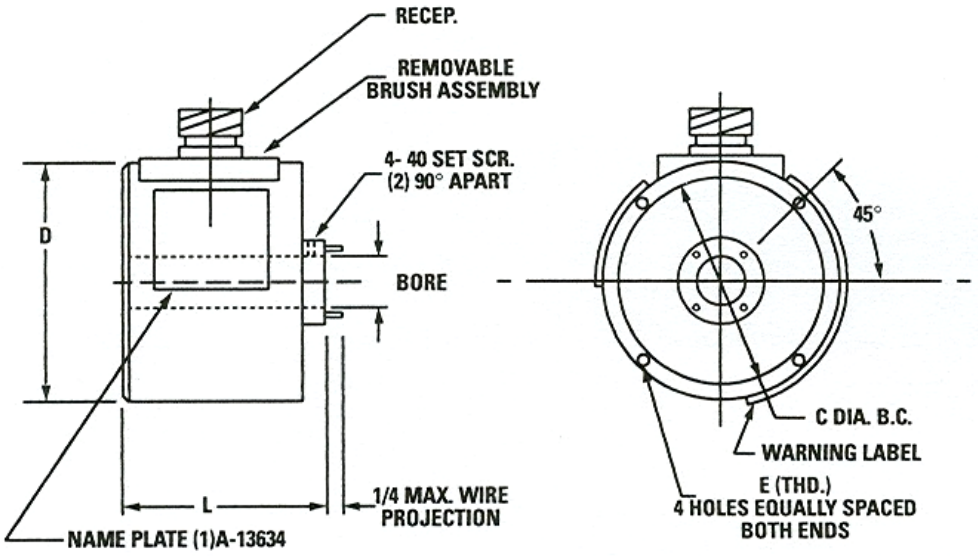

Figure 3.8 Sectional view of the slip ring (Lebow Products, Inc. MI).

3.4.2.5 Soil containers

Two custom-designed, soil containers were fabricated from acrylic sheets (Plexiglas®). One was used as sample preparation and the other for testing. The material was selected because it is durable and lightweight. The smooth walls of container were important in minimizing friction between soil and the sides of the container. The soil preparation container had a base of 306 mm x 306 mm and 172 mm height. It was used for preparing the soil with uniform moisture content. The test container (Figure 3.9) had a base of 254 mm x 254 mm and 158 mm height, which was used to prepare the soil sample with a predefined compaction level at a particular moisture content across its profile. The width and height of the test container were limited by the access space of the table and column based on its original design of the 10-inch Drill Press (Mastercraft 10-inch Drill Press, Model 55-5917-0). However, considerations were made that there was no influence of side effects of the container wall on the soil deformation due to the vane action. One side of the test container had a rectangular slot near the base to make it properly set on the table.

Figure 3.9 Custom-designed Plexiglas® container.

3.4.2.6 Data Acquisition system

Data acquisition (DAQ) system consists of a data logger, an amplifier and signal conditioner. A Campbell 21X data logger (Campbell Scientific Inc., Logan, UT) was used for data acquisition to collect the data. A computer program written in Edlog programming environment for Campbell 21X data logger collected data that were monitored on the computer screen.

3.5 Testing of the soil rheometer

Input parameters required for the CFD simulation: bulk density, viscosity and yield stress. Independent variables that influenced the output were moisture content and cone index (soil compaction level).

3.5.1 Calibration

The sensitivity of the torque sensor was calibrated prior to test by applying torque using a custom designed calibration device. A torque arm was made of a flat iron and attached to the chuck of the head spindle as shown in Figure 3.10. A rope was attached to the other end of the torque-arm and known mass was put on the hanger connected to the rope over a frictionless pulley. Thus, a known amount of torque was applied to the head

spindle and the output was observed using a multi-meter in terms of voltage. A calibration curve is given in Fig. 3.11 relating torque and voltage.

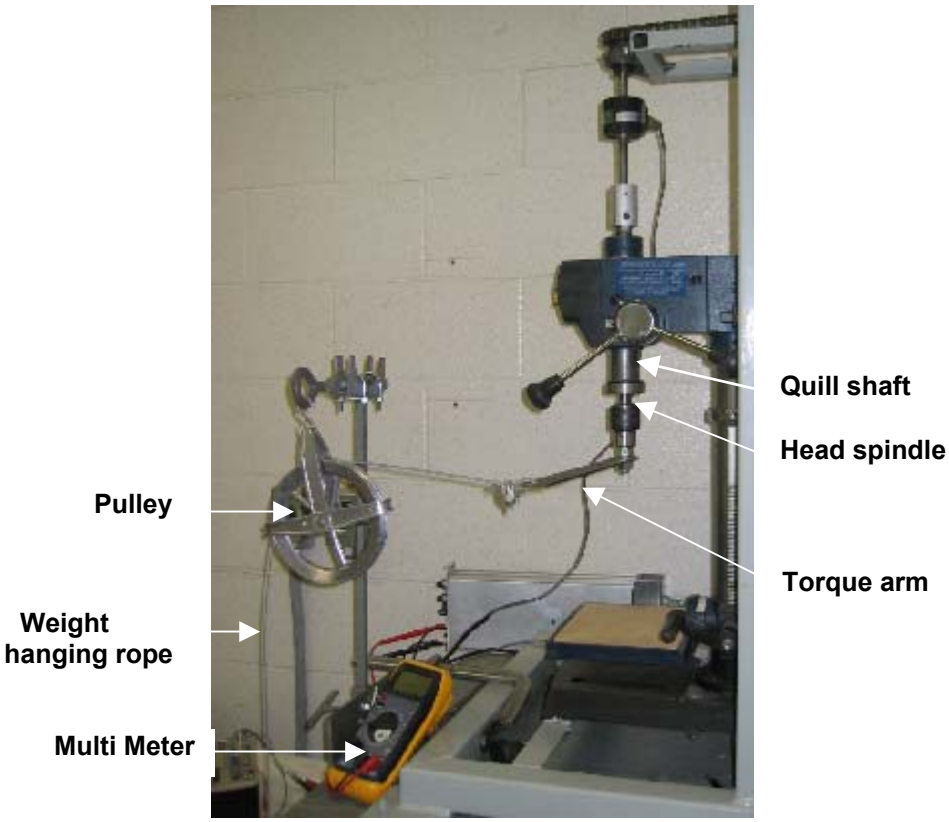

Figure 3.10 Calibration of the torque sensor.

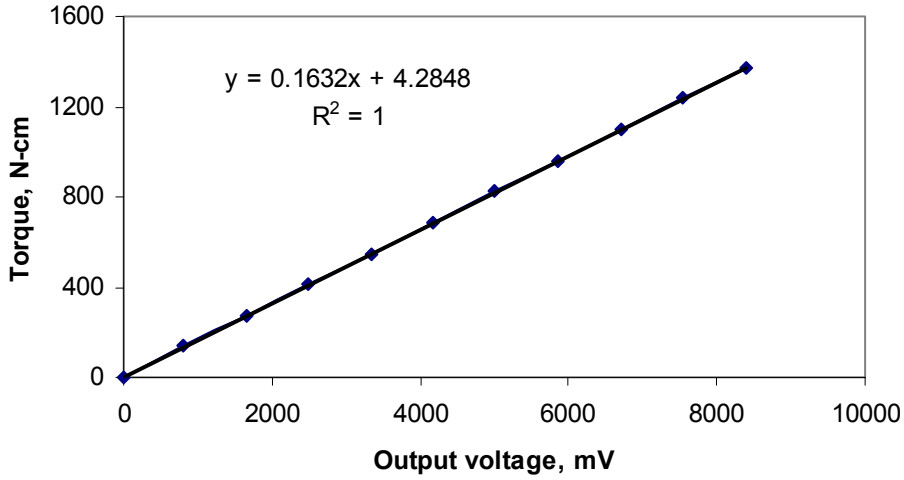

Figure 3.11 Calibration curve for the torque sensor.

The coefficients of the straight line relationship of the calibration curve were used in the data logger programming.

3.5.2 Soil preparation

Though the soil parameters vary with soil type and soil conditions, tests are conducted for a particular type of clay-loam soil with some variations in the soil conditions. The soil used was a clay loam containing 29% clay, 24% silt and 47% sand. The following soil parameters were used for finding the visco-plastic properties:

- Four levels of moisture content: 10-11%, 13-14%, 16-17% and 19-20%.
- Five levels of soil compaction: 100-110 kPa, 150-160 kPa, 200-210 kPa, 300-320 kPa and 400-450 kPa.

3.5.2.1 Soil preparation in the sample container

Soil was prepared for a particular moisture content by adding a calculated amount of water to the dry soil. The soil was mixed with water to obtain the desired moisture contents of 10%, 14%, 17% and 20%. After mixing, the soil was left for 24 h for the moisture to reach equilibrium. The moisture content was then checked by taking samples from three different location of the sample container and by standard oven dry method (ASTM 2216-90).

3.5.2.2 Soil preparation in test container

Soil prepared in the sample container was shifted to the test container in three layers. Each layer was compacted by pounding a wooden block to the predetermined compaction level. Predetermined compaction levels were controlled by the height of fall of the wooden block and the number of blows per layer. Soil compaction was measured in terms of cone index using standard Cone Penetrometer (ASAE S313.2, 1984).

3.5.3 Procedure

After the soil was prepared in the test container, it was placed on the table of the soil rheometer and the vane was inserted in to the soil by raising the table using the crank

and lowering the Quill tube using the knob. The vane is rotated in the soil at a predetermined speeds of 1/4, 1/6, 1/9, 1/16, 1/25 and 1/30 RPM. The speed was controlled by an inverter which was run at a specific frequency (Hz). Soil response to the shearing vane was observed for predetermined soil conditions. The program written for the data logger recorded the torque required to shear the soil with respect to time.

3.6 Results and discussion

Soil visco-plastic properties observed in this study have been depicted in the following sections.

Figure 3.12 shows a typical relationship between torque and shearing time. The steadily increasing displacement caused an increasing shear force applied to the soil at the peripheral region of the vane. The soil sustained the applied torque until the induced stress reached a maximum value. The torque at which the soil failed was termed as peak torque. Shear stress related to this torque was the shear strength of soil. With increasing displacement, the shear stress decreased until it attained a residual stress level. Residual stress level is a critical shear stress value when shearing continues at constant volume (Craig, 2003).

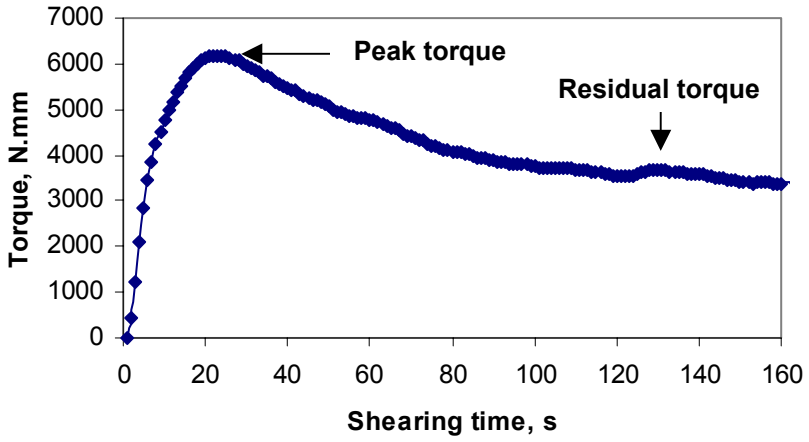

Figure 3.12 Shearing curve for 13% moisture content and 200 kPa compaction at shearing rate of ¼ RPM.

Shearing curve was obtained for peak torque at different shear rates (Fig. 3.13). The peak torque or the shear strength was increased with shearing rate. Soil failed earlier in case of high shear rates. The detailed shearing curve showing the peak and residual soil strength at lower rates for this soil condition has been included in Appendix A.

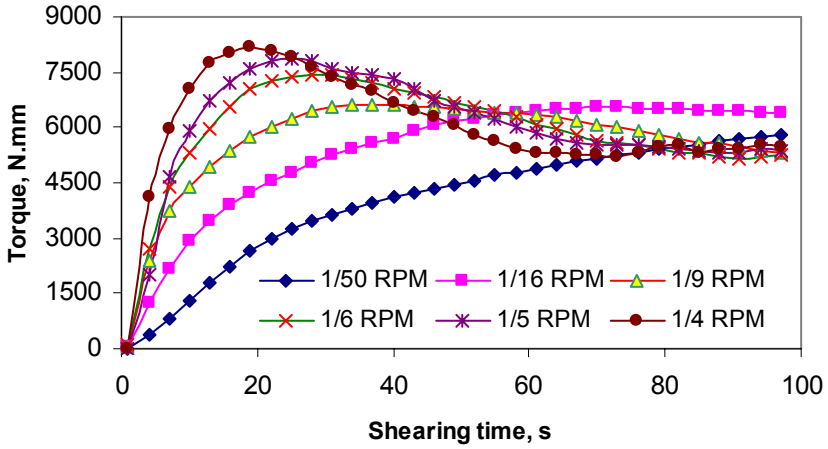

Figure 3.13 Shearing curve at different shearing rates for 300 kPa compaction at 17% moisture content.

Shear stress variation with respect to shear rate at different moisture content is shown in Fig. 3.14. This relationship enabled to obtain yield stress and soil viscosity. All the curves have been fitted to the Bingham model. The interception of the linear model with the Y-axis gave the yield stress values; while the slope of the fitted lines gave the viscosity values. Figure 3.15 shows that for 300 kPa compaction level and 13% moisture content, yield stress is 12.527 kPa and viscosity is 212.62 kPa.s.

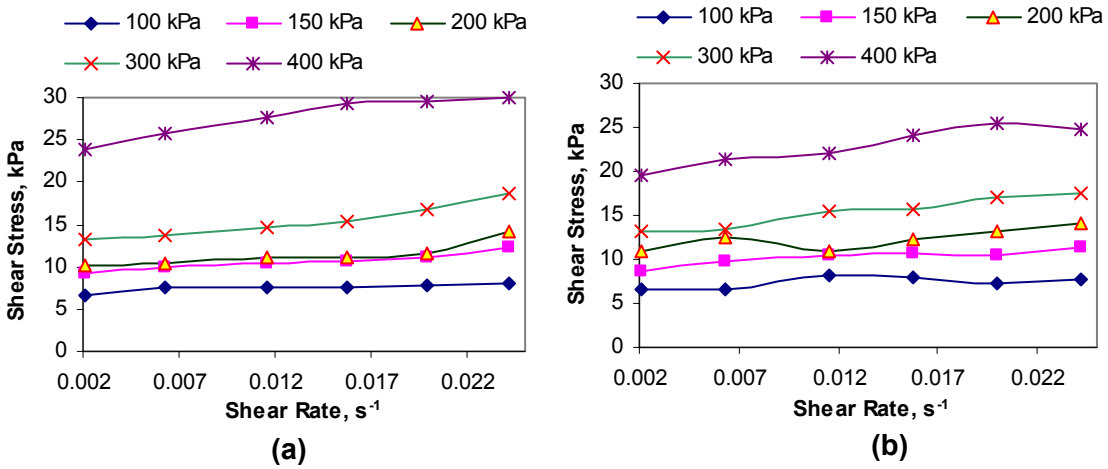

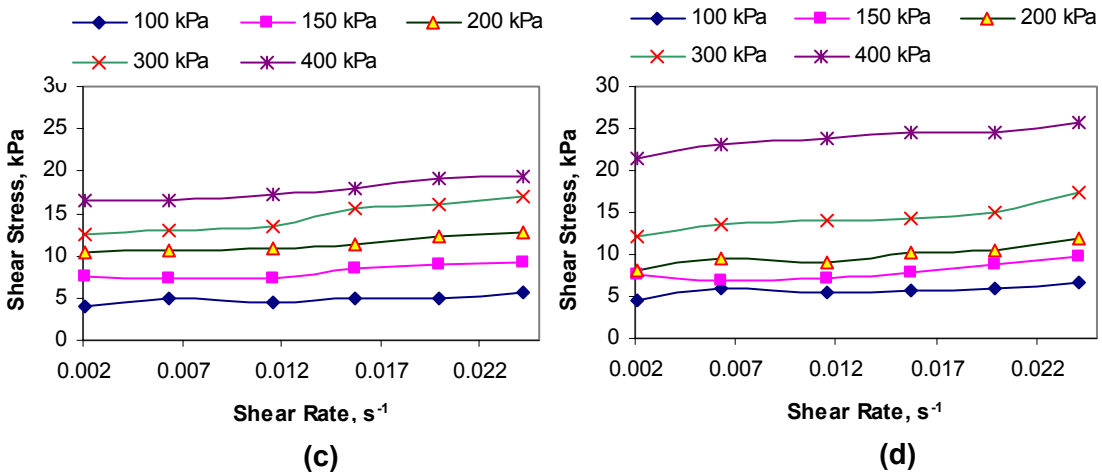

Figure 3.14 Relationship between shear stress and shear rate at different compaction levels; (a) 10%, (b) 13%, (c) 17% and (d) 20% moisture content

Soil testing for visco-plastic parameters using the developed soil rheometer resulted in soil viscosity and soil yield stress values at different moisture content and soil compaction levels (Table 3.1).

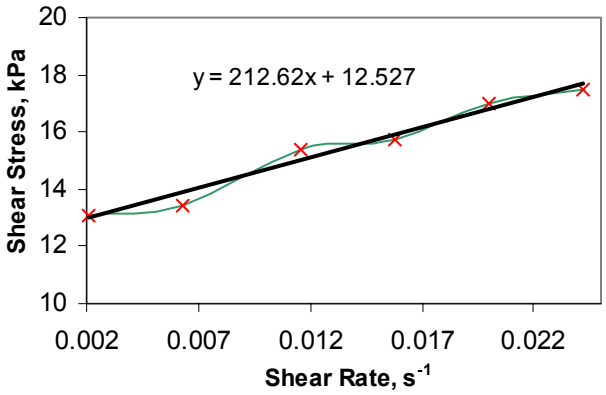

Figure 3.15 Relationship between shear stress and shear rate for 13% moisture content and 300 kPa compaction.

3.6.1 Soil viscosity

Steady-state, constant rate measurements conducted at different moisture contents and compaction levels provided relationships of shearing stress vs. shear rates. In this present study, the values of viscosity of the clay loam soil were found to spread in the range of $53x10^3$ to $28x10^4$ Pa.s. This result is in agreement with the lower range of soil

viscosity data (10^5 to 10^{16} Pa.s) obtained by Vyalov (1986). However, this result is not comparable to the viscosity values (1.5 x 10^6 to 1.8 x 10^9 Pa.s) of clay soil with high moisture content as reported by Ermolaeva (1968) and Maslov (1968). Based on these relationships, viscosity values have been obtained and plotted with respect to the moisture content (Fig. 3.16) and soil compaction (Fig. 3.17).

Table 3.1 Soil viscoplastic parameters obtained using the Soil Rheometer.

	Moisture content (d.b)							
Compaction level, kPa	**10%**		**13%**		**17%**		**20%**	
	Viscosity*	**Yield stress****	**Viscosity**	**Yield stress**	**Viscosity**	**Yield stress**	**Viscosity**	**Yield stress**
100	55.218	6.74	53.23	6.42	53.67	4.14	65.46	4.8201
150	119.08	8.99	99.34	8.93	86.62	6.57	105.48	6.59
200	145.80	10.66	124.06	10.30	104.27	9.50	151.32	7.86
300	235.11	12.20	212.62	12.26	195.51	11.72	185.99	11.83
400	283.10	23.90	257.78	19.40	169.11	15.80	175.98	21.50

* Viscosity in kPa.s ** yield stress in kPa.

3.6.1.1 Effect of moisture content

The generalised feature was that increasing moisture content was accompanied by a decreasing viscosity. At a microscopic scale, an increase in moisture content would increase the spacing between soil particles and reduces the solid-solid interactions. Thus, the soil viscosity decreased. This trend was observed for all the soil conditions up to the moisture content of 17%. After 17% moisture content, there was slight increase in the viscosity. This may be due to the increase in soil cohesion at higher moisture content. Data were analysed by SAS statistical program. Factorial ANOVA was obtained for Duncan's multiple range analysis. Effect of moisture content on viscosity values was significant at 95% confidence level with an R-square value of 0.91.

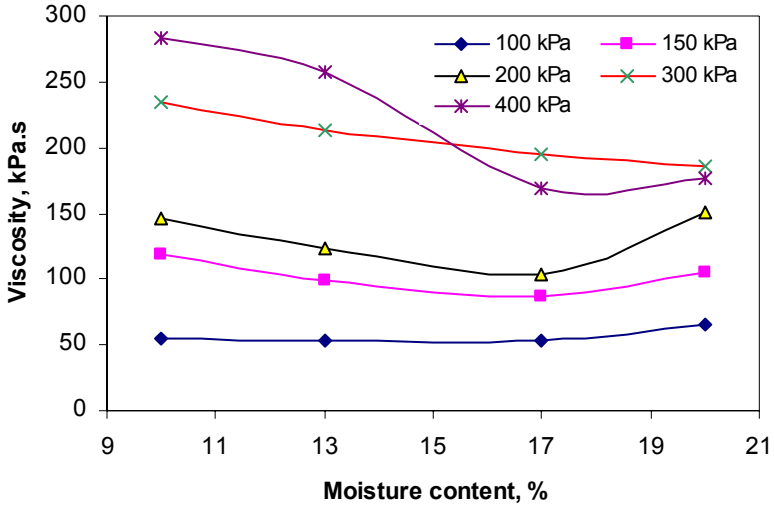

Figure 3.16 Relationship between moisture content and soil viscosity as affected by compaction levels.

3.6.1.2 Effect of soil compaction

Soil viscosity was highly affected by the compaction levels for all the moisture contents. Increase in soil compaction was accompanied by a sharp increase in soil viscosity. With an increase in soil compaction, the volume of pore spaces would reduce and cause more solid-solid contact, thereby increasing the viscosity. There was no significant effect of increasing compaction from 150 to 200 kPa and 300 to 400 kPa.

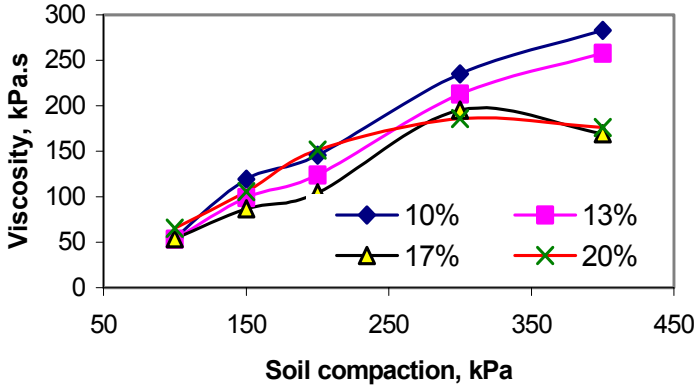

Figure 3.17 Relationship between soil compaction and viscosity as affected by moisture content.

3.6.2 Soil yield stress

3.6.2.1 Effect of moisture content

Yield stress has been found to decrease with increasing moisture content (Fig. 3.18). This trend agrees with the studies of soil rheology using a parallel plate rheometer by Ghezzehei and Or (2001). These phenomena can be attributed to the liquid water between clay sheets and solid- solid friction. With increasing moisture content, there would be an increased ability of water molecules to flow freely, and thus reducing solid-solid friction. However, it was observed that after 17% moisture content yield stress was increased slightly for 100 and 150 kPa compaction levels and appreciably for 400 kPa compaction. It may be due to increased cohesion at higher water levels.

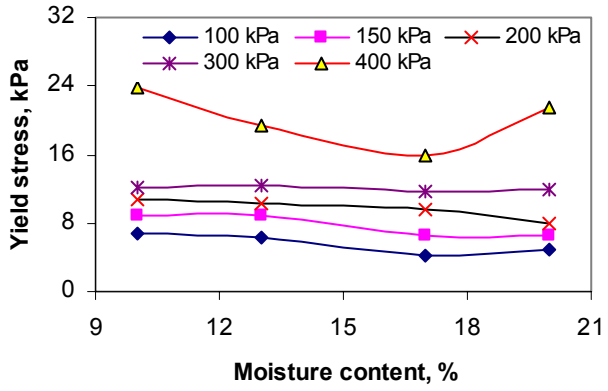

Figure 3.18 Relationship between moisture content and yield stress as affected by compaction levels.

3.6.2.2 Effect of soil compaction

Yield stress increased with soil compaction for all the levels of moisture content (Fig. 3.19). There was a steep increase in yield stress when the compaction level was increased from 300 kPa to 400 kPa. Statistically the compaction level was effective on yield stress values at the 95% level of significance with an R-square value of 0.95. There was no effect for an increase of compaction from 150 to 200 kPa. The mean values were different for the levels of 100, 150-200, 300 and 400 kPa levels.

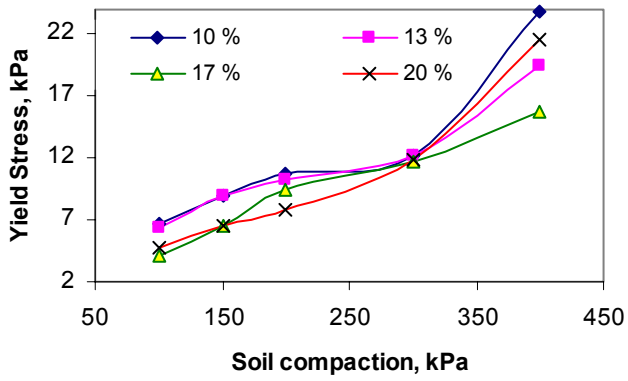

Figure 3.19 Relationship between soil compaction and yield stress as affected by moisture content.

3.7 Conclusions

Following conclusions can be drawn from the experiments conducted using the Soil Rheometer:

1. A soil rheometer was successfully developed to obtain soil visco-plastic parameters. The apparatus may also be used to explore the soil dynamic properties for geotechnical engineering problems, like land slides and excavation etc.
2. The values of viscosity of the clay loam soil were found to spread in the range of $53x10^3$ to $280x10^3$ Pa.s. Increasing moisture content was accompanied by a decreasing viscosity.
3. Soil viscosity was highly affected by the compaction levels for the moisture contents tested. Increase in soil compaction was accompanied by a sharp increase in soil viscosity.
4. The values of yield stress of the clay loam soil were found to spread in the range of 4 to 23 kPa. Yield stress has been found to decrease with increasing moisture content. Yield stress also increased with soil compaction for the levels of moisture content tested. There was a steep increase in yield stress when the compaction level increased from 300 kPa to 400 kPa. The moisture content of 17% (d.b) was found to have a reduced viscosity and yield stress. There was no effect for an increase of compaction from 150 to 200 kPa.

3.8 References

ASAE S313.2, 1984. ASAE Standards, 31st edition. Soil cone penetrometer. St. Joseph, MI.: ASAE.

ASTM D 2216-90 (revision of 2216-63, 2216-80). 1990. Standard method for laboratory determination of water (moisture) content of soil and rock. ASTM International.

ASTM D 2573-72 (revised 2004). Standard test method for Field vane shear test in cohesive soil. ASTM International.

Beris, A. N., J. A. Tsamopoulos, R. C. Armstrong and R. A. Brown. 1985. Creeping motion of a sphere through a Bingham plastic. J Fluid Mech 158: 219-244.

Bird, R. B., G. C. Dai and B.J. Yarusso. 1983. The rheology and flow of visco-plastic materials. Rev Chem Eng 1: 1-70.

Chandler, R. J. 1988. Vane Shear Strength Testing in Soils: Field and Laboratory Studies, ASTYM STP 1014, A. F. Richards, Ed., American Society for Testing and Materials, Philadelphia, 1988, pp.13-44.

Chhabra, R. P. and J. F. Richardson. 1999. Non-Newtonian Flow in the Process Industries, Fundamentals and Engineering Applications. Oxford, UK: Butterworth Heinemann Publishing Ltd.

Collocott, T. C. (Ed.). 1971. Chambers Dictionary of Science and Technology, W. R. Chambers, Edinburgh.

Craig, R. F. 2003. Soil Mechanics, 6th Edition. London and NY: Spon Press.

Davison, J., R. K. Calay, T. Sands and M. England. 2002. CFD simulation of soil flow over augers. Proceedings of 2002 ASME PVP Conference, Vancouver, Canada.

Day, P. R. and G. G. Holmgren. 1952. Microscopic change in soil structure during compression. Soil Sci Soc Am Proc 16: 73-77.

Ghavami, M., J. Keller and I. S. Dunn. 1974. Predicting soil density following irrigation. Trans ASAE 17: 166-171.

Ghezzehei, T. A. and Or, Dani. 2001. Rheological properties of wet soils and clays under steady and oscillatory stresses. Soil Sci Soc Am J 65: 624-637.

Gill, W R and G E Vanden Berg. 1967. Soil Dynamics in Tillage and Traction. Agriculture Handbook No. 316. United States Department of Agriculture.

Gupta, C. P. and A. C. Pandya. 1966. Rheological behavior of soil under static loading. Trans ASAE 9(5): 718-728.

Hiller, D. 1980. Fundamentals of Soil Physics. New York: Academic Press.

Illingworth, V. (Ed.). 1991. Penguin Dictionary of Physics. London, UK: Penguin Books.

Karube, D., S. Sibuya, T. Baba and Y. Kotera. 1988. Vane Shear Strength Testing in Soils: Field and Laboratory Studies, ASTYM STP 1014, A. F. Richards, Ed., American Society for Testing and Materials, Philadelphia, 1988, pp.131-149.

Lebow Products, Inc. 1728 Maplelawn Dr. Troy, MI 48084

Lipscomb, G. G. and M. M. Denn. 1984. Flow of Bingham fluids in complex geometries. J Non-Newtonian Fluid Mech 14: 337-346.

Maslov, N. N. 1968. Fundamentals of Soil Mechanics and Engineering Geology. Vysshaya Shkola, Moscow (in Russian).

McMurdie, J. L. and P. R. Day. 1958. Compression of soil by isotropic stress. Soil Sci Soc Am Proc 22: 18-22.

Oida, A. 1992. The rheological model for agricultural soil. J Japanese Soc Agric Machinery (JSAM) 54 (1): 1-7.

Ram, R. B. and C. P. Gupta. 1972. Relationship between rheological coefficients and soil parameters in compression test. Trans ASAE 15(6): 1054-1058.

Robinson, M. (Ed.). 1996. Chambers 21st Century Dictionary, W. R. Chambers, Edinburgh.

SAS Institute. 2000. The SAS system for windows. Version 8. SAS Inst., Cary, NC.

Skelland, A. H. P. 1967. Non-Newtonian Flow and Heat Transfer. New York: John Wiley and Sons Inc.

Stokoe, K.H., M.B Darendeli, R.D. Andrus and L.T. Brown, "Dynamic Soil Properties: Laboratory, Field and Correlation Studies," Theme Lecture, Second International Conference Earthquake Geotechnical Engineering, Vol. 3, Lisbon, Portugal, June, 1999, pp. 811-845.

Vyalov, S. S. 1986. Rheological Fundamentals of Soil Mechanics. Amsterdam, The Netherlands: Elsevier Science Publishing Company.

Walters, K. 1975. Rheometry. London, UK: Chapman and Hall.

Zisis, T. and E. Mitsoulis. 2002. Visco-plastic flow around a cylinder kept between parallel plates. J Non-Newtonian Fluid Mech 105: 1-20.

Chapter 4

Numerical Modeling of Soil Flow Behavior with Tool Interaction

4.1 Significance

This chapter relates to objective 3 of the thesis, and contributes to one of the main goals of the research on flow behavior of soil. Chapter 2 demonstrated the need for numerical modeling of soil-tool interaction and the potential of a fluid flow approach. The research in the previous chapter enabled the determination of the soil dynamic parameters required for numerical modeling using computational fluid dynamics (CFD). The main objectives of the research presented in this chapter are to explore the possibilities of implementation of a CFD model for tillage by observing the soil flow pattern as a non-Newtonian material and to find the influence of a tool as a bluff body in the flow domain. A paper has been published on the results of three-dimensional CFD simulations of soil deformation around a tool in the Transaction of the ASAE (*Karmakar, S. and R. L. Kushwaha. 2005. Simulation of soil deformation around a tillage tool using computational fluid dynamics. Transactions of the ASAE 48(3):923-932*). The paper in its published format has been included in the thesis as Appendix H.

4.2 Introduction

The basic objective of tillage is to break down the soil by disturbing its original structure for preparing a desired seed bed. During tillage, soil particles move ahead and around the tool as they fail in shear. As the tool engages soil, the high stiffness of

undisturbed soil sustains the exerted tool thrust up to its elastic limit, and the soil then fails in shear. Accurate measurement of the soil failure geometry caused by a tillage tool is a prerequisite for understanding the soil-tool mechanics (Durairaj and Balasubramanian, 1997). In a study on soil microtopography, soil deformation due to sweep interaction has been described as 'soil shift', 'ridge height' and 'change of surface height' (Hanna et al., 1993b). Soil shift is a measure of horizontal soil movement perpendicular to the travel direction, ridge height is the vertical peak-to-furrow distance after the tool has passed and the change in surface height is a measure of loosening of the surface soil.

Dynamic analysis of soil-tool interaction is an essential area of research to predict the propagation of the soil failure front or advancing of the soil failure zone with respect to the tool motion. Soil failure front is an indicator of soil disturbance and is directly associated with slip surfaces generated by yielding and plastic deformation. The advancement of the soil failure front, influenced by the tool action, depends on the operating speed, tool shape and size, tool orientation, and the soil conditions. Extensive research has been conducted for modeling the energy requirement of a tillage tool using analytical and numerical methods. However, little information is available on the physical and mechanical soil deformation pattern that results from the soil-tool interaction. High speed operation, practiced in conservation or reduced tillage, necessitates optimization of soil disturbance coupled with energy efficiency.

4.3 Literature Review

4.3.1 Soil disturbances due to tillage tool action

Soil movement due to tillage has been studied for narrow and wide tools using different approaches. Söhne (1960) studied soil movement perpendicular to the travel direction with a wide tool in high-speed plowing and observed that the magnitude of the lateral soil displacement increased with the lateral directional angle at the end of the moldboard. Similar study on the effect of speed on soil failure patterns by Olson and

Weber (1966) revealed that the size of the disturbed zone increased with increasing speed.

McKyes and Ali (1977) proposed a three dimensional model (soil wedge model with crescent failure) which was able to predict both the draft forces and the volume of soil disturbed in front of a narrow blade. The forward distance of the failure crescent from the blade on the surface was related to the rake angle, the rupture angle, and the depth of operation. The area disturbed by a tool across its direction of travel was approximated as a function of tool width, operating depth and the lateral distance of the soil failure crescent from tool and soil surface interaction.

Desai and Phan (1980) generalized the case of three dimensional soil-structure interactions, where the structure is moving in the soil. Since the structure and soil move relative to each other, there is shear transfer through relative slip. The lateral soil movement was an idealization as the flow of soil particles around the tool, while the vertical soil movement was idealized as soil flow parallel to the soil shear failure planes.

Grisso and Perumpral (1981) studied the basis for the analytical models, the assumptions involved and the capabilities of the models to predict soil-tool interaction. It was concluded that a majority of the assumptions involved with the models were the same as those associated with the earth pressure theory which neglected the inertial forces and were suitable only for predicting the behavior of a narrow tine moving at extremely slow speeds.

McKyes and Desir (1984) measured the disturbed soil mass of narrow tools in different soil conditions at a speed of 1.4 m s^{-1}. Failure area was calculated by means of passive earth pressure theory and the shape of the soil failure wedges was determined by soil weight and strength using the same expression proposed by McKyes and Ali (1977). The soil wedge model overestimated the cross sectional area of thoroughly disturbed

soil in tillage operations primarily because the real tilled areas were bounded by curved boundaries and only completely remolded soil was included in the field experiments.

Hanna et al. (1993a) compared the soil flow path of a sweep with the Goryachkin theory (1968). Soil shift, or lateral movement, and ridge height were affected by both tool operating speed and sweep rake angle. Faster speeds and steeper rake angles created larger ridges. Changes in surface height, an indicator of soil loosening, was significantly affected by tool depth and speed, but not by sweep rake angle. The Goryachkin theories did not adequately predict observed soil flow on a sweep (Hanna et al., 1993b). In agreement with the Goryachkin theories, observed soil flow changed with rake angle, but did not change with the speed or depth.

Durairaj and Balasubramanian (1997) developed a technique to measure the three-dimensional soil failure front owing to a tool under dynamic conditions. The procedure involved scanning and sensing the relative movement of failed soil with respect to the tool at millisecond timings by the sensors embedded in the soil-tool front.

Rosa (1997) investigated soil disturbance by measuring the soil cross sectional area affected by the tool pass. Disturbed area and geometry of the seeding furrow were measured by a roughness meter. It was concluded that the soil disturbance increased as operating speed increased. However, no method had been adopted, in a standard form, to quantify the soil disturbance and no statistical data were reported on disturbed soil area because of the difficulty in measurement by the roughness meter.

Little information is available on the soil mechanical behavior during high speed tillage. There exists a critical speed range at which the relationship between draft and speed changes i.e. the draft increases less with speed above the critical speed (Kushwaha and Linke, 1996). A critical speed range of 3 and 5 m s^{-1} was observed for the conditions investigated. It was also expected that the amount of soil deformation would decrease near and above the critical speed. Sarifat and Kushwaha (1998) measured soil movement by narrow tillage tools (45^{o} triangle, 90^{o} triangle, flat and elliptical) at high

speeds of operation (10 to 25 km h^{-1}) in the soil bin and reported that increasing the tool operational speed resulted in an increase in soil movement for all the tools. A series of experiments was conducted (Zhang and Kushwaha, 1999) in a soil bin with a concern about the critical speed at which the continuously increasing soil advancement failure zone started decreasing. However, a speed effect of only up to 1.8 ms^{-1} was reported and the critical speed could not be reached due to technical limitations. Sarifat and Kushwaha (2000) developed a model using MATLAB for horizontal soil movement in front of the tool. The influence zone, as a function of speed of operation, was considered to be of circular shape attached to the tillage tool in the travel direction.

Assumptions on the orientation of the soil shear failure plane are needed before the soil failure front can be quantified using analytical methods. Some researchers have considered configuration of the rupture plane as slightly curved (Payne, 1956), and log spiral (Reece, 1965), while others have assumed it as a straight line (McKyes and Ali, 1977; and Perumpral et al., 1983). Optimization of high speed tillage operation is a current concern. The speed at which the continuously increasing soil advancement failure zone starts decreasing can be termed as the critical speed (Zhang and Kushwaha, 1999). The tool velocity where the distance of the failure front from the tool face ceases to increase could be set as the critical velocity for high speed tillage to obtain minimum soil disturbance for a particular soil condition. The study of soil deformation due to tool interaction as a visco-plastic material from a fluid flow perspective is anticipated to represent the dynamic behaviors of tillage.

4.3.2 Flow of visco-plastic materials

4.3.2.1 Conduit flow

Abdali and Mitsoilis (1992) reported the excess pressure losses at the entrance of a non circular conduit flow for Bingham fluids and presented as a function of the dimensionless yield stress or Bingham number. At a very low shear rate the material will be mostly unyielded; as the throughput increases and the shear rates get higher, the material behaves more like a fluid having a reduced solid region.

Taylor and Wilson (1997) studied the flow pattern of a steady, incompressible flow of Bingham visco-plastic material along a non circular duct. The flow has been observed to consist of a plug in the centre of the duct with dead regions of 'no flow' at the corners, due to the rectangular cross section. Finite difference numerical solutions were obtained for square and rectangular duct with different aspect ratio. The 'plug region' of highly viscous fluid in the centre of the cross section got larger as the dimensionless yield stress increased.

Wang (1998) analysed noncircular duct flow of nonlinear visco-plastic fluid through finite element method and the location of the yield surface was determined by the regularised technique. The flows were seen to consist of mobile plug zones in the centre of the duct with stagnant plugs near the apex of corners in a square duct at large Bingham number. He also noted that the contours of the stagnant plugs are concave toward the duct centre. The velocity contours for Bingham number, B_n=0.4 are shown in Fig. 4.1.

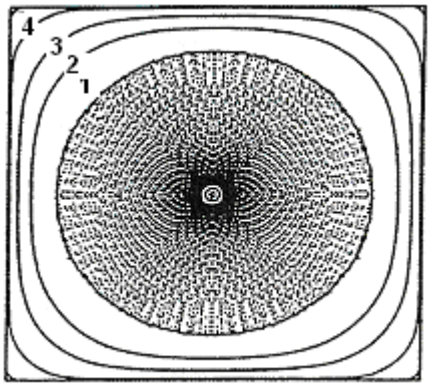

Figure 4.1 Velocity contours in a square duct (Wang, 1998).

Davidson et al. (2000) studied the "slump Test" of concrete and concentrated suspensions and conducted numerical simulation by CFD, considering the material as a Bingham fluid. They have developed a homogenous two fluid (liquid-air) model representing flow of an equivalent single phase with variable properties. Predictions were in reasonable agreement with published experimental data for high yield stress materials.

4.3.2.2 Open channel flow

The flow of debris in channels, the process which transports granular solids mixed with water and air along gentle slopes, and glacier flows are other geophysical examples of flow of Bingham substances (Taylor and Wilson, 1997). Debris flows are seen to exhibit behavior similar to that of Bingham materials (Johnson, 1970); observations of debris moving in a wide, open channel show that the upper part of the flow is rigid (plug flow) and the bottom part is sheared (plastic flow).

Zisis and Mitsoulis (2002) studied creeping pressure driven visco-plastic flow around a cylinder kept between parallel plates for a wide range of Bingham numbers and gap/cylinder diameter ratios considering wall effects. They confirmed that a dramatic increase of drag coefficient occurred as the dimensionless yield stress or the Bingham number increased. Schematic of the flow pattern (Fig. 4.2) shows the unyielded (shaded) regions forming polar caps around the stagnation points and islands near the equator.

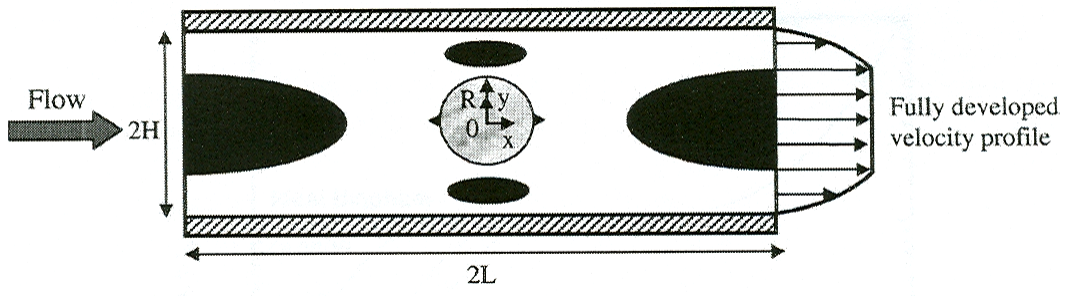

Figure 4.2 Visco-plastic flow around a cylinder (Zisis and Mitsoulis, 2002).

4.3.3 Computational fluid dynamics (CFD): The numerical method

Computational fluid dynamics (CFD) is based on the finite volume method. It uses the integral form of the conservation law as its starting point. The solution domain is sub-divided into a finite number of control volumes and the conservation equations are applied to each control volume. At the centroid of each control volume there is a computational node at which the variable values are to be calculated. Discrete equations

must be used in order to numerically simulate the laminar and turbulent duct flow. The key step of the finite volume method is the integration of the governing equation over a control volume to yield discretised equation at its nodal point. The discretisation process gives a system of linear algebraic equations that are solved numerically (on a computer) for the flow field variables at each node. Advantages of CFD can be categorized as:

- It provides a details understanding of flow distributions
- It makes it possible to evaluate geometric changes with much less time and cost than would be involved in the laboratory testing.
- It can answer many 'what if' questions in short time
- It is able to reduce scale up problems because the models are based on fundamental physics and are scale independent
- It is particularly useful to simulate the situations where it is not possible to take detailed measurements.

In general three different major tasks should be done to perform CFD simulation (Shaw, 1992).

a) Pre-processing: flowing steps are performed in this section.
    - Statements of the physics of the problem.
    - Creating geometry of the problem
    - Meshing: creating shape of the problem domain by subdividing the domain into numerous elements or volumes
    - Defining boundary of the geometry
    - Specifying the boundary conditions
    - Defining initial conditions
    - Setting fluid properties
    - Setting the numerical control parameters

b) Processing

- Meshing is completed
- Model input values are specified
- Mathematics equations of the fluid flow is solved by a computer software by
    - Discretisation of the equations applied to the individual cells/meshes
    - Solving of equations by iteration until convergence is achieved.

c) Post processing

- Evaluates the data generated by CFD analysis in the preceding steps
- Results expressed numerically and graphically
- Numerical expressions are by
    - Vector plots of velocity field
    - Contour plots of scalar variable (eg. Pressure)
- Graphical expressions are done by
    - 2-D visualization
    - 3-D visualization.

4.4 Soil duct flow around a simple tool

Preliminary investigations were conducted to understand the features of soil visco-plastic flow in a conduit. The dimensions of the conduit were benchmarked on the basis of tool influence zone during tillage. A tool has been placed in the flow domain to observe the tool influence in the visco-plastic soil flow. Soil flow in a rectangular channel in its Bingham fluid behavior has been analyzed. To simulate the soil flow around the tool, the tool was considered to be stationary and soil (visco-plastic fluid) was moving around the tool. Three dimensional CFD simulations were carried out in isothermal conditions using the commercial software CFX4.4 from AEA Technologies (2001).

4.4.1 Benchmark

A vertical blade with 20 mm thickness, 50 mm width and 100 mm height was considered for simulation. The width of the channel was varied to observe the effect of the wall influence. It was intended to have negligible effect of the confining channel on the flow pattern with the same channel height.

Initially, the influence zone considered by Chi and Kushwaha (1991) for their Finite Element Method was taken as a benchmark as the problem domain. That is for a vertical blade, the region of influence had a length of six times the operating depth behind the tool and five times ahead of the tool and a width of six times the width of the tool. The schematics of the flow domain with the tool is shown in Fig. 4.3.

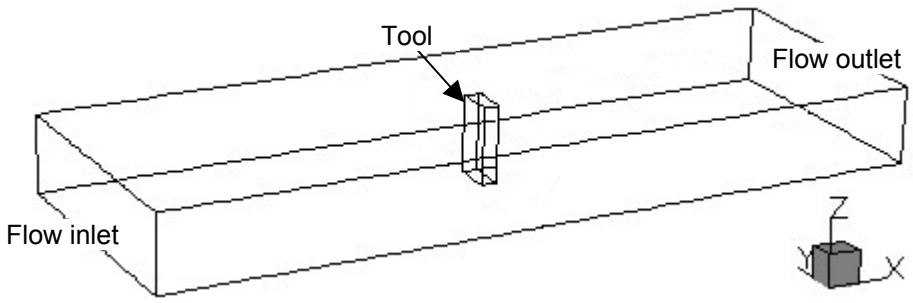

Figure 4.3 Schematics of the conduit flow field.

4.4.2 Mathematical modeling

Navier-Stokes equation is the basis of numerical solutions of any fluid flow (Patankar, 1980). Assuming the conservation of mass through the control volume the continuity equation was

$$\frac{\partial \rho}{\partial t} + \frac{\partial}{\partial x_i}(\rho U_i) = 0 \tag{4.3}$$

where:

ρ = density of the fluid (Kg m^{-3}),

U_i = directional velocity of the fluid (m s^{-1}),

t = time (s),

x_i = directional displacement of the fluid element in time t (m).

At any location of the flow, time rate of the change of density was balanced by the net mass flux at that point. For initial simulations, the soil was considered incompressible, with a constant density and was treated as a single-phase continuous medium. Thus, the value of ρ was that of a bulk density including any pore water that may have been present within the soil. Hence, Eq. (4.3) reduced to the following simplified form indicating that the volume of the differential fluid element did not change.

$$\frac{\partial}{\partial x_i}(\rho U_i) = 0 \tag{4.4}$$

Newton's second law enabled to relate the acceleration of a fluid parcel or element to the net force action on it through the following momentum equation,

$$\rho \frac{DU}{Dt} = \rho g_i - \frac{\partial p}{\partial x_i} + \frac{\partial \tau_{ij}}{\partial x_j} \tag{4.5}$$

where:

g = acceleration due to gravity (m s^{-2}),

p = hydrostatic pressure (Pa),

τ_{ij} = shear stress tensor (Pa).

The material or substantial derivative is a function of both temporal and spatial changes.

$$\frac{DU}{Dt} = \frac{\partial U}{\partial t} + U_j \frac{\partial U}{\partial x_j} \tag{4.6}$$

The above expressions indicate that the acceleration of the fluid element is balanced by the gravitational force, pressure (hydrostatic stress) and viscous stress (hydrodynamic). In this way, the fluid flow approach addresses different aspects of dynamic soil-tool interaction, such as (a) forces due to the velocity and acceleration of the tool; (b) soil pressure on the tool surface considering the weight of soil mass, and (c) soil failure due to visco-plastic soil deformation.

The following constitutive relation for the Bingham model represents the shear stress tensor in the momentum equation.

$$\tau_{ij} = \tau_y + \mu \dot{\gamma} \text{, for } \left|\tau_{ij}\right| > \tau_y \tag{4.7}$$

$$\dot{\gamma} = 0 \text{, for } \left|\tau_{ij}\right| \leq \tau_y \tag{4.8}$$

where:

$\dot{\gamma}$ = shear rate (s^{-1}),

τ_y = yield stress (Pa),

μ = plastic viscosity (Pa.s).

During tillage, as the tool encounters stiff soil, there would be no soil failure until the applied stress exceeds the soil yield stress. This continued applied stress, exceeding the threshold yield stress, results in visco-plastic soil flow due to soil shear failure.

4.4.3 Soil failure criteria

The soil yield stress in shear was considered to be the failure criteria. During tillage, as the tool encounters stiff soil, there would be no soil failure until the applied stress would exceed the soil yield stress. This continued applied force that exceeds the threshold yield stress, would result in visco-plastic soil flow due to soil shear failure.

4.4.4 Boundary conditions and solution approach

Boundary conditions are determined for the fictitious nodes. Soil was drawn into the channel from the inlet with a particular velocity. Therefore, the velocity component normal to the inlet boundary was set to that specific velocity. Simulations were conducted for a inlet velocity ranging from 0.3 m s^{-1} to 6 m s^{-1}. Elsewhere no slip boundary condition was applied. The channel wall and the tool surface have been considered as wall boundary.

The geometry was simple, so a rectangular coordinate system was used. A value of 10^{-5} has been employed as the convergence criterion at every step of the iteration for the sum of the normalized residuals over the whole fluid domain for all the governing fluid flow equations. A relaxation factor less than 0.3 was found to be a good value for attaining stable convergence, though it increased the computation time compared to larger relaxation factors.

4.4.5 General considerations

Soil visco-plastic parameters, soil viscosity and yield stress required for the simulations have been found using the constant rate Soil Rheometer, developed in the department of Agricultural and Bioresource Engineering, University of Saskatchewan. The data correspond to medium soil compaction (CI = 300 kPa) and 13% moisture content were:

Soil bulk density = 1300 kg m^{-3}

Yield stress = 12.5 kPa

Soil viscosity = 213 kPa.s.

Reynolds number for the considered for the fluid and flow parameters for a inlet velocity of 6 m s^{-1}:

$$N_{\mathrm{Re}} = \frac{\rho VL}{\mu} = \frac{1300x6x0.82}{213x10^{3}} = 0.03$$

4.4.6 Numerical modeling

The numerical procedure involved grid generation, discretisation, solving the governing equations with specific fluid and flow parameters. The solution domain is divided into a finite number of cells. Geometry was created in the CFX-Build 4.4 with a specific dimension which comprised of blocks. The tool block was specified as solid, while the other blocks as conducting body. Boundary conditions have been specified as patches. Discretisation was done by specifying mesh seeds and the geometry was meshed. This meshing was done in one way, two way and uniform bias form to take care of the accuracy at the sensitive zones in the domain. As the flow is expected to vary most rapidly near to the edge of the plate, finer meshes have been placed in that region by

two-way bias and comparatively number of control volumes (finer mesh). The geometry was then analyzed for its correctness regarding the nodes and elements.

Figure 4.4 shows the pattern of one way and two way bias mesh seed placement for discretizing the geometry. The area near the tool was discretised to have comparatively more nodes.

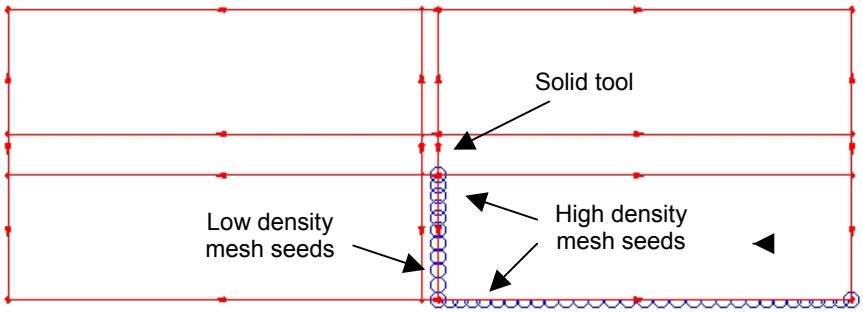

Figure 4.4 Plan view of the flow geometry with typical mesh seeding in two way and one way bias.

4.4.7 Results and Discussions

4.4.7.1 Visco-plastic soil flow

It was important to understand the soil flow behavior before observing the influence of the tool. It is customary to define an entry length, as the distance from the inlet at which the centerline velocity is 99% of that for the fully developed flow (White, 1999). The velocity profile in the entry region was different from that in the fully developed flow since it was a function of the velocity and pressure gradients (Fig. 4.5). With the no slip boundary condition, the higher velocity gradients in the wall region resulted in greater frictional losses and some pressure energy was converted into kinetic energy. Consequently, the pressure gradient influenced the velocity profile in the entry region and the fluid in the central core accelerated. The retardation of the fluid in the wall region must be accompanied by a concomitant acceleration in the central region in order to maintain continuity (Chhabra and Richardson, 1999). Thus, the acceleration of the inlet velocity near the inlet can be attributed to the principle of mass and momentum conservation.

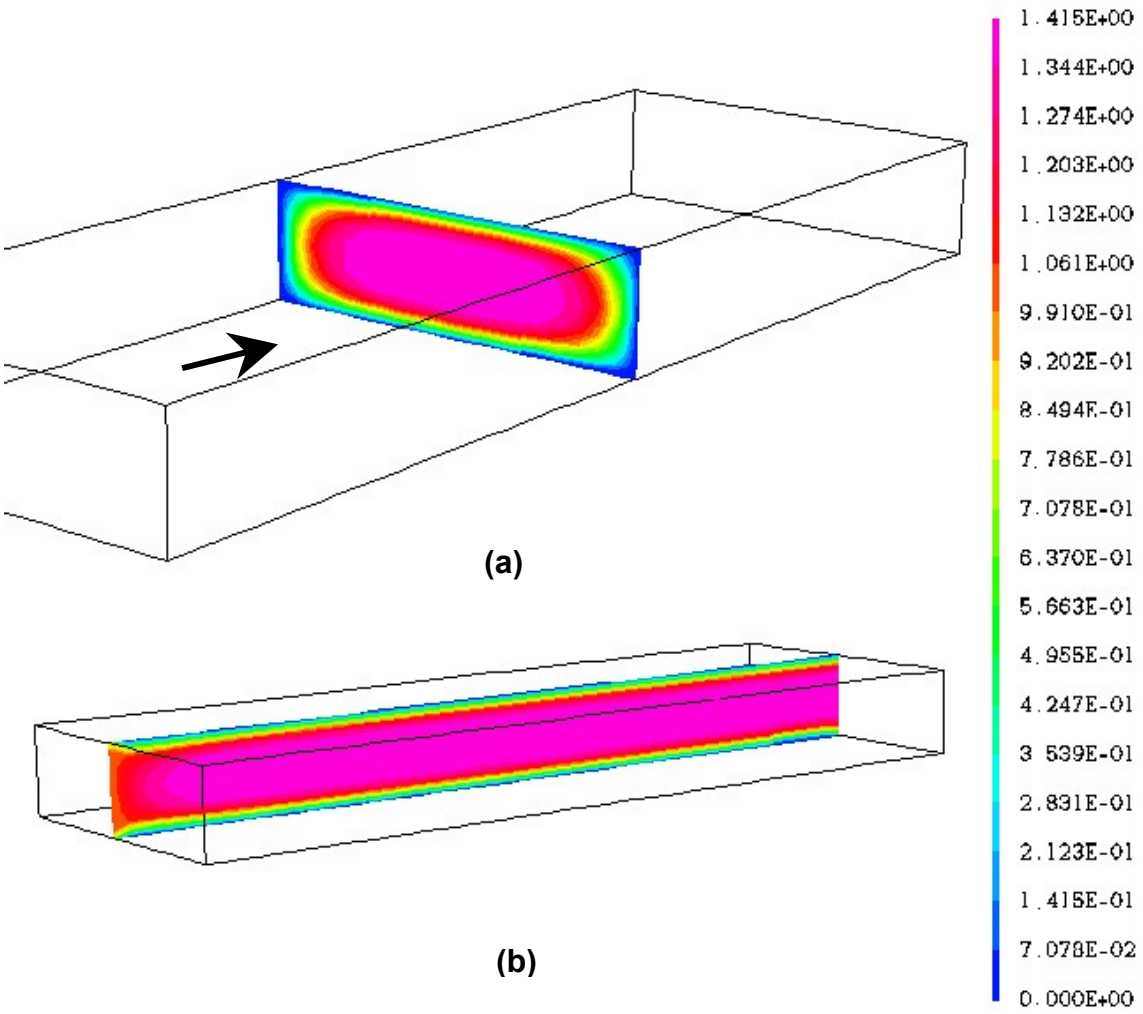

Figure 4.5 Fringe plot of velocity (m s^{-1}) profile of soil flow in the conduit for an inlet velocity of 1 ms^{-1}; (a) across flow section, (b) across flow depth.

A longitudinal velocity profile for an inlet velocity of 3 m s^{-1} (Fig. 4.6) showed that the velocity suddenly increased near the inlet (entry region) and then it was stabilized at a fully developed velocity of about 4.35 m s^{-1}. The thickness of the boundary layer is theoretically zero at the entrance and increases progressively along the flow line. The velocity reached its stabilized shape where the boundary layer converged at the centerline of the flow.

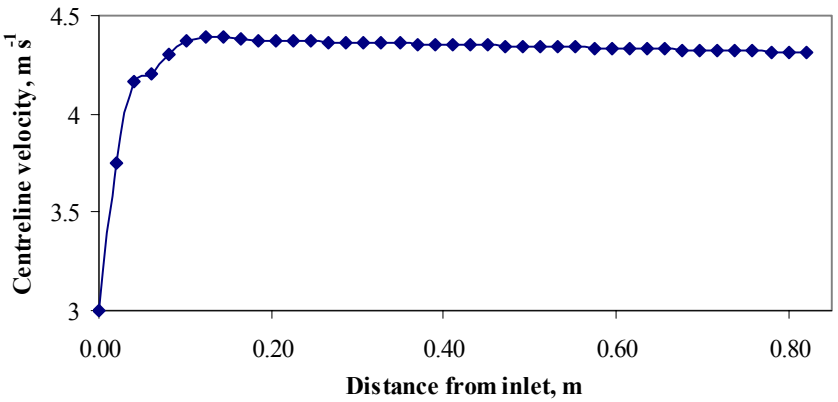

Figure 4.6 Velocity profile along the centerline of the flow domain.

Velocity profile for the fully developed flow for an inlet velocity of 4 m s^{-1} (Fig. 4.7) shows the behavior of the non-Newtonian material. Since the non-Newtonian fluid (soil) has been modeled by Bingham constitutive law, the velocity profile in this perspective was observed to have "plug flow region" and "plastic flow regions". There was a solid plug-like core flowing in the middle of the flow channel where the deviatoric stress was less than the yield stress. Thus the yield surface can be located at the point where the shear stress was equal to the yield stress.

The flow behavior of soil in the problem domain has been investigated in different sections with respect to the axial velocity (Fig. 4.8 and Fig. 4.9). These contour plots specify the regions of the plastic and plug flow zones. Thus the failure or the yield surface can be detected on the flow domain. A characteristic peculiarity on problems of the fluidity of a visco-plastic medium is the locations of the boundaries which divide the flow fields into fluid regions and rigid plug regions (Adichi and Yoshioka, 1973). The flow behavior of soil as observed in the above figures agrees very much with the existing results (Taylor and Wilson, 1997; Wang, 1998) of Bingham flow behavior.

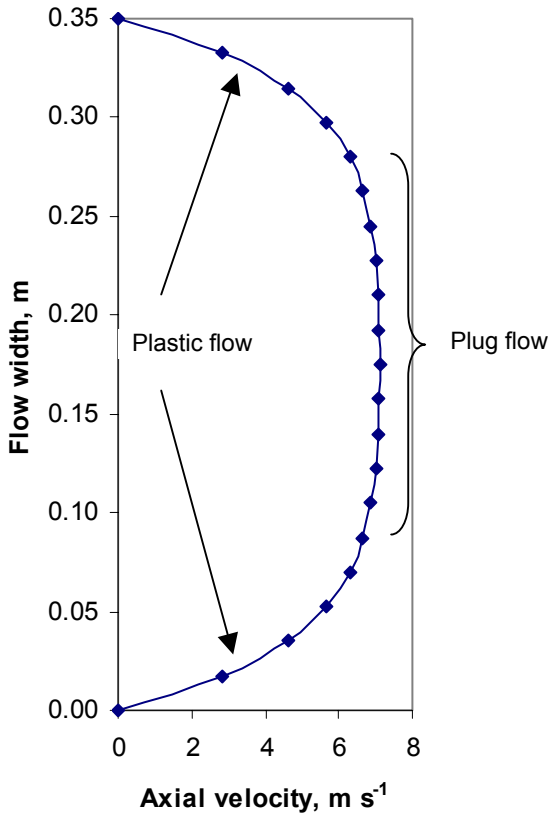

Figure 4.7 Fully developed velocity profile of non-Newtonian soil flow pattern across the flow width observed at the middle of flow depth.

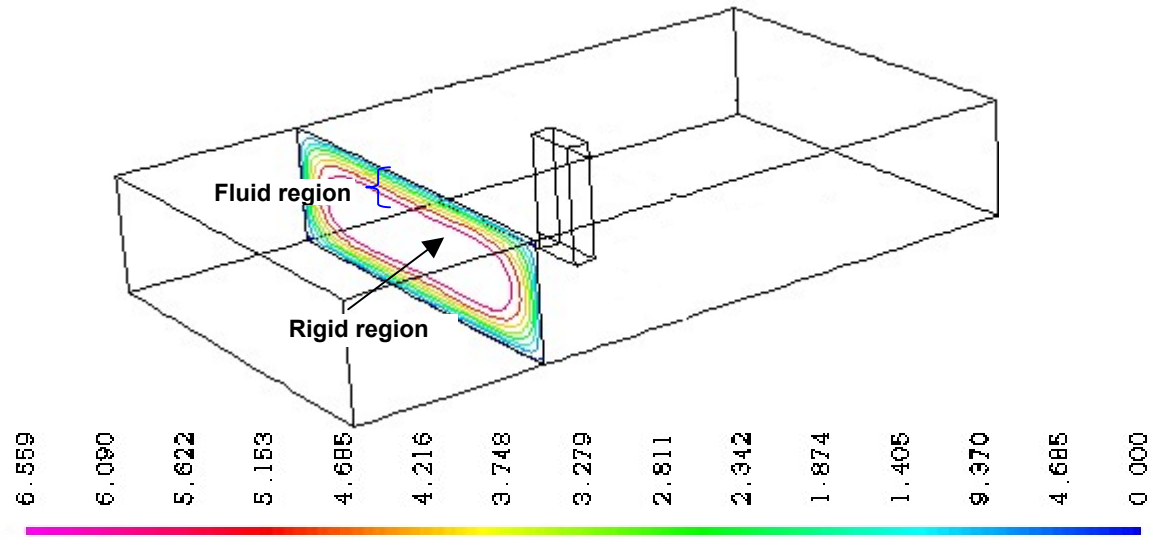

Figure 4.8 Velocity contours away from the tool in the upstream flow in the conduit.

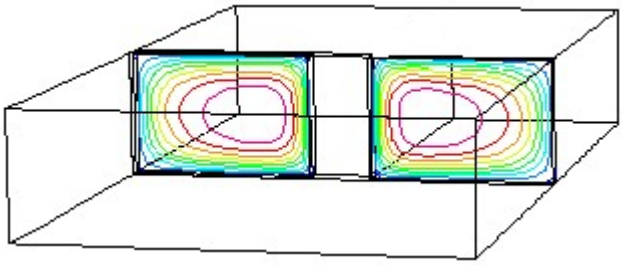

Figure 4.9 Velocity contours across the flow at the tool section along the tool width in the conduit.

The fully developed velocity is always more than the inlet velocity. This velocity for a particular inlet velocity would be considered as the tool velocity when the tillage tool would be simulated in the same flow geometry considering the soil as stationary and the influence zone of the tool would be determined. The following section describes the simulation of soil tillage tool interaction in the perspective of soil disturbance zone and failure front advancement.

4.4.7.2 Soil failure front

A general feature of the influence of tool placed in the fully developed flow is as shown in Fig. 4.10. The fully developed plug flow is observed at a distance after the inlet as a Bingham material moving like a solid in the central region of the channel. Figure 4.11 shows the disturbance of the flow due to the interaction with the tool. The velocity just in front and rear of the tool is zero because of the stagnation points in the flow domain. Because of the presence of the tool, the region of influence behaves like a plastic or viscous flow as the pressure near the tool would be very high and the shear stress would exceed the yield stress. Thus the yield surface related to the axial velocity should give the soil disturbance zone. The unyielded zone at the lateral tool position of the flow and at the stagnation points are defined respectively as *islands* and *polar caps* (Zesis and Mitsoulis, 2002).

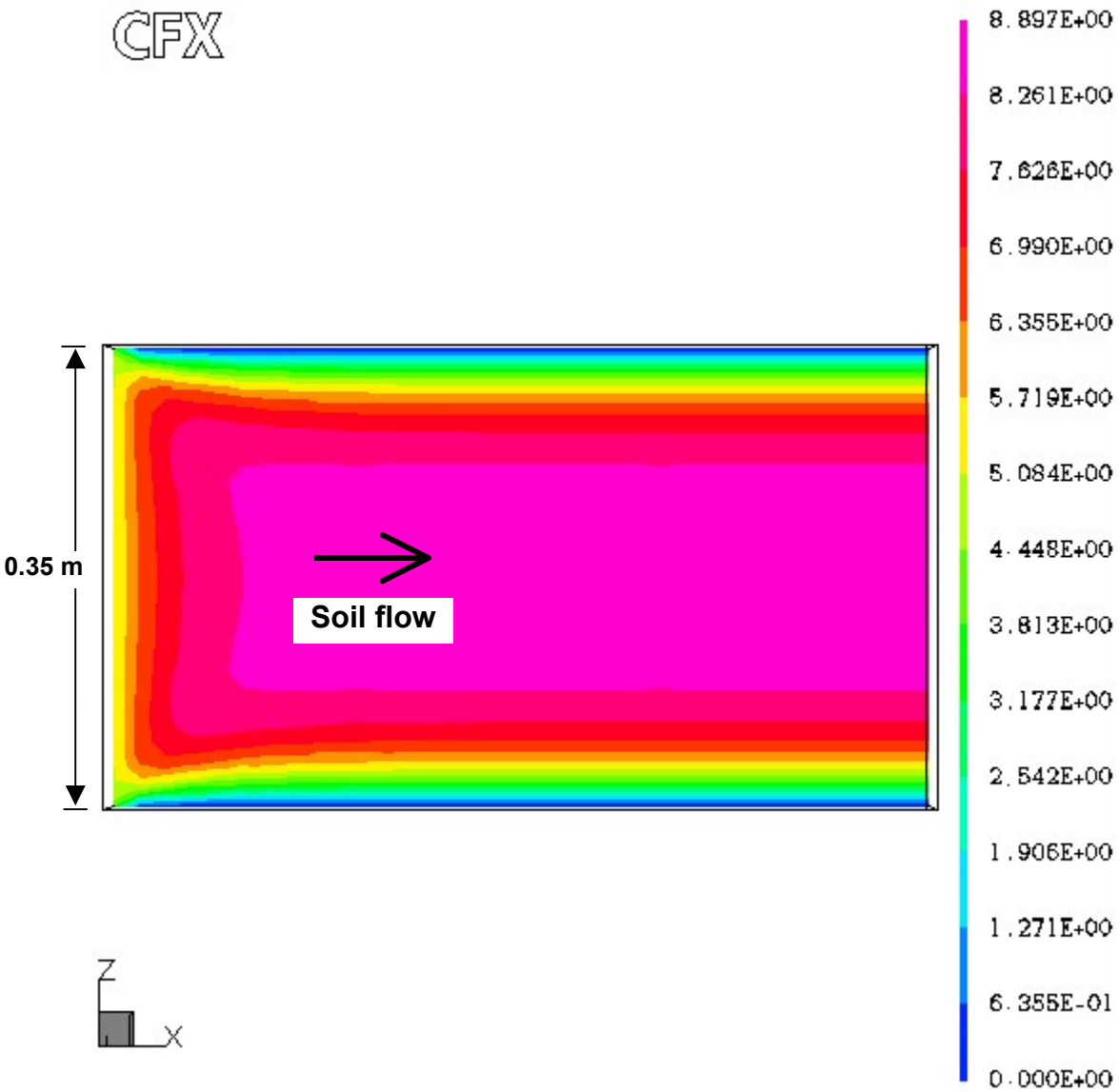

Figure 4.10 Fringe plot of soil flow pattern (velocity profile, m s^{-1}) observed across the width of the conduit at the middle of the flow depth for an inlet velocity of 5 m s^{-1}.

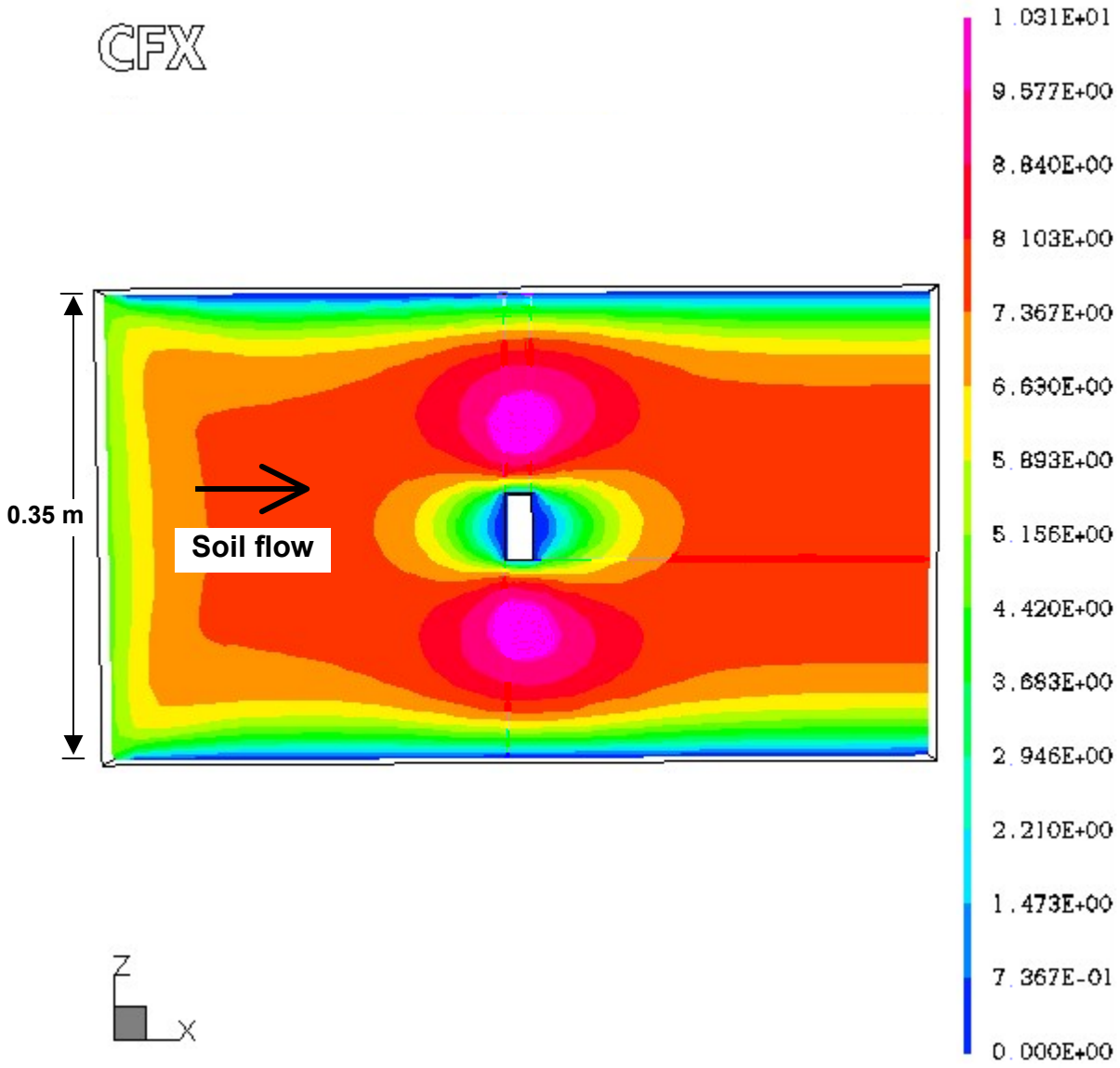

Figure 4.11 Fringe plot of soil flow pattern (velocity profile, m s^{-1}) in a conduit as influenced by the tool (bluff body) for an inlet velocity of 5 m s^{-1}.

4.5 Soil free-surface or open channel flow around a simple tool

Free-surface computational simulations were performed with a geometry modified to the benchmarked one for conduit flow. This was done with the objective of getting the soil surface deformation due to tool interaction.

4.5.1 Soil-tool model

The soil-tool model consisted of a rectangular flow field with a flat plate (representing tillage tool) as an obstruction (the bluff body) in the flow. A simple vertical blade (bluff body) of 20 mm thickness (T) and 50 mm width (W), operating at 100 mm depth (H) was modeled in this study. The flow geometry (Fig. 4.12) consisted of an open channel of 350 mm width (7W), 820 mm length (L) and 300 mm depth (3H). For a vertical blade, the region of influence had a length of four times the operating depth ahead and behind of the tool and a width of six time the width of the tool. However, during the CFD simulations, it was observed that a channel width of seven times the tool width eliminated the effect of channel wall on the flow pattern with respect of tool influence.

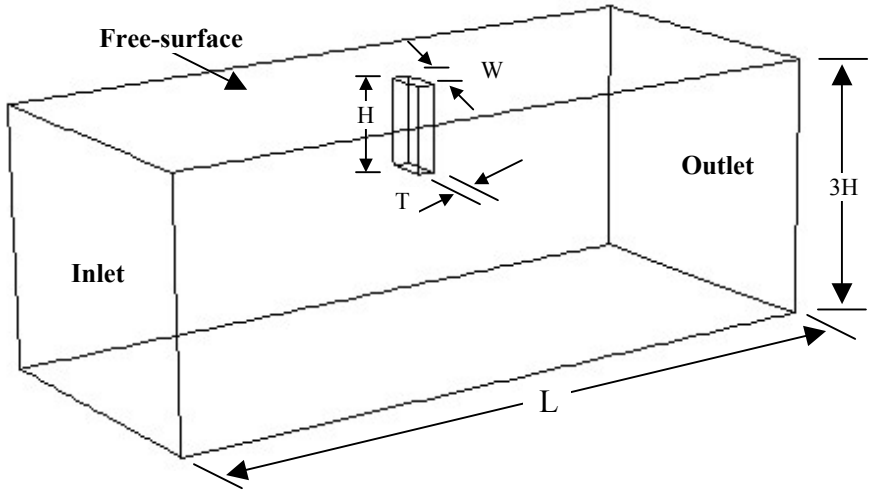

Figure 4.12 Schematics of the flow field for free-surface flow.

4.5.2 General considerations

For a soil with 1270 kg m^{-3} bulk density, 400 kPa cone index and 17% moisture content (dry basis), viscosity was found to be 149 kPa.s and yield stress as 12 kPa using the soil rheometer. These visco-plastic parameters have been used for the simulations.

Soil was considered to be cut by a narrow tool operating at a constant speed. The system was idealized with the following assumptions:

(1) The tool is narrow, rigid and works as a vertical blade.

(2) The tool operates at a constant depth.

(3) Soil flow type is laminar and the state of flow is transient.

(4) Flow is symmetrical about the vertical section of the tool.

(5) Soil failure is three-dimensional.

(6) The soil is an isotropic and homogeneous continuum.

(7) Soil behaves as a Bingham material with definite yield stress.

(8) Soil pore spaces are negligible and it is an incompressible material.

4.5.3 Boundary conditions

Soil was drawn into the flow channel with an inlet velocity. Therefore, the velocity component normal to the inlet boundary was set to that value. Boundary conditions imposed in the simulation with respect to the flow domain are;

1. Inlet velocity was specified from 3 to 10 m s^{-1}.
2. The outlet was specified as pressure boundary.
3. No slip wall boundaries were at the bottom and the sides of the channel.
4. Top of the flow domain was specified as free-surface with pressure boundary.
5. Surface regions were also specified as 3D regions to which free-surface grid movement was confined.

4.5.4 Numerical modeling

Surface meshing was done in the forms of one way, two way and uniform bias to take account of the sensitive zones in the domain. As the flow was expected to vary most rapidly near to the edge of the tool, finer meshes were placed in that region using two-way bias. Several simulations were conducted with the same condition to attain a grid-independent solution.

The differential equation governing the conservation of momentum was solved using the solution scheme for non-Newtonian material with control volume approach. A user subroutine written in FORTRAN (Compaq Visual, version 6.5) was incorporated in the main solver program for the numerical solution with free-surface grid movement. When

the Moving Grid feature was used, additional terms were included in the governing equations to account for the movement of the grid. These terms accounted for the velocity of each grid node, since the position of the grid nodes changed with time. The grid topology and number of nodes remained constant whereas the nodal position and velocity changed with each time step. At the start of each time step, user-coded routines were called that specified the way in which the grid was moved. The free-surface grid algorithm allowed the grid near the surface to change in time. Free-surface grid movement was convection controlled with a specified false time step for slow convergence to avoid oscillation in the solution process.

4.5.5 Results and discussion

Results of simulation were interpreted with the soil as stationary and the tool moving at a constant velocity. Some significant results are discussed below.

The velocity profile at the fully developed region represented the non-Newtonian Bingham flow pattern the same way as it was observed for a conduit flow. Figure 4.12 shows the velocity profiles of the fully developed soil flow in the channel across the flow depth and the channel width. Central core being the visco-plastic plug flow. In the fully developed non-Newtonian soil flow pattern outside the tool influence zone (Fig. 4.13), free-surface boundary condition at the top of the flow domain allowed a velocity close to plug flow near the top of the channel. The plug flow at the central core of the channel represents Bingham visco-plastic flow where the shear stress is below the yield stress. The velocity profile across the channel width depicts that soil deforms and a plastic flow takes place at the wall region. Zero velocity at the channel walls due to no-slip boundary conditions causes very high shear stress, which is more than the yield stress.

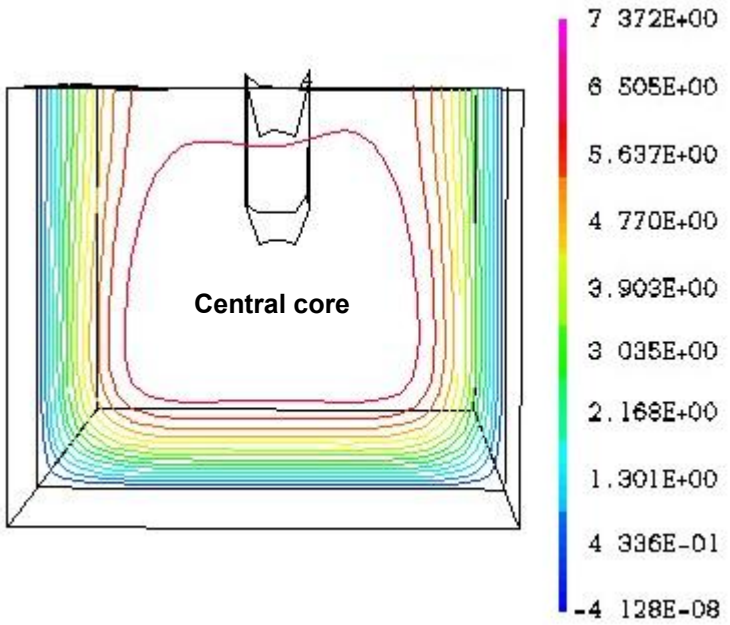

Figure 4.13 Cross sectional velocity profile (m s^{-1}) for the axial velocity before the tool influence zone.

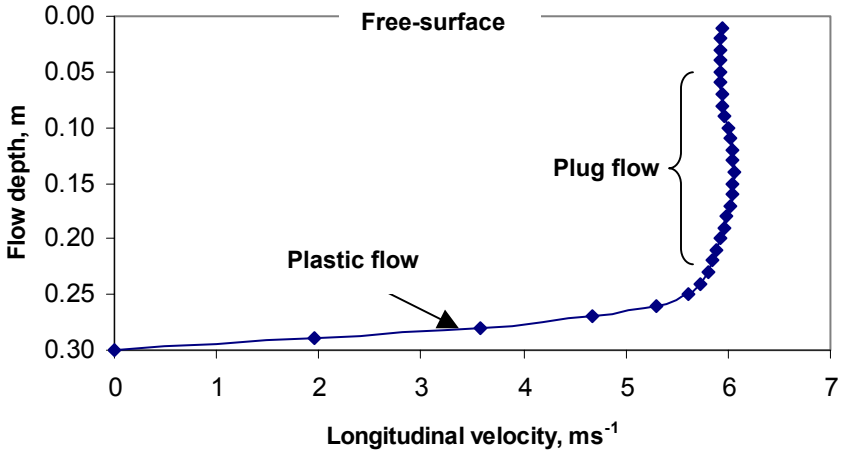

Figure 4.14 Free-surface velocity profile at the centerline of the channel.

Velocity vectors as influenced by the presence of the tool in the flow domain are shown in Figure 4.15. Soil flow around the tool at the free-surface has been depicted in this figure. Velocity vectors shows soil build up in front of the tool and furrow formation behind the tool (side view of the channel). A prominent wave formation exists at the inlet of the flow. Due to no slip boundary condition at the channel base and at the walls

of flow channel, velocity close to the channel base and walls gets reduced after the flow starts at a particular inlet velocity. Free-surface at the top allows the soil to bulge out following the principle of mass and momentum conservation. Velocity vectors in front of the tool shows the height of soil build up and size and shape of the furrow formed behind the tool. As the fully developed plug flow encounters the tool, due to free-surface boundary condition, velocity of the soil particles increased and is directed upwards.

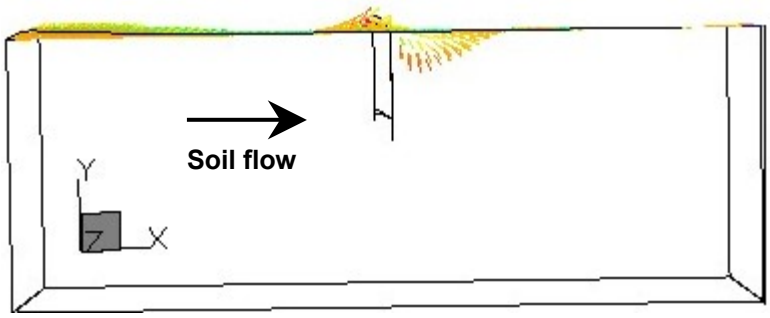

Figure 4.15 Velocity vectors at free-surface showing furrow formation.

The flow dynamics near the tool in the flow domain is of major interest with respect to soil failure front. Flow pattern of longitudinal velocity at the tool section (vertical plane) is shown in Figure 4.16. Contour plot of axial velocity at the centre line of the channel across the tool vertical section, shows the tool influence zone (X). Soil disturbance zone due to the tool interaction can be obtained from this axial velocity profile of the soil particles. Large soil deformation due to tool interaction causes soil to build up at the front of the tool and furrow behind it. In a tool operating environment, soil particles scour the tool face as the tool moves ahead in soil cutting and a furrow is formed behind the tool. It is observed that the fully developed flow was disturbed due to the presence of the vertical tool in the flow domain and the flow pattern is influenced. Thus the longitudinal soil disturbance zone can be found for a particular tool velocity and soil condition. The distance between the tool face and the furthermost disturbed zone is the soil failure front.

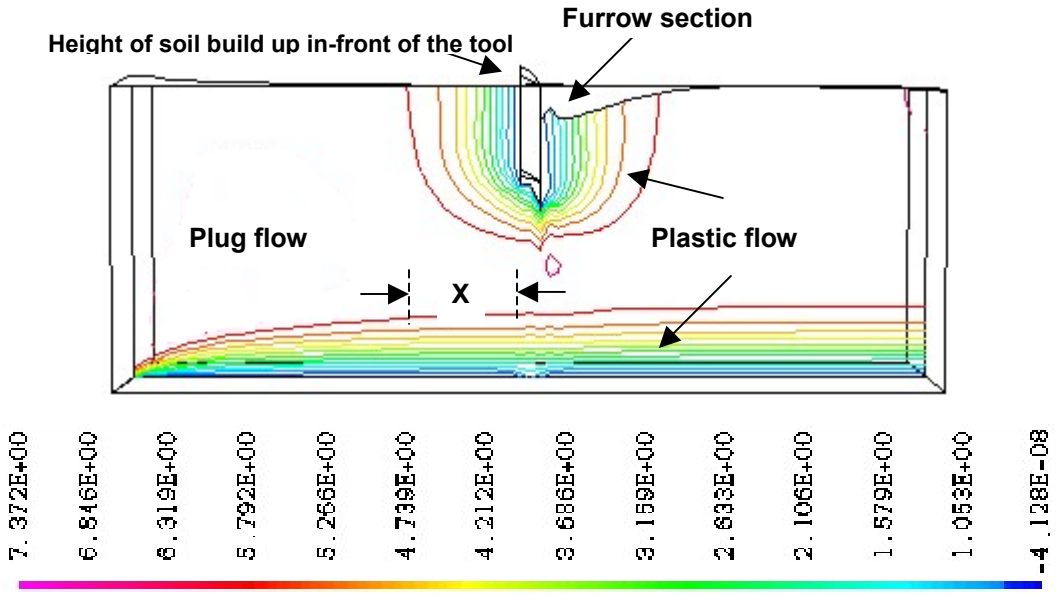

Figure 4.16 Contour plot of axial velocity (m s^{-1}) at the centre line of the channel (vertical plane).

The velocity profile along the flow length helped determine the tool influence zone. Fully developed velocity reduces to zero at the tool surface. At the rear of the tool, the discontinuity of the velocity profile is due to the presence of the furrow. This velocity distribution can be used to interpret the case of a real tool operating condition. With this fluid flow approach, considering soil as a fluid and the tool as a stationary solid, interpretation can be made in the reverse mode.

Considering the tool operating condition, a particular fully developed velocity has been considered as the tool speed operating in the same flow domain of stationary soil. Thus, the soil failure front can be determined (Fig. 4.17) from the longitudinal velocity profile. For a tool operating speed of 6 m s^{-1}, the soil failure front ('S') was observed to be 160 mm.

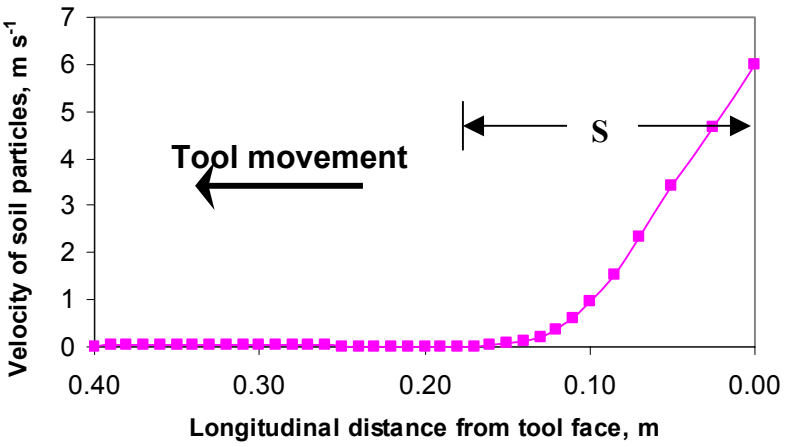

Figure 4.17 Soil failure front for the moving tool.

4.5.5.1 Effect of operational velocity on soil failure front

Simulations were conducted with different inlet velocities, thereby causing different fully developed soil flow velocities, and these were used to estimate frontal failure zones. Figure 4.18 shows the relationship between soil failure front (extended at a depth of 10 mm below the soil surface) and tool velocity for a 50 mm wide tool.

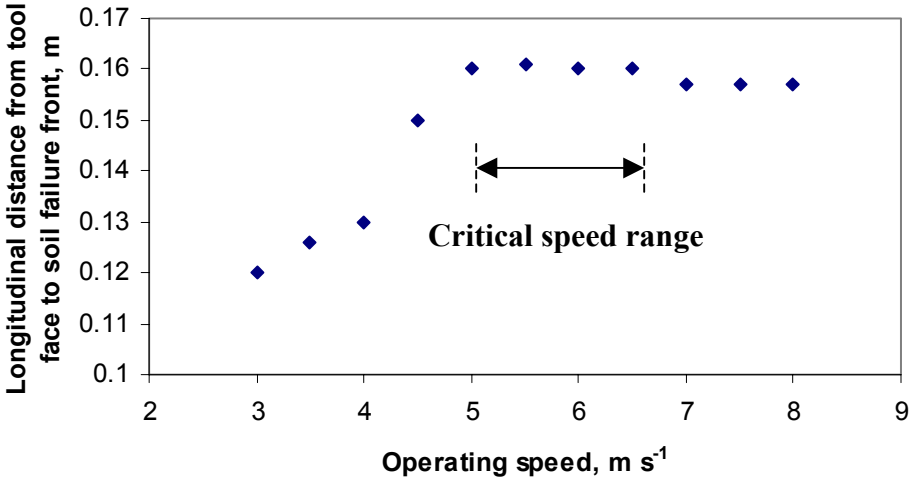

Figure 4.18 Relationship between soil failure fronts and tool velocity.

Initially the failure front increased with the tool velocity. After reaching a critical level, there was little or no increase in the longitudinal distance from the tool face to the soil failure front. These results satisfy the theoretical arguments by Russian scientists

(Azyamova, 1963; and Vetro and Stanevski, 1972) on the effect of operating speed during tillage. An extensive soil stress or energy concentration occurred in front of the tool when the tool speed was less than the velocity of the wave propagation of the soil stress. As the tool speed increased faster than the wave of soil stress propagation, plastic zone of soil in front of the tool decreased or even disappeared.

Figure 4.19 shows the effect of tool velocity on the profile of soil failure front at three depths for the 100 mm tool operating depth. It is seen that the longitudinal distance of the soil failure front from the tool face increases with the tool operating speed in initially at a higher rate and then the rate of increase declines. For the 10 mm soil depth, the closest to the soil surface, the soil failure front has been found to decline after the tool operating speed of 5 m s^{-1}. For the other two soil depths of 30 mm and 50 mm the range of optimum operating speed was found to be 4 to 6 m s^{-1}, where the longitudinal distance of the soil fronts did not increase much with the increase with the operating speed. For 50 mm depth of the tool, soil failure front was found to decrease. This may be attributed to the fact that at higher depth, due to higher 'hydrostatic' stress, the stress concentration was near the tool face. Shear band formation appears to be the cause of soil failure at high shear rates (Yamamuro, 2004). Thus at higher depth and higher speed, the energy concentration was near the tool and soil disturbance would be less.

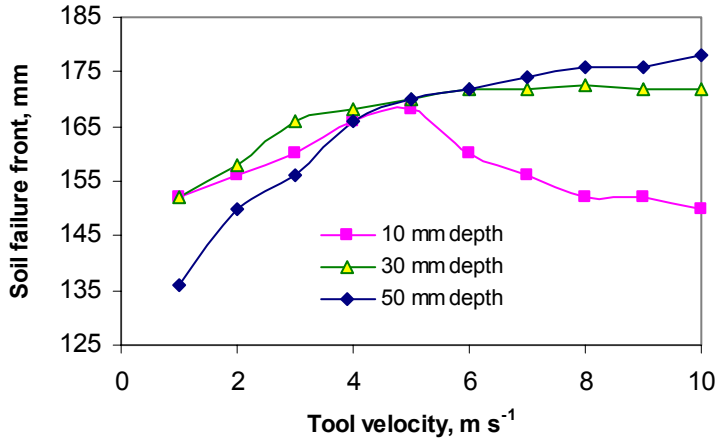

Figure 4.19 Soil failure fronts at different soil depths.

4.5.6 Comparison of CFD results with published data

The longitudinal distance of the soil failure front from the tool surface could not be validated with experimental results due to the limitations of the soil-bin facility for high speed tillage. However, the critical speed range agrees well with the published literature.

With current simulations, the critical speed range has been found to be between 5 to 6.5 ms^{-1} which is within the values reported by Kushwaha and Linke (1996). Investigation of draft-speed response using Artificial Neural Network (ANN) revealed a critical speed range of 3.5-6.0 m s^{-1} (Zhang and Kushwaha, 1999).

4.6 Conclusions

The following conclusions were derived from the results of this study.

1. The soil was successfully modeled as Bingham material in these CFD simulations.
2. The Bingham model successfully depicted soil visco-plastic failure with respect to the formation of plastic and plug regions in the flow domain.
3. The longitudinal distance of the soil failure front from the tool face for a 50 mm wide tool operating at about 6 m s^{-1} was found to be about 160 mm.
4. The critical speed range was found to be in the range of 4 to 6.5 m s^{-1}.
5. Dynamic analysis of soil-tool interaction in a conduit enabled visualization of the visco-plastic soil flow phenomena.
6. Free-surface simulation improved the prediction and description of the dynamics of soil-tool interaction.

4.7 References

Adichi, K. and N. Yoshioka. 1973. On creeping flow of a visco-plastic fluid past a circular cylinder. Chem Eng Sc 28: 215-226.

AEA Technologies. 2001. CFX Release 4.4 User Guide. Harwell, Didcot, UK: CFX International.

Azyamova, E. N. 1963. Studies of dynamics of deformation of soil. Trudy Minsk 1:131-139. Translated by W. R. Gill, Auburn, AL, USA: National Tillage Machinery Laboratory, USDA.

Chhabra, R. P. and J. F. Richardson. 1999. Non-Newtonian Flow in the Process Industries, Fundamentals and Engineering Applications. Oxford, UK: Butterworth Heinemann Publishing Ltd.

Chi, L. and R. L. Kushwaha. 1991. Three dimensional Finite Element Interaction between soil and Simple Tillage Tool. Trans ASAE 34(2): 361-366.

Davidson, M. R., N. H. Khan and Y. L. Yeow. 2000. Collapse of a cylinder of Bingham fluid. J. ANZIAM 42(E): C-499-C517.

Desai, C. S. and H. V. Phan. 1980. Computational Methods in Nonlinear Mechanics. Ed. J. T. Oden. New York: North Holland Publishing Company.

Durairaj, C. D. and M. Balasubramanian. 1997. A method for dynamic measurement of soil failure patterns caused by tillage tools. Soil Tillage Res 41: 119-125.

Goryachkin, V. P. 1968. Collected works in three volumes. N. D. Luchinski, eds. Translated 1972. Jerusalem, Israel: Ketter Press.

Grisso, R. D. and J. V. Perumpral. 1981. Models for predicting narrow tillage tool behavior in soil- A review and comparison. ASAE Paper No. 81-1535, St. Joseph, MI.:ASAE.

Hanna, H. M., S. J. Marley, D. C. Erbach and S. W. Melvin. 1993a. Change in soil microtopography by tillage with a sweep. Trans ASAE 36(2): 301-307.

Hanna, H. M., D. C. Erbach, S. J. Marley and S. W. Melvin. 1993b. Comparison of the Goryachkin theory to soil flow on a sweep. Trans ASAE 36(2): 293-299.

Johnson, A. M. 1970. Physical processes in Geology. San Francisco: Freeman, Cooper.

Kushwaha, R. L. and C. Linke. 1996. Draft-speed relationship of simple tools at high operating speeds. Soil Tillage Res 39: 61-73.

Linke, C. and R. L. Kushwaha. 1992. High speed evaluation of draft with a vertical blade. ASAE Paper No. 92-1019, St. Joseph, MI.:ASAE.

Mckyes, E. and F. L. Desir. 1984. Prediction and field measurement of tillage tool draft forces and efficiency in cohesive soils. Soil Tillage Res 4: 459-470.

McKyes, E. and O. S. Ali. 1977. The cutting of soil by narrow blades. J Terramech 14(2): 43-58.

Patankar, S.V. 1980. Numerical Heat Transfer and Fluid Flow. Washington, DC: Hemisphere Publishing.

Payne, P. C. J. 1956. The relationship between the mechanical properties of soil and the performance of simple cultivation implements. J Agric Eng Res 1(1): 23-50.

Perumpral, J.V., R. D. Grisso and C. S. Desai. 1983. A soil-tool model based on limit equilibrium analysis. Trans ASAE 26(4): 991-995.

Reece, A. R. 1965. The fundamental equations of earth-moving mechanics. Proc. Symp. Earth Moving Machinery: Institute of Mechanical Engineering 179 (3F): 8-14.

Rosa, U. A. 1997. Performance of narrow tillage tools with inertial and strain rate effects. Unpublished Ph.D thesis. Saskatoon, Saskatchewan: Department of Agricultural and Bioresource Engineering, University of Saskatchewan.

Sarifat, K. and R. L. Kushwaha. 1998. Soil translocation by narrow tillage tools at high speeds. CSAE/SCGR Paper No. 98-409. Mansonville, QC: SCAE/SCGR.

Sarifat, K. and R. L. Kushwaha. 2000. Modeling soil movements by tillage tools. Canadian Agric Eng 42(4): 165-172.

Söhne, W. 1960. Suiting the plow body shape to higher speeds. National Institute of Agricultural Engineering Translation No. 101 (12): 51-62.

Taylor, A. J. and S. D. R. Wilson. 1997. Conduit flow of an incompressible yield-stress fluid. J Rheology 41(1): 93-101.

Vetrov, Yu. A. and V. P. Stanevaski. 1969. The investigation of the factors of the speed of cutting soils. Mining Constructions and Highway Machines 8: 21-26. Tekhnika Publishing House, Kiev, USSR. (Russian Edition).

Wang, Y. 1998. Non circular duct flow of nonlinear visco-plastic fluids. J Chinese Inst Chem Eng 29(2): 85-97.

White, F. M. 1999. Fluid Mechanics. 4th ed. Columbus, OH: McGraw-Hill Companies.

Zhang, Z. X. and R. L. Kushwaha. 1999. Operating speed effect on the advancing soil failure zone in tillage operation. Canadian Agric Eng 41(2): 87-92.

Zisis, T. and E. Mitsoulis. 2002. Visco-plastic flow around a cylinder kept between parallel plates. J Non-Newtonian Fluid Mech 105: 1–20.

Chapter 5

Computational Fluid Dynamics Modeling of Pressure Distribution on Tool Surface

5.1 Significance

This chapter relates to objective 4 of the thesis. Chapter 4 demonstrated the potential of CFD modeling of tool interaction with visco-plastic soil flow. Since there has not been previous research on the soil velocity or soil failure pattern around a tillage tool, the results from simulation presented in chapter 4 could not be validated for soil failure front. Only the critical speed range has been validated with the published literature. Moreover, due to the limitations of soil bin facility to carry out high speed experiments at this state, it was not possible to validate the results with experimental values. Hence, as a next step, numerical modeling has been carried out on the pressure distribution on a tool, on which there are available literatures (though limited). The objective of this chapter was, thus, to investigate the pressure distribution on a tool surface and the stress pattern on soil due to the advancing tool.

5.2 Introduction

In order for a soil working tool to perform according to some desirable criteria, proper tool design based on its geometry is a critical parameter. The common criteria of tillage tool design have been draft required to operate the tool, the volume of soil failed by the

device and total energy requirement. The modified condition of the tilled soil due to tool action depends on the soil mechanical behavior and its initial condition. Pressure exerted by soil on the tillage tool and its distribution with respect to tool wear is an important parameter in determining tool size and shape. There has been extensive research on force prediction modeling due to soil-tool interaction. However, very little research is available on studies related to soil deformation focusing the pressure on tool or stresses exerted on the soil and its stress profile in the vicinity of the tool.

The power requirements of a tillage tool depend on several factors related to soil type and conditions, design of the tool, and operating parameters. Depth of tillage and the forward speed contribute significantly to the draft requirement and these are the only factors that could be controlled by the operator. Hence, establishing the relationship between speed and draft is important for optimizing soil-tool interaction. Soil pressures on the tool is of interest for several reasons, including the power requirement to pull the implement, mechanical design of the tool in respect of size and shape and optimum soil condition obtained from tool operation at different operating conditions.

Many force prediction models have been developed for tillage tools using analytical and numerical methods. Soil, in most of the earlier studies, has been considered as an elastic solid, elasto-plastic material or rigid body. Dynamic visco-plastic nature of soil during tillage has not been given proper consideration. The objective of this research was to gain an insight into soil forces and the pressure distribution on a simple tool considering the dynamics of soil-tool interaction from fluid flow approach. Pressure distribution over the surface of a flat tillage tool was investigated using computational fluid dynamics (CFD) for high speed tillage using a commercial CFD software CFX4.4 (AEA Technologies, 2001). Soil stress patterns due to the tool interaction at different speeds were also analyzed, besides investigating the draft requirement. Three dimensional simulations were conducted by control volume method with structured mesh. Soil was characterized as a Bingham material in its rheological behavior.

5.3 Literature Review

5.3.1 Pressure distribution on a tillage tool

The pressure pattern due to a horizontally applied load has not been studied much. The pressure profile on the tool or soil due to a horizontally applied force has not been studied much. Zelenin (1950) studied the stress distribution in front of a tillage tool working in a sandy loam soil and observed lines of equal stress in front of the tool. It was concluded that for normal soil conditions, stress distribution in the soil can be considered to have a circular shape for modeling purposes, although the actual stress distribution may not follow an exact circular pattern.

Elijah and Weber (1971) conducted research on soil failure and pressure patterns for flat cutting blades in soils of three different strengths. Soil pressures on the tool at 45 deg operating at a depth of 150 mm with an operating velocity of about 3 km h^{-1} were observed using pressure transducers. Pressure distribution on the blade surface was found to vary with the position of the blade surface and with the type of soil. Maximum pressure was observed on the cutting edge. Average normal pressures varied from 14 to 50 kPa at the tool edge for soils with low strength to high strength (the soil strength values have not been specified). However, the peak normal pressure ranged from 0 to 500 kPa.

Chi and Kushwaha (1990) developed a nonlinear 3-D finite element model to predict the soil forces on a tillage tool. The theoretical force on the tool edge was found to be larger than the force at the centre of the tool. The stress also increased with the increase in depth, with the maximum force occurring at the outer edges of the tool at the bottom. For a vertical tool of 50 mm wide operating at a depth of 100 mm in a loamy soil with a bulk density of 1434 kgm^{-3} and soil cohesion of 7.2 kPa, soil stress on the tool ranged from 250 kPa near the bottom corners to 100 kPa close to the tool centre line running through two third depths. During the FEM analysis using the incremental method, the change in displacement was very small in each small increment. Since, the difference in

strain at each increment could be considered as infinitesimal strain, the dynamics of tillage can not be inferred from the data completely.

5.3.2 Draft requirement with respect to operating speed

Increased forward speed increases the draft with most tillage implements, mainly because of the more rapid acceleration of moving soil (Kepner et al., 1978). Draft required to pull minor tillage tools operating at shallower depths is primarily a function of the width of the implement and the speed at which it is pulled (ASAE, 2003). For tillage tools operated at deeper depths, draft also depends on the soil texture, depth and the geometry of the tool and can be calculated using the following equation

$$D = F_i[A + B(S) + CS^2]WT \tag{5.1}$$

where:

D = implement draft (N),

F = dimensionless soil texture adjustment parameter (i=1 for fine, 2 for medium and 3 for coarse textured soils), A, B and C are machine-specific parameters (values have been tabulated in the Standard, ASAE D497),

S = operating speed (Km h^{-1}),

W = machine width (m),

T = tillage depth (cm).

For many years it was assumed that increases in tillage tool forces at high speed were due to the acceleration forces of disrupted soil. Researchers have demonstrated that soil acceleration accounts for only a fraction of the increased reaction (Wismer and Luth, 1970), but that the increase was mainly due to the change in soil strength with speed. Based on their Russian literature review on high speed tillage, Hendrick and Gill (1973) stated that there were interfaces that at cutting velocities in the range of 10 -12 m s^{-1}, a body may pass through the soil faster than the soil can compact ahead of the tool, resulting in a potential reduction in the energy requirement at higher velocities. The existence of such a phenomena was suggested to be proved or disproved.

Performance of plane soil cutting blades was studied in sandy soil for an operating speed up to 2.5 m s^{-1} (Luth and Wismer, 1971). Draft appeared to be related to the square of velocity. This velocity term was suggested to be included as an additive term with a draft amount at zero velocity in the prediction equation. Draft requirement of tillage tools as a function of the tool operating speed is very important for high speed tillage. Many empirical and analytical models were developed correlating the draft and tool speed. Results of the analytical models (Payne, 1956; Rowe and Barnes, 1961; Wismer and Luth, 1970) were compared with the experimental results. Draft of mould board and disc ploughs has been found to increase as the square of the operating speed. However, the draft of many other implements has been found to have a linear relationship with the speed.

Stafford (1979) reported that both the magnitude of draft and the relationship between speed and force depended on the mode of soil failure. With brittle failure (low confining stress around the tool at low speed), a second order polynomial could be fitted to the draft-speed relationship, i.e. force increased with increasing rate with the speed. With flow failure (high confining stress around the tool at high speed), the relationship was satisfactorily approximated by an exponential expression, i.e. force increased at a decreasing rate with speed with a tendency towards an asymptotic value. The range of speed at which the failure pattern was observed to change was 1 mm s^{-1} to 5 m s^{-1}. An approximate set of force prediction equations was developed by Stafford (1984) for brittle and flow failures. The force equations were functions of tool width and depth, rake angle, soil cohesion, angle of internal friction and a coefficient. The value of the coefficient, which is a function of rake angle, failure plane angle and angle of internal friction, could be obtained from the graph developed by Hettiaratchi and Reece (1974) for the force equation pertaining to brittle failure. However, it was not possible to determine the value of the coefficient in flow failure due to undefined failure geometry, while, it was easy for the brittle failure due to simplified failure geometry based on passive earth pressure theory for quasi-static conditions.

In the analytical models, the prediction of draft forces was basically dependant on how the soil failure planes were assumed for the analysis. Some simplification of the failure zones were made in order to develop the force equation, such as circular side crescent, log-spiral bottom failure plane and straight bottom rupture plane. The over-prediction of the Hettiaratchi-Reece model was possibly caused by the assumption of the forward failure and transverse failure at the same time in which the effect of the centre wedge might be considered twice (Grisso and Perumpral, 1981). On the other hand, Perumpral-Grisso-Desai (1983) models ignored the soil weight of the side crescents leading to the predicted forces were slightly lower for narrow tillage tools.

Summers et al. (1986) investigated the effects of speed and depth on draft of four different tillage tools, in three different soils. Draft was found to be a linear function of speeds for chisel plows, disks and sweep plows, and a quadratic function of speed for the mould board plows. The speed of operation was varied from 1 to 3 m s^{-1}. Al-Janobi and Al-Suhaibani (1998) developed regression equations to predict draft of three different primary tillage implements on sandy loam soils based on the effects of speed and depth. An increasing response in specific draft was observed with an increase in tillage depth and operating speed for all the implements, chisel plow, offset disc harrow, disc plow and mould board plow. Specific draft was found to have a quadratic relationship with speed for disc and mould board plows. The maximum speed in the investigation was 2.5 m s^{-1}.

Kushwaha and Linke (1996) conducted field experiments with five different blades in sandy loam and clay soil types to determine the draft-speed relationship at high speeds. The results showed that draft increased less above a critical speed range of 3 to 5 m s^{-1}. This critical speed was found to be related to the speed of disruption. Further laboratory and field studies were suggested to be conducted to establish such a relationship.

The results reported in the literature appear to have some contradiction regarding the effect of speed on draft. The relationship was of square law form in air-dry sand (Luth and Wismer, 1969), but in saturated clay it was of power law form with a power of less

than unity, i.e. the draft tended to an asymptotic value at higher speed (Wismer and Luth, 1970). It has generally been found that the draft increases with speed. Most of the studies have focused on mould board plow and disc plow. The relationship between the draft and speed for mould board plow has been found in most of the cases as a square law. Soil movement due to narrow tool interaction with soil is comparatively less and the inertia effect contributes only a small amount of the draft increase (Stafford and Tanner, 1976). However, for only cohesionless soils, the draft increase with speed is due mainly to the inertia forces (Luth and Wismer, 1969). Again, the range of operating speed of these studies, conducted on the effect of speed on draft, was not very high (less than 5 ms^{-1}). This has motivated the present study on a narrow tool used for high speed tillage.

5.4 CFD modeling of pressure distribution on tool surface

Simulations were performed using the commercially available computational fluid dynamics (CFD) code, CFX4.4 from AEA Technologies (2001) for analysing the soil pressure exerted on the tool surface. The subroutine is usually coded in FORTRAN and compiled and linked in CFX. Subroutine URSBCS was used to allow the programmer to specify real information at walls, inlets, mass flow boundaries and other 2D patches, both at the start of a run and on each iteration or time step. Subroutine USRBF was used to allow the programmer to specify body forces.

The soil-tool model (Fig. 5.1) is the same as described in Chapter 4. However, for computational convenience, the geometry has been reduced to half by introducing a symmetrical plane along the flow direction.

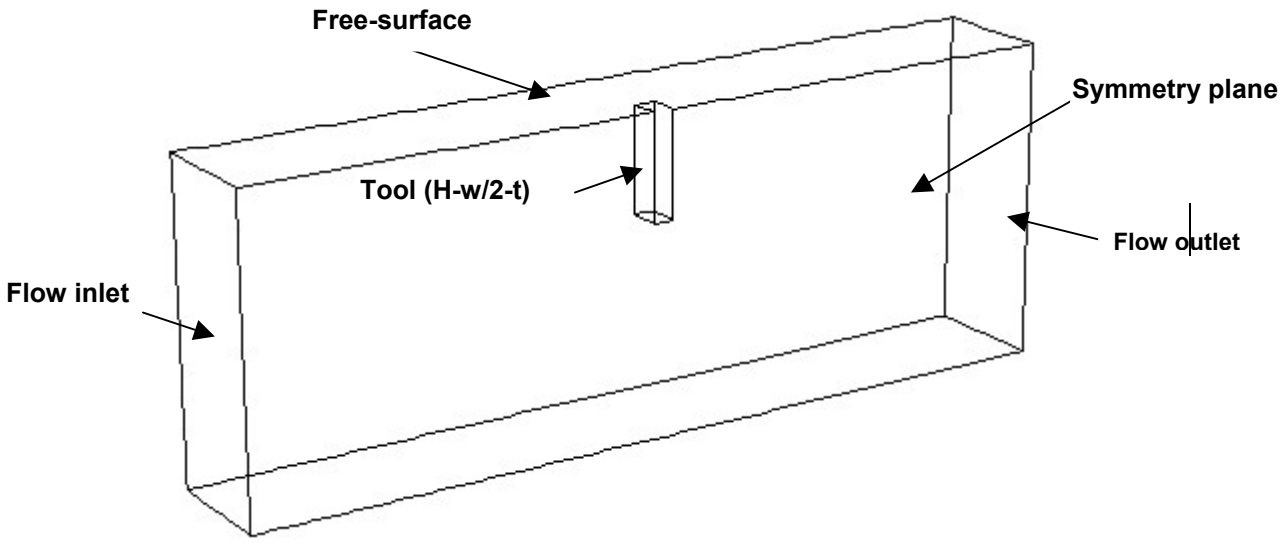

Figure 5.1 Schematic of the flow field.

5.4.1 Drag of Immersed Bodies

Any body of any shape when immersed in a fluid will experience forces from the flow. The force on the body along the axis, parallel to the mainstream flow is called drag, which is essentially a flow loss and must be overcome if the body is to move against the stream (White, 1999). Drag coefficients are defined by using a characteristic area which may differ depending upon the body shape:

$$C_D = \frac{drag}{\frac{1}{2}\rho V^2 A} \tag{5.2}$$

where,

C_D = drag coefficient,

ρ = fluid density

V = fluid velocity and

A = characteristic area.

Drag on an immersed body is comprised of two components, pressure drag and viscous or friction drag. Thus,

$$C_D = C_{D,press} + C_{D,fric} \tag{5.3}$$

where:

$C_{D,press}$ = pressure drag and

$C_{D,fric}$ = friction drag.

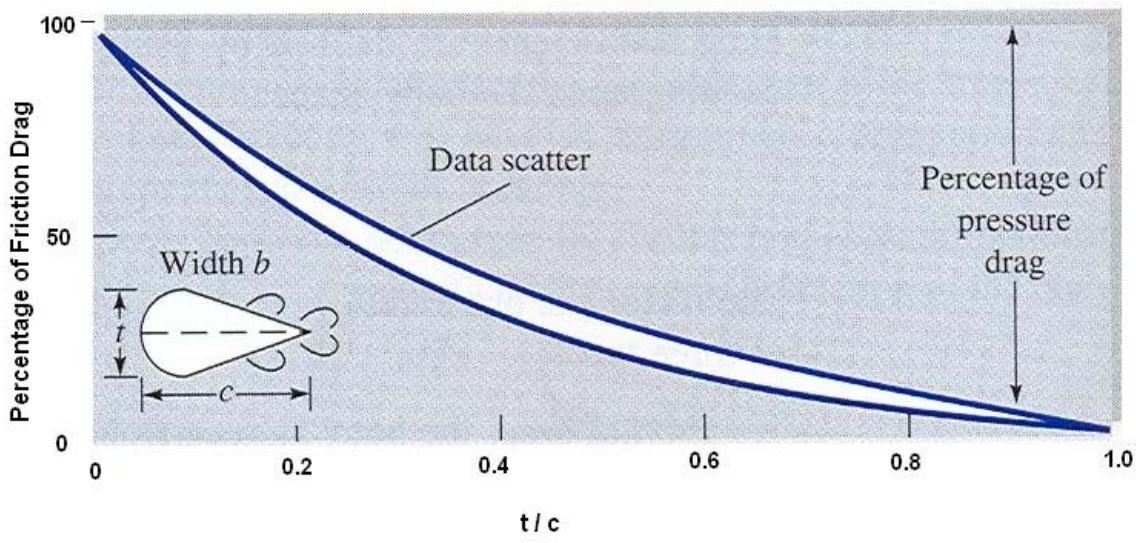

Figure 5.2 Contribution of pressure and viscous component on drag force (White, 1999).

The contribution of friction and pressure drag depends on the bluff body shape. This is explained in Fig. 5.2 as a function of the thickness and width ratio. Since the value of t/c is 2.5 for the tool considered for simulation (Fig. 1), pressure drag can be considered as major contributing part for calculating the drag force (draft) on the tool.

5.4.2 Mathematical modeling and Boundary conditions

The physics of the problem governed by the fluid flow equations are the same as described in Chapter 4. Boundary conditions were also the same as previous simulations for finding soil failure pattern.

For the purpose of obtaining shear stress on the tool surface, a 'thin surface' wall boundary condition has been imposed close to the face of the tool. This has enabled to find the tangential force acted on the tool surface.

5.4.3 Soil parameters for dynamic analysis

Soil dynamic parameters such as soil viscosity and yield stress were determined by a strain rate controlled torsional Soil Rheometer, developed in the Agricultural and Bioresource Engineering Department, University of Saskatchewan. For a soil with 1456 kg m^{-3} bulk density (d.b.), 400 kPa cone index and 17% moisture content, the viscosity was found to be 169 kPa.s and yield stress was 15.8 kPa. Simulations were carried out with these soil parameters.

5.5 Results and Discussion

The distribution of pressure over the surface of the tillage tool was investigated using computational methods considering the dynamic condition of tillage. Soil pressures on the tool is of interest for several reasons, including the power requirement to pull the implement, mechanical design of the tool with respect to size and shape and the state of soil conditions obtained from tool operation. The tool draft can be estimated by integrating the soil pressure on the tool surface.

Figure 5.3 shows the pressure distribution on the tool surface (50 mm x 100 mm) for four different tool operating speeds. The distortion of the top and bottom edge of the tool section is due to the free-surface simulations. Because of free-surface grid movements, the discretised tool conforms to the soil deformation pattern. The color fringe plots show that the pressure on the tool surface increases with tool operating speed. The maximum pressure on the tool surface increased from 250 kPa to 1240 kPa with increase in tool speed from 1 ms^{-1} to 10 ms^{-1}. The percentage increase of the maximum pressure on the tool for an increase in speed from 1 to 4, 4 to 7 and 7 to 10 ms^{-1} were 120, 67 and 35 % respectively. Thus the rate of increase in pressure decreases with speed. For low operating speed, the pressure concentration is at the tool bottom and it extends towards the tool upper sections with increase in tool speed.

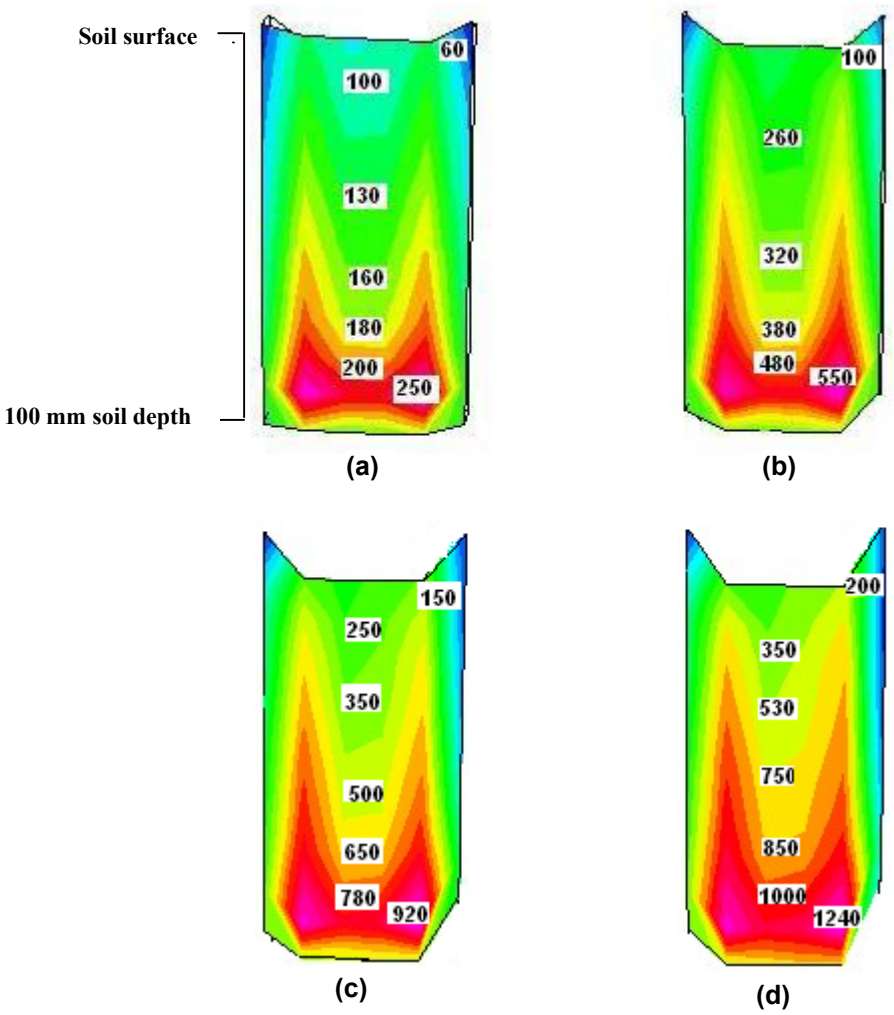

Figure 5.3 Pressure (kPa) distribution on the tool surface for different tool operating velocity; (a) 1 m s^{-1}, (b) 4 m s^{-1} (c) 7 m s^{-1} (d) 10 m s^{-1}.

Figures 5.4-5.7 show the pressure bulbs in front of the tool and the pattern of pressure distribution on the soil around the tool. The contour lines depict the range of pressure on a horizontal plane at half way below the soil surface i.e., at 50 mm depth. It is seen that the pressure around the tool increases with speed. The extent of soil disturbance can also be explained by this pressure distribution. Contour density increases with increase in speed. This indicates that at slow speed, soil fails creating some soil segments in terms of blocks and at higher velocities, the soil failure is like a flow failure with a high range of pressure distribution in the vicinity of the tool. The lateral soil disturbance is

also observed to increase with operating speed. It is clear that with increase in speed, the size of the pressure bulb increases up to some extent and then decreases.

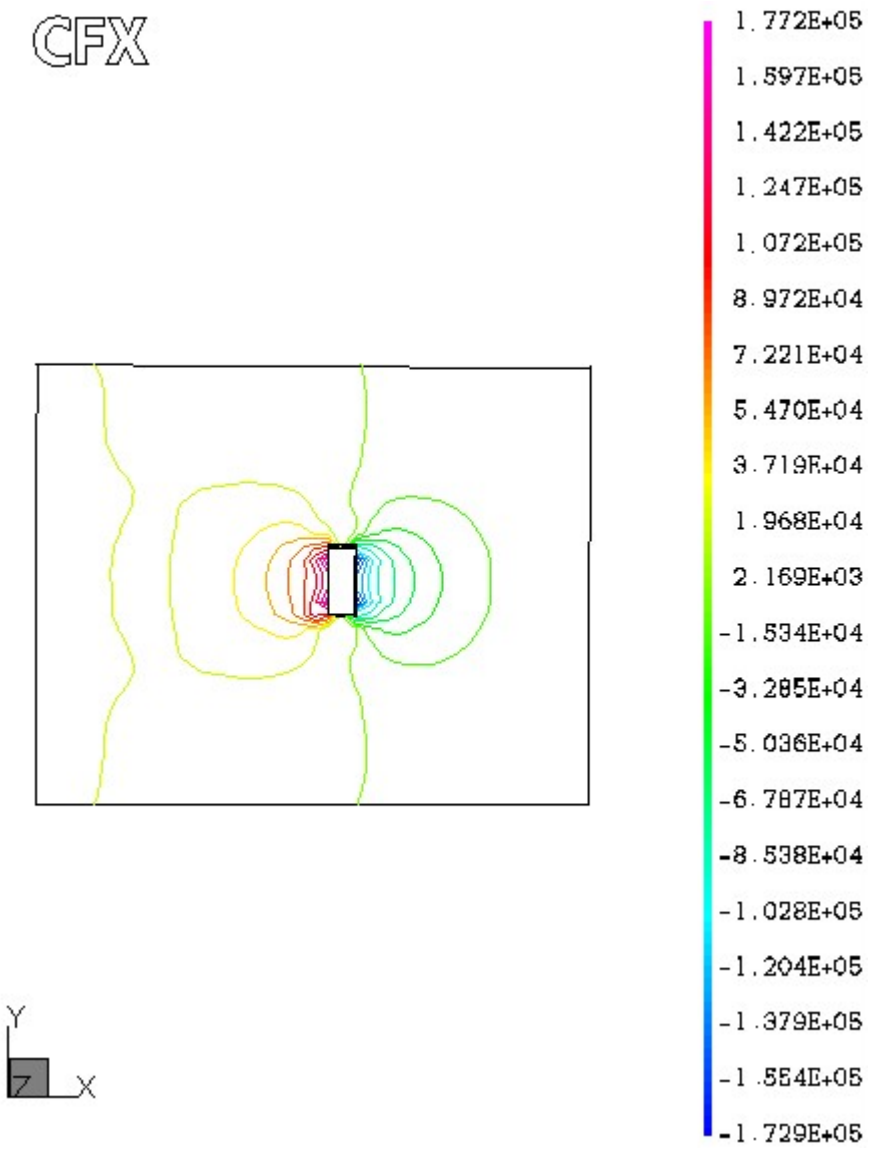

Figure 5.4 Pressure distribution (Pa) on the soil around the tool at tool speed of 1 m s^{-1}

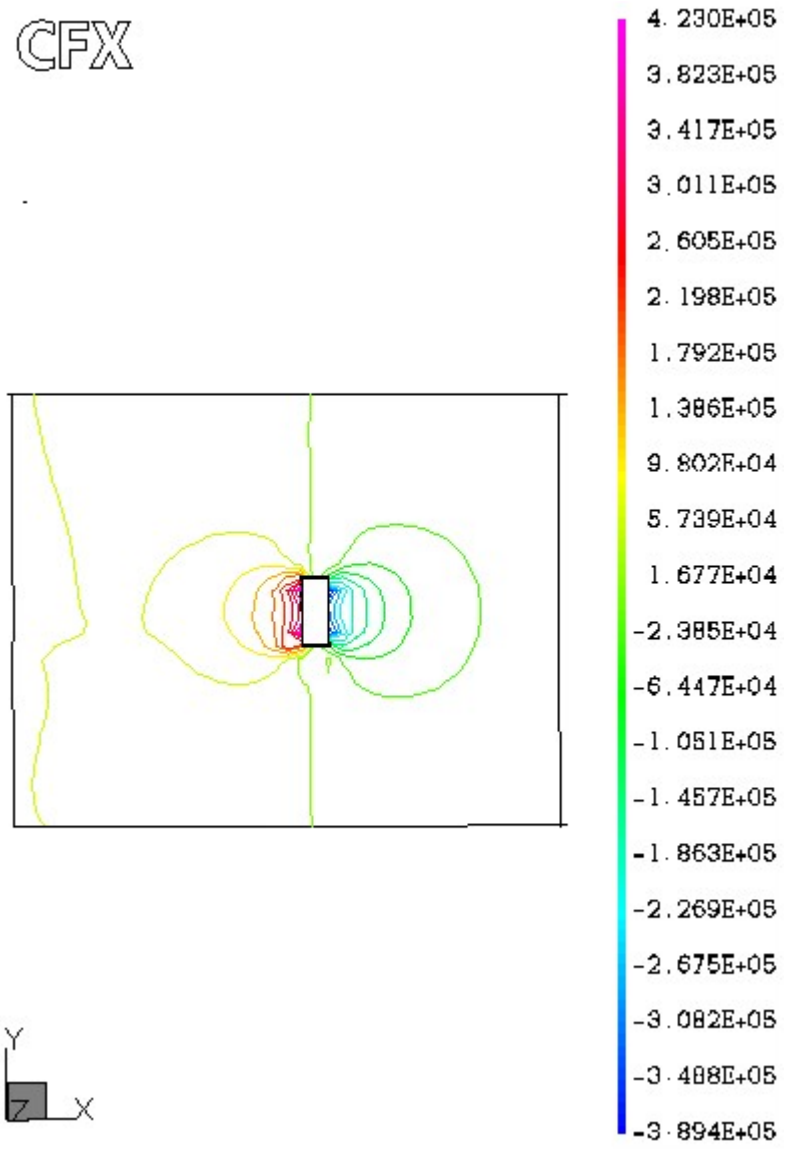

Figure 5.5 Pressure distribution (Pa) on the soil around the tool at tool speed of 4 m s^{-1}

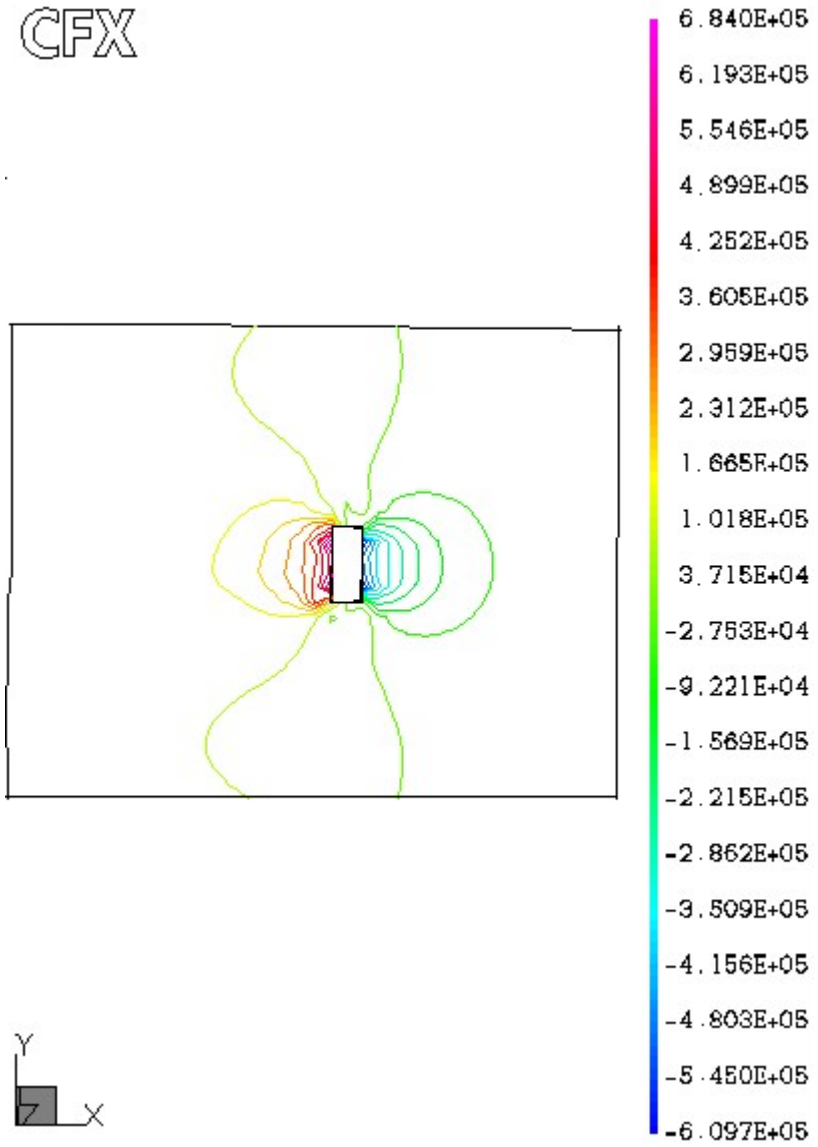

Figure 5.6 Pressure distribution (Pa) on the soil around the tool at tool speed of 7 m s^{-1}

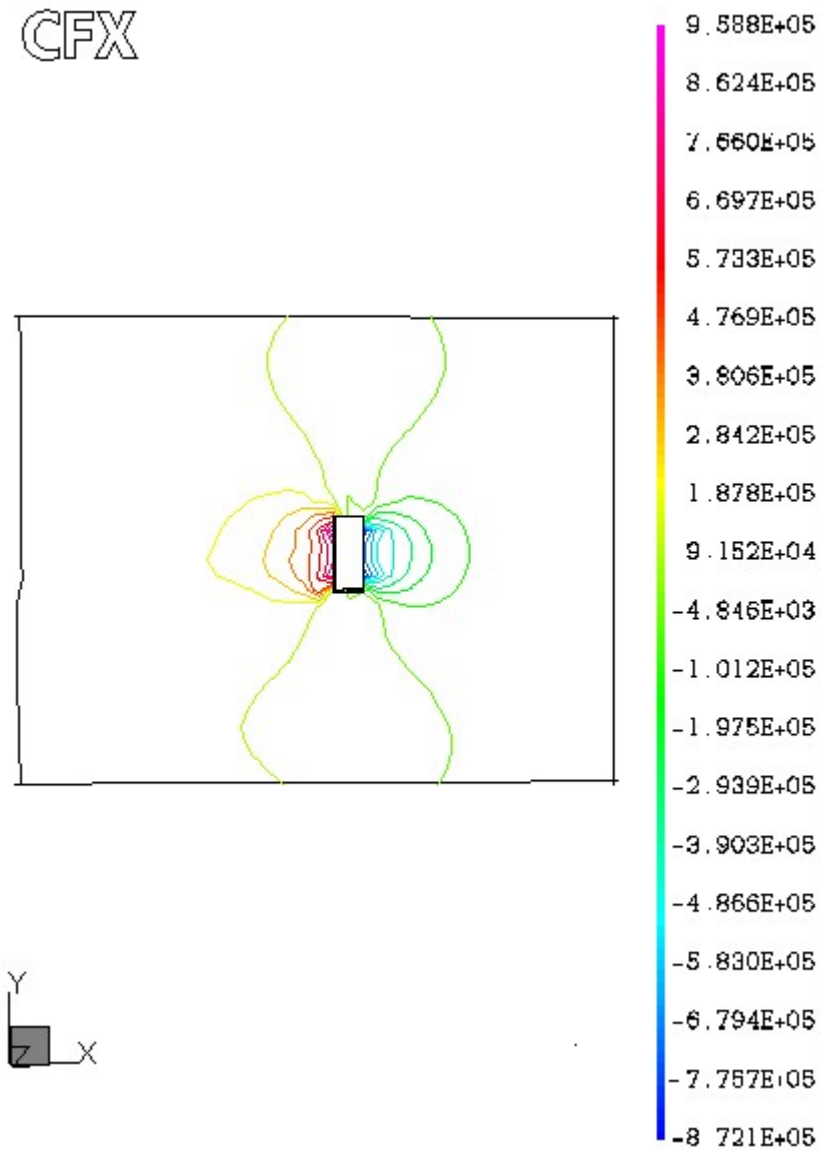

Figure 5.7 Pressure distribution (Pa) on the soil around the tool at tool speed of 10 m s^{-1}

The longitudinal expansion of the pressure contours determines the soil plastic failure zones. Soil flows as a fully developed visco-plastic material which is termed as plug flow. In the plug flow region, the shear stress is less than the yield stress. When this solid like flow approaches the tool, due to the influence of the tool, shear stress in the vicinity of the tool increases and it exceeds the soil yield stress. Soil then exhibits plastic flow with a yield surface demarcating the transition of the plug flow and plastic flow zone. The variation of the soil stress with respect to speed in front of the tool is

shown in Figure 5.8. The longitudinal distance of the pressure bulb does not increase after a certain speed or the rate of increase with speed decreases. This speed range can be termed as critical speed for high speed tillage.

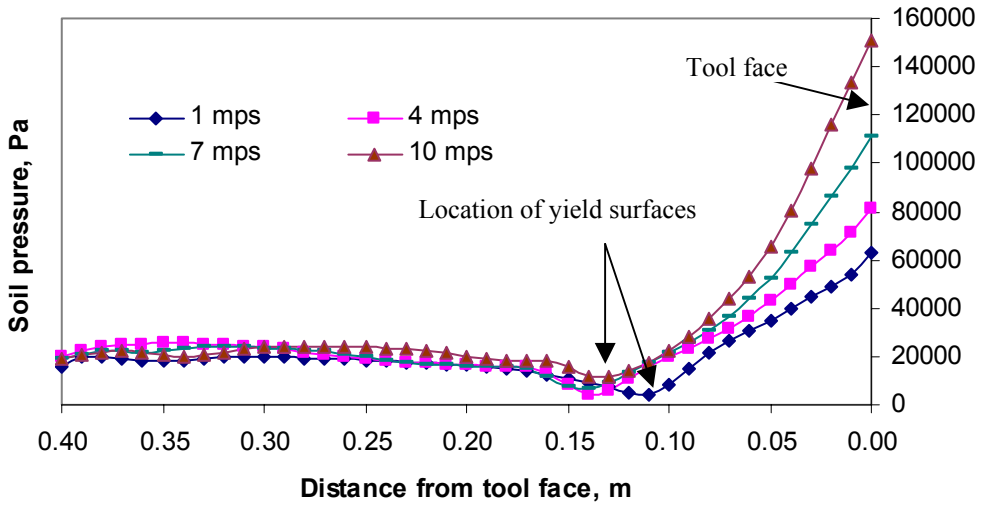

Figure 5.8 Location of yield surface at different tool speeds; (a) 1 m s^{-1}, (b) 4 m s^{-1} (c) 7 m s^{-1} (d) 10 m s^{-1}.

In the analytical modeling of soil-tool interaction, this pressure bulb was explained with the formation of three-dimensional failure crescents around the tool. Godwin and Spoor (1977) noted that the shape of soil failure crescents on the surface and to the sides of narrow blades was elliptical, but not very far from perfectly circular. This radius of the side crescents was called as rupture distance, which was equal to the total forward distance of soil failure on the surface from the tool face. From the perspective of a visco-plastic fluid flow, the rupture plane is termed as yield surface. The variation of the further most yield surface with respect to the operating velocity is shown in Figure 5.9. The distances where the plastic flow became the plug flow at a depth of 50 mm below the free-surface have been observed at the different speeds. The range of 4-6 m s^{-1} can be termed as the critical speed range where the rupture distance or the yield surface does not increase much with the increase of speed. This feature can be attributed to the face that as the velocity of the tool moving through the soil is increased, the zone of plastic deformation near the tool decreased (Hendrick and Gill, 1972). When the

velocity of the tool exceeds the velocity of the plastic deformation, soil compaction around and ahead of the tool may not occur.

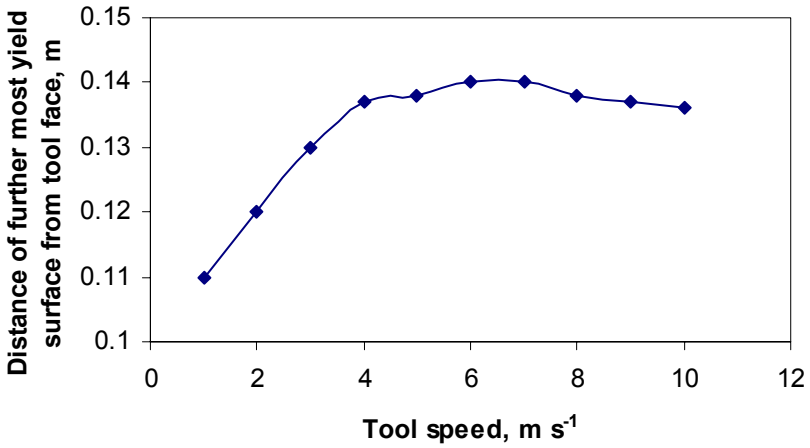

Figure 5.9 Effect of speed on the plastic failure zone.

Soil shear failure can be explained from the slip surfaces (internal rupture surfaces) generated due to the mechanical failure of soil. It has long been assumed in the analytical models of soil-tool interactions that a shear plane existed to run from the base of the tine to the soil surface ahead of the tine, meeting the soil surface at an angle of $(45\text{-}\phi/2)^{o}$. A succession of shear planes is formed as blocks of soil separate from the soil mass (Stafford, 1984). Figures 5.10-5.13 show the stress distribution on the soil near the tool face in the vertical plane. The color contours show the slip surfaces representing the soil shear failure planes or the rupture planes. It is observed that the shear failure lines start from the tool tip in log-spiral shape attesting the passive earth pressure theory of soil failure with tillage tool. The effect of operating speed in the soil failure pattern is also very interesting. Higher tool speed is accompanied by an increase in tool influence zone below the operating depth. The inclination of the rupture plane with horizontal also increases with operating speed. The free-surface grid movement with speed also distorted the shape of the tool. This phenomenon was inherent to the CFD software.

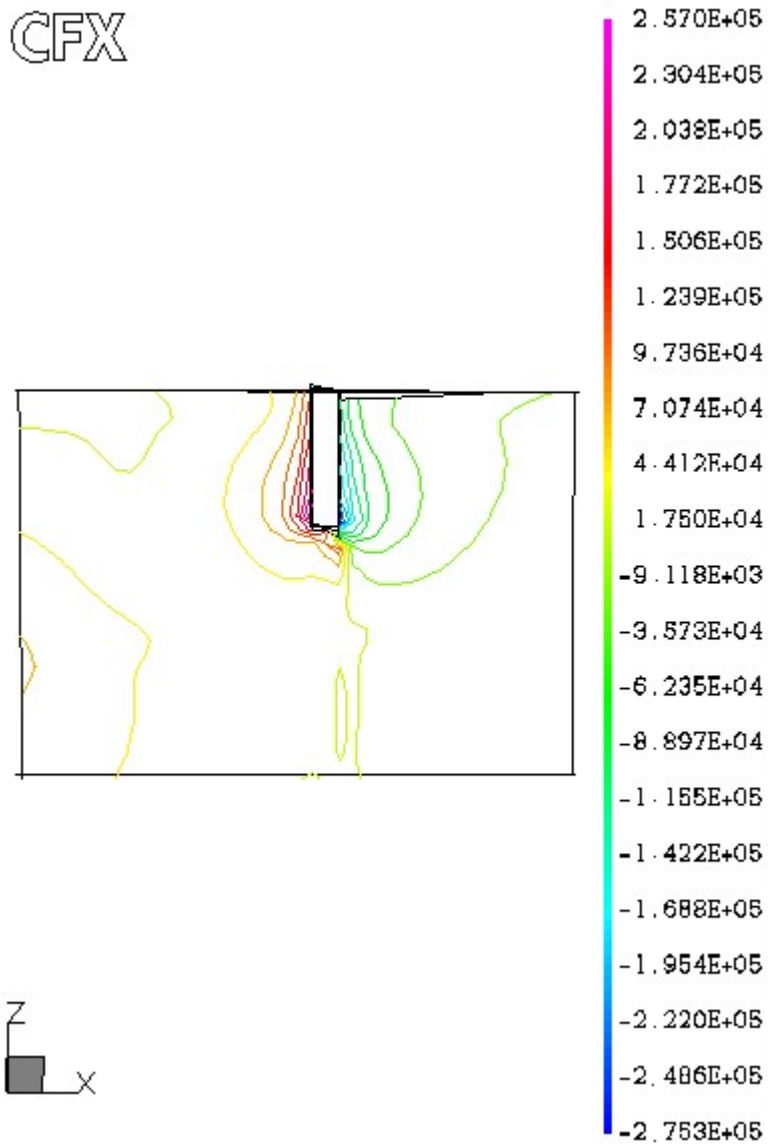

Figure 5.10 Pressure (Pa) contours on the vertical plane showing slip surfaces at tool operating speed of 1 m s^{-1}.

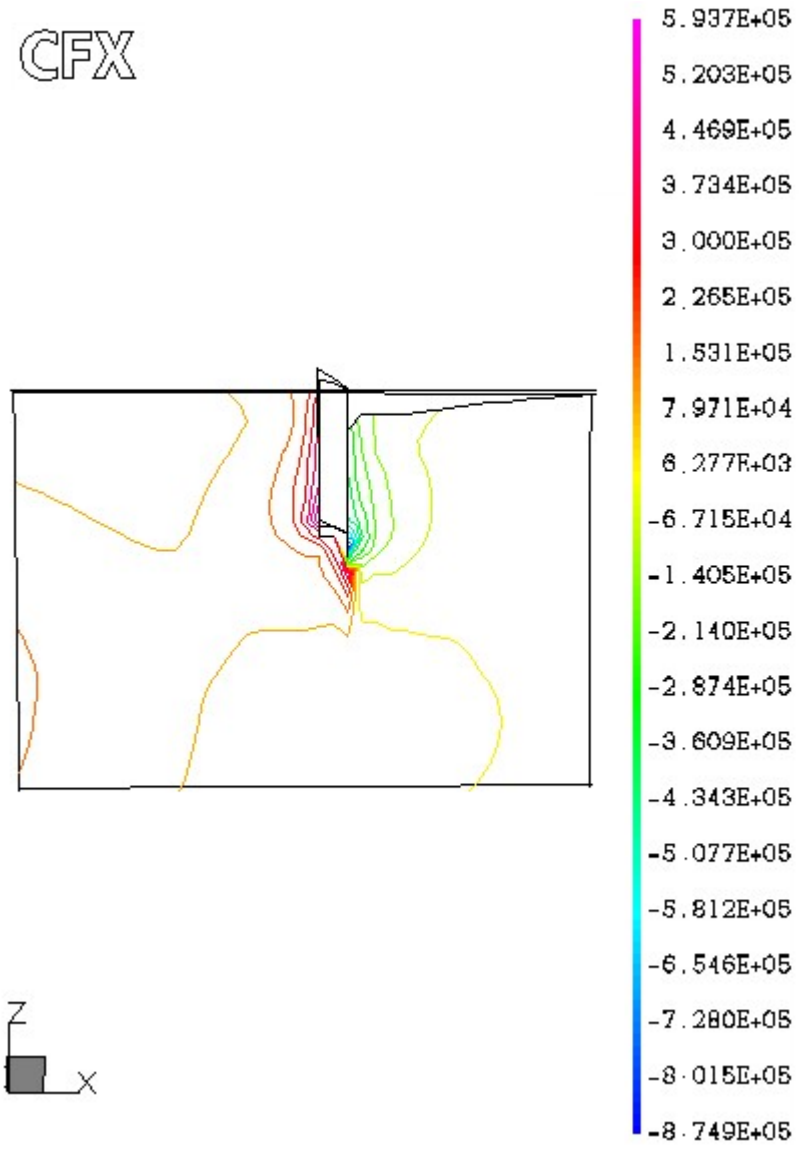

Figure 5.11 Pressure (Pa) contours on the vertical plane showing slip surfaces at tool operating speed of 4 m s^{-1}.

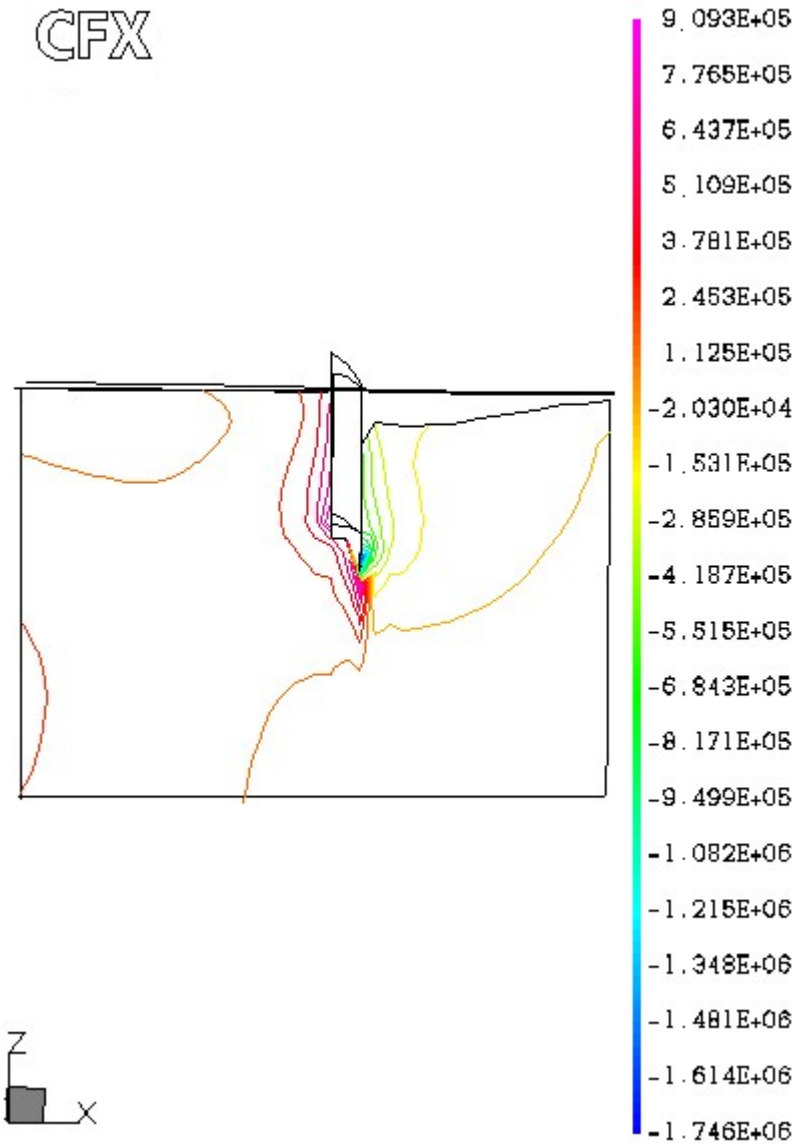

Figure 5.12 Pressure (Pa) contours on the vertical plane showing slip surfaces at tool operating speed of 7 m s^{-1}.

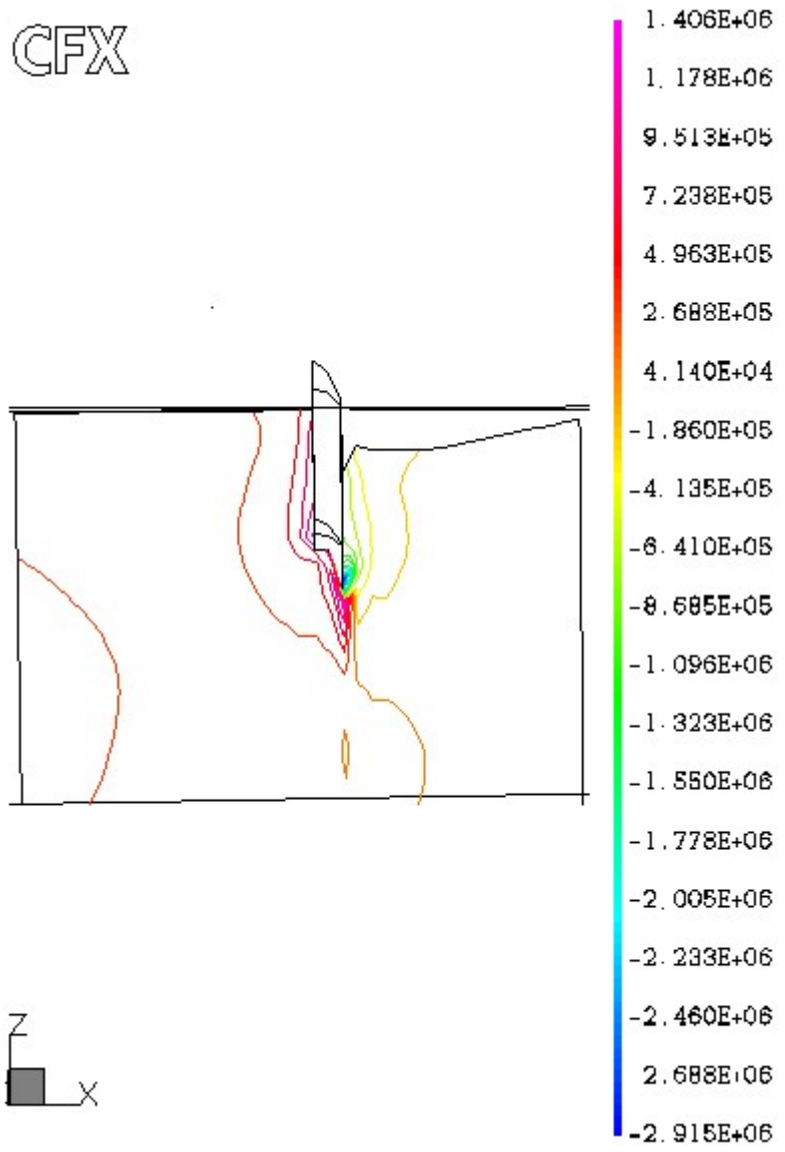

Figure 5.13 Pressure (Pa) contours on the vertical plane showing slip surfaces at tool operating speed of 10 m s^{-1}.

The total normal force exerted on the vertical blade can be considered as the draft of the tool. With the experimentally found soil parameters, the simulation results reveal that the draft of the tool increases with speed with a polynomial form having the square function of velocity (Fig. 5.14). The hypothesis of Hendrick and Gill (1973) that a critical speed exists where the energy requirement decreases with speed could not be supported by this numerical solution of the problem. However, it conforms with the

basic conception of tillage energy requirement that the draft is related to the square of velocity as was found by many other studies.

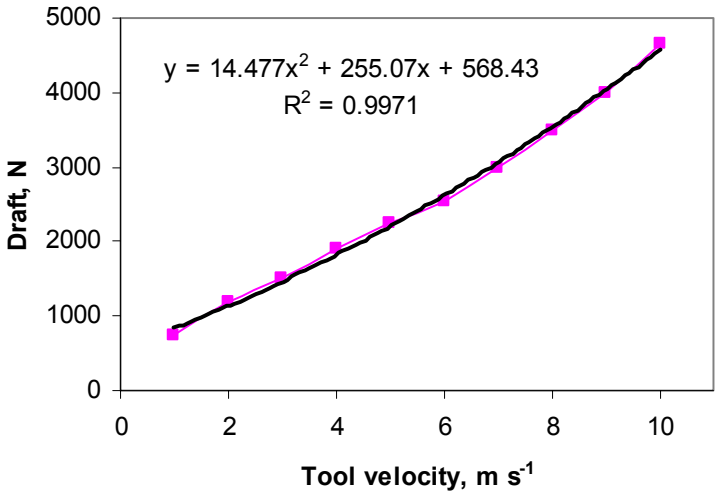

Figure 5.14 Variation of draft with speed.

Draft obtained from the present CFD simulations for a tool operating speed of 2 m s^{-1} and particular soil conditions was about 1100 N. For the same tool size (10 x 5 cm), Chi and Kushwaha (1993) found a draft force of 800 N from their FEM simulations. However, the operating speed was 0.7 m s^{-1}. Onwualu and Watts (1998) observed a tool draft of 900 N for a tool operating speed 2 m s^{-1} from their experimental analysis. Thus, the data obtained from CFD simulations seems to be realistic.

There is a speed range at which the direct relationship between draft and speed changes (Linke and Kushwaha, 1992). Since the draft equation standardized by ASAE (2003) is primarily for tillage tools operating at higher depths and no specific speed range has been mentioned with respect to the draft-speed relationship, the results obtained from the computational modeling could not be compared. The polynomial feature of this draft prediction needs to be verified with experimental data at high speed operation for shallow depth of tillage.

5.6 Comparison of CFD results with published data

5.6.1 Pressure distribution

Soil pressure exerted on the tool surface has been validated with the published results based on finite element analysis (FEM). Comparisons of the pressure patterns were realistic for similar tool shape, size and rake angles. Figure 5.8a shows the results of CFD simulations and Fig. 5.8b shows that of FEM simulations.

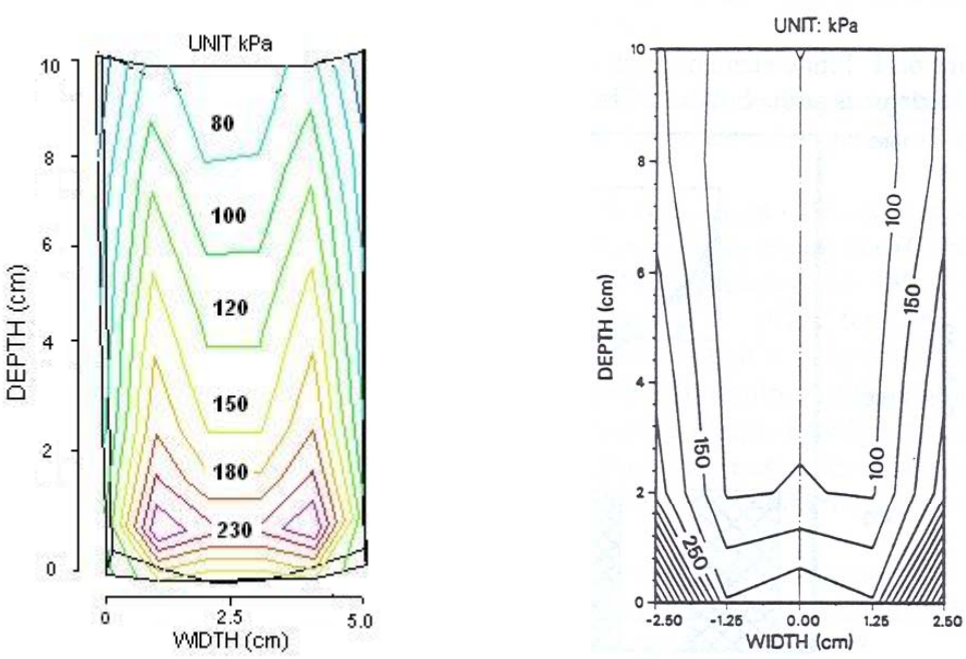

(a) (b)

Figure 5.15 Comparison of numerical modeling of pressure distribution on tool surface (a) results obtained by CFD modeling; (b) results by FEM modeling (Chi and Kushwaha, 1990).

Finite element modeling results represent the pressure contours on a tool surface (50x100 mm) with 90^{o} rake angle (vertical blade) for an operating velocity of 2 km h^{-1} (0.7 m s^{-1}). For comparison, CFD simulations were also carried out at a velocity of fully developed soil flow of 0.7 m s^{-1} with other parameters as stated in section 5.3.2.

In both the cases, high pressure zone lies at the tool bottom. Pressure at the tool tip centre by FEM (200-250 kPa) agrees very well with that of the CFD results (200-230 kPa). The variation in system parameters like soil conditions in these two numerical modeling can be attributed to the differences in the prediction models. FEM demonstrated pressure concentration at the bottom corners of the tool. However, CFD predictions for pressure concentration are at centre of the tool tip. During CFD modeling, the tool was considered stationary and soil was flowing. Thus, there was flow around the tool, which caused pressure drop due to flow past the tool and friction at the tool wall. This can be attributed to the shifting of the pressure concentration towards the tip centre of the tool.

5.6.2 Draft requirement

Total normal force on the tool surface is considered as the draft of the tool. In the comparison (section 5.6.1), FEM analysis resulted a draft of about 820 N, while CFD analysis predicted a draft of 740 N. When soil compressibility will be taken into account considering the pore spaces, predicted draft by CFD analysis will further reduce. It was anticipated, if the strength parameters were specified on the basis of triaxial compression test, an analysis using isotropic elasto-plastic soil model would result in an over prediction of the required tillage force (Karmakar et al., 2004). This is due to the fact that an anisotropic soil mobilizes shear strength in extension that is only about 50 to 60% of its shear strength in compression (Kulhawy and Mayne, 1990).

Variation of draft with tool depth is shown in Fig. 5.9. The comparison of the predicted draft variation with tool depth by CFD analysis is very close to that of the FEM analysis (Chi and Kushwaha. 1990). This is highly encouraging results of CFD analysis.

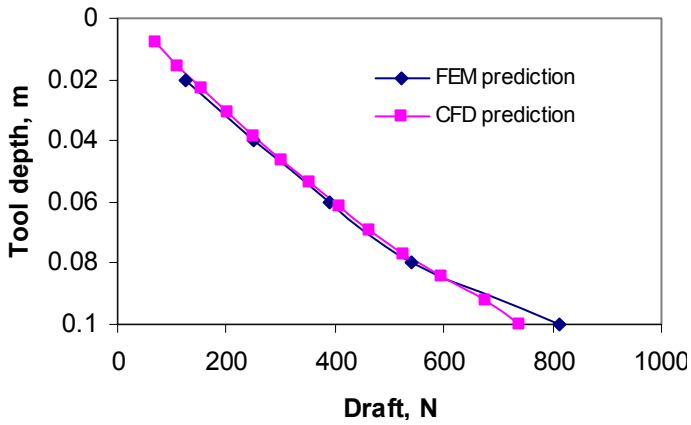

Figure 5.16 Comparison for draft variation with tool depth by FEM and CFD analysis.

5.7 Free surface simulations without free-surface grid movement

With an effort to avoid tool distortion, simulations were carried out without free-surface grid movement. Slip boundary conditions at the channel walls and the channel base were imposed to get rid off any influence of the side and bottom walls. Few results have been described in the following sections. Soil parameters and other modeling variables are same as described in section 5.4.3.

Figure 5.17 shows the axial velocity profile as a fringe plot taken at a depth of 50 mm from the free surface. The fully developed flow is influenced by the presence of the tool. However, sudden acceleration of the flow at the entrance region (Fig 4.11) has been avoided by imposing slip boundary condition at the channel wall and pressure boundary at the channel outlet, besides having the free surface condition at the top of the flow domain.

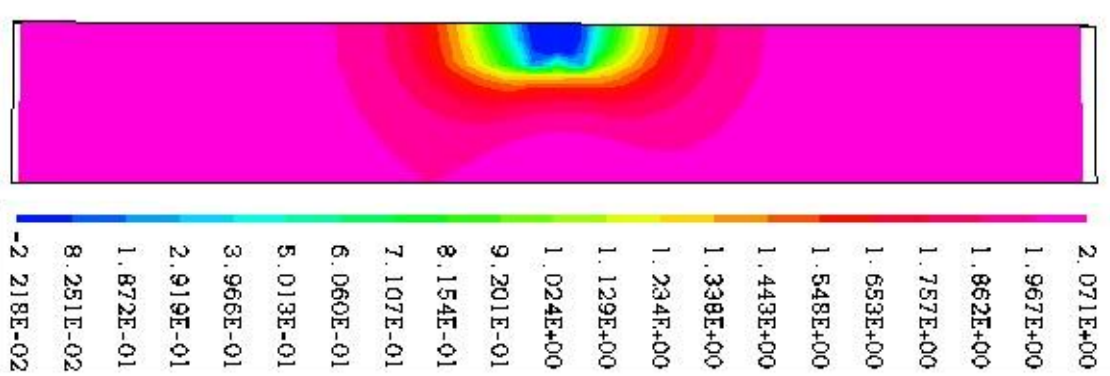

Figure 5.17 Fringe plot of axial velocity (m s^{-1}) at 50 mm depth along the flow channel.

Velocity distribution across the tool section in the flow domain is shown in Figure 5.18 for an inlet velocity of 2 m s^{-1}. The plastic flow region at the channel side walls and near the bottom (Figure 4.13) has been avoided. Thus, the influence of the walls of the flow domain is expected to be avoided.

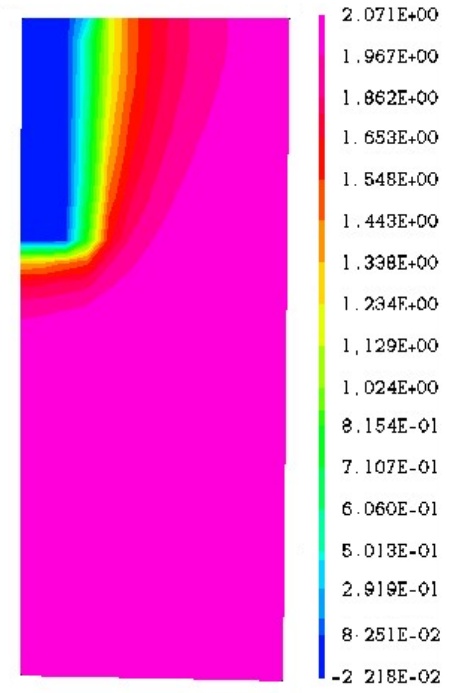

Figure 5.18 Fringe plot of axial velocity (m s^{-1}) at the tool section.

Figure 5.19 shows the contours of pressure distribution on the tool surface. It is observed that the maximum pressure for the tool speed of 0.7 ms^{-1} (2 km h^{-1}) is about 100 kPa. The pressure values are less than the corresponding predictions as shown in Figure 5.15 (a). This may be due to the changes in boundary conditions. Importantly, the tool distortion has been avoided by having no grid movement at the free surface.

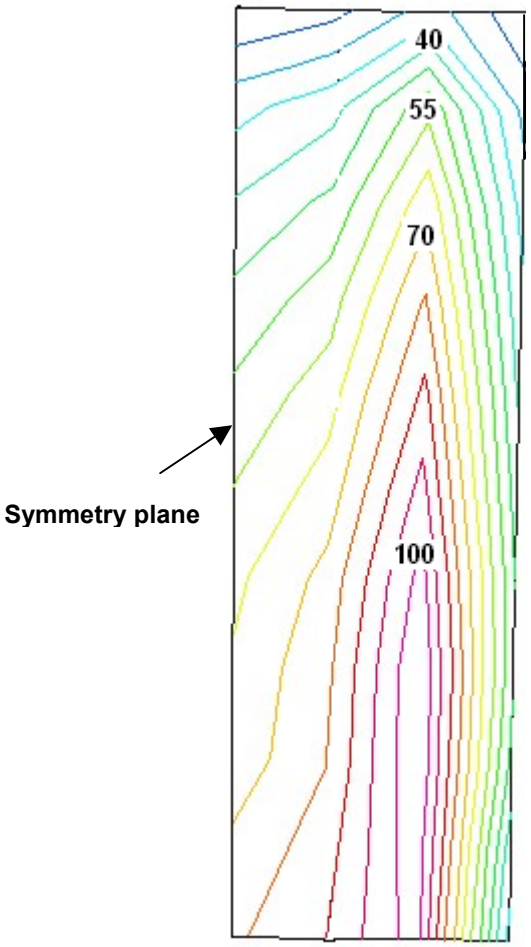

Figure 5.19 Pressure contours (kPa) for a tool speed of 0.7 m s^{-1} (2 km h^{-1}).

Variation of pressure distribution on the tool surface with tool operating speed has been shown in the Figures 5.20-5.23. Tool distortion as was observed in Fig. 5.3 has been avoided by imposing no grid movement at the free surface.

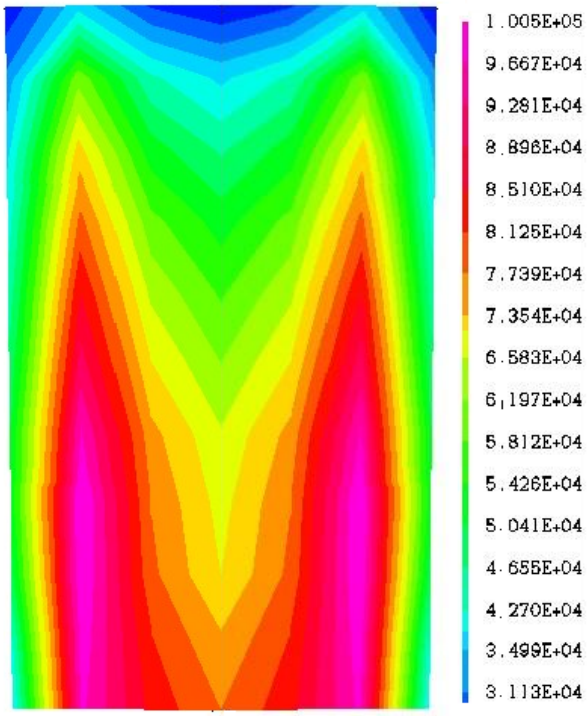

Figure 5.20 Pressure distribution (kPa) on the tool surface at a tool operating speed of 1 m s^{-1}.

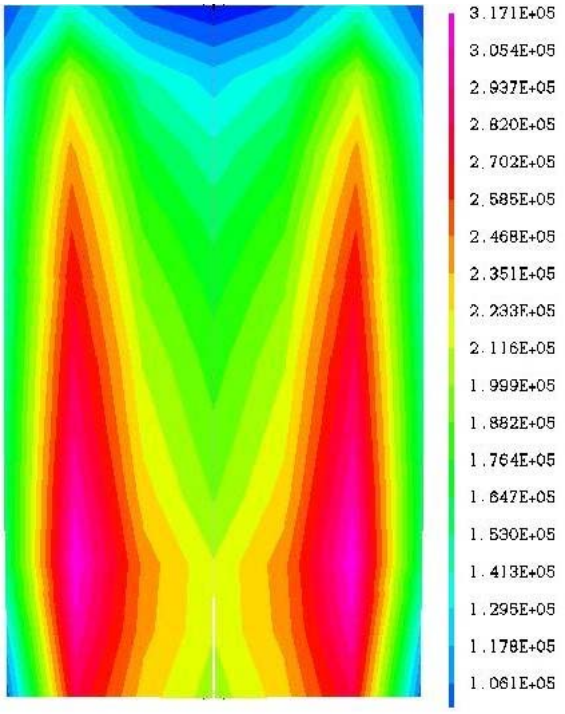

Figure 5.21 Pressure distribution (kPa) on the tool surface at a tool operating speed of 4 m s^{-1}.

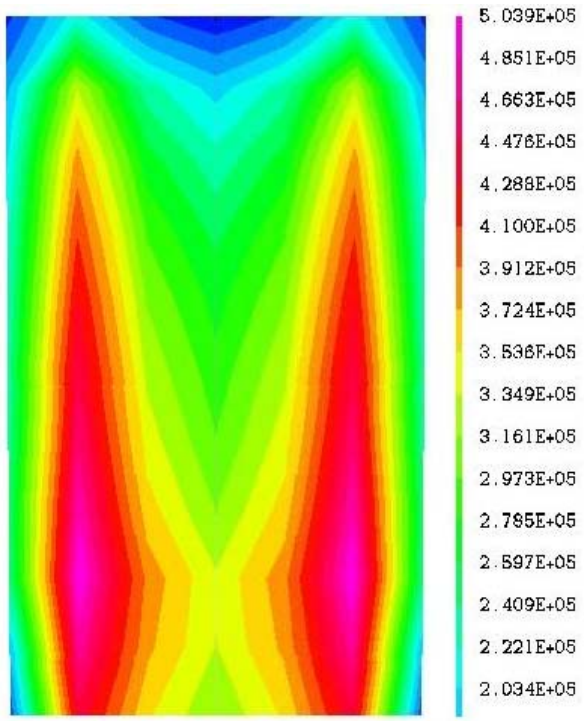

Figure 5.22 Pressure distribution (kPa) on the tool surface at a tool operating speed of 7 m s^{-1}.

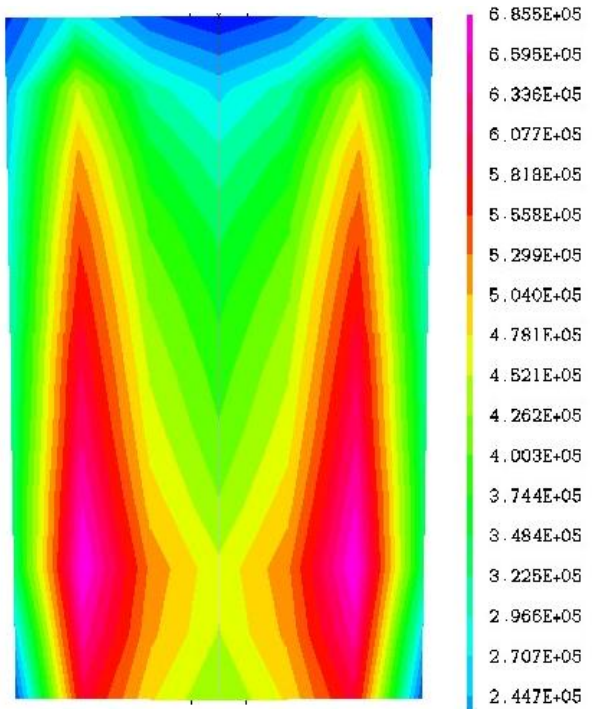

Figure 5.23 Pressure distribution (kPa) on the tool surface at a tool operating speed of 10 m s^{-1}.

With an attempt to check the effect of symmetry plane in the previous simulations, further simulations were carried out with the complete tool in the flow domain. Solution strategy was modified by improving the convergence of the solution with higher number of iterations and lower relaxation factors. However, the spike formation of the pressure pattern still existed as shown in Figure 5.24.

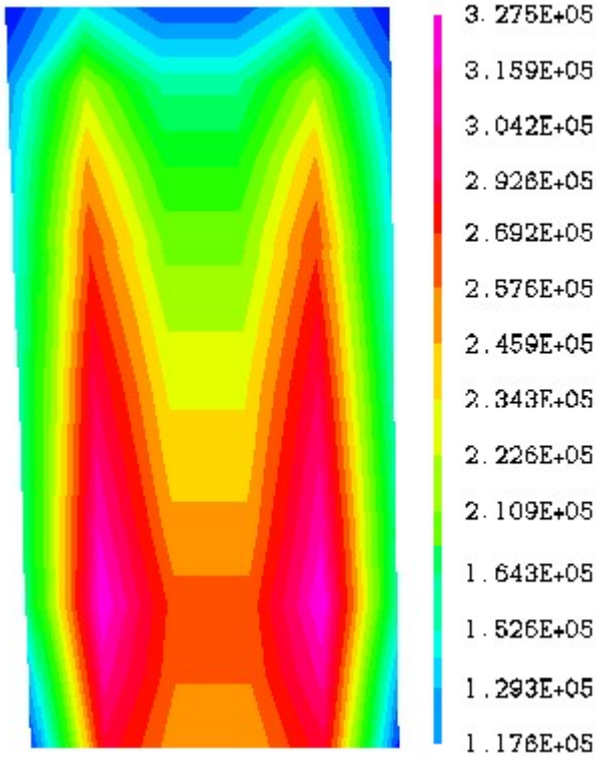

Figure 5.24 Pressure distribution (kPa) on the tool surface at a tool operating speed of 4 m s^{-1} (from simulations with the complete tool).

Draft for a tool speed of 0.7 m s^{-1} was found to be 564 N which is about 24% less than the previous predicted value for the same tool operating speed. Draft values obtained for five different tool operating speeds have been shown in Figure 5.25 as a comparison with the previous predictions.

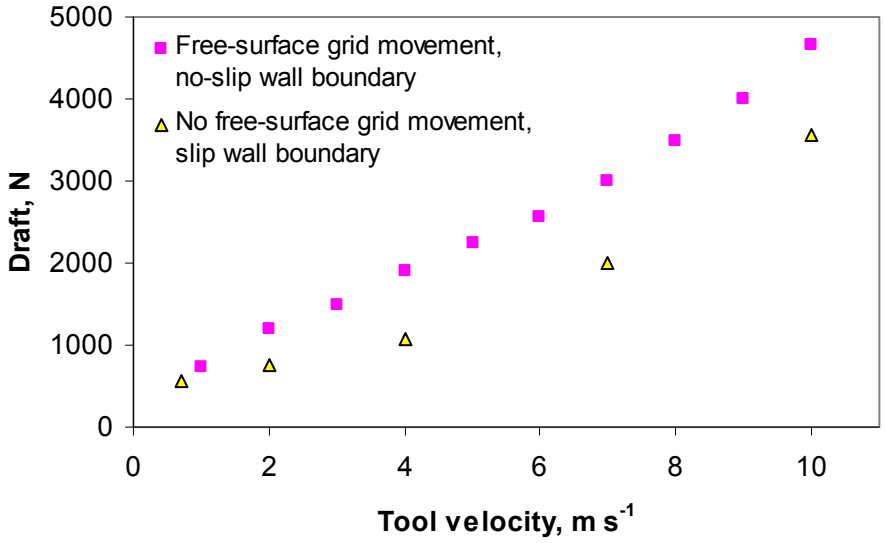

Figure 5.25 Variation of tool draft with speed.

5.8 Conclusions

Major findings obtained from this research can be summarized in the following points.

1. Soil pressure on the tool surface increased with speed. Rate of increase of pressure on the tool decreased with speed. Pressure concentration was highest at the tool tip; decreased towards the soil surface.
2. Pressure concentration extended over greater area on the tool surface with increase in tool speed.
3. The longitudinal distance of the pressure bulb from the tool face (yield surface) initially increased with speed and after a critical speed range of 4-6 m s^{-1}, it did not respond much to the increase in speed.

4. Soil failure front as observed from the location of the yield surfaces due to tool pressure on soil at different operating speed agrees with that obtained from the longitudinal velocity profile.
5. Draft was related as a square function of speed. No critical speed range was observed where draft ceases to increase with speed.
6. The comparison of tool draft and its variation with depth agreed very well with that of FEM modeling.
7. Tool distortion has been avoided by imposing no grid movement at the free surface. However, the soil surface deformation due to tool interaction with the formation of furrow behind the tool and soil build up in front of the tool have not been observed with no free surface grid movement. The modification of this solution approach along with the changed boundary conditions at the channel walls (two sides and one bottom) have resulted in reduction of soil pressure prediction over the tool surface.
8. Draft was found to reduce from the simulations with no free-surface grid movement and slip boundary conditions at the channel walls. The percent reductions were 37, 44, 33 and 24 for the tool operating speeds of 1, 4, 7 and 10 ms^{-1} respectively.

5.9 References

AEA Technologies. 2001. CFX Release 4.4 User Guide, CFX International, Harwell, Didcot, UK.

Al-Janobi, A. A. and S. A. Al-Suhaibani. 1998. Draft of primary tillage implements in sandy loam soil. Applied Eng Agric 14(4): 343-348.

ASAE D497. 2003. Agricultural Machinery Management Data,. St. Joseph, MI.: ASAE.

Chi, L. and R. L. Kushwaha. 1990. A non-linear 3-D finite element analysis of soil failure with tillage tools. J Terramech 27(4): 343-366.

Elijah, D. L. and J. A. Weber. 1971. Soil failure and pressure patterns for flat cutting blades. Tran ASAE 14(4): 781-785.

Godwin, R. J. and G. Spoor. 1977. Soil failure with narrow tines. J Agric Eng Res 22: 213-228.

Grisso, R. D. and J. V. Perumpral. 1981. Models for predicting narrow tillage tool behavior in soil: A review and comparison. ASAE Paper No. 811535. St. Joseph, MI.: ASAE.

Hendrick, J. G. and W. R. Gill. 1972. A critical soil deformation velocity. Proceedings of the conference on Rapid Penetration of Terrestrial Materials Feb. 1-3, Texas: Texas A &M University.

Hendrick, J. G. and W. R. Gill. 1973. Soil Reaction to High Speed Cutting. Trans ASAE 16(3): 401-403.

Hettiaratchi, D. R. P. and A. R. Reece. 1974. The calculation of passive soil resistance. Geotechnique 24(3): 289-310.

Kepner, R. A., R. Bainer and E. L. Barger. 1978. Principles of Farm Machinery. Third Edn. Westport, Connecticut: AVI Publishing Company, Inc.

Kulhawy, F.H. and P.W. Mayne. 1990. Manual on estimating soil properties. Report EL-6800, EPRI, California, USA.

Karmakar, S., J. Sharma and R. L. Kushwaha. 2004. Critical state elasto-plastic constitutive models for soil failure in tillage – A Review. Canadian Biosystems Eng 46: 2.19-2.23.

Kushwaha, R. L. and C. Linke. 1996. Draft-speed relationship of simple tillage tools at high operating speeds. Soil Tillage Res 39: 61-73.

Linke, C. and R. L. Kushwaha. 1992. High speed evaluation of draft with a vertical blade. ASAE Paper No. 921019. St. Joseph, MI.: ASAE.

Luth, H. J. and R. D. Wismer. 1969. Performance of plane soil cutting blades in sand. ASAE Paper No. 69-115. St. Joseph, MI.: ASAE.

Luth, H. J. and R. D. Wismer. 1971. Performance of plane soil cutting blades in sand. Trans. ASAE 1(1): 255-260.

Onwualu, A. P. and K. C. Watts. Draught and vertical forces obtained from dynamic soil cutting by plane tillage tools. Soil & Tillage Res., 48: 239-253.

Payne, P. C. J. 1956. The relationship between the mechanical properties of soil and the performance of simple cultivation implements. J. Agric Eng Res 1(1): 23-50.

Perumpral, J. V., R. D. Grisso and C. S. Desai. 1983. A soil-tool model based on limit equilibrium analysis. Trans ASAE 26(4): 991-995.

Rowe, R. J. and K. K. Barnes. 1961. Influence of speed on elements of draft of a tillage tool. Trans ASAE 4: 55-63.

Stafford, J. V. 1979. The performance of a rigid tine in relation to soil properties and speed. J Agric Eng Res 24: 41-56.

Stafford, J. V. 1984. Force prediction models for brittle and flow failure of soil by draught tillage tools. J Agric Eng Res 29: 51-60.

Stafford, J. V. and D. W. Tanner. 1976. An investigation into the effect of speed on the draught requirements of a chisel tine. Paper No. 40. Wageningen The Netherlands: ISTRO.

Summers, J. D., A. Khalilian and D. G. Batchelder. 1986. Draft relationships for primary tillage in Oklahoma soils. Trans ASAE 29(1): 37-39.

Wismer, R. D. and H. J. Luth. 1970. Performance of plane soil cutting blades in a clay. Trans ASAE 15(2):211-216.

Zelenin, A. N. 1950. Basic Physics of the Theory of Soil Cutting. Moscow, Russia: Kolos.

Chapter 6

Summary and Conclusions

This chapter regroups the conclusions of chapters 2 through 5 of the thesis. Chapter 1 was an introductory work focusing on the mechanics of soil tillage and brief review of soil-tool modeling approaches towards project formulations. Specific chapter wise conclusions have been summarised in the following sections.

6.1 Chapter 2

Chapter 2 was associated to the objective 1 of the thesis and was dedicated to a case study on soil crack propagation related to the soil failure front, review work on soil-tool modeling and features of large soil deformation with respect to soil rheology.

From the case study, following specific conclusions have been drawn:

1. Features of soil crack development and propagation indicated the nonlinear characteristics of soil.
2. Shallower depth of operation caused short and intermittent soil crack propagation with lower growth rate.
3. The growth rate or the acceleration of the crack propagation followed a sinusoidal response.
4. Longitudinal component of a crack had higher displacement and growth rate than the lateral component during the deformation process.

5. Soil cracks indicated four distinct phases: as, ‘soil compression’ or elastic failure, ‘crack initiation’, ‘crack propagation’ or crack growth, and ‘particle retardation’ or plastic failure (post-tilling phase).

In second part of Chapter 2, several elasto-plastic soil constitutive models for possible use in the soil-tool interaction have been reviewed. It was concluded that certain key aspects such as strain-dependent stiffness and strength as well as anisotropy should be considered in order to obtain significant results from such analyses, though it is a daunting task to model all aspects of soil behavior when analyzing tillage.

The last part of Chapter 2 was focused on the review of different tillage tool modeling approaches to solve problems in the area of soil-tool interaction and failure mechanism. So far, five major methods, namely empirical and semi-empirical, dimensional analysis, finite element method, discrete or distinct element method and artificial neural network have been used. The limitations of the constitutive relations in numerical modeling of dynamic soil-tool interactions have been pointed out. From the discussion of soil rheology and fluid flow features, it was clear that soil could be considered as a visco-plastic material and its mechanical behavior during tillage can be studied from a fluid flow perspective with non-Newtonian flow behavior. It was concluded that computational fluid dynamics (CFD) should be applied to analyze the dynamic soil-tool interaction considering the visco-plastic nature of soil from its rheological behavior.

6.2 Chapter 3

Chapter 3 was related to the objective 2 of the research project and was dedicated to the development and testing of the soil rheometer to evaluate dynamic soil parameters required for CFD simulations (objectives 3 and 4).

The soil rheometer worked on the principle of torsional shear applied to a standard vane with controlled strain rate. Specific results from soil test can be concluded as:

1. The developed soil rheometer was successfully able to produce soil visco-plastic parameters.
2. The values of viscosity of the clay loam soil were found to spread in the range of $53x10^3$ to $28x10^4$ Pa.s. Increasing moisture content was accompanied by a decreasing viscosity.
3. Soil viscosity was highly affected by the compaction levels for all the moisture contents. Increase in soil compaction was accompanied by a sharp increase in soil viscosity.
4. Yield stress has been found to decrease with increasing moisture content. Yield stress increased with soil compaction for all the levels of moisture content. There was a steep increase in yield stress when the compaction level was increased from 300 kPa to 400 kPa. The moisture content of 17% (d.b) was found to have a reduced viscosity and yield stress. There was no effect for an increase of compaction from 150 to 200 kPa.

6.3 Chapter 4

Chapter 4 was associated with objective 3 and was dedicated to the CFD simulations of soil flow and the analysis of tool influence in the soil-flow domain using the soil parameters obtained in chapter 3. Major findings can be concluded as:

1. Soil characterization as a Bingham model successfully depicted soil visco-plastic failure with respect to the formation of plastic and plug regions in the flow domain.
2. The longitudinal distance of the soil failure front from the tool face for a 50 mm wide tool operating at 6 m s^{-1} was found to be about 160 mm.
3. Soil failure front has been related to the velocity profile of the flow. The prediction can be further improved and compared when the tool influence would be related to displacement vector of the visco-plastic flow.
4. The critical speed range was found to be in the range of 5 to 6.5 m s^{-1}.
5. Dynamic analysis of soil-tool interaction in a conduit enabled visualization of the visco-plastic soil flow phenomena.

6. Free-surface simulation improved the prediction and description of the dynamics of soil-tool interaction.

6.4 Chapter 5

Chapter 5 was related to objective 4 of the thesis. It focused on the investigation of pressure distribution over the surface of a flat tillage tool. Specific results can be concluded as:

1. Soil pressure on the tool surface increases with speed. Rate of increase of pressure on the tool increases with speed. Pressure concentration was highest at the tool tip; it decreased towards the soil surface.
2. Pressure concentration extended over greater area on the tool surface with increase in tool speed. The maximum pressure on the tool surface (50 mm x 100 mm) increased from 115 kPa to 175 kPa with increase in tool speed from 1 ms^{-1} to 10 ms^{-1}. Pressure distribution agreed well with that of finite element analysis.
3. The longitudinal distance of the pressure bulb from the tool face (yield surface) initially increased with speed and after a critical speed range of 4-6 m s^{-1}, it did not respond much to the increase in speed.
4. Draft was related as a square function of speed. No critical speed range was observed where draft ceases to increase with speed.
5. Tool distortion has been avoided by imposing no grid movement at the free surface. However, the soil surface deformation due to tool interaction with the formation of furrow behind the tool and soil build up in front of the tool have not been observed with no free surface grid movement. The modification of this solution approach along with the changed boundary conditions at the channel walls (two sides and one bottom) have resulted in reduction of soil pressure prediction over the tool surface.
6. Draft was found to reduce from the simulations with no free-surface grid movement and slip boundary conditions at the channel walls. The percent reductions were 37, 44, 33 and 24 for the tool operating speeds of 1, 4, 7 and 10 ms^{-1} respectively.

Chapter 7

Contribution and Recommendations

7.1 Contributions

The contributions of this research to engineering knowledge can be stated in two major aspects. Firstly design and development of a unique apparatus to determine soil visco-plastic parameters and, secondly, analysis of tillage dynamics using fluid flow approach.

Soil Rheometer: A soil rheometer was developed and used to determine soil yield stress and viscosity according to the ASTM (ASTM 2004 D2573-01) standard. For the clay loam soil (29% clay, 24% silt and 47% sand) used in the experiment, the range of values for yield stress was 4 to 23 kPa and that for viscosity was $53x10^3$ to $28x10^4$ Pa.s. This apparatus could also be used for measuring dynamic soil parameters for civil and geotechnical engineering problems associated with land slides, excavation etc.

CFD Applications: This is the first known attempt of numerical analysis of tillage process using computational fluid dynamics modeling. The results of simulation revealed the behavior of soil failure front with respect to operating speed that would be an important aspect for tillage tool design. Critical speed range of soil failure front was in agreement with two published literatures based on experimental and numerical study. Another aspect of the CFD modeling was the analysis of draft requirement. Comparison of soil pressure on tool and resulting draft were very close to the published data based on finite element modeling. Since CFD predictions were in good agreement with published data, it indicates that computational fluid dynamics has great potential for in depth study of soil-tool interaction.

7.2 Limitations of the current CFD modeling

The main objective of this research was to investigate the possibility of the application of computational fluid dynamics to soil-tool interaction for dynamic analysis of tillage. The results demonstrated it positively. However, from fluid dynamics point of view, following limitations have been experienced:

1. Due to the very low Reynolds' Number < 10^{-01}, the flow pattern that was assumed to be laminar would better be observed as a pressure driven creeping flow. This however is unrealistic for very fast moving soil.
2. Due to the very high viscosity, flow analysis which assumes conventional relationships of Reynolds number for boundary layer thickness etc does not give intuitively correct results.
3. Displacement vector and shear stress profiles were not determined with the solution approach applied in this study.
4. CFD assumes no density change (either compaction or loosening). Although viscosity is seen to be a high function of compaction, this is ignored in this first attempt.
5. Only viscous failure is assumed. (p 36)
6. The scale of motion (p 40) seen in turbulent flow and in soil failure patterns is not seen in this CFD simulation.
7. The normal force is ignored in the pressure calculations.
8. The drag force is ignored in the draft computations.
9. Other physical properties (internal friction) of the soil (p 51) have not been considered in CFD simulations for analyzing soil movement.

7.3 Recommendations for future research

Further research can be conducted on the following areas as an extension to this project:

1. Rheological properties of soil should be measured for different soil physical conditions and soil types. These visco-plastic properties may be grouped based on soil types and their physical parameters.

2. The developed rheometer can also be used for measuring visco-plastic parameters of slurry, mixed fertilizers and bio-materials and manure products with high density that can not be tested with the currently available rheometer for low range viscosity or by direct shear tests accurately.

3. Simulations have been conducted considering the soil as a single continuous phase incompressible medium. Further study should be conducted on the compressible soil considering the pore spaces at different soil conditions.

4. Soil failure front related to the tool influence zone needs to be investigated with respect to displacement vector and shear stress profile in the flow domain.

5. Some criteria analogous to Reynolds number, based on viscosity range, are expected to address change in state of soil due to tool interaction. Sensitivity studies need to be conducted on the effect of soil visco-plastic parameters on soil failure front, soil furrow formation and energy requirement.

6. Study need to be conducted for soil deformation pattern and force prediction with different rake angles of the tool and with different shapes of the tool. Dynamic analysis of tillage for an implement with multiple tines for optimization of soil disturbance with the perspective of conservation tillage should also be investigated.

List of Appendices

Appendix A

Complete shearing curve as an extension of Figure 3.13

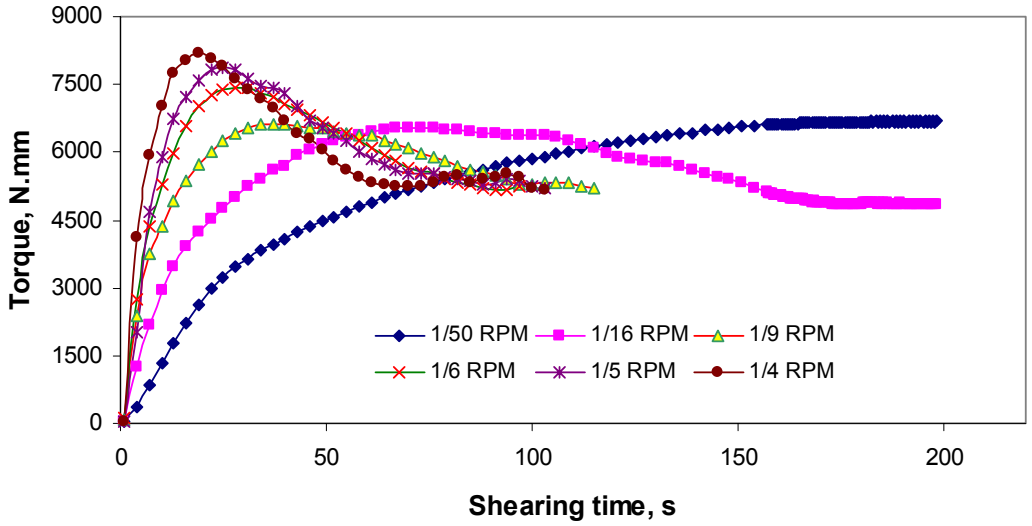

Shearing curve at different shearing rates for 300 kPa soil compaction at 17% moisture content showing peak and residual soil strength occurring at different time span.

Appendix B

Typical CFX 4.4 program samples

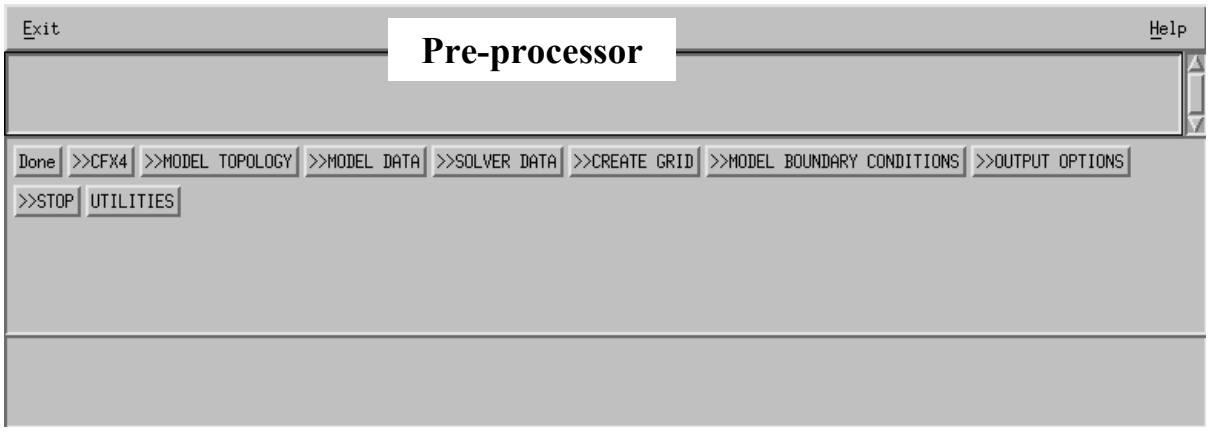

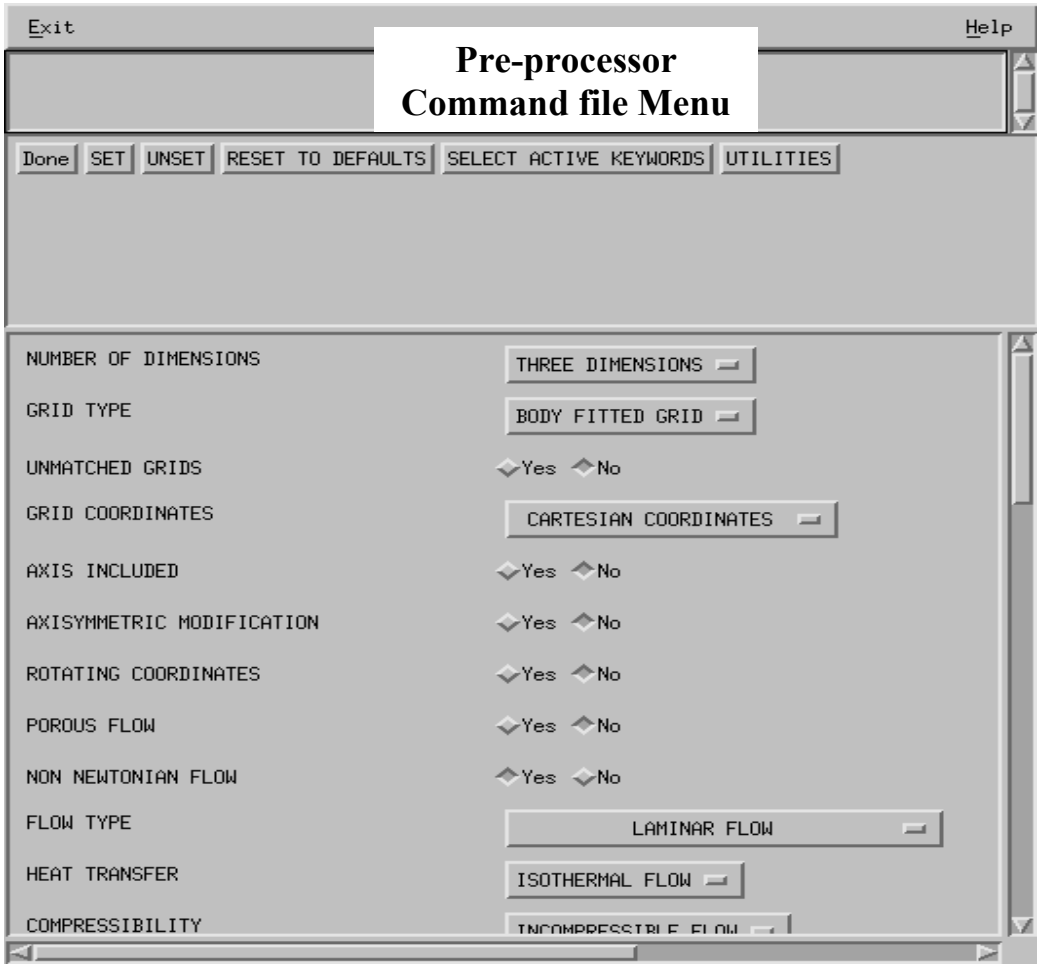

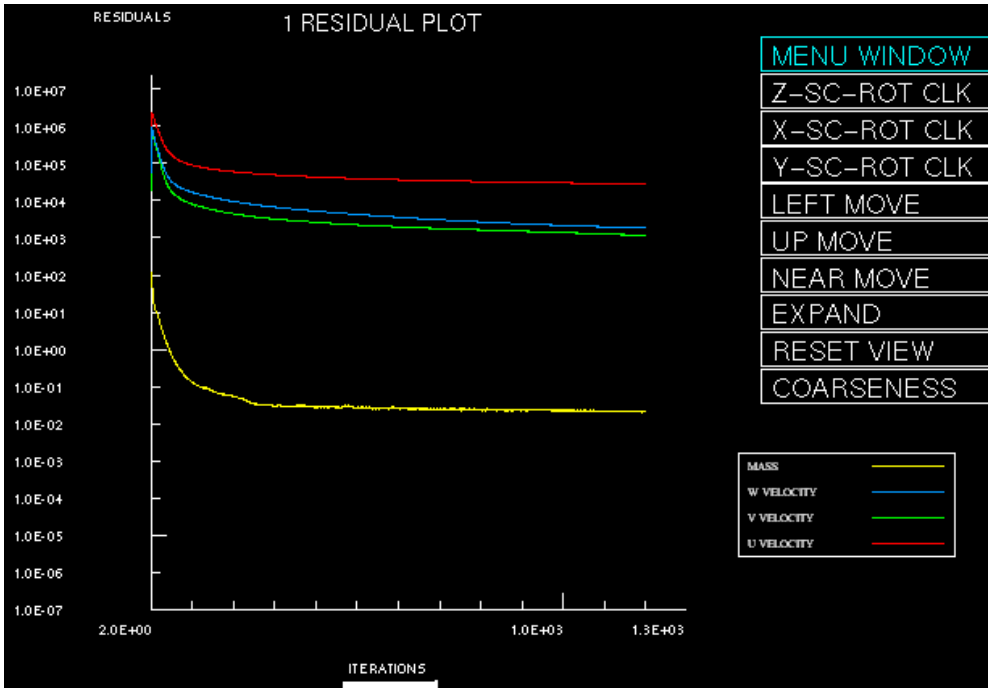

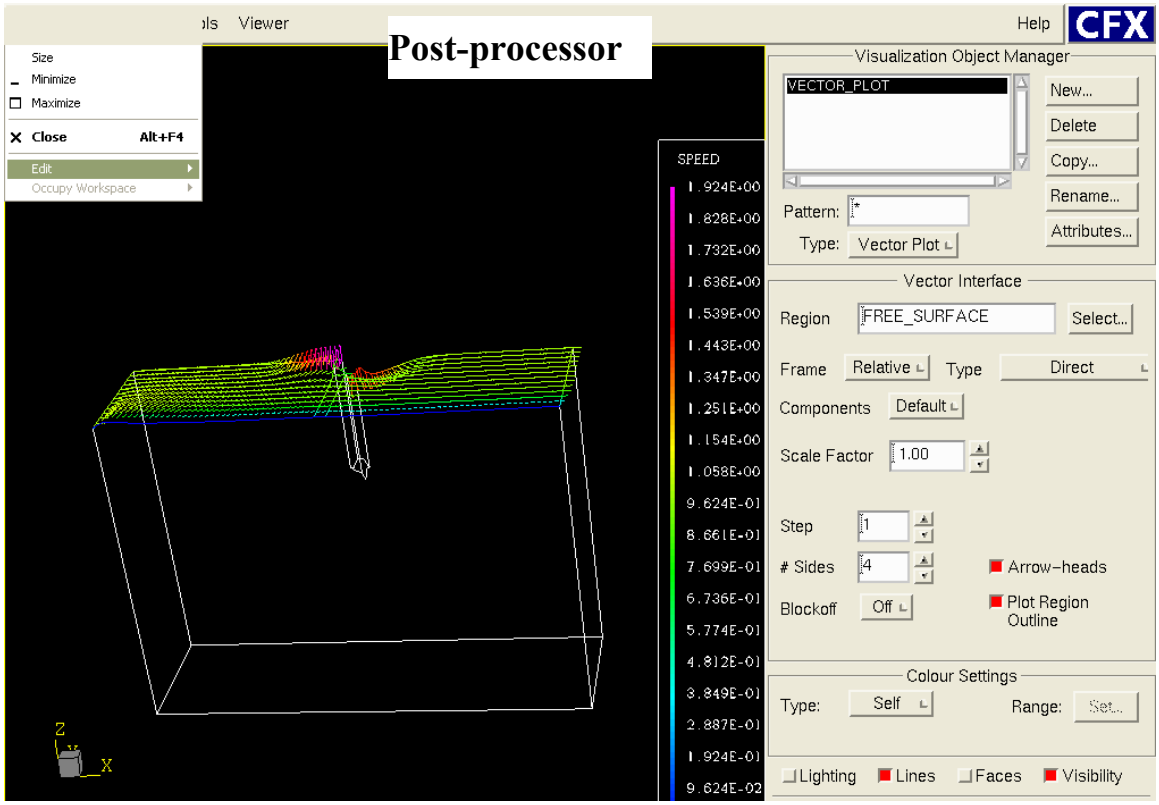

Free-surface simulation showing soil surface deformation due to tool interaction

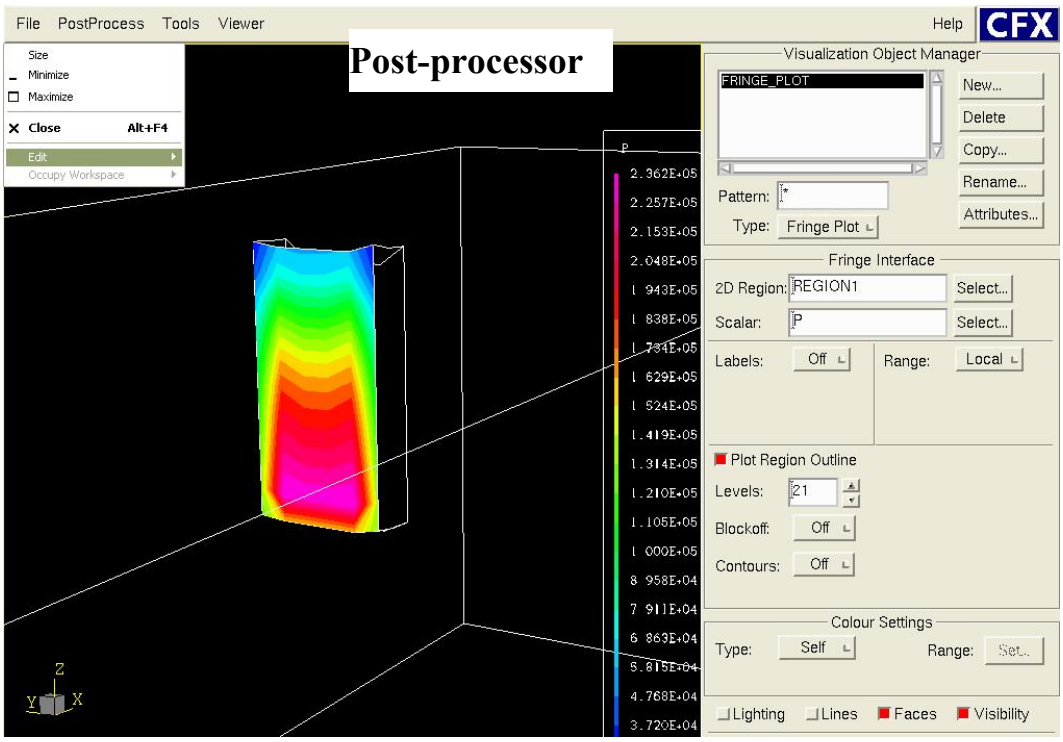

Pressure distribution on the tool surface

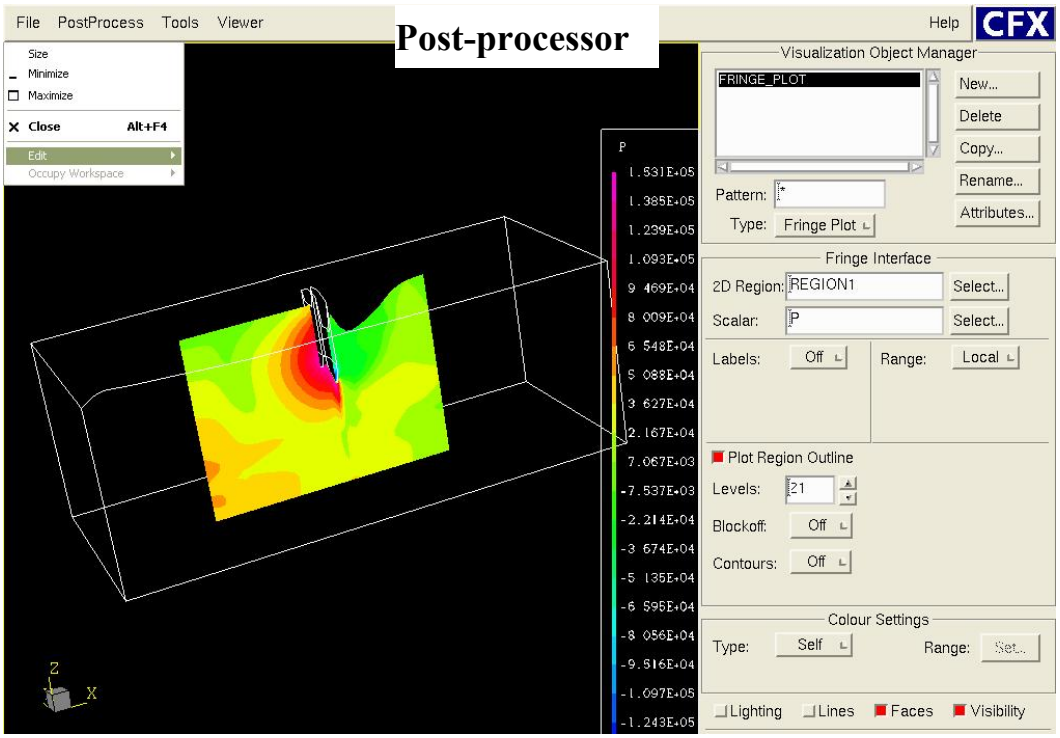

Stress pattern on soil due to advancing tool

Appendix C

Typical data obtained from the Soil Rheometer.

DURATION		TORQUE
HOUR	SECOND	N-cm
1240	56	2.282
1240	56.5	61.89
1240	57	149.3
1240	57.5	232.4
1240	58	308.2
1240	58.5	366.8
1240	59	412.4
1240	59.5	453.6
1241	0	488.1
1241	0.5	519.1
1241	1	546.8
1241	1.5	572.2
1241	2	595.2
1241	2.5	617
1241	3	636.7
1241	3.5	653.1
1241	4	670.4
1241	4.5	687.3
1241	5	704
1241	5.5	718
1241	6	733
1241	6.5	744
1241	7	754
1241	7.5	766
1241	8	773
1241	8.5	781
1241	9	787
1241	9.5	793
1241	10	796
1241	10.5	800
1241	11	804
1241	11.5	810
1241	12	814
1241	12.5	817
1241	13	818
1241	13.5	819
1241	14	819
1241	14.5	817
1241	15	818
1241	15.5	816
1241	16	815
1241	16.5	811
1241	17	807
1241	17.5	805
1241	18	801
1241	18.5	798
1241	19	796
1241	19.5	794
1241	20	790
1241	20.5	785
1241	21	780
1241	21.5	775
1241	22	770
1241	22.5	765
1241	23	762
1241	23.5	757
1241	24	754
1241	24.5	752
1241	25	749
1241	25.5	745
1241	26	740
1241	26.5	733
1241	27	728
1241	27.5	725
1241	28	722
1241	28.5	720
1241	29	717
1241	29.5	716
1241	30	713
1241	30.5	710
1241	31	705
1241	31.5	702
1241	32	697.8
1241	32.5	693.5
1241	33	690.4
1241	33.5	684.9
1241	34	679.6
1241	34.5	673.3

1241	35	669.5	1242	0	526.8
1241	35.5	665.3	1242	0.5	527.5
1241	36	661.4	1242	1	527.1
1241	36.5	656.2	1242	1.5	526.3
1241	37	651.4	1242	2	526.4
1241	37.5	647.9	1242	2.5	527
1241	38	643.7	1242	3	526.3
1241	38.5	642.7	1242	3.5	526.2
1241	39	639.3	1242	4	526.4
1241	39.5	637	1242	4.5	524.4
1241	40	633.6	1242	5	524.4
1241	40.5	631.8	1242	5.5	524.1
1241	41	628.2	1242	6	523
1241	41.5	623.4	1242	6.5	521.3
1241	42	618.7	1242	7	521.8
1241	42.5	614.7	1242	7.5	522.7
1241	43	612.8	1242	8	523
1241	43.5	610.1	1242	8.5	526.7
1241	44	607.1	1242	9	527.8
1241	44.5	603	1242	9.5	529.4
1241	45	600.1	1242	10	530.4
1241	45.5	595.3	1242	10.5	531.1
1241	46	589.9	1242	11	532.5
1241	46.5	584.6	1242	11.5	534.6
1241	47	580.3	1242	12	537.4
1241	47.5	577.2	1242	12.5	539.2
1241	48	573.8	1242	13	541.3
1241	48.5	571.5	1242	13.5	542.9
1241	49	568.7	1242	14	545
1241	49.5	566.7	1242	14.5	546.6
1241	50	562.4	1242	15	548.6
1241	50.5	556.6	1242	15.5	548.9
1241	51	549.7	1242	16	550.3
1241	51.5	546.6	1242	16.5	550.1
1241	52	542.4	1242	17	550.8
1241	52.5	544.8	1242	17.5	551.6
1241	53	544.3	1242	18	546.6
1241	53.5	541.9	1242	18.5	539.9
1241	54	539.5	1242	19	536.3
1241	54.5	536.9	1242	19.5	534.3
1241	55	535.3	1242	20	533.2
1241	55.5	531.7	1242	20.5	535.2
1241	56	532.3	1242	21	535.2
1241	56.5	532.3	1242	21.5	535.8
1241	57	531.8	1242	22	538.6
1241	57.5	532.1	1242	22.5	541.5
1241	58	531.9	1242	23	542.1
1241	58.5	532.5	1242	23.5	541.9
1241	59	530.5	1242	24	542.6
1241	59.5	529.1	1242	24.5	543.6

1242	25	546
1242	25.5	545.5
1242	26	544.3
1242	26.5	545.6
1242	27	546.4
1242	27.5	548.7
1242	28	551.3
1242	31.5	547.5
1242	32	545.9
1242	32.5	542.9
1242	33	538.6
1242	33.5	532.9
1242	34	530.8
1242	34.5	526.6
1242	35	522.2
1242	35.5	520.6
1242	36	523.3
1242	36.5	525.2
1242	37	522.7
1242	37.5	520.3
1242	38	518.2
1242	38.5	517.5
1242	39	515
1242	39.5	513.2
1242	40	508.2
1242	40.5	503.8
1242	41	499.1
1242	41.5	494
1242	42	491.4
1242	42.5	486.6
1242	43	482
1242	43.5	477.4
1242	44	474.2
1242	44.5	471.2
1242	45	470.4
1242	45.5	469.3
1242	46	468.7
1242	46.5	468.8
1242	47	469.2
1242	47.5	468.1
1242	48	467.9
1242	48.5	467.9
1242	49	467.1
1242	49.5	466.2
1242	50	463.5
1242	50.5	462.5
1242	51	461.9
1242	28.5	553.2
1242	29	552.3
1242	29.5	551.8
1242	30	551.3
1242	30.5	550.3
1242	31	549.3

Appendix D

Permission to include published manuscripts in the thesis.

Date: Wed, 10 Aug 2005 14:10:37 -0400
RE: Permission to use.

We are pleased to grant permission.

Donna M. Hull
Director, Publications

American Society of Agricultural and Biological Engineers
2950 Niles Rd. St. Joseph, MI 49085
hull@asabe.org
(269) 428-6326 Fax (269) 429-3852
See the ASABE Online Technical Library at http://asae.frymulti.com

-----Original Message-----
From: Subrata Karmakar [mailto:s.karmakar@usask.ca]
Sent: Wednesday, August 10, 2005 12:02 PM
To: Donna M. Hull
Subject: Permission to use.

Dear Ms. Hull,

I would like to get permission from ASABE to include article PM5461 in my doctorate thesis. My thesis is structured as a series of manuscripts written suitable for publication in scientific journals. Article PM5461 has already been published in the Transactions of the ASAE [48(3): 923-932].

Please feel free to contact me for any further information.

Thank you for your collaboration,
Best regards,

Subrata KARMAKAR

PhD Candidate
Department of Agricultural and Bioresource Engineering
University of Saskatchewan
57 campus Drive, Saskatoon, SK, CANADA S7N 5A9
Phone: 306-966-5325/6 Fax: 306-966-5334
Email: s.karmakar@usask.ca

Date: Mon, 22 Aug 2005 10:22:37 -0600
From: Don Norum <donald.norum@usask.ca>

To: Subrata Karmakar <s.karmakar@usask.ca>
Subject: Re: Permission to use.

Subrata Karmakar:

This email gives you permission to use article "Critical state elasto-plastic constitutive models for soil failure in tillage - A review" with authors S. Karmakar, J. Sharma and R.L. Kushwaha published in Canadian Biosystems Engineering/Le génie des biosystèmes au Canada, Volume 46 (2004) 2.19-2.23 in your Ph.D. thesis at the University of Saskatchewan.

D.I. Norum
Publisher, Canadian Biosystems Engineering.

-----Original Message-----

Date: Wed, 10 Aug 2005 10:27:17 -0600
From: Subrata Karmakar <s.karmakar@usask.ca>
To: "D. I. Norum" <norum@engr.usask.ca>
Subject: Permission to use.

Subrata Karmakar wrote:

Dear Dr. Norum,

I would like to get permission from CSAE/SCGR to include article c0346 in my doctorate thesis. My thesis is structured as a series of manuscripts written suitable for publication in scientific journals. Article c0346 has already been published in the Canadian Biosystems Engineering [46: 2.19-2.23].

Please feel free to contact me for any further information. Thank you for your collaboration,

Best regards,

Subrata KARMAKAR

PhD Candidate
Department of Agricultural and Bioresource Engineering
University of Saskatchewan
57 campus Drive, Saskatoon, SK, CANADA S7N 5A9
Phone: 306-966-5325/6 Fax: 306-966-5334
Email: s.karmakar@usask.ca

Appendix E

Manuscript 1: Soil failure associated with crack propagation for an agricultural tillage tool.

Chapter 2 (part-1) has been published in Soil & Tillage Research as Article in Press.

Available online at www.sciencedirect.com
SCIENCE DIRECT®
Soil & Tillage Research 84 (2005) 119–126
Soil & Tillage Research
www.elsevier.com/locate/still

Soil failure associated with crack propagation for an agricultural tillage tool

S. Karmakar *, R.L. Kushwaha, D.S.D. Stilling

Department of Agricultural and Bioresource Engineering, University of Saskatchewan, 57 Campus Drive, Saskatoon, Sask., Canada S7N 5A9

Received 28 November 2003; received in revised form 8 September 2004; accepted 4 October 2004

Abstract

Tillage loosens soil to depths of 75–150 mm (3–6 in.). As the soil is tilled, the failure path precedes the motion of the tillage tool. Previous studies have examined soil forces acting on a tine by predicting different soil failure patterns. This paper quantifies the rate and the path of the cracks associated with soil failure front. The propagation of the soil failure path by observing the temporal profile of the leading edge of the failure crack with respect to the tool motion was examined. Crack propagations were analysed for sweep operating at 4 km h^{-1} speed, and two operating depths of 75 and 100 mm using high-speed digital videography. Higher depth of operation showed distinct phases for crack development and propagation. Short and intermittent soil crack propagation with lower propagation growth rates was observed for shallow depth of operation. Crack growth rate has been observed to have a sinusoidal relation with time.

Keywords: Tillage; Crack propagation; Soil failure front

1. Introduction

Development of force prediction models with analytical approach have been based on the assumptions on different soil failure patterns during soil–tool interaction. Soil failure patterns were also assumed conveniently based on passive earth pressure theory (Terzaghi, 1943) in empirical and semi-empirical models. The efficiency of the models in terms of their prediction capabilities depends largely to the assumption on position, and orientation of soil failure plane or slip lines associated with the forward most failure front. The tool influence zone, represented by the regions of these failure fronts, depends on the development of individual soil cracks. As a tine is advanced through the ground, the soil close to its path is subjected to a compressive stress. The forward motion of the tool through the soil (a medium with high compressive strength) is possible by soil shear failure. As the tool interacts with soil, cracks develop from different areas of the tool section depending on the tool shape and orientation.

* Corresponding author. Tel.: +1 306 966 5326; fax: +1 306 966 5334.
E-mail address: S.Karmakar@usask.ca (S. Karmakar).

0167-1987/$ – see front matter © 2005 Elsevier B.V. All rights reserved.
doi:10.1016/j.still.2004.10.005

Soil–tool interaction has been analysed in two- and three-dimensional soil failure patterns. Two-dimensional failures may be in a vertical plane with tools operating at shallow depths or in horizontal plane for tools operating at deeper depths and is applicable to wider tools. A three-dimensional failure (Payne, 1956) involves a failure pattern in both planes and is generally considered for narrow tools. These models have been useful in estimating the force exerted on a tillage tool, the stress experienced at different sections of the tool, soil displacement and other parameters. These common features improved understanding of the soil–tool interaction during tillage with the intent of optimizing tool design and minimizing energy requirements. However, the mechanics of the soil crack development and propagation have been studied to a very limited extent. The objective of this research was to examine the propagation of the soil cracks associated with the action of a tillage tool.

Previous studies on the mechanism of soil failure front were based on the cleavage development due to the interaction of a vertical tool (flat blade) with soil (O'Calleghan and Farrely, 1964; Godwin and Spoor, 1977; Rajaram and Gee-Clough, 1988). Soil mechanical behaviour in the perspective of crack development and its propagation for soil interaction with commonly used tillage tools is not available in the literature. Sweep, the commonly used tool for tillage operation, has been considered for this study.

2. Literature review

Studies on the mechanics of agricultural soil failure, and a comparison of the experimental results with the passive earth pressure against retaining wall, concluded that tines caused progressive failure rather than instantaneous failure (Payne, 1956; Sohne, 1956).

Considering soil deformations that occur when load is applied to the soil by a flat vertical plate, two modes of ruptures are predicted in 'shallow' and 'deep' regimes depending on the depth/width ratio of the tine (O'Calleghan and Farrely, 1964; Godwin and Spoor, 1977). O'Callaghan and Farrelly attributed this aspect ratio as the sole parameter determining the mechanism of cleavage from the perspective of slip surfaces in a vertical plane. A vertical tine acted as a 'retaining wall' with less than 0.6 aspect ratio, and as a 'footing' with an aspect ratio more than 0.6. At shallow depth, the tine displaced a chip of soil, slightly wider than the tine face width, immediately in front of it; while for deep operations, a fissure was developed in the soil some distance in front of the tine face and across the path of the tine. The fissure curved backwards on both sides of the tine forming a triangular wedge. The process of soil cleavage or cracks was considered.

Elijah and Weber (1971) studied the soil failure pattern in the vertical plane perpendicular to the direction of travel for an inclined flat blade of full scale and 1/8th scale in a soil bin using film. They observed and defined four distinct types of soil failure, namely shear-plane, flow, bending and tensile. The study revealed that 'shear-failure' and 'flow' occurred in granular-brittle material at relatively slow tool speeds. 'Bending' was evident in relatively high-moisture clays, which had enough toughness to prevent failure planes, yet sufficient plasticity to allow considerable strain with the formation of a minimum number of tension cracks occurred.

Godwin and Spoor (1977) observed that a change in soil failure mechanism occurred with depth for narrow tines. Above a certain 'critical depth' (small aspect ratio), the soil was displaced forwards, sideways and upwards creating a 'crescent failure', and below this depth (high aspect ratio), the displaced soil had components only in forward and sideways direction with no formation of distinct shear plane from the tine base creating a 'lateral failure'.

The study of soil failure and corresponding force–distance behaviour for flat tines in clay soil under quasi-static conditions with varying soil moisture, tine width and constant working depth revealed that the nature of failure depended on the soil moisture level (Rajaram and Gee-Clough, 1988). They also observed four mechanisms of soil failure, namely collapsing, fracturing, chip forming and flow failure. When the tine interacted with the virgin soil, the stress conditions were different from those during subsequent passes. During the tine's initial movement, soil was continuously displaced upwards and part of the displaced mass fell into the trench cut by the tine. After a few failures, the rate of upward flow became equal to the rate of sideways flow into the trench, and therefore the volume of the surcharging soil mass

reached a stable value. The number of failures after which the surcharge stabilized depended on the width of the tine. They also observed, for given moisture content and tine width, a sinusoidal time relation of the force on the tine existed. Rajaram (1990) found the soil failure pattern caused due to collapsing of soil in front of the tine is periodic, the frequency and magnitude of which depended on tine width.

Failure surface propagation of landslides has been studied in the context of stability of slopes, where progressive failure was the key focus. Kamai (1993) conducted a similar study using an experimental approach with ring shear creep test following 'Sohmen method' on landslide clay. Four stages of the soil failure process in the context of creep test were proposed. The 'preceding stage' is characterised by small displacement rate and corresponds to the second stage of creep with no failure surface yet developed. The second is a 'seeding stage' when several failure zones are formed arbitrarily and are disconnected from each other with an accelerated displacement rate. Next, the 'propagation stage', where the failure zones formed in the previous stage propagate to each area completing the failure surface. Fourth, the 'post-failure stage', sliding occurs along the failure surface that has been formed completely.

Soil failure is related to different factors like soil type, moisture content, size and shape of the tool, speed of operation etc. Literature available on soil failure crack and deformation pattern with tillage tool interaction is mostly based on flat blade and narrow tillage tools. This research examined both qualitatively and quantitatively the soil crack propagation and failure patters for a commonly used cultivating tool. Contrary to the previous studies on soil cleavage formation due to the vertical flat blade in a vertical plane, this study focused mainly on the process of crack propagation due to soil–sweep interaction in the horizontal plane.

3. Methodology

Tillage is a dynamic process and to observe failure patterns under dynamic conditions, high-speed videography were recorded during the soil bin experiments with a sweep. Visual interpretations were made from segments of the video clips, their still images, and soil

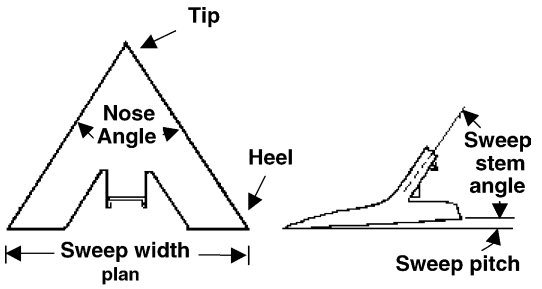

Fig. 1. Details of sweep.

crack propagations were analysed by digitizing the data using commercial software.

Experiments were conducted in the soil bin facilities of the Department of Agricultural and Bioresource Engineering of the University of Saskatchewan. The sweep (1/2–1/4 in.) used for the experiment has 50° nose angle and 50° stem angle (Fig. 1). Tool operating speed was slightly above 1 m s^{-1} for operating depths of 75–100 mm. The soil was a clay loam (sand 47%, silt 24% and clay 29%). Soil preparation involved a roto tiller, a flat surface packing roller, a sheep foot roller, a soil leveller and a water spray boom for maintaining soil moisture content. The soil bed was prepared to have a moisture content of 12.4% (d.b) and an average compaction level with cone index of 492 kPa. The soil compaction levels were measured using a cone penetrometer.

A 10 cm grid was chalked on the soil surface using a white powder substance for scaling. A high-speed video camera was mounted to the carriage frame where the tillage tool was mounted. Therefore, the recorded field of view had the tillage tool in the same location (the camera and the tool moved in unison). The digital film was transferred to standard video allowing the soil failure pattern to be observed conveniently. In addition, the film was converted to audio video interleave (AVI) format to allow for subsequent video processing.

For qualitative assessment, video clips (moving pictures) have been converted to still pictures using a commercial moving picture experts group (MPEG) Encoder TMPGEnc at fraction of seconds. For the quantitative assessment, a commercial software package for Automatic Motion Analysis, 'WINanalyze', was used to digitize the crack tip (x–y coordinates) frame-by-frame. The program calibrated

the distance based on the known grid and calculated crack tip growth (velocity), and rate of growth (acceleration) using finite differences in the respective directions. The analysis involved determining resultant displacement, velocity and acceleration for the soil failure crack.

4. Results and discussions

4.1. Visual interpretation

Analysis of the still images obtained by encoding the moving pictures revealed sequential soil crack development and propagation associated with soil deformation. For the sweep, operating at a depth of 100 mm in a soil of 12.4% (d.b) moisture content and 492 kPa cone index, the following visual interpretations were observed (Fig. 2).

As the tool started tilling undisturbed soil, elevated nose of the sweep pushed the soil sideways (clear from the shifting of chalk marks sideways), and cracks developed from the base of the sweep stem along the direction of motion and at about 45° to both the sides (Fig. 2a). Then, the crack following the sweep tip widened and propagated after splitting again at 45° to both sides of sweep nose (Fig. 2b). With further widening of the central crack, the cracks developed from sideways also widened and propagated (Fig. 2c). In this way, the soil around the stem base completely deformed (Fig. 2d) into small chips and was pushed sideways (clear from the disappearance of the chalk marks near the stem base). At the same time, the crack development region extended from the sweep stem

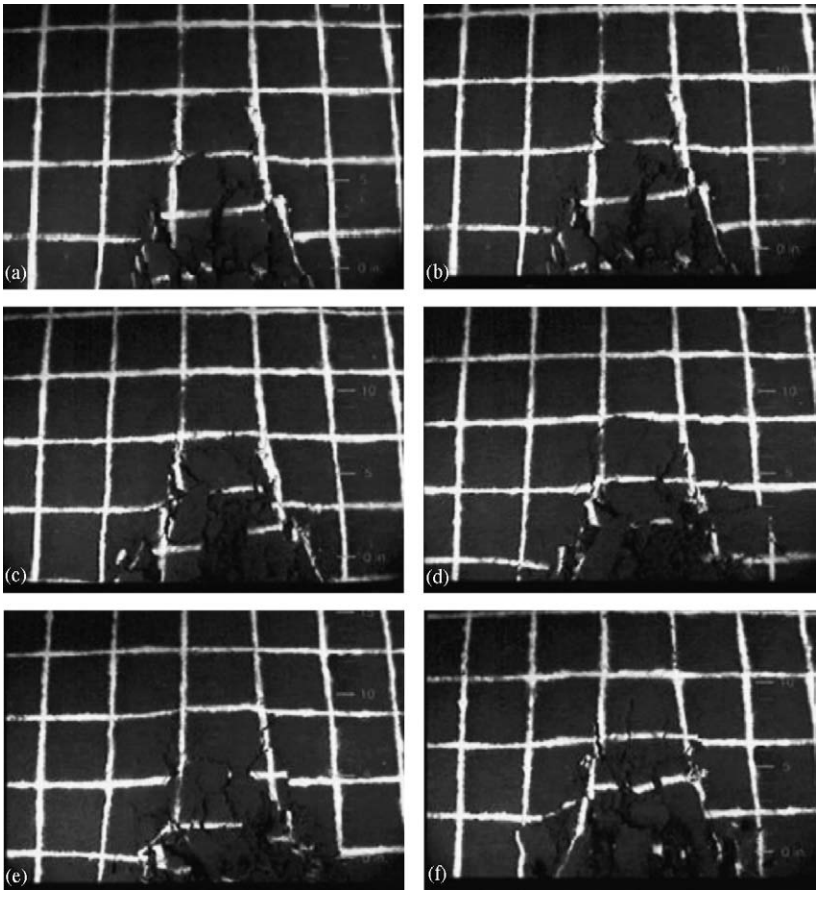

Fig. 2. Crack propagation with 100 mm depth of operation.

base and new cracks developed from the whole plan area of the tool and propagated to the direction of motion and at angles ranging 30–60°. With the tool forward motion, new cracks develop from stem base and earlier developed cracks propagate and widen (Fig. 2e) as a part of the cyclic process. Due to the stabilised soil deformation process, the propagation seems to be faster with simultaneous crack development (Fig. 2f).

Significant still images obtained by encoding the video clips for 75 mm depth of operation are shown in Fig. 3 for visual interpretation. As soon as the tool engaged the soil, cracks developed from the stem base and propagated in different directions. Number of cracks developed was very high in comparison to that of 100 mm depth. Crack initiation, development and subsequent processes were not as distinct as that for 100 mm depth of operation. Soil displacement to the sideways was also higher in this case.

The differential feature of soil crack development and propagation with the sweep in respect of the operating depth was similar to the observation by O'Calleghan and Farrely (1964) for a flat vertical plate. However, experiments with more operating depths would be required for specifying two- and three-dimensional soil failure patterns with a well-defined critical depth for sweep based on its shape.

The generalized feature of the observed soil failure cracks and their propagation can be illustrated as in Fig. 4. Thus, failure advancement of soil relative to the tool can be written as $\frac{d}{dt}(\overline{x_s} - \overline{x_t})$, where $\overline{x_t}$ is the average tool displacement and $\overline{x_s}$ is the average resulting soil failure propagation. Since the camera was mounted on the tool carrier, the observed soil

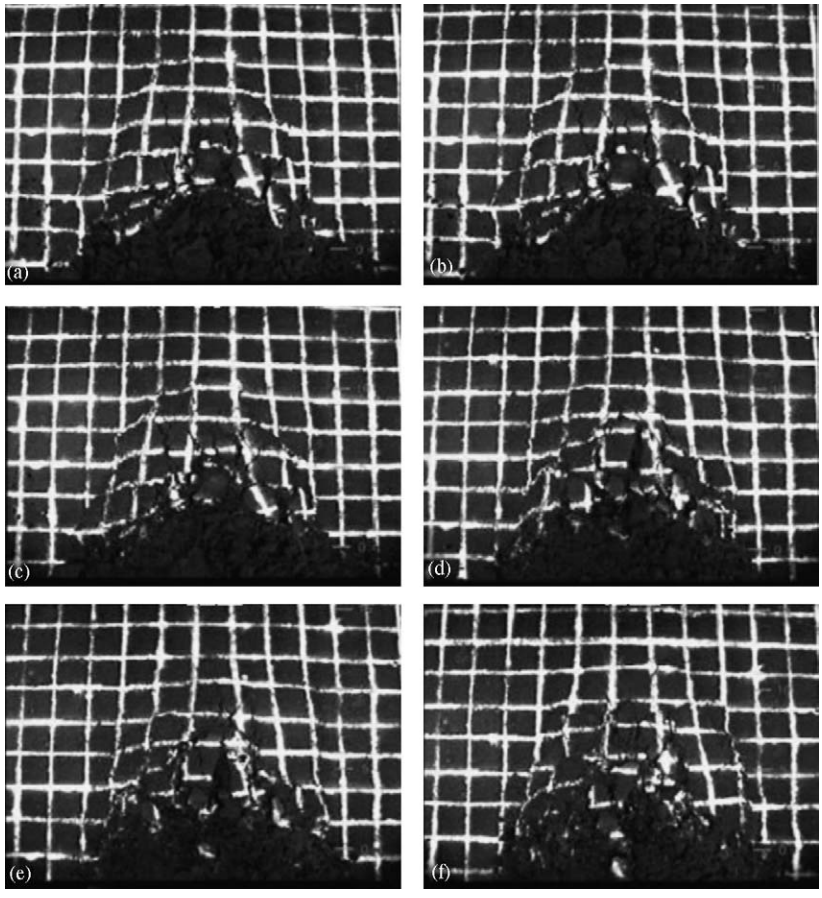

Fig. 3. Crack propagation with 75 mm depth of operation.

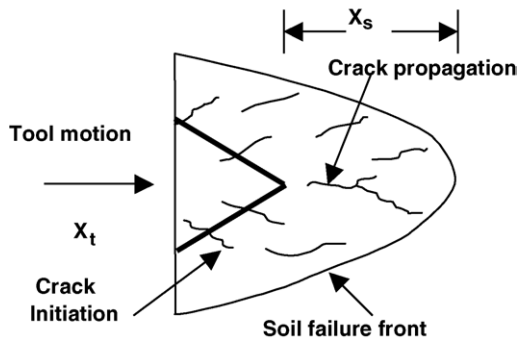

Fig. 4. Schematics of crack propagation and failure front advancement.

failure propagation is the relative soil failure advancement.

4.2. Analytical interpretation

Image analysis of the soil failure pattern allowed the crack propagation to be quantified. The observation of soil movement with respect to the advancing tool revealed a process of crack initiation and its development. Cracks developed from the stem base of the sweep were considered for analysis.

Fig. 5 shows the process of crack propagation of a particular crack with respect to its lateral and longitudinal components. After a crack was initiated, for a little duration it sustained the compressive force without any displacement and then propagated suddenly until it deformed completely. For this particular crack, which completes the whole process in less then 15 ms, the longitudinal component is seen to have higher displacement of about 50 mm, and than the lateral component of about 25 mm before complete deformation.

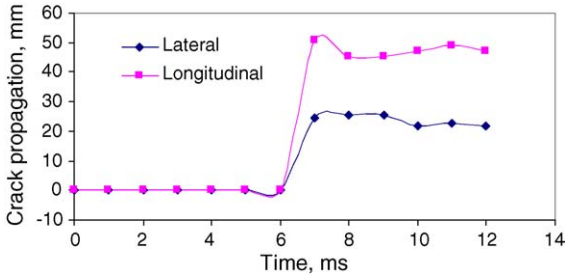

Fig. 5. Directional crack development and soil deformation.

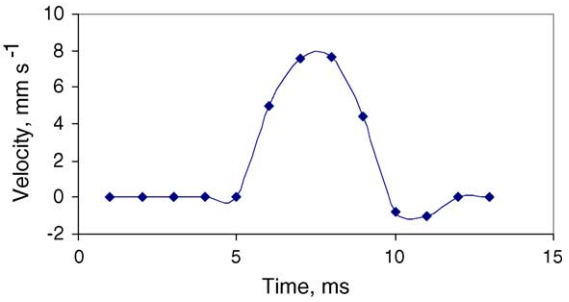

Fig. 6. Velocity of soil crack propagation.

For 75 mm depth of operation a maximum of about 8 mm s^{-1} crack velocity occurred during the crack propagation (Fig. 6). The acceleration of the crack propagation followed a sinusoidal response (Fig. 7) with a higher growth rate in longitudinal direction than in lateral direction. For this particular soil crack, developed with 75 mm depth of operation, the maximum accelerations in longitudinal and lateral direction were found to be 0.28 and 0.15 mm s^{-2}, respectively.

The process of soil crack propagation and soil deformation due to soil–tool interaction can be explained in a general form as shown in Fig. 8. The growth rate (acceleration) of a crack showed sinusoidal response after it was initiated. In the next phase of propagation, it decelerated and finally came to rest. Simultaneously, other crack initiated and continued with the same process. For the 100 mm depth of operation, the longitudinal component of acceleration was found to be maximum of about 2.0 mm s^{-2} and that of lateral component was about 1.5 mm s^{-2}.

The features of crack propagation for a shallower depth are shown in Fig. 9. The crack development and propagation process is found to last for very small

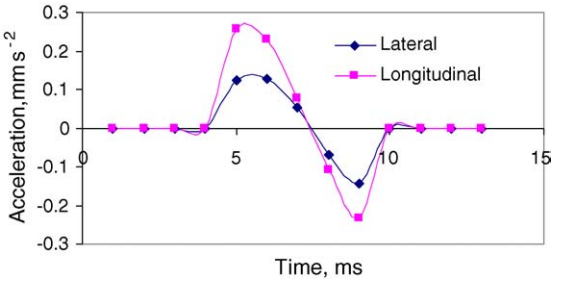

Fig. 7. Growth rate of soil crack.

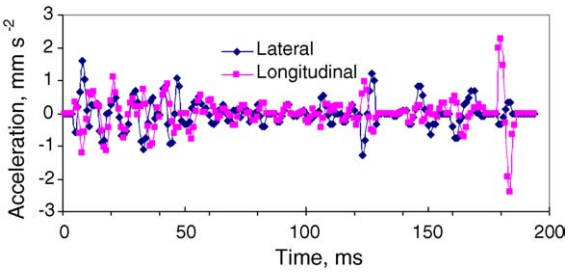

Fig. 8. Phases of soil failure for 100 mm depth of operation.

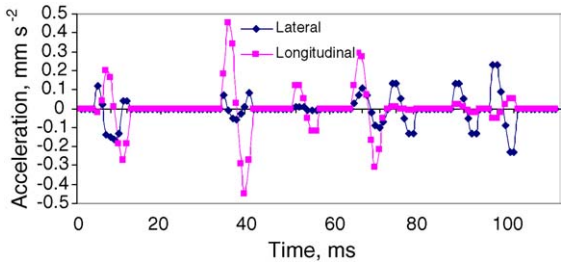

Fig. 9. Phases of soil failure for 75 mm depth of operation.

period for each individual crack. This supports the visual interpretation for 75 mm depth of operation. The process is not distinct as that of the 100 mm depth of operation. In this case, the maximum longitudinal and lateral components of crack growth rate were found to be about 0.5 and 0.3 mm s^{-2}, respectively.

Various stages of soil failure during landslide (Kamai, 1993) do not correspond to the soil failure pattern by a tillage tool, since soil–tool interaction is very quick with an external loading. As the tillage tool advances, the soil gets compressed (elastic deformation) and the crack is initiated. The crack grows rapidly and then the growth rate (propagation) is reduced considerably. This is followed by soil plastic failure and soil particles come to a rest (post-tilling phase). Thus, the soil failure feature in the case of tillage tool may be divided into the phases of soil compression and elastic deformation, crack initiation, crack propagation or crack growth and plastic failure or post-tilling phase.

5. Conclusions

The objectives of this study were to observe the initiation and development of individual soil cracks for soil–sweep interaction and to analyse their propagation as individual cracks. Following conclusions can be drawn from the above experimental study, and visual and analytical observations of soil crack propagation for a sweep operating at two different depths:

- Features of soil crack development and propagation indicated the non-linear characteristics of soil.
- Crack initiation appeared as fine, hair like fissures mainly from the sweep stem base area in the direction of motion and at angles ranging from 30° to 60° to the direction of motion.
- Crack development and propagation was distinct for higher depth of operation.
- Shallower depth of operation caused short and intermittent soil crack propagation with lower growth rate.
- The growth rate or the acceleration of the crack propagation followed a sinusoidal response.
- Longitudinal component of a crack had higher displacement and growth rate than the lateral component during the deformation process.
- Soil cracks indicated four distinct phases: ‘soil compression’ or elastic failure, ‘crack initiation’, ‘crack propagation’ or crack growth and ‘particle retardation’ or plastic failure (post-tilling phase).

Acknowledgements

The authors gratefully acknowledge the financial support provided by the Natural Science and Engineering Research Council of Canada, the Department of National Defence, Canada, and University of Saskatchewan Partnership Research Program.

References

Elijah, D.L., Weber, J.A., 1971. Soil failure and pressure patterns for flat cutting blades. Trans. ASAE 14 (4), 781–785.

Godwin, R.J., Spoor, G., 1977. Soil failure with narrow tines. J. Agric. Eng. Res. 22, 213–228.

Kamai, T., 1993. Failure propagation process in landslide clay. In: Proceedings of the Seventh International Conference and Field Workshop on Landslides, Brastislava, Slovakia, pp. 243–248.

O'Calleghan, J.R., Farrely, K.M., 1964. Cleavage of soil by tined implements. J. Agric. Eng. Res. 9 (3), 259–270.

Payne, P.C.J., 1956. The relationship between the mechanical properties of soil and the performance of simple cultivation implements. J. Agric. Eng. Res. 1 (1), 23–50.

Rajaram, G., 1990. Collapse failure in dry clay soils caused by implements. J. Terramech. 27 (2), 69–78.

Rajaram, G., Gee-Clough, D., 1988. Force–distance behaviour of tine implements. J. Agric. Eng. Res. 41, 81–98.

Sohne, W., 1956. Some basic considerations of soil mechanics as applied agricultural engineering. Grundlagen der Landtechnik, 7:11 (NIAH Transaction No. 53).

Terzaghi, K., 1943. Theoretical Soil Mechanics. Wiley, New York.

Appendix F

Manuscript 2: Critical state elasto-plastic constitutive models for soil failure in tillage – A Review.

Chapter 2 (part-2) has been published in the Canadian Biosystems Engineering 46: 2.19-2.23.

Critical state elasto-plastic constitutive models for soil failure in tillage – A review

S. Karmakar[1], J. Sharma[2] and R.L. Kushwaha[1]

[1]Agricultural and Bioresource Engineering Department; and [2]Department of Civil asnd Geological Engineering, University of Saskatchewan, Saskatoon, Saskatchewan, Canada S7N 5A9

Karmakar, S., Sharma, J. and Kushwaha, R.L. 2004. **Critical state elasto-plastic constitutive models for soil failure in tillage – A Review**. Canadian Biosystems Engineering/Le génie des biosystèmes au Canada **46**: 2.19-2.23. Soils, in general, undergo both elastic and plastic deformations upon loading. A realistic constitutive model of soil behaviour must be able to distinguish between the elastic and plastic deformations. A large number of isotropic elasto-plastic constitutive models have been developed for sand, clay, and rock during the last four decades. These models have been used for analysing tillage tool interaction with soil. To describe the behaviour of soil subjected to a tillage tool with a rather complex loading path, the model should also account for the dependency of certain material properties on the stress history of the soil. In this article, an attempt has been made to review some of these critical state elasto-plastic models with reference to their application in soil-tool interaction. Strain dependant anisotropic elasto-plastic models have been found to be a need for realistic modeling for agricultural soil-tool mechanics. **Keywords**: tillage, constitutive model, elasto-plastic, isotropic, anisotropic, critical state model.

De façon générale, les sols subissent des déformations élastiques et plastiques lorsque soumis à des chargements mécaniques. Un modèle constitutif de comportement des sols réaliste doit être capable de distinguer entre les déformations élastiques et plastiques. Un grand nombre de modèles isotropiques élasto-plastiques constitutifs ont été développés pour le sable, l'argile et le roc au cours des quarante dernières années. Ces modèles ont été utilisés pour analyser les interactions entre les outils de travail du sol et le sol. De manière à décrire le comportement du sol remanié sous l'effet d'un outil exerçant une charge complexe, les modèles doivent aussi tenir compte de la dépendance de certaines propriétés du matériau sur les variations temporelles du chargement. Cet article constitue une revue de quelques-uns de ces modèles d'état critique élasto-plastique en référence à leur application sur les intéractions sol-outil. Il en ressort que des modèles anisotropiques élasto-plastiques et affichant une dépendance aux variations temporelles des déformations sont nécessaires pour la modélisation réaliste des interactions sol-outil en agriculture. **Mots clés**: travail du sol, modèle constitutif, élasto-plastique, isotropique, anisotropique, modèle à l'état critique

INTRODUCTION

Soil undergoes both elastic and plastic deformation when subjected to loading. The basic requirement for integrated analyses of movements and failure of a soil mass is a constitutive relationship capable of modeling stress-strain behaviour of soil up to and beyond failure. Development of such a relationship generally involves separating the elastic and plastic behaviour. This is achieved using a well-defined curve known as the yield locus located in a shear stress – normal stress space (Wood 1990). If the stress state of a soil plots inside the yield locus, it is considered to be elastic and undergoes recoverable deformation. On the other hand, if a particular stress path puts the stress state of the soil on or outside the yield locus, plastic or irrecoverable deformation of soil occurs. Elasto-plastic constitutive models help distinguish between the recoverable and irrecoverable deformations for understanding the stress strain behaviour of soil during loading and unloading. Kushwaha and Shen (1994) reported that a substantial soil deformation is associated with the generation of non-linearity in stress-strain relation in agricultural soil failure with tillage tool interaction. This leads to a large amount of irreversible deformation after the removal of the load, indicating that plastic deformation dominates in agricultural operations.

Tillage is concerned with the top soil strata (up to about 1000 mm depth). Thus the metric suction and pore pressures, which are significant in geotechnical engineering problems like stability of slope, foundation of structures, etc., do not contribute much to the constitutive modeling for tillage. Elastic and plastic models, primarily based on the assumption of soil isotropy, have been used to model tillage tool interaction with soil. The force experienced by a tillage tool is influenced by both the stiffness and the strength of the soil. This is also affected by the stress history of soil with an anisotropic behaviour. The modeling of soil-tool interaction using numerical methods can be improved further by incorporating strain-dependent stiffness and strength of soil associated with soil anisotropy. Therefore, the objective of this paper was to study the pertinent soil constitutive models based on critical state soil mechanics in relation to their application to soil failure in tillage.

CRITICAL STATE SOIL MECHANICS

Elasto-plastic soil constitutive models

A soil is said to be in critical state when it undergoes large shear deformations at constant volume and constant shear and normal effective stress (Schofield and Wroth 1968). A locus of critical states of all shear tests on a soil is called a Critical State Line (CSL). The CSL is plotted in a three-dimensional space consisting of deviatoric stress, mean normal effective stress, and void ratio. Where a particular soil sample will end up on the CSL depends on its initial void ratio, initial mean normal effective stress, and the stress path. All the elasto-plastic models based on the critical state concept have a well-defined yield locus that can be either isotropic or anisotropic. These models are not based on the Mohr-Coulomb failure criterion although the slope of the CSL can be readily correlated with the critical state angle of internal friction. However, some of these models

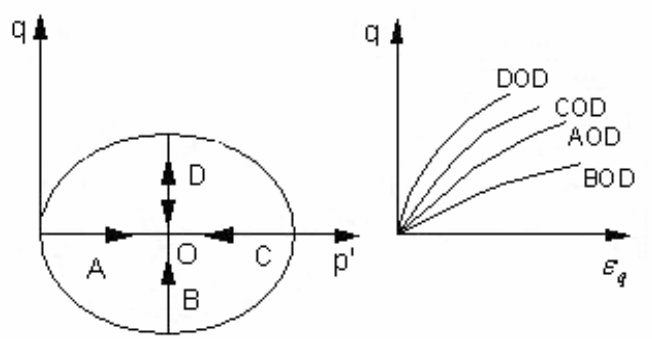

Fig. 1. Effect of stress history on the strength and stiffness of soil (Atkinson et al. 1990)

(e.g. Cam Clay) give a unique strain response to an increment of stress but do not give a unique stress response to an applied strain increment. Therefore, these models cannot be used for finite element computations without some modifications (Simpson 1973).

Effect of stress history

The stress-strain response of soil not only depends on the current stress state but also on the recent stress history of the soil (Stallebrass 1990). Problems involving unidirectional stress path (e.g. one-dimensional consolidation) may be described by a relatively simple non-linear elasto-plastic model. However, for situations where the stress path directions may vary either because of the stress history or because of loading, a strain dependent non-linear elasto-plastic model is desirable. The magnitude of the effect of recent stress history (Fig. 1) is determined largely by the difference in direction of loading between the current and previous stress path (Atkinson et al. 1990). The stress-strain behaviour for a common stress path OD is shown after various histories. The DOD stress path is stiffest as the stress path changes its direction by 180° followed by COD and AOD where stress path changes its direction by 90° in deviatoric stress (q) vs mean normal effective stress (p') space. The stress path BOD is the softest as it continues its previous direction. Soil offers resistance to change in direction of loading which implies stress-strain behaviour of current stress path depends on the stress history of soil.

Isotropic models – Cam Clay and Modified Cam Clay

Cam Clay (Roscoe et al. 1958) and Modified Cam Clay (Roscoe and Burland 1968) were developed by the Geotechnical Group at Cambridge University in the United Kingdom. These models were proposed on the basis of experimental evidence obtained from axisymmetric shear tests (the so-called triaxial tests) on remoulded soil samples of clay that were isotropically consolidated. For this reason, these models cannot be applied to conditions other than axisymmetry without attempting a generalization based on certain assumptions. The most important assumption made in this regard is that of isotropy. An isotropic soil constitutive model gives the same value of stiffness and strength irrespective of the direction of principal stresses. For such a model, there is no "preferred" direction that the stresses in soil can choose in order to mobilize minimum stiffness and strength and the yield curve is symmetric about the space diagonal – a line in principal stress space on which the three principal stresses are equal.

The yield locus for the Cam Clay model (Roscoe et al. 1958) is defined using a logarithmic spiral as shown in Fig. 2(a). The position of the yield surface is defined by p_o'. The point C represents the point of the yield curve with horizontal slope. At this point. plastic volumetric strain is zero and the yield surface becomes stationary. A point like C is the final state for a soil taken to failure, independently of initial conditions. This state is called critical state. If a soil element yields at a point to the right of C ('wet' or subcritical side), plastic volumetric strains are positive and hardening is ensured. If yielding takes place to the left of C ('dry' or supercritical side), plastic volumetric strains are negative and softening results. The Cam Clay model assumes that the elastic shear strain is zero and the soil dissipates the applied energy by undergoing plastic shear

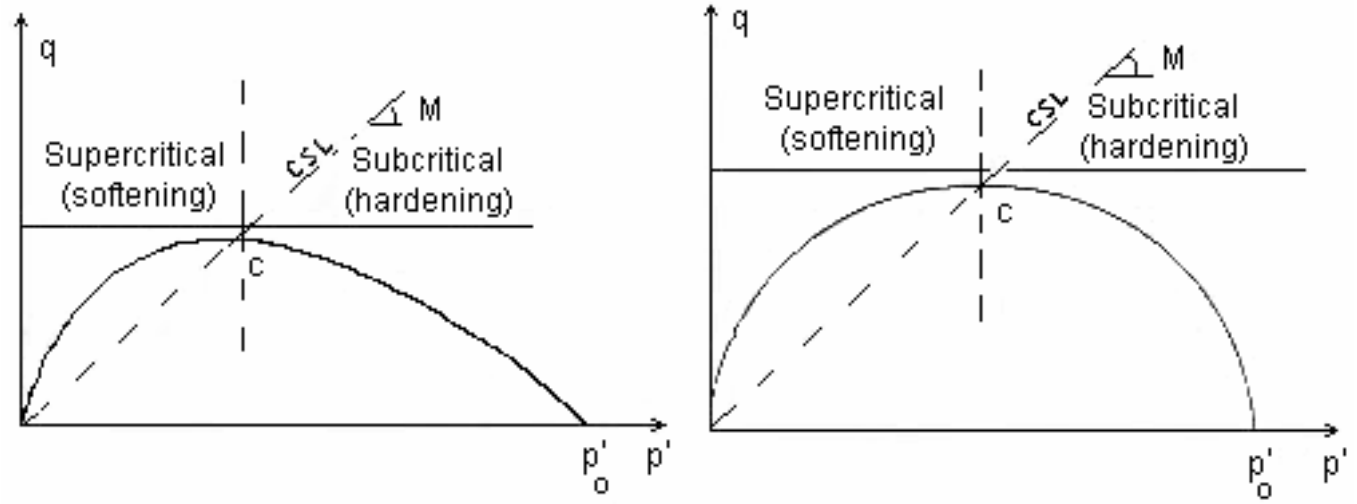

(a) (b)

Fig. 2. (a) Cam Clay Model; (b) Modified Cam Clay Model.

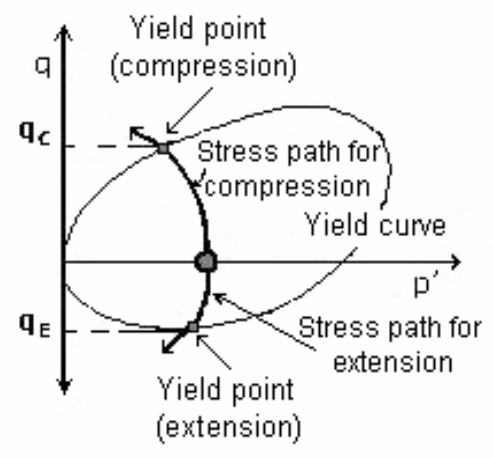

Fig. 3. Yielding of a cross-anisotropic soil.

strains. On the other hand, the Modified Cam Clay (MCC) model developed by Roscoe and Burland (1968) assumes that the dissipation of energy is due to both the elastic and plastic shear strains and thus the yield curve is elliptical as shown in Fig 2(b).

Anisotropic models

Naturally occurring soil is essentially a cross-anisotropic material. The main reason for the anisotropy is that most natural soils have been subjected to one-dimensional consolidation with a horizontal effective stress that is smaller than the vertical effective stress (coefficient of lateral earth pressure at-rest, K_o, is about 0.5 to 0.75 for most soils). The main implication of such a deposition process is that the yield locus is no longer symmetrical about the mean normal effective stress (p') axis. An asymmetric yield curve implies that the stiffness and strength of a soil in the vertical direction is significantly different than that in the horizontal direction. For a cross-anisotropic material, it is important to know the direction of the principal stresses because it influences the magnitude of the mobilized shear strength. A cross-anisotropic soil undergoing pure vertical compression (vertical major principal stress) would mobilize higher shear strength compared to that undergoing pure shear (major principal stress at 45°) or pure vertical expansion (horizontal major principal stress). This effect is illustrated in Fig. 3 that shows that a cross-anisotropic soil will yield at a much lower value of deviatoric stress in extension (q_E) than that in compression (q_C).

Strain dependent models

Simpson et al. (1979) developed a London Clay (LC) model to predict the effect of stiffness variation with elastic, intermediate, and plastic strain. The model also takes into account the variation of stiffness with mean normal stress and of plastic flow at large strains by relating increments of effective stress to increments of strain, given the current stress state. For this model, a kinematic yield surface (KYS), which depicts a small zone in the stress or strain space representing a higher stiffness at small strain, was defined in terms of strain. Straining within the KYS is purely elastic, though non-linear. The dependency of soil stiffness on the level of soil strain is modeled in a stepwise manner (Fig. 4). At very small strain, the soil is completely elastic and very stiff. As straining proceeds, plastic strain develops and there is a drop in the overall stiffness of soil.

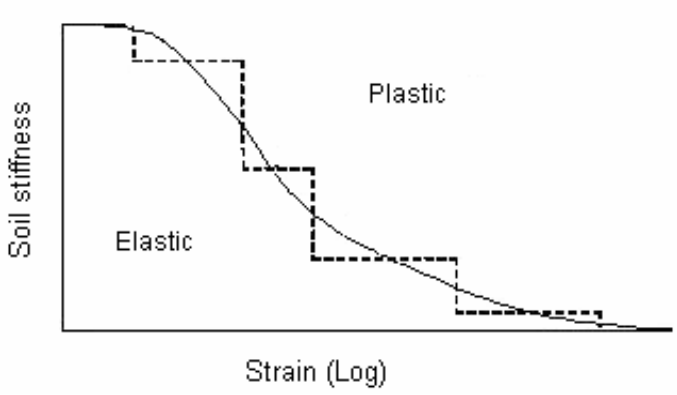

Fig. 4. Stepwise simulation of the stiffness vs strain curve (Simpson 1992).

APPLICATION OF CRITICAL STATE MODELS TO TILLAGE

Elastic and plastic models have been used to model soil-tool interaction, taking into account the formation of two and three dimensional soil failure patterns. A non-linear hyperbolic elastic model developed by Kondner and Zelasko (1963) and later modified by Duncan and Chang (1970) has been extensively used in tillage tool modeling (Chi and Kushwaha 1989; Pollock et al. 1986; Bailey et al. 1984; Yong and Hanna 1977). Chi et al. (1993) developed an elasto-plastic model using the incremental Lade and Nelson (1984) model and applied it to finite element analysis of soil tillage. The soil-tool interaction modeling using numerical methods can be improved further by incorporating strain-dependent stiffness and strength of soil.

The force experienced by a tillage tool is influenced by both the stiffness and the strength of the soil as shown in Fig. 5(a). At the beginning of the tilling activity, most of the soil is elastic and offers significant resistance. Therefore, the force required to till soil is quite high. As the tool moves, more and more soil begins to yield and fail, resulting in the propagation of failure planes or cracks from the tip of the tillage tool to the surface (Fig. 5(b)). Once the soil begins to yield, the magnitude of the required force drops and reaches a residual level as the soil in front of the tool reaches a steady state in terms of crack propagation.

As the tillage tool is dragged further, new failure planes are initiated in the soil in front of the tool and this cycle of peak and residual force repeats itself as shown in Fig. 6. The frequency of the cycle and the magnitude of the peak tillage force are influenced by the speed at which tilling is carried out. Zhang and Kushwaha (1998) reported a similar repeated soil failure pattern as demonstrated by shank vibrations.

The inclination of successive failure planes with respect to horizontal (θ in Fig. 5(b)) is a function of the critical state angle of internal friction (ϕ'_{cs}) as well as the angle of dilation (α) of the soil. The angle of dilation increases as the effective confining stress decreases (Wood 1990). The peak tillage force is a function of both the stiffness and the strength of the soil whereas the residual tillage force depends primarily on the strength of the soil. As shown in the previous sections of this

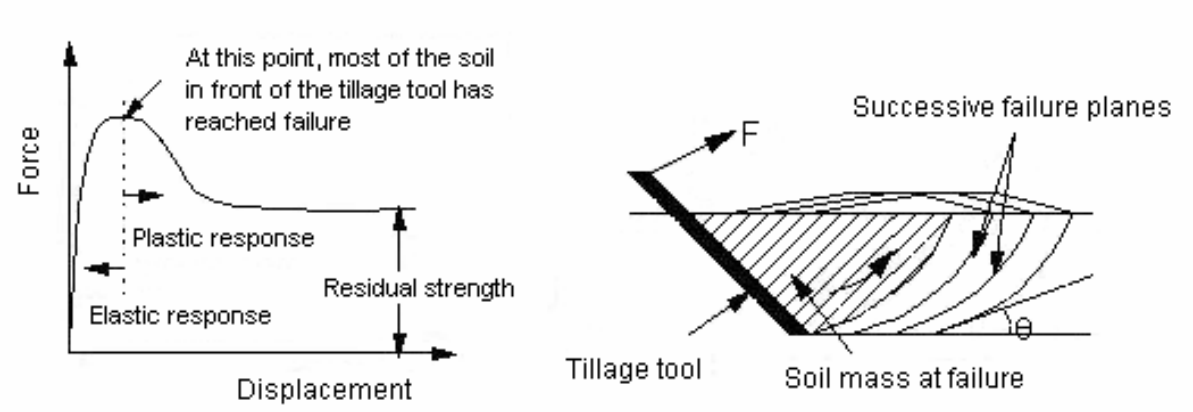

Fig. 5. (a) Force required for tillage; (b) Successive failure planes in front of the tool.

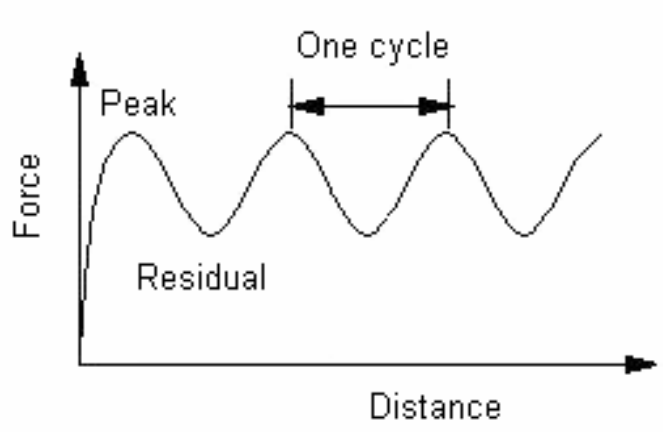

Fig. 6. Fluctuations in the tillage force due to formation of failure planes in the soil.

paper, both the stiffness and the strength of the soil are influenced significantly by the past stress (or strain) history of the soil. Therefore, to predict the magnitude of the tillage force, it is crucial to choose a strain dependent elasto-plastic constitutive model for the soil.

In addition to strain dependency, the change in the direction of the strain path is also a crucial factor in the analysis of soil-tool interaction during tillage. Before the tilling activity, the soil has experienced a strain path that is primarily vertical due to one-dimensional compaction or consolidation of the ground. During tillage, the soil experiences a strain path inclined at an angle of 30 to 90° with respect to the horizontal depending on the type of the tillage tool being used (Fig. 7). This change in the strain path reversal means that the soil is likely to have a higher stiffness as demonstrated experimentally by Atkinson et al. (1990). The increased stiffness of the soil will influence mainly the peak required tillage force.

As mentioned above, most soils are formed anisotropically by the process of deposition and subsequent consolidation in horizontal layers. Therefore, the magnitude of mobilized shear strength for these soils will be affected by the rotation of principal stresses experienced during tillage. Before the tillage activity, the major principal stress direction is vertical and the minor principal stress direction is horizontal (Fig. 8). During tillage, the soil in front of the tillage tool undergoes shear and passive failure. Therefore, the major principal stress direction changes from vertical to nearly horizontal close to the ground surface as shown in Fig. 8 and the soil is deemed to have failed in extension (negative deviatoric stress q as shown in Fig. 3). An anisotropic soil mobilizes shear strength in extension that is only about 50 to 60% of its shear strength in compression (Kulhawy and Mayne 1990). If the strength parameters are specified on the basis of, say, triaxial compression test, an analysis using isotropic elasto-plastic soil model will result in an overprediction of the required tillage force. Therefore, it may be necessary to use an anisotropic elasto-plastic soil model for achieving accurate simulation of soil tillage.

It is also important to recognize that most of the agricultural topsoil is unsaturated and therefore, a strain-dependent elasto-plastic model incorporating essential aspects of unsaturated soil behaviour may be necessary for numerical modeling of soil-tool interaction during tillage. Although several such models have been proposed (e.g. Wheeler and Sivakumar 1992; Fredlund and Rahardjo 1993), the science of coupled poro-mechanical analysis of an unsaturated soil is in a fairly nebulous stage. Therefore, special attention has to be taken for application of such models in machine-tool interactions.

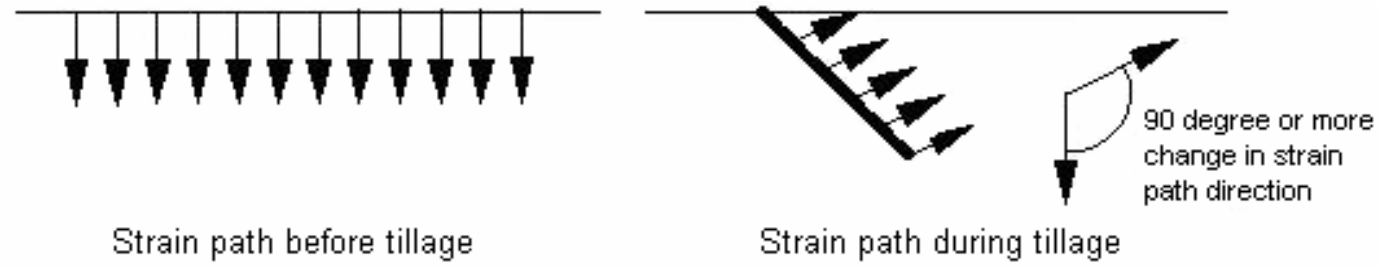

Fig. 7. Change in strain path direction due to tillage.

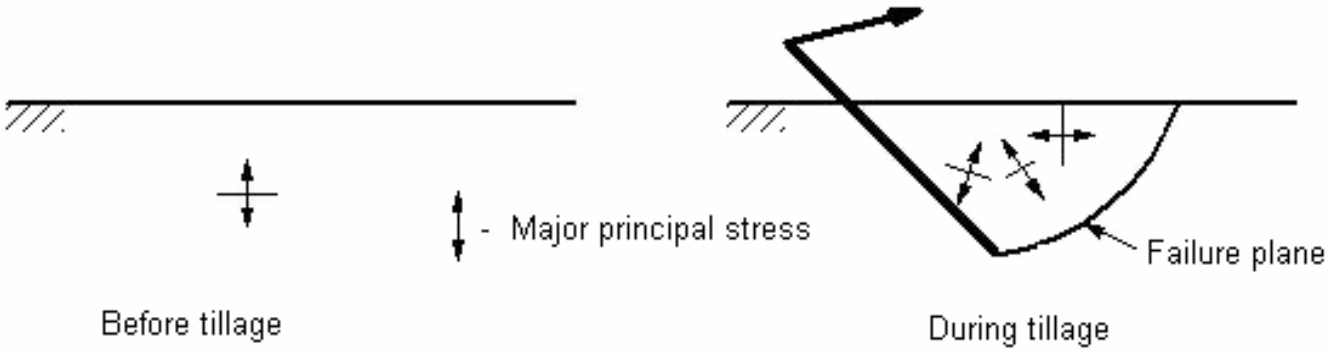

Fig. 8. Rotation of principal stresses in the ground due to tillage.

CONCLUSIONS

An attempt has been made to review several elasto-plastic soil constitutive models for possible use in the soil-tool interaction analysis during tillage. A wide range of such models is available from rather simple isotropic models requiring a few parameters to fairly complex models requiring 15 or more parameters. It is recognized that soil is an anisotropic material and its strength and stiffness are influenced by the past stress history as well as rotation of the direction of principal stresses. It is a daunting task to model all aspects of soil behaviour when analyzing tillage. However, certain key aspects such as strain-dependent stiffness and strength as well as anisotropy should be considered in order to obtain significant results from such analyses.

ACKNOWLEDGEMENT

The authors gratefully acknowledge the financial support provided by the Natural Science and Engineering Research Council of Canada, the Department of National Defence, Canada, and University of Saskatchewan Partnership Research Program.

REFERENCES

Atkinson, J.H., D. Richardson and S.E. Stallebrass. 1990. Effect of recent stress history on the stiffness of overconsolidated soil. *Géotechnique* 40(4):531-541.

Bailey, A.C., C.E. Johnson and R.L. Schafer. 1984. Hydrostatic compaction of agricultural soils. *Transactions of the ASAE* 27(4): 925-955.

Chi, L. and R.L. Kushwaha. 1989. Finite element analysis of forces on a plane soil blade. *Canadian Agricultural Engineering* 31(2):135-140.

Chi, L., R.L. Kushwaha and J. Shen. 1993. An elasto-plastic constitutive model for agricultural cohesive soil. *Canadian Agricultural Engineering* 35(4):245-251.

Duncan, J.M. and C.Y. Chang. 1970. Nonlinear analysis of stress and strain in soil. *Journal of the Soil Mechanics and Foundations Division, ASCE* 96(SM5):1629-1653.

Fredlund, D.G. and H. Rahardjo. 1993. *Soil Mechanics for Unsaturated Soils*. New York, NY: John Wiley.

Kondner, R.L. and J.S. Zelasko. 1963. A hyperbolic stress-strain response: Cohesive soil. *Journal of the Soil Mechanics and Foundations Division, ASCE* 89(SM1):115-143.

Kulhawy, F.H. and P.W. Mayne. 1990. *Manual on Estimating Soil Properties for Foundation Design*. Report EPRI-EL6800. Palo Alto, CA: Electric Power Research Institute.

Kushwaha, R.L. and J. Shen. 1994. The application of plasticity in soil constitutive modeling. ASAE Paper No. 941072. St Joseph, MI: ASAE.

Lade, P.V. and R.B. Nelson. 1984. Incrementalization procedure for elasto-plastic constitutive model with multiple, intersecting yield surface. *International Journal for Numerical and Analytical Methods in Geomechanics* 8:311-323.

Pollock, D. Jr., J.V. Perumpral and T. Kuppusamy. 1986. Finite element analysis of multipass effects of vehicles on soil compaction. *Transactions of the ASAE* 29(1):45-50.

Roscoe, K.H. and J.B. Burland. 1968. On the generalized stress-strain behaviour of wet clay. In *Engineering Plasticity*, eds. J. Heyman and F.A. Leckie, 535-609. Cambridge, England: Cambridge University Press.

Roscoe, K.H., A.N. Schofield and C.P. Wroth. 1958. On the yielding of soils. *Géotechnique* 8: 22-53.

Schofield, A.N. and C.P. Wroth. 1968. *Critical State Soil Mechanics*. London, England: McGraw-Hill.

Simpson, B. 1973. Finite elements applied to earth pressure problems. Unpublished Ph.D. thesis. Cambridge, UK: Department of Engineering, University of Cambridge.

Simpson, B. 1992. Retaining structures: Displacement and design. *Géotechnique* 42(4): 541-576.

Simpson, B., N.J. O'Riordon and D.D. Croft. 1979. A computer model for the analysis of ground movements in London Clay. *Géotechnique* 29(2): 149-175.

Stallebrass, S.E. 1990. Modelling the effect of recent stress history on the deformation of over-consolidated soils. Unpublished Ph.D. thesis. London, UK: Department of Geotechnical Engineering, City University.

Wheeler, S.J. and V. Sivakumar. 1992. Critical state concepts for unsaturated soil. In *Proceedings of Seventh International Conference on Expansive Soils*, 167-172. Lubbock, TX: Texas Tech University Press.

Wood, D.M. 1990. *Soil Behaviour and Critical State Soil Mechanics*. Cambridge, England: Cambridge University Press.

Yong, R.N. and A.W. Hanna. 1977. Finite element analysis of plane soil cutting. *Journal of Terramechanics* 15(1):43-63.

Zhang, J. and R.L. Kushwaha. 1998. Dynamic analysis of a tillage tool: Part I – Finite element method. *Canadian Agricultural Engineering* 40(4):287-292.

Appendix G

Manuscript 3: Dynamic modeling of soil-tool interaction: An overview from a fluid flow perspective.

Chapter 2 (part-3) has been accepted for publication in the Journal of Terramechanics on 17 June, 2005.

Available online at www.sciencedirect.com
SCIENCE DIRECT®
Journal of Terramechanics xxx (2005) xxx–xxx
Journal of Terramechanics
www.elsevier.com/locate/jterra

Dynamic modeling of soil–tool interaction: An overview from a fluid flow perspective

Subrata Karmakar *, R. Lal Kushwaha

Department of Agricultural and Bioresource Engineering, University of Saskatchewan, 57 Campus Drive, Saskatoon, Canada S7N 5A9

Abstract

The study of tillage tool interaction centers on soil failure patterns and development of force prediction models for design optimization. The force-deformation relationships used in models developed to date have been considering soil as a rigid solid or elasto-plastic medium. Most of the models are based on quasi-static soil failure patterns. In recent years, efforts have been made to improve the conventional analytical and experimental models by numerical approaches. This paper aims at reviewing the existing methods of tillage tool modeling and exploring the use of computational fluid dynamics to deal with unresolved aspects of soil dynamics in tillage. The discussion also focuses on soil rheological behaviour for its visco-plastic nature and its mass deformation due to machine interaction which may be analyzed as a Bingham plastic material using a fluid flow approach. Preliminary results on visco-plastic soil deformation patterns and failure front advancement are very encouraging. For a tool operating speed of 5.5 m s^{-1}, the soil failure front was observed to be about 100-mm forward of the tool.

Keywords: Tillage; Elasto-plastic; Visco-plastic; Computational fluid dynamics (CFD)

* Corresponding author. Tel.: +1 306 966 5326; fax: +1 306 966 5334.
E-mail address: S.Karmakar@usask.ca (S. Karmakar).

0022-4898/$20.00 © 2005 Published by Elsevier Ltd on behalf of ISTVS.
doi:10.1016/j.jterra.2005.05.001

1. Introduction

Tool interaction with agricultural soil basically deals with soil cutting, with the objective of attaining suitable conditioning for crop production. Tillage is the mechanical manipulation of the soil in the tillage layer in order to promote tilth, i.e. desired soil physical condition in relation to plant growth. Performance efficiency of tillage is measured in terms of draft or input energy [1]. Optimization in tillage tool design necessitates minimization of the input energy. It is estimated that tillage accounts for about one half of the energy used in crop production [2]. The draft requirement to cause soil failure to a desired tilth depends on the soil failure pattern which is a combined effect of the soil, tool and system parameters.

Methods of classical soil mechanics are often applied to agricultural soil mechanics with little modification for studying soil deformation [3]. Soil mechanics dealing with agricultural soil has the distinction from those of civil and geotechnical engineering problems in the context of the soil behaviour. Tillage is mostly concerned with soil loosening at shallow depths with the interaction of relatively low loads. During the last four decades, much research has been conducted on parametric studies for soil–tool interaction with different approaches. These parameters have primarily been studied in a quasi-static condition considering the equilibrium of the soil–tool system. Recently few studies have been conducted taking the dynamic feature of soil–tool interface due to machine interaction by numerical modeling. These studies, in contrast to the conventional assumption of passive earth pressure theory (quasi-static), considered velocity and acceleration of the tool during the soil–tool interaction. However, the large scale deformation of soil is still an area in which little research has been conducted. Force prediction models for tillage tools have been relying on the classical soil failure theory for quasi-static conditions. A better understanding of the soil–tool interface mechanism can be obtained by correlating soil rheological behavior with its dynamic characteristics. This article attempts to briefly review the conventional practices in tillage tool modeling and to explore the possible application of a fluid dynamics modeling framework to this large and irrecoverable soil deformation.

2. Different approaches for soil–tool modeling

Studies of soil–tool interaction have been carried out mostly for development of force prediction models using different soils, tools, and operating conditions (speed and depth of operation, tool orientation, etc.). The formation of two- and three-dimensional soil failure patterns, with their validity established by comparing the predictions with experimental results, have been taken into account. So far, five major methods, namely empirical and semi-empirical, dimensional analysis, finite element method (FEM), discrete or distinct element method (DEM) and artificial neural network (ANN), have been used as approaches to solve problems in the area of soil–tool interaction and failure mechanism.

Mathematical solutions based on empirical and semi-empirical models have been developed to describe soil–tool interaction which helps designers and researchers develop an understanding through parametric studies. These analytical models are based on the physics of soil and system parameters, tool configuration and simple assumptions. Experimental models are cost and time effective. The relation between the variables is expressed by a suitable curve that fits best to the observed data and an appropriate model is developed. Similitude or dimensional analysis techniques involve representing different parameters of a tillage system by 'PI' terms and developing relations between dependent and independent variables. Effectiveness of a similitude model depends on the completeness of the list of parameters [4]. Here, scaling of parameters is a complicating factor, which results in distorted models. Improper scaling may lead to obscurity in two- and three-dimensional problems. High speed computers and commercial software have allowed numerical models to be developed to take care of complex tool geometry and other parameters which are difficult to consider in analytical modeling. The finite element method can partly overcome the shortcomings of analytical methods in supplying more information about the progressive soil failure zone, field of stress, displacement, velocity, and acceleration of soil–tool interaction [5].

Different types of failure mechanisms have been considered towards analysing the power requirement for a tillage tool. Passive shear failure has been considered with respect to passive earth pressure theory. Progressive shear type of failure formed soil blocks at uniform intervals. An analytical method with crescent-shaped soil blocks was used and was helpful in analysis of the force system. Rigid-brittle type of failure was considered for soil water content values below the plastic range and flow type was considered for soil water content values above the plastic range [6]. In brittle failure, shear planes are formed as blocks of soil separated from the soil mass. It was observed that the force on the tool was of periodic nature in brittle failure. Speed did not affect the shear strength under the conditions of brittle soil failure, whereas, under flow failure conditions, soil–metal friction has been observed to be a logarithmic function of speed. Collapse-type failure was observed for cyclic behaviour of soil forces with tine movement, particularly for wide tools [7]. Relationships have been established between draft force and operating speed. The soil worked by tines has been assumed to obey the Mohr–Coulomb failure criterion of classical soil mechanics in most of the models. The Cambridge theory of critical state soil mechanics, which deals with the saturated soil and postulates the effect of stress on pore pressure, has also been adopted for soil tillage study [8]. Following the methods of fracture mechanics for partially saturated soil, Hettiaratchi [9] developed a critical state soil mechanics model for agricultural soils.

Analytical models are primarily based on the logarithmic spiral method and passive earth pressure theory for calculating soil resistance. Osman [10] initiated a study on the mechanics of simple two-dimensional soil cutting blades based on the theories concerning the passive pressure on large retaining walls. The basic formulation for soil cutting was proposed by Reece [11] based on Terzaghi's passive earth pressure theory [12] incorporating an additional parameter to the bearing capacity;

$$P = \gamma z^2 N_\gamma + czN_c + c_a zN_a + qzN_q, \quad (1)$$

where P is the force necessary to cut soil with a tillage tool, γ is the specific weight of soil, c is the soil cohesion, c_a is the soil–metal adhesion, z is the depth of cut, q is the surcharge, The 'N' terms represent gravitational, cohesive, adhesive and surcharge components of soil reaction per unit width of interface, respectively.

Based on Reece's equation, models [11,13] have been developed for two-dimensional soil failures. Improvement in prediction models was achieved by three-dimensional soil failure models [14–17]. Two-dimensional failures may be in a vertical plane with tools operating at shallow depths or in a horizontal plane for tools operating at deeper depths and are applicable to wider tools. A three-dimensional failure [18] involves a failure pattern in both planes and is generally considered for narrow tools. Models have been developed by calculating the total force on a tillage tool due to forward (*crescent*) and side failures, soil–metal and soil internal frictional forces with some modification from one to the other. Some of the models have also considered a critical depth with respect to describing a failure pattern in two and three dimensions for precise calculation of the draft. Godwin and Spoor [15] considered three-dimensional crescent failure above critical depth and two-dimensional lateral failure below critical depth for narrow tillage tools. Models developed with the limit equilibrium method [16,17] of analytical approach assume that the failure surface emanates from the tool tip and intersects the soil surface at a failure angle. These methods can only be used to obtain information of the maximum forces that are generated inside soil because of soil–tool interaction, without providing much information about how the soil body deforms [19].

The above stated type of models are not based on actual soil failure patterns that vary with rake angle, moisture content, soil density, etc. The soil failure profile varies with tool shape, operating speed, and soil physical properties. Therefore, the use of the analytical models, based on passive earth pressure theory and assumptions of a preliminary soil failure pattern, is limited for optimum design of a tillage tool [20]. Numerical methods help analyse the soil–tool interaction of complex shaped machines with the development of a suitable constitutive relation for a specific working condition with a proper algorithm. Several models [21–25] have been developed based on finite element analysis. For agricultural soils, which are usually unsaturated, a hyperbolic stress–strain model developed by Duncan and Chang [26] has been adopted by many researchers in their FEM applications. FEM can partly overcome the shortcomings of analytical methods in supplying more information about the progressive soil failure zone, field of stress, displacement, velocity, and acceleration of soil–tool interaction [5].

Studies using distinct element method (DEM) are based on mechanical behaviors of granular assemblies. If the soil model by the DEM is constructed with high accuracy, it could be applied to many mechanical and dynamic problems between soil and machines in the field of Terramechanics [27]. A technique based upon the DEM has been developed to model the dynamic interaction of an implement (a typical dozer blade) with cohesively bonded particles by simulating cohesive soils [37].

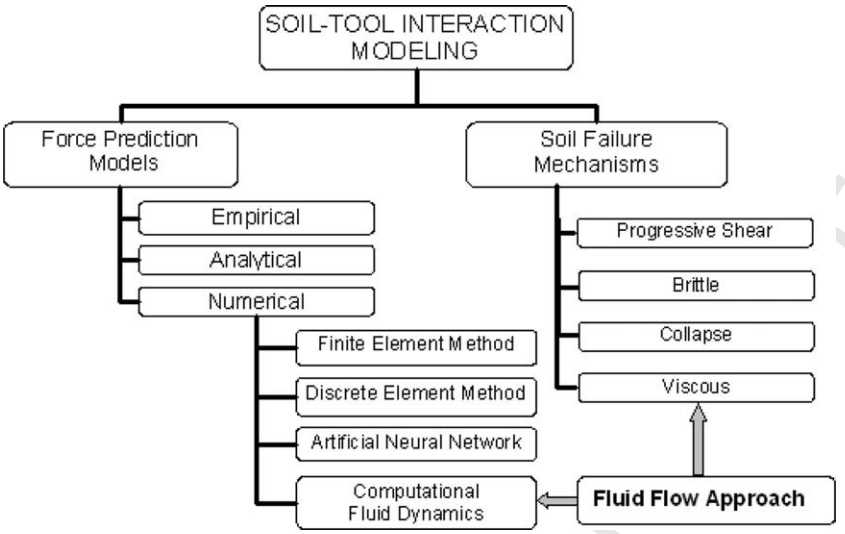

Fig. 1. Schematics of soil–tool modeling.

Comparisons with test data showed good correlation for cutting forces, but poor correlation for penetration forces.

The proposed model [28] based on artificial neural network seemed to be a better solution for soil–tool interaction modeling as it can handle fuzzy and non-uniform input variables for the dynamic range of problems [29]. A generalized flow-chart has been drawn (Fig. 1) based on the researches conducted on soil–tool modeling.

3. Issues and challenges

From the above discussion, the following points can be highlighted as problem areas in tillage tool design.

3.1. Tool geometry

Analytical models are good for simple geometries. Design of tillage tools with complex shape cannot be handled with this conventional and lengthy method for varying soil–tool parameters. Numerical methods are capable of analyzing the physics of a problem with complex tool geometry using computer aided design (CAD). The CAD files are loaded in the respective computer program and parametric studies are carried out by sensitivity analysis in a very short time.

3.2. Dynamic modeling

Tillage is primarily a dynamic operation. Though the analytical models serve the purpose to a certain extent, one of the weaknesses is that they do not adequately

define the influence of tool speed on soil failure pattern [19]. With a dynamic process, two possible effects, which are an inertia effect and a rate-effect, might need to be considered in an analysis. The tillage energy requirement, tool wear, and the final soil conditions are rate-dependent, which necessitates optimization of parameters for tillage operations to take account of the effects of soil–tool dynamics on tillage performance [5]. The engineering soil mechanics approach is based on equilibrium state stress–strain relationships for the study of soil deformation, while deformations in agricultural soils rarely reach equilibrium [30]. In soil tillage, the soil is lifted and accelerated and thereby given potential and kinetic energies, and it is manipulated such that a change of state occurs. These processes occur under non-equilibrium conditions [31]. Also, soil tillage is conducted in the unsaturated soil zone, where it is difficult to achieve the critical state condition (no volume change due to external loading). Thus, tillage is a non-equilibrium process.

Most of the assumptions involved with the models based on earth pressure theory neglect the inertial forces and are suitable only for predicting the forces on a narrow tine moving at very slow speed. Though the application of existing numerical techniques like FEM and ANN have been found to predict the soil–tool system in a better approximation to the exact solution, soils have been considered for static analysis and the mass soil deformations have been ignored. Recently, a few studies [32–34] based on numerical methods have been conducted using FEM with the dynamic perspective of tillage. However, in this case, prior knowledge of shear strain at failure for determining the position of a shear failure boundary is required. With a few exceptions, the finite element method, the boundary element method, and the finite difference method require the fabric to be continuous in nature, not allowing for separation, rotation, large scale deformation and displacement [35]. For dynamic modeling, the conventional DEM model for calculation of contact forces between elements has some problems; for example, the movement of elements is too discrete to simulate real soil particle movement [36]. The distinct element method has been shown to predict the horizontal force on implements, such as dozer blades, with reasonable accuracy. The vertical force predictions on the dozer blade, however, do not correlate well with measured data. It appeared, in general, that more capable computational methods are required to effectively simulate the dynamic response characteristics of cohesive earthen materials and their interaction with components of off-road machines. The challenge is daunting, but the need is great [37].

Simulations were performed using FEM [25] to evaluate the effects of moldboard settings and operating speed on plow performance in a clay soil. They have suggested that other numerical tools should be combined with FEM to enable evaluation of overall behaviors of tillage implements. This is because the current formulation of FEM alone cannot solve such a complex behavior and field experiments may not allow clear depiction of the effect of changing a single part.

Soil shear rate with respect to the tool operational speed plays a very important role in analyzing and optimizing high speed tillage. The size of the furrow formed behind the tool is a function of the operating speed. Photographic and video camera analysis indicated increasing soil crumbling with increasing tool speed. While

trying to estimate the furrow profile using a soil profilometer, difficulties arose and quantification could not be addressed [38].

3.3. Material complexity and stress path variation

Most soils are formed anisotropically by the process of deposition and subsequent consolidation in horizontal layers. Soil complexity is compounded by the influences of moisture content, structural disturbance, stress history, time, and environmental conditions. Different soil formation phases and previous activities cause agricultural soil to be basically an anisotropic material. An anisotropic soil tends to fail due to shear strength in extension that is only about 50–60% of its shear strength in compression [39]. Modeling of soil–tool interaction using FEM, soil strength parameters have been based in triaxial compression tests. Before the tillage activity, the major principal stress direction is vertical and the minor principal stress direction is horizontal. During tillage, the soil undergoes shear and passive failure. Therefore, the major principal stress direction changes from vertical to nearly horizontal close to the ground surface and soil is deemed to fail in extension. Thus, analyses that use isotropic elastic–plastic soil models result in an over prediction of the required tillage forces [40].

3.4. Limitations of existing base models

The peak tillage force is a function of both stiffness and strength of the soil, whereas the residual tillage force depends primarily on the strength of soil. Both the stiffness and the strength of soil are influenced significantly by the past stress (or strain) history of the soil. Therefore, in order to predict the magnitude of the tillage force, it is crucial to choose a strain-dependent elasto-plastic model for the soil [41]. Although several such models have been proposed [41,42], the science of coupled poro-mechanical analysis of an unsaturated soil is in a fairly nebulous stage. Therefore, application of such models in tillage tool interaction is not anticipated in the near future. Thus, analysis of soil–tool interaction taking the dynamic feature into consideration remains unsatisfied.

4. Application of CFD to tillage

Movies have shown the fundamental behavior of an artificial soil failure to change from shear to plastic flow as the tool velocity was increased [43]. Olson and Weber [44] also observed that an increase in the speed of a blade could cause a transition between the shear-plane and flow failures. As the speed was increased, there was more general shear and less sliding of one soil block on another, until the shear failure plane no longer formed and only a flow failure occurred. At high speed, soil underwent plastic failure when both dry and wet soils were used [45]. It was believed that the soil strength parameters, cohesion and angle of internal friction, were dependant on strain rate. Successive study by Stafford and Tanner [46] on sandy and clay

soils revealed that deformation (shear) rate had a very significant effect on the shear strength over a wide range of moisture content.

In design and development, computational fluid dynamics (CFD) programs are now considered to be standard numerical tools for predicting not only fluid flow behavior, but also the transfer of heat and mass, phase change, chemical reaction, mechanical movement and stress or deformation of structures [47]. The programs provide a detailed description of flow distributions, making it possible to evaluate geometric changes with much less time and cost than would be involved in laboratory testing.

4.1. Soil rheological behaviour

The rheology of soil is very complex. In the case of Newtonian fluids, like air and water, the shear stress versus shear rate relationship is linear and the fluids have a constant viscosity at a particular temperature. However, high molecular suspensions of fine particles, pastes and slurries are usually non-Newtonian [48]. Soils, like most real bodies, deform at a variable rate. Only at the certain stage of the process is the rate of deformation constant [49].

Upon close examination of experimental stress–strain rate relationships of several soils, Vyalov [49] concluded that a simple linear model of visco-plasticity, the Bingham rheological model, can describe soil deformation under steady-state stress. Soil visco-plastic behaviour has been reported in several studies [50–52]. The relation between the stress and rate of flow is non-linear in soil, and the flow is induced by the difference between total stress and the yield stress. The generalized observation was that flow of soil is initiated only when the stress acting upon the inter-aggregate contact exceeds a '*critical yield point*' (threshold stress value). This threshold stress is termed as yield stress. Beyond this stress, soil aggregates flow in a manner similar to viscous material at a rate proportional to the stress in excess of the yield stress. Visco-plastic fluids behave like solids when the applied shear stress is less than the yield stress; once it exceeds the yield stress, it will flow just like a fluid [53].

4.2. Soil flow phenomena

Fornstrom et al. [31] proposed non-equilibrium process concepts for tillage with emphasis on the notion of change of state. The theory considers the energy balance taking into account a stress tensor to represent internal mechanical effects involving kinetics and kinematics. The externally applied force was related to the changes in internal energy and specific volume (dilation) and to viscous flow. Since soil flow is not always a continuous process, '*scale of motion*', represented by '*integral or macro scale*' and '*micro scale*' was recommended for consideration. Macro scale is a measure of the average longest distance over which the motion of a particle or group of particles persists in a given direction. Micro scale is some measure of the average shortest distance travelled by a particle or group of particles before a change of direction occurs.

The feature of large deformation of soil due to tillage tool interaction can be viewed as soil flow around the tillage tool. By definition, a fluid is a material

continuum that is unable to withstand a static shear stress. Unlike an elastic solid which responds to a shear stress with a recoverable deformation, a fluid responds with an irrecoverable flow [54]. Fluid flow can be of generally either an internal flow or an external flow type. Examples of internal flow are pipe flow of air or water or any other fluids. Flow of air over an aircraft is a perfect example of external flow. When a tool is operated for soil cutting, this dynamic process can be viewed as an external flow over a bluff body; soil flow over the tool. Desai and Phan [55] presented the general case of the three-dimensional soil–tool interaction in which the tool is moving relative to the soil as shown in Fig. 2. Thus, the soil shear failure due to the translation of the tool is analogous to the fluid flow over a blunt body. The velocity vectors of the soil particles as they encounter with the tool and soil failure front propagation can be derived from a fluid mechanistic approach.

4.3. Soil flow pattern

Soil flow around the tool can be categorized and analyzed from the perspective of fluid and flow parameters. Fluid parameters are concerned with the physical properties of the fluid, while flow parameters represent the feature of the flow with respect to the system as a whole. Though both air flow over an aircraft and soil flow over a tillage tool are external flows, much difference exists in the fluid characteristics. A fluid flow could be laminar or turbulent depending on several factors, including flow velocity, fluid viscosity and length scale, etc. The general demarcation of the two

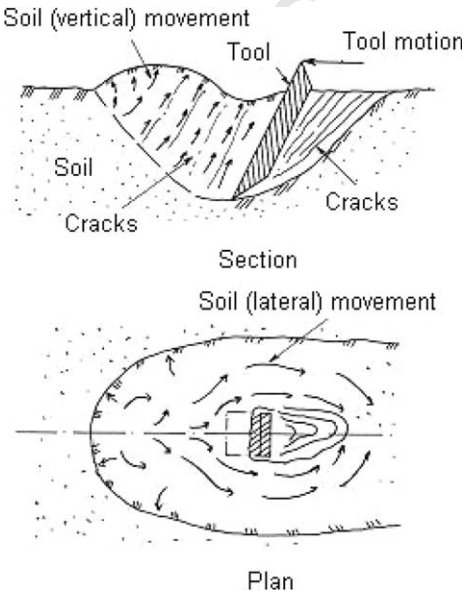

Fig. 2. Soil tool idealization [55].

types of flow is specified by the Reynolds number, which is the ratio of inertia and viscous forces. Even in high speed tillage, due to the high molecular weight of soil, the soil flow pattern is expected to remain a laminar flow.

4.4. Soil flow hypothesis

From the discussion of soil rheology and fluid flow features, it is clear that soil can be considered as a visco-plastic material and its mechanical behaviour during tillage can be studied from a fluid flow perspective with non-Newtonian flow behaviour. Predicting the changes of complex soil mechanical behavior with different texture and structures at different places is either intractable or very costly. However, for many interactive applications, realistic appearance is more important than accuracy. Hence, for simulation purposes, initially, soil could be considered to be homogeneous and incompressible. Soil could also be modeled as a compressible material in this fluid flow approach. In this case, a multiphase fluid flow would have to be considered. The specific volume fraction of solid, water, and air with their mechanical characteristics would be analyzed using a volume of fluid approach. However, since this was the first attempt, for simplification, the soil has been considered to be incompressible.

Changes in void ratio due to soil loading by interaction with a tillage tool, and hence density change which causes the rheological behavior to be altered can be neglected. Thus, soil can be considered as a single-phase continuous medium and its rheological properties can be analyzed and used to simulate the soil deformation process associated with tillage. The approach could be to consider the tool as stationary and visco-plastic soil flow over the tool. The flow domain could be decided based on the tool influence zone. Thus, the influence of the tool in a fully developed flow could be utilized to calculate the soil disturbance and force imposed on the tool.

4.5. Mathematical modeling of CFD

With CFD, particle movement of a system can be observed with its velocity and stress distribution field in a well defined form. The basic principle is to solve the constitutive equations of fluids which are based on the conservation of mass and momentum equations. Thus, the general equations of motion can be obtained in an acceptable form. Soil tilling could be modeled by incorporating non-Newtonian parameters in the following basic Navier–Stokes equation (continuity and momentum equations):

$$\frac{\partial \rho}{\partial t} + \nabla \cdot (\rho V) = 0, \tag{2}$$

$$\rho g - \nabla p + \nabla \cdot \tau_{ij} = \rho \frac{\partial V}{\partial t}, \tag{3}$$

where ρ is the density of the fluid, V is the velocity, p is the pressure, τ_{ij} is the stress tensor. The stress tensor is

$$\tau_{ij} = \eta\left(\frac{d^2V}{dx^2} + \frac{d^2V}{dy^2} + \frac{d^2V}{dz^2}\right), \tag{4}$$

where η is the viscosity of the fluid; x, y, z, are the coordinate axes.

Soil, being non-linear and visco-plastic in nature, possesses a variable coefficient of viscosity. This parameter can be modeled by a user subroutine in any commercial CFD software package to analyze the soil–tool interaction. The stress tensor would be replaced by the following constitutive relation of a Bingham plastic material:

$$\tau = \tau_y + \mu\dot{\gamma}, \quad |\tau| > \tau_y, \tag{5}$$

$$\dot{\gamma} = 0, \quad |\tau| \leqslant \tau_y, \tag{6}$$

where τ is the shear stress, $\dot{\gamma}$ is the shear rate, τ_y is the yield stress, μ is the viscosity coefficient, analogous to Newtonian viscosity, usually referred to as plastic viscosity.

5. Preliminary results

Preliminary studies have been carried out to analyze soil flow behavior as a Bingham visco-plastic material in a rectangular flow domain using computational fluid dynamics with pertinent soil parameters. The numerical simulations were performed using a commercially available CFD code, CFX4.4 from AEA Technologies [56]. Simulations were carried out for a tool with 50-mm width operating vertically in clay loam soil. Soil parameters for simulations were obtained using vane-type shear tests in a strain rate controlled torsional soil rheometer developed in the Department of Agricultural and Bioresource Engineering, University of Saskatchewan. The soil was precompressed by applying a normal stress of 300 kPa to the surface of the soil contained in a soil box. The soil had a bulk density of 1250 kg m^{-3}, and a moisture content of 17% d.b., and the yield stress and the viscosity were found to be 12 kPa and 850 Pa s, respectively. The depth of the tool as well as the flow channel was 100 mm. A contour plot (longitudinal velocity) of soil flow behavior with tool interaction was observed to have two distinct features of plastic and plug flow (Fig. 3(a)). Plastic flow (near the tool and the wall boundary) occurred where the soil shear stress exceeded the compressive yield stress, while plug flow (solid-like flow) occurred where the shear stress was less than the compressive yield stress. For a soil flow situation with the tool modeled as stationary, the velocity of soil at the tool surface is zero due to a no slip boundary condition. Soil flow velocity increases towards the fully developed flow approaching from the flow inlet. Thus, at the region near the tool, the shear stress is very high and it exceeds the yield stress of soil and soil fails, i.e. visco-plastic soil deformation is observed.

In a tool operating environment, the soil front propagation or soil disturbance zone would be interpreted from the distribution of the longitudinal velocity of soil flow (Fig. 3(b)). It is seen that the fully developed soil flow was disturbed due to the presence of the tool in the flow domain. Thus, the influence zone which is also an indication of the plastic flow region could be referred to as the soil disturbance area for a particular tool velocity. For a tool velocity (fully developed soil flow

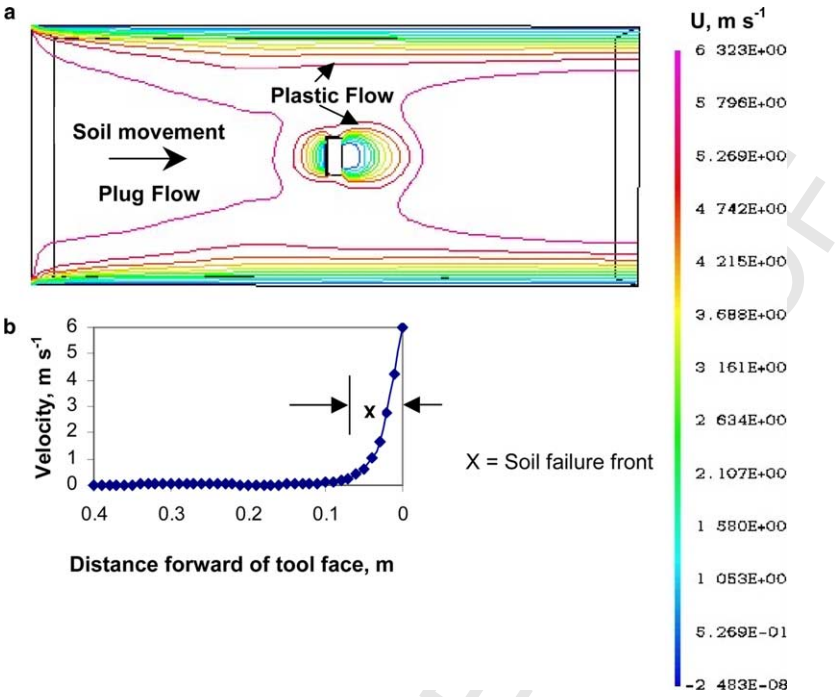

Fig. 3. (a) Top view showing soil flow pattern around a stationary tool. Contour lines show longitudinal velocity of soil particles, U (m s^{-1}). (b) Soil front propagation for the moving tool.

velocity) of 5.5 m s^{-1}, the soil front propagation ('X') in the direction of tool movement (opposite to the direction of soil flow) was observed to be about 100-mm forward of the tool.

In addition to showing the soil failure pattern and calculating soil disturbance area due to tool interaction, CFD analysis would also provide soil stress analysis and force requirement. The fluid flow approach, thus, plays an important role for addressing many unresolved areas in tillage tool modeling.

6. Conclusions

Existing soil–tool modeling techniques have been reviewed with their relative merits and weaknesses. A wide range of such models is available to predict the force required to operate a tillage tool. Improvements have been achieved by the recent numerical methods. However, the behavior of large soil deformation during tillage needs to be explored. Problem areas and information gaps existing with soil–tool interaction have been identified.

Preliminary investigations using computational fluid dynamics showed promising results for modeling soil–tool interaction. Results clearly showed the soil failure front advancement and soil velocity profile with a tool velocity of 5.5 m s^{-1}.

Application of CFD in the area of tillage is anticipated to bring a new dimension to the tool design and study of soil behavior for different agro-climatic conditions. The following pathways could be speculated for advanced research using computational fluid dynamics:

1. Soil dynamic behavior using the CFD simulation will help in optimizing the design of tools with different shapes in order to reduce tool draft and energy demand over a wide speed range.
2. Soil deformation features like ridge and furrow formation, stress distribution, energy requirement etc. due to soil–tool interaction are expected to be obtained from this approach in a realistic manner. Dynamic analysis of high speed tillage with respect to the soil disturbance and quantifying the furrow profile could be achieved using free surface CFD simulations.
3. Dynamic analysis in this fluid flow perspective would help modeling different types of soils based on their visco-plastic parameters. Some criteria analogous to Reynolds number, based on viscosity range, are expected to address change in state of soil due to tool interaction.

References

[1] Gill WR, Vanden Berg GE. Soil dynamics in tillage and traction. Agriculture handbook, No. 316. USDA; 1967.
[2] Kushwaha RL, Bigsby FW. Tillage practices. In: Gillies JA, Kushwaha RL, editors. Handbook on conservation agriculture. Saskatoon (SK): University of Saskatchewan; 1989.
[3] Koolen AJ. Agricultural soil mechanics. Advanced series in agricultural sciences. Berlin: Springer-Verlag; 1983.
[4] Luth HJ, Wismer RD. Performance of plane soil cutting blades in sand. Trans ASAE 1971;14:255–9.
[5] Kushwaha RL, Zhang ZX. Evaluation of factors and current approaches related to computerized design of tillage tools: a review. J Terramech 1998;35(2):69–86.
[6] Stafford JV. Force prediction models for brittle and flow failure of soil by draught tillage tools. J Agric Eng Res 1984;29:51–60.
[7] Rajaram G, Gee-Clough D. Force distance behaviour of tine implements. J Agric Eng Res 1988;41:81–98.
[8] Hettiaratchi DRP, O'Callaghan JR. Mechanical behaviour of Agricultural soils. J Agric Eng Res 1980;25:239–59.
[9] Hettiaratchi DRP. A critical state soil mechanics model for agricultural soils. J Soil Use Manage 1987;3:94–105.
[10] Osman MS. The mechanics of soil cutting blades. J Agric Eng Res 1964;9(4):313–28.
[11] Reece AR. The fundamental equations of earth-moving mechanics. In: Proceedings of the symposium on earth moving machinery, vol. 179, No. 3F. Institute of Mechanical Engineering; 1965. p. 8–14
[12] Terzaghi K. Theoretical soil mechanics. New York: Wiley; 1943.
[13] Hettiaratchi DRP, Witney BD, Reece AR. The calculation of passive pressure in two-dimensional soil failure. J Agric Eng Res 1966;11(2):89–107.
[14] Hettiaratchi DRP, Reece AR. Symmetrical three-dimensional soil failure. J Terramech 1967;4(3):45–52.
[15] Godwin RJ, Spoor G. Soil failure with narrow tines. J Agric Eng Res 1977;22:213–28.
[16] McKyes E, Ali OS. The cutting of soil by narrow blades. J Terramech 1977;14(2):43–58.

[17] Perumpral JV, Grisso RD, Desai CS. A soil–tool model based on limit equilibrium analysis. Trans ASAE 1983;26(4):991–5.
[18] Payne PCJ. The relationship between the mechanical properties of soil and the performance of simple cultivation implements. J Agric Eng Res 1956;1(1):23–50.
[19] Shen J, Kushwaha RL. Soil–machine interactions – a finite element perspective. Marcel Dekker; 1998.
[20] Kushwaha RL, Chi L, Shen J. Analytical and numerical models for predicting soil forces on narrow tillage tools – a review. Can Agric Eng 1993;35(3):183–90.
[21] Yong RN, Hanna AW. Finite element analysis of plane soil cutting. J Terramech 1977;14(3):103–25.
[22] Liu Y, Hou ZM. Three-dimensional non-linear finite element analysis of soil cutting by narrow blades. In: Proceedings of the international conference on soil dynamics, Auburn (AL), vol. 2; 1985. p. 338–47.
[23] Chi L, Kushwaha RL. A non-linear 3-D finite element analysis of soil failure with tillage tools. J Terramech 1990;27(4):343–66.
[24] Wang J, Gee-Clough D. Deformation and failure in wet clay soil. II. Simulation of tine soil cutting. In: Proceedings of IAMC conference, Beijing, China, Session 2; 1991. p. 219–26.
[25] Plouffe C, Laguë C, Tessier S, Richard MJ, McLaughlin NB. Moldboard plow performance in a clay soil: simultaneous and experiment. Trans ASAE 1999;42(6):1531–9.
[26] Duncan JM, Chang C-Y. Non-linear analysis of stress and strain in soils. J Soil Mech Found Div ASCE 1970;96(SM5):1629–53.
[27] Tanaka H, Momozu M, Oida A, Yamazaki M. Simulation of soil deformation and resistance at bar penetration by the distinct element method. J Terramech 2000;37(1):41–56.
[28] Zhang ZX, Kushawaha RL. Application of neural networks to simulate soil–tool interaction and soil behaviour. Can Agric Eng 1999;41(2):119–25.
[29] Jayasuriya HPW, Salokhe VM. A review of soil–tine models for a range of soil conditions. J Agric Eng Res 2001;79(1):1–13.
[30] Or D. Wetting induces soil structural changes: the theory of liquid phase sintering. Water Resour Res 1996;32:3041–9.
[31] Fornstrom KJ, Brazee RD, Johnson WH. Tillage tool interaction with a bounded, artificial soil. Trans ASAE 1970;13(4):409–16. p. 418.
[32] Swick WC, Perumpral JV. A model for predicting soil–tool interaction. J Terramech 1988;25(1):43–56.
[33] Zeng D, Yao Y. A dynamic model for soil cutting by blade and tine. J Terramech 1992;29(3):317–27.
[34] Shen J, Kushwaha RL. Investigation of an algorithm for non-linear and dynamic problems in soil–machine systems. Comput Electron Agric 1995;13:51–66.
[35] Nordell LK. Particle flow modeling: transfer chutes other applications. In: Chute design conference BELTCON, Republic of South Africa; 1997.
[36] Momozu M, Oida A, Yamazaki M, Koolen AJ. Simulation of a soil loosening process by means of the modified distinct element method. J Terramech 2003;39:207–20.
[37] Hofstetter K. Analytic method to predict the dynamic interaction of a dozer blade with earthen material. In: Proceedings of the 14th international conference on ISTVS, Vicksburg (MS); 2002 [on CD-ROM].
[38] Rosa UA. Performance of narrow tillage tools with inertial and strain rate effects. Doctoral Thesis, University of Saskatchewan, Saskatoon; 1997.
[39] Kulhawy FH, Mayne PW. Manual on estimating soil properties. Report EL-6800, Electric Power Research Institute, Davis (CA); 1990.
[40] Karmakar S, Sharma J, Kushwaha RL. Critical state elasto-plastic constitutive models for soil failure in tillage – a review. Can Biosyst Eng 2004;46:219–23.
[41] Wheeler SJ, Shivakumar V. Critical state concepts for unsaturated soil. In: Proceedings of the 7th international conference on expansive soils, Dallas (TX); 1992. p. 167–72.
[42] Fredlund DG, Rahardjo H. Soil mechanics for unsaturated soils. New York: Wiley; 1993.
[43] Schimming BB, Hass HJ, Saxe HC. A comparison of the dynamic and static shear strengths of cohesion less, cohesive, and combined soils. Tech Report No. AFWL TR-65-48, Department of Civil Engineering, University of Notre Dame; 1965.

[44] Olson DJ, Weber JA. Effect of speed on soil failure patterns in front of model tillage tools. Trans SAE 1966;74(4):298–310.
[45] Stafford JV. The performance of rigid tine in relation to soil properties and speed. J Agric Eng Res 1979;24(1):41–56.
[46] Stafford SV, Tanner DW. Effect of rate on soil shear strength and soil–metal friction. Soil Tillage Res 1983;3:245–60.
[47] Sethian JA. Computational fluid dynamics. From desktop to teraflop: exploiting the US lead in high performance computing. Washington (DC): NSF Publications; 1993.
[48] Skelland AHP. Non-newtonian flow and heat transfer. Wiley; 1967.
[49] Vyalov SS. Rheological fundamentals of soil mechanics. Amsterdam, The Netherlands: Elsevier; 1986.
[50] Day PR, Holmgren GG. Microscopic change in soil structure during compression. Soil Sci Soc Am Proc 1952;16:73–7.
[51] McMurdie JL, Day PR. Compression of soil by isotropic stress. Soil Sci Soc Am Proc 1958;22:18–22.
[52] Ghavami M, Keller J, Dunn IS. Predicting soil density following irrigation. Trans ASAE 1974;17:166–71.
[53] Bird RB, Dai GC, Yarusso BJ. The rheology and flow of visco-plastic materials. Rev Chem Eng 1983;1:1–70.
[54] White FM. Fluid mechanics. 4th ed.. WCB McGraw Hill; 1999.
[55] Desai CS, Phan HV. In: Oden JT, editor. Computational methods in non-linear mechanics. North-Holland Publishing Company; 1980. p. 205–24.
[56] CFX release 4.4 user guide, AEA Technologies. Harwell, Didcot, UK: CFX International; 2001.

Appendix H

Manuscript 4: Simulation of soil deformation around a tillage tool using computational fluid dynamics.

Chapter 4 has been published in the Transactions of the ASAE 48(3): 923-932.

SIMULATION OF SOIL DEFORMATION AROUND A TILLAGE TOOL USING COMPUTATIONAL FLUID DYNAMICS

S. Karmakar, R. L. Kushwaha

ABSTRACT. *Tillage tool modeling is primarily concerned with analysis of soil deformation patterns and development of force prediction models. During the last four decades, most of the studies conducted on analytical and numerical modeling have considered soil as a solid or elasto-plastic material with quasi-static conditions. Large soil deformation, resulting from the dynamic tool action with respect to the soil mechanical behavior, has not been given much attention. This article deals with preliminary modeling of soil deformation around a tool using the computational fluid dynamics (CFD) approach. The main objective of this research was to characterize the soil as a visco-plastic material to determine soil flow pattern around the tool. Analyses were based on the governing equations of non-Newtonian fluid flow with the Bingham constitutive relationship. Simulations were carried out using CFX 4.4, a commercial CFD software. Free-surface simulation of an open channel visco-plastic soil flow indicated soil deformation patterns and the effect of speed on the failure front propagation. Soil deformations, as the flow of a visco-plastic material with yield stress, were observed to possess "plastic flow" and "plug flow" patterns. For a tool speed of 6 m s^{-1}, with a vertical tool of 20 mm thick and 50 mm wide, operating at 100 mm depth, the soil failure front was observed to be 160 mm at a depth of 10 mm below the top soil surface. The critical speed range was found to be 5 to 6.5 m s^{-1}. Further studies with this fluid flow approach are expected to reveal details of dynamic soil behavior with tool interaction.*

Keywords. *Bingham visco-plastic, CFD, Computational Fluid Dynamics, Elasto-plastic, Plastic flow, Plug flow, Soil failure front, Tillage.*

The basic objective of tillage is to break down the soil by disturbing its original structure for preparing a desired seed bed. During tillage, soil particles move ahead and around the tool as they fail in shear. As the tool engages soil, the high stiffness of undisturbed soil sustains the exerted tool thrust up to its elastic limit, and the soil then fails in shear. Accurate measurement of the soil failure geometry caused by a tillage tool is a prerequisite for understanding the soil-tool mechanics (Durairaj and Balasubramanian, 1997). In a study on soil microtopography, soil deformation due to sweep interaction has been described as "soil shift," "ridge height," and "change of surface height" (Hanna et al., 1993a). Soil shift is a measure of horizontal soil movement perpendicular to the travel direction, ridge height is the vertical peak-to-furrow distance after the tool has passed, and the change in surface height is a measure of loosening of surface soil.

Article was submitted for review in August 2004; approved for publication by the Power & Machinery Division of ASAE in April 2005. Presented at the 2004 ASAE/CSAE-SCGR Annual International Meeting, Ottawa as Paper No. 041014.

The authors are **Subrata Karmakar, ASAE Student Member,** Doctoral Student, Department of Agricultural and Bioresource Engineering, University of Saskatchewan, Canada, and Lecturer (on leave), Faculty of Agricultural Engineering, Bidhan Chandra Krishi Viswavidyalaya, West Bengal, India; and **Radhey Lal Kushwaha, ASAE Fellow Engineer**, Professor, Department of Agricultural and Bioresource Engineering, University of Saskatchewan, Canada. **Corresponding author**: Subrata Karmakar, Department of Agricultural and Bioresource Engineering, University of Saskatchewan, 57 Campus Drive, Saskatoon, SK S7N 5A9, Canada; phone: 306-966-5326, fax: 306-966-5334, e-mail: s.karmakar@usask.ca.

Soil failure front is an indicator of soil disturbance and is directly associated with slip surfaces generated by yielding and plastic deformation. The advancement of the soil failure front, influenced by the tool action, depends on the operating speed, tool shape and size, tool orientation, and the soil conditions. Extensive research has been conducted on modeling the energy requirement of a tillage tool using analytical and numerical methods. However, little information is available on the physical and mechanical soil deformation pattern that results from the soil-tool interaction. High-speed operation, practiced in conservation or reduced tillage, necessitates optimization of soil disturbance coupled with energy efficiency.

In contrast to classical elasto-plastic materials, the soil medium can experience significant volume changes. Soil is usually highly nonlinear and should be characterized as a nonlinear plastic or visco-plastic material (Desai and Phan, 1980). Many non-Newtonian materials have "yield stress," a critical value of shear stress below which they do not flow; they are sometimes called visco-plastic materials (Bird et al., 1983). Thus, visco-plastic fluids behave like solids when the applied shear stress is less than the yield stress. Once it exceeds the yield stress, the visco-plastic material flows just like a fluid. The most elementary constitutive equation in common use that describes a visco-plastic material that yields is the Bingham fluid (Lipscomb and Denn, 1984).

Dynamic analysis of soil-tool interaction is an essential area of research to predict the propagation of the soil failure front or advancing of the soil failure zone with respect to the tool motion. Numerical approaches like the finite element method (FEM) require prior knowledge of shear strain at failure for determining the position of a shear failure

boundary. Due to computational limitations, FEM has not been able to simulate dynamic tillage with high shear rates. Study of soil mechanical behavior from a visco-plastic fluid flow perspective using computational fluid dynamics (CFD) and its interaction with a tool is anticipated to be useful in representing the tillage dynamics. The main objectives of this research were to explore the possibilities of implementation of a CFD model for tillage by observing the soil flow pattern as a non-Newtonian material and to find the influence of a tool as a bluff body in the flow domain. The study of the dynamic influence zone moving in front of the tool for high-speed tillage is the main focus of this article.

LITERATURE REVIEW

Soil movement due to tillage has been studied for narrow and wide tools using different approaches. Söhne (1960) studied soil movement perpendicular to the travel direction with a wide tool in high-speed plowing and observed that the magnitude of the lateral soil displacement increased with the lateral directional angle at the end of the moldboard. Similar study on the effect of speed on soil failure patterns by Olson and Weber (1966) revealed that the size of the disturbed zone increased with increasing speed.

Goryachkin (1968) explained the soil flow phenomena over an inclined tillage tool surface using a trihedral wedge and three theories. The crushing theory considered the absolute soil motion normal to the tool surface, the lifting theory considered the relative position of the soil aggregates within a soil slice to remain the same, and the shearing theory considered soil motion parallel to the planes of soil shear failure.

Fornstrom et al. (1970) proposed a theory considering the energy balance concepts for tillage with emphasis on the change of state. They considered a stress tensor to represent internal mechanical effects involving kinetics and kinematics. The externally applied force was related to the changes in internal energy and specific volume (dilation) and to viscous flow. Since soil flow is not always a continuous process, "scale of motion," represented by "integral" (or "macro") scale and "micro" scale, was recommended to be used. Macro scale is a measure of the average longest distance over which the motion of a particle or group of particles persists in a given direction. Micro scale is a measure of the average shortest distance traveled by a particle or group of particles before a change of direction occurs.

McKyes and Ali (1977) proposed a three-dimensional model (soil wedge model with crescent failure) that was able to predict both the draft forces and the volume of soil disturbed in front of a narrow blade. The forward distance of the failure crescent from the blade on the surface was related to the rake angle, the rupture angle, and the depth of operation. The area disturbed by a tool across its direction of travel was approximated as a function of tool width, operating depth, and the lateral distance of the soil failure crescent from the tool and soil surface interaction.

Desai and Phan (1980) generalized the case of three-dimensional soil-structure interactions, where the structure is moving in the soil. Since the structure and soil move relative to each other, there is shear transfer through relative slip. The lateral soil movement was idealization as the flow of soil particles around the tool, while the vertical soil movement was idealized as soil flow parallel to the soil shear failure planes.

Grisso and Perumpral (1981) studied the basis for the analytical models, the assumptions involved, and the capabilities of the models to predict soil-tool interaction. It was concluded that a majority of the assumptions involved with the models were the same as those associated with the earth pressure theory and neglected the inertial forces and were suitable only for predicting the behavior of a narrow tine moving at extremely slow speeds.

McKyes and Desir (1984) measured the disturbed soil mass of narrow tools in different soil conditions at a speed of 1.4 m s^{-1}. Failure area was calculated by means of passive earth pressure theory, and the shape of the soil failure wedges was determined by soil weight and strength using the same expression proposed by McKyes and Ali (1977). The soil wedge model overestimated the cross-sectional area of thoroughly disturbed soil in tillage operations, primarily because the real tilled areas were bounded by curved boundaries and only completely remolded soil was included in the field experiments.

Hanna et al. (1993b) compared the soil flow path of a sweep with the Goryachkin theory. Soil shift, or lateral movement, and ridge height were affected by both tool operating speed and sweep rake angle. Faster speeds and steeper rake angles created larger ridges. Changes in surface height, an indicator of soil loosening, were significantly affected by tool depth and speed, but not by sweep rake angle. The Goryachkin theories did not adequately predict observed soil flow on a sweep (Hanna et al., 1993a). In agreement with the Goryachkin theories, observed soil flow changed with rake angle, but did not change with the speed or depth.

Durairaj and Balasubramanian (1997) developed a technique to measure the three-dimensional soil failure front owing to a tool under dynamic conditions. The procedure involved scanning and sensing the relative movement of failed soil with respect to the tool at millisecond timings by the sensors embedded in the soil-tool front.

Rosa (1997) investigated soil disturbance by measuring the soil cross-sectional area affected by the tool pass. Disturbed area and geometry of the seeding furrow were measured by a roughness meter. It was concluded that the soil disturbance increased as operating speed increased. However, no method had been adopted, in a standard form, to quantify the soil disturbance, and no statistical data were reported on disturbed soil area because of the difficulty in measurement by the roughness meter.

Little information is available on soil mechanical behavior during high-speed tillage. There exists a critical speed range at which the relationship between draft and speed changes, i.e., the draft increases less with speed above the critical speed (Kushwaha and Linke, 1996). A critical speed range of 3 to 5 m s^{-1} was observed for the conditions investigated. It was also expected that the amount of soil deformation would decrease near and above the critical speed. Sarifat and Kushwaha (1998) measured soil movement by narrow tillage tools (45° triangle, 90° triangle, flat, and elliptical) at high speeds of operation (10 to 25 km h^{-1}) in the soil bin and reported that increasing tool operational speed resulted in an increase in soil movement for all the tools. A series of experiments was conducted (Zhang and Kushwaha, 1999) in a soil bin to investigate the critical speed

at which the continuously increasing soil advancement failure zone started decreasing. However, a speed effect of only up to 1.8 ms^{-1} was reported, and the critical speed could not be reached due to technical limitations. Sarifat and Kushwaha (2000) developed a model using MATLAB for horizontal soil movement in front of the tool. The influence zone, as a function of speed of operation, was considered to be of circular shape attached to the tillage tool in the travel direction.

Passage of farm implements through soil for a short duration causes transient stress (Ghezzehei and Or, 2001). Movies have shown the fundamental behavior of an artificial soil failure to change from shear to plastic flow as the tool velocity was increased (Schimming et al., 1965). Olson and Weber (1966) also observed that an increase in the speed of a blade could cause a transition between the shear-plane and flow failures. As the speed was increased, there was more general shear and less sliding of one soil block on another, until the shear failure plane no longer formed and only a flow failure occurred.

Based on several experiments on stress-strain rate relationships of several soils, Vyalov (1986) concluded that a simple linear model of visco-plasticity, the Bingham rheological model, can describe soil deformation under steady-state stress. Several studies (Day and Holmgren, 1952; McMurdie and Day, 1958; Ghavami et al., 1974) on soil visco-plastic behavior have reported that the relation between the stress and rate of flow is non-linear in soil, and the flow is induced by the difference between total stress and the yield stress. The generalized observation was that flow of soil is initiated only when the stress acting upon the inter-aggregate contact exceeds a “critical yield point” (threshold stress value). This threshold stress is termed the yield stress. Visco-plastic fluids behave like solids when the applied shear stress is less than the yield stress; once it exceeds the yield stress, it will flow just like a fluid (Bird et al., 1983).

Assumptions on the orientation of the soil shear failure plane are needed before the soil failure front can be quantified using analytical methods. Some researchers have considered configuration of the rupture plane as slightly curved (Payne, 1956) and log spiral (Reece, 1965), while others have assumed it as a straight line (McKyes and Ali, 1977; Perumpral et al., 1983). Optimization of high-speed tillage operation is a current concern. The speed at which the continuously increasing soil advancement failure zone starts decreasing can be termed the critical speed (Zhang and Kushwaha, 1999). The tool velocity at which the distance of the failure front from the tool face ceases to increase could be set as the critical velocity for high-speed tillage to obtain minimum soil disturbance for a particular soil condition. The study of soil deformation due to tool interaction as a visco-plastic material from a fluid flow perspective is anticipated to represent the dynamic behaviors of tillage.

PROBLEM GEOMETRY

The problem domain consisted of a rectangular flow field with a flat plate as an obstruction (the bluff body) in the flow. The side and bottom walls were so placed that the effects of the boundary wall on the flow characteristics were negligible. A simple vertical blade (bluff body) with 20 mm thickness (T) and 50 mm width (W), operating at 100 mm depth (H), was considered for the study. The flow geometry (fig. 1) consisted of an open channel of 350 mm width (7W), 820 mm length (L) and 300 mm depth (3H). The tool influence zone considered by Chi and Kushwaha (1991) for their finite element analysis was taken as a benchmark for this analysis. For a vertical blade, the region of influence had a length of four times the operating depth ahead of and behind the tool, and a width of six times the width of the tool. However, during the CFD simulations, it was observed that a channel width of seven times the tool width eliminated the effect of the channel wall on the flow pattern with respect to tool influence.

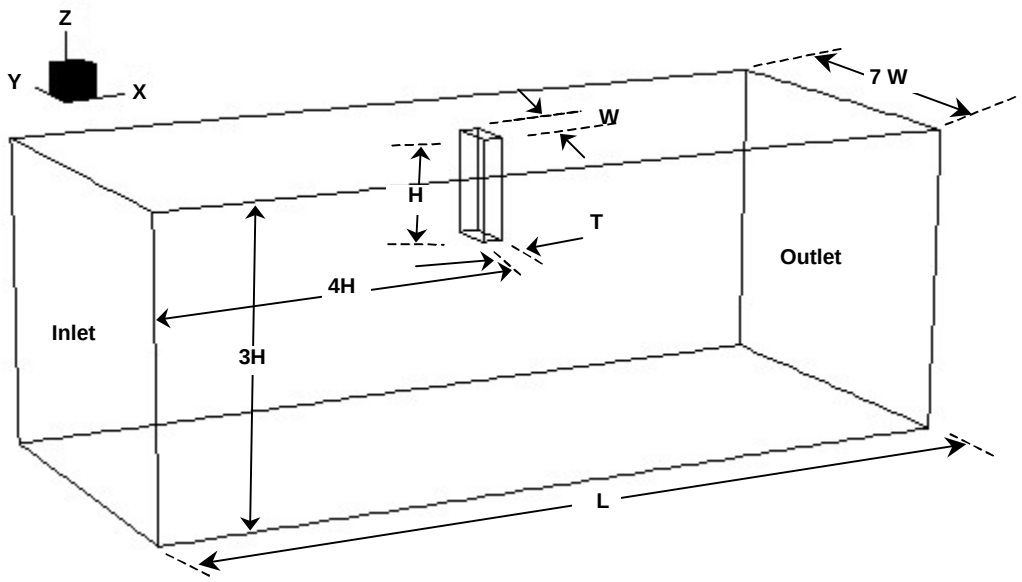

Figure 1. Schematic of the flow field: T = 20 mm, W = 50 mm, H = 100 mm, and L = 820 mm.

MATHEMATICAL MODELING

The Navier-Stokes equation is the basis of numerical solutions of any fluid flow (Patankar, 1980). By assuming the conservation of mass through the control volume, the continuity equation was:

$$\frac{\partial \rho}{\partial t} + \frac{\partial}{\partial x_i}(\rho U_i) = 0 \quad (1)$$

where

ρ = density of the fluid
U_i = directional velocity of the fluid
x_i = directional displacement of the fluid element in time t.

At any location of the flow, the local time rate of the change of density is balanced by the net mass flux at that point. For initial simulations, the soil was considered incompressible, with a constant density, and was treated as a single-phase continuous medium. Thus, the value of ρ was that of a bulk density including any pore water that may be present within the soil. Hence, the above equation reduced to the following simplified form, indicating that the volume of the differential fluid element does not change:

$$\frac{\partial}{\partial x_i}(\rho U_i) = 0 \quad (2)$$

Newton's second law enables us to relate the acceleration of a fluid parcel or element to the net force action on it through the following momentum equation:

$$\rho \frac{DU}{Dt} = \rho g_i - \frac{\partial p}{\partial x_i} + \frac{\partial \tau_{ij}}{\partial x_j} \quad (3)$$

where

g = acceleration due to gravity
p = hydrostatic pressure
τ_{ij} = shear stress tensor.

The material or substantial derivative is a function of both temporal and spatial changes:

$$\frac{DU}{Dt} = \frac{\partial U}{\partial t} + U_j \frac{\partial U}{\partial x_j} \quad (4)$$

The above expressions indicate that the acceleration of the fluid element is balanced by the gravitational force, pressure (hydrostatic stress), and viscous (hydrodynamic) stress. In this way, the fluid flow approach addresses different aspects of dynamic soil-tool interaction, such as forces due to the velocity and acceleration of the tool, soil pressure on the tool surface considering the weight of the soil mass, and soil failure due to visco-plastic soil deformation.

The following constitutive relation for the Bingham model represents the shear stress tensor in the momentum equation:

$$\tau_{ij} = \tau_y + \mu \dot{\gamma} \quad \text{for} \quad |\tau_{ij}| > \tau_y \quad (5)$$

$$\dot{\gamma} = 0 \quad \text{for} \quad |\tau_{ij}| \le \tau_y \quad (6)$$

where

$\dot{\gamma}$ = shear rate
τ_y = yield stress
μ = constant viscosity, also known as plastic viscosity.

During tillage, as the tool encounters agricultural stiff soil, there is no soil failure until the applied stress exceeds the soil yield stress. Then, visco-plastic soil flow takes place due to soil shear failure with the applied stress exceeding the threshold yield stress.

ANALYSIS

GENERAL CONSIDERATIONS

To simulate the soil flow around the tool, the tool was considered to be stationary, and the soil (Bingham visco-plastic material) was considered to be moving in the flow domain, having an interaction with the tool. Three-dimensional CFD simulations were carried out in isothermal conditions for steady-state soil flow to determine dynamic soil deformation patterns and the tool influence. Soil visco-plastic parameters, soil viscosity, and yield stress required for the simulations have been found using a constant-rate soil rheometer, developed in the Department of Agricultural and Bioresource Engineering, University of Saskatchewan. For a soil with 1250 kg m^{-3} bulk density, 400 kPa cone index, and 17% moisture content (dry basis), viscosity was found to be 900 Pa·s and yield stress was found to be 12 kPa. Simulations were conducted with the following fluid and flow parameters:

Fluid inlet velocity = 1.0 to 8.0 m s^{-1}

Soil bulk density = 1250 kg m^{-3}

Yield stress = 12 kPa

Apparent viscosity = 900 Pa·s.

The soil was considered to be cut by a narrow tool operating at a constant speed. The system was idealized with the following assumptions:

- The tool is narrow, rigid, and works as a vertical blade.
- The tool operates at a constant depth.
- Soil flow type is laminar, and the state of flow is transient.
- Flow is symmetrical about the vertical section of the tool.
- Soil failure is three-dimensional.
- The soil is an isotropic and homogeneous continuum.
- The soil behaves as a Bingham visco-plastic material with definite yield stress.
- Soil pore spaces are negligible, and the soil is an incompressible material.

BOUNDARY CONDITIONS AND SOLUTION APPROACH

Soil was drawn into the flow channel with an inlet velocity. Therefore, the velocity component normal to the inlet boundary was set to that value. Boundary conditions imposed in the simulation with respect to the flow domain are:

- Inlet velocity was specified from 3 to 8 m s^{-1}.
- The outlet was specified as pressure boundary.
- No-slip wall boundaries were specified at the bottom and the sides of the channel.
- The top of the flow domain was specified as free-surface with pressure boundary.
- Surface regions were also specified as 3D regions to which free-surface grid movement was confined.

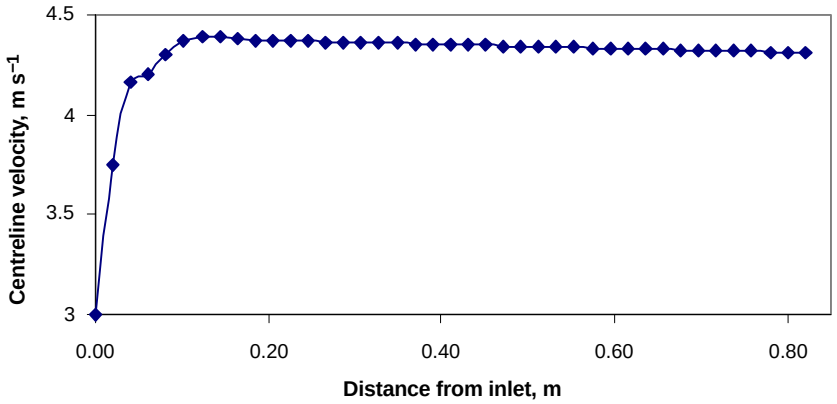

Figure 2. Velocity profile along the centerline of the flow domain.

The geometry was simple, so a rectangular coordinate system was used. A value of 10^{-4} has been employed as the convergence criterion at every step of the iteration for the sum of the normalized residuals over the whole fluid domain for all the governing fluid flow equations. A relaxation factor less than 0.3 was found to be a good value for attaining stable convergence, although it increased the computation time compared to larger relaxation factors. Fixed time stepping was applied for the transient grid movement. The program was controlled with a mass source tolerance value of 10^{-5}.

Numerical Procedures: The Finite Volume Method

The computational simulations were performed using a commercially available CFD code, CFX4.4 (AEA Technologies, 2001). The numerical procedure was based on the finite volume method and involved grid generation, discretization, and solving the governing equations with specific fluid and flow parameters. Surface meshing was done in the forms of one-way, two-way, and uniform bias to take account of the sensitive zones in the domain. As the flow was expected to vary most rapidly near to the edge of the tool, finer meshes were placed in that region using two-way bias. Several simulations were conducted with the same condition to attain a grid-independent solution.

The differential equation governing the conservation of momentum was solved using the solution scheme for a non-Newtonian material with the control volume approach. A user subroutine written in FORTRAN was incorporated into the main solver program for the numerical solution with free-surface grid movement. When the moving grid feature was used, additional terms were included in the governing equations to account for the movement of the grid. These terms accounted for the velocity of each grid node, since the position of the grid nodes changed with time. The grid topology and number of nodes remained constant, whereas the nodal position and velocity changed with each time step. At the start of each time step, user-coded routines were called that specified the way in which the grid was moved. The free-surface grid algorithm allowed the grid near the surface to change in time. Free-surface grid movement was convection controlled with a specified false time step for slow convergence to avoid oscillation in the solution process.

Results and Discussion

Dynamic soil-tool interactions were carried out by the control volume method with fluid flow phenomena. Simulations were carried out with the soil flowing as a Bingham material in an open channel with an obstruction or bluff body in the flow domain. Results of the simulation were interpreted with the soil as stationary and the tool moving at a constant velocity. Some significant results are discussed below.

It was important to understand the soil flow behavior before observing the influence of the tool. It is customary to define an entry length, i.e., the distance from the inlet at which the centerline velocity is 99% of that for the fully developed flow (White, 1999). A longitudinal velocity profile for an inlet velocity of 3 m s^{-1} (fig. 2) showed that the velocity suddenly increased near the inlet (entry region) and then stabilized at a fully developed velocity of about 4.35 m s^{-1}.

The thickness of the boundary layer is theoretically zero at the entrance and increases progressively along the flow line. The velocity reached its stabilized shape where the boundary layer converged at the centerline of the flow. The velocity profile in the entry region was different from that in the fully developed flow since it was a function of the

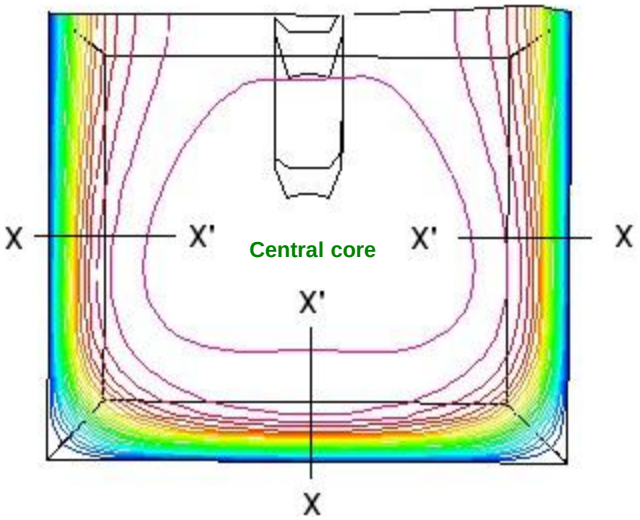

Figure 3. Contour plot of the fully developed longitudinal velocity profile away from the tool influence zone in the open channel (X-X′: 0 to 6.35 m s^{-1} for an inlet velocity of 6 m s^{-1}).

velocity and pressure gradients. With the no-slip boundary condition, the higher velocity gradients in the wall region resulted in greater frictional losses, and some pressure energy was converted into kinetic energy. Consequently, the pressure gradient influenced the velocity profile in the entry region, and the fluid in the central core accelerated. The retardation of the fluid in the wall region must be accompanied by a concomitant acceleration in the central region in order to maintain continuity (Chhabra and Richardson, 1999). Thus, the acceleration of the inlet velocity near the inlet can be attributed to the principle of mass and momentum conservation.

The velocity profile at the fully developed region represented the non-Newtonian Bingham flow pattern. The contour plot (fig. 3) of the longitudinal velocity across the channel section shows the features of fully developed soil flow away from the tool influence zone. Zero velocities at the walls of the flow domain were due to the no-slip boundary conditions. Since the non-Newtonian fluid (soil) has been modeled by the Bingham constitutive law, the velocity profile in this perspective was observed to have "plug flow" regions and "plastic flow" regions. There was a solid plug-like core flowing in the middle of the flow channel where the deviatoric stress was less than the yield stress. Thus, the yield surface is located at the point where the shear stress is equal to the yield stress. At this point, the regions of rigid solid and inelastic fluid behavior were separated in terms of the von Mises yield criterion (Beris et al., 1985). A characteristic peculiarity of problems concerning the fluidity of a visco-plastic medium is the locations of the boundaries that divide the flow fields into fluid regions and rigid regions (Adichi and Yoshioka, 1973). Fluid regions, or the plastic flow regions, were near the wall boundary of the flow where the pressure gradient was very high and the shear stress exceeded the yield stress, causing the soil to fail in plastic deformation.

Figure 4 shows the velocity profiles of the fully developed soil flow in the channel across the flow depth and the channel width. With the no-slip boundary condition at the bottom, a plastic flow region (fig. 4a) is observed at the base of the channel. However, the free-surface boundary condition at the top of the flow domain allowed a velocity close to plug flow near the top of the channel. The plug flow at the central core of the channel represents Bingham visco-plastic flow where the shear stress is below the yield stress (fig. 4b). The velocity profile across the channel width shows that the soil deforms and plastic flow takes place at the wall region. Zero velocity at the channel walls due to no-slip boundary conditions causes very high shear stress, which is more than the yield stress.

Velocity vectors as influenced by the presence of the tool in the flow domain are shown in figure 5. A prominent wave formation exists at the inlet of the flow. Due to the no-slip boundary condition at the channel base and at the walls of flow channel, velocity close to the channel base and walls gets reduced after the flow starts at a particular inlet velocity.

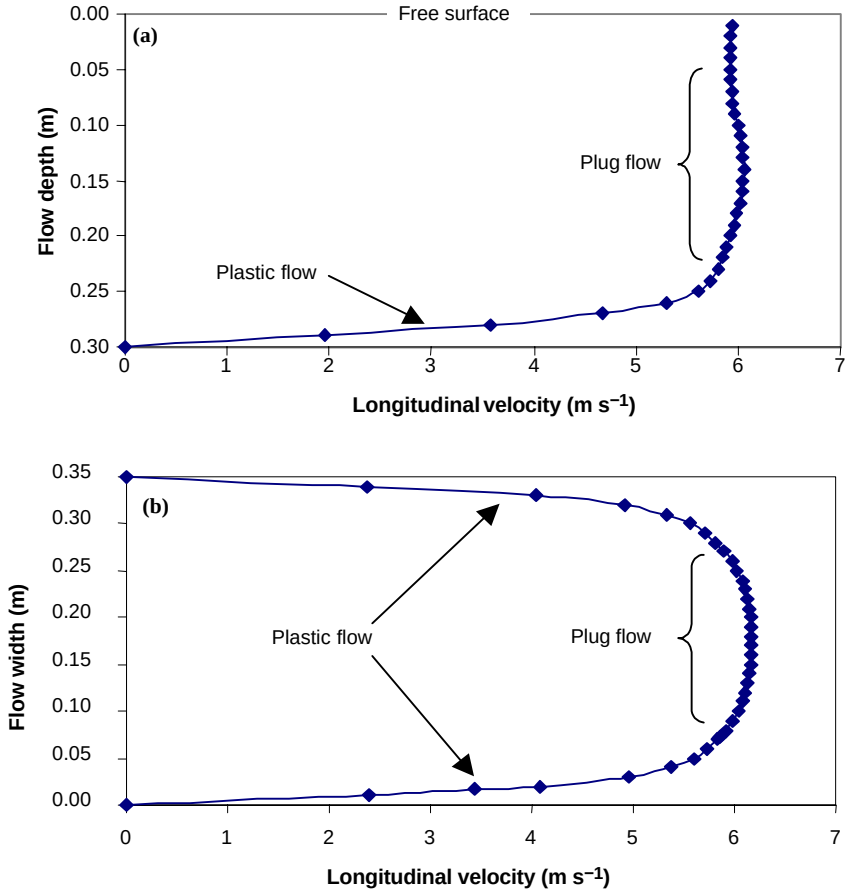

Figure 4. Fully developed non-Newtonian soil flow pattern outside the tool influence zone: (a) velocity profile across the flow depth at the centerline of the channel, and (b) velocity profile across the channel width at midway in the channel depth.

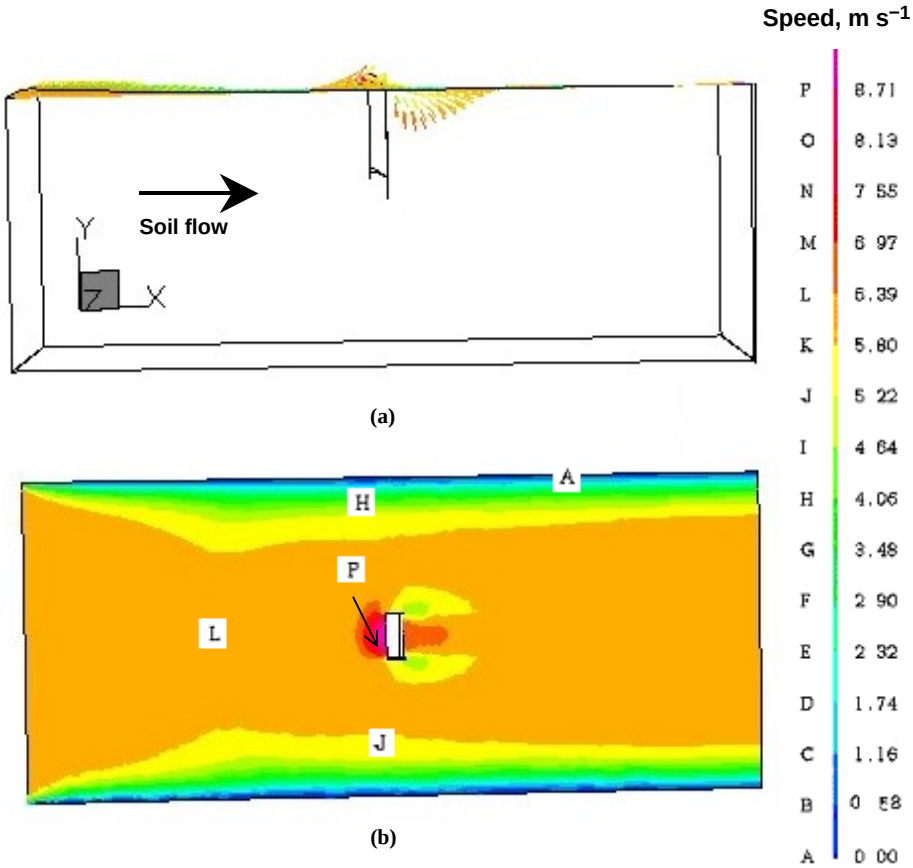

Figure 5. Soil flow around the tool at the free surface. Soil flow is from left to right: (a) velocity vectors showing soil buildup in front of the tool and furrow formation behind the tool (side view of the channel), and (b) fringe plot of the speed of soil particles at the free surface (top view of the channel).

The free-surface boundary condition at the top allows the soil to bulge out, following the principle of mass and momentum conservation. Velocity vectors in front of the tool show the height of soil buildup and the size and shape of the furrow formed behind the tool. As the fully developed plug flow encounters the tool, due to the free-surface boundary condition, the velocity of the soil particles increases and is directed upwards. The high velocity at the vicinity of the tool can also be seen in the fringe plot (fig. 5b) describing the variation of the speed of soil particles at the free surface.

A generalized feature of the influence of the tool placed in the fully developed flow is shown in figure 6a. This flow was influenced and disturbed due to the presence of the tool. The disturbed area can be considered the soil failure zone, and the total area of influence can be determined for a particular tool velocity and soil parameters. It is also seen that with the CFD analysis, the soil failure zones can be precisely quantified in the front, to the side, and to the rear of the tool. The velocity just in front of and behind the tool is zero because of the stagnation points in the flow domain. Soil failed in plastic deformation near the tool due to high pressure gradients. Thus, the yield surface related to the axial velocity should give the boundary of the soil disturbance zone.

The tool influence zone due to soil interaction can be obtained from the axial velocity profile of the soil particles (fig. 6b). The soil failure front can be obtained from the predicted longitudinal velocity distribution at the soil surface or at a particular tool operating depth considering the tool influence zone. The contour plot of longitudinal velocity at the free surface indicates that the fully developed flow reduces to zero at the tool face due to the stagnation point. For the real situation, where the tool moves in stationary soil, the zone of this velocity reduction can be interpreted as the tool influence zone or the soil failure front for a particular fully developed velocity or tool operating velocity.

The flow dynamics near the tool in the flow domain is of major interest with respect to the soil failure front. The flow pattern of longitudinal velocity at the tool section (vertical plane) is shown in figure 7. Fully developed soil flow gets largely deformed due to the tool interaction. Large soil deformation due to tool interaction causes soil to build up at the front of the tool and furrow behind it. In a tool operating environment, soil particles scour the tool face as the tool moves ahead in soil cutting, and a furrow is formed behind the tool. From the contour plot, it can be observed that the soil failure front extends more below the top soil surface.

The velocity profile along the flow length helps determine the tool influence zone. The fully developed velocity reduces to zero at the tool surface. At the rear of the tool, the discontinuity in the velocity profile is due to the presence of the furrow. This velocity distribution can be used to interpret a real operating condition. With this fluid flow approach, considering the soil as a fluid and the tool as a stationary solid, interpretation can be made in the reverse mode.

Considering a real tool operating condition, a particular fully developed velocity can be considered as the tool operating speed in the same flow domain with stationary soil. Thus, the soil failure front can be determined (fig. 8) from the longitudinal velocity profile. For a tool operating speed of 6 m s^{-1}, the soil failure front (S) was observed to be 160 mm.

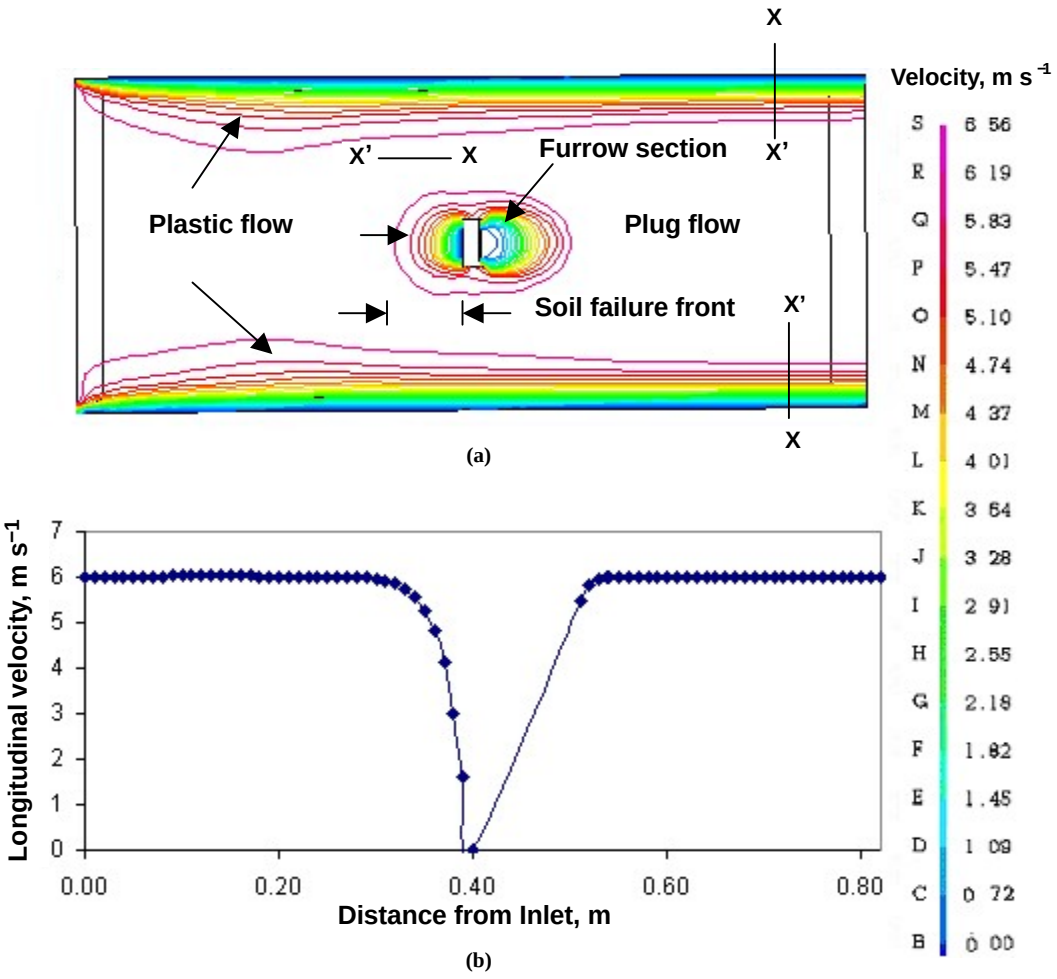

Figure 6. Dynamic soil-tool interaction: (a) visco-plastic soil flow pattern at a horizontal plane 10 mm below the free surface (X-X′: 0 to 6.56 m s^{-1}), and (b) longitudinal velocity profile at the centerline midway between the sides of the flow field, with the tool influence shown.

Effect of Operational Velocity on Soil Failure Front

Simulations were conducted with different inlet velocities, thereby causing different fully developed soil flow velocities, and these were used to estimate frontal failure zones. Figure 9 shows the relationship between soil failure front (extended at a depth of 10 mm below the soil surface) and tool velocity for a 50 mm wide tool.

The soil failure front initially increased with tool velocity. After reaching a critical level, there was little or no increase in the longitudinal distance from the tool face to the soil failure front. These results satisfy the theoretical arguments of earlier researchers (Azyamova, 1963; Vetro and Stanevski, 1972) on the effect of operating speed during tillage. An extensive soil stress or energy concentration occurred in front of the tool when the tool speed was less than the velocity of

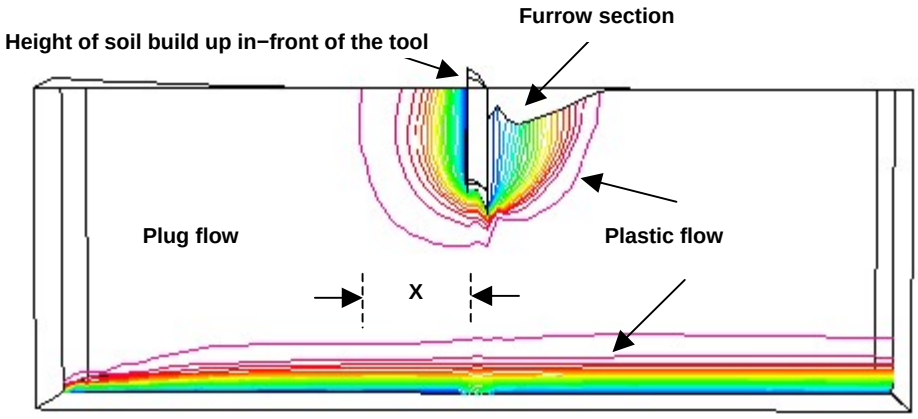

Figure 7. Contour plot of longitudinal velocity at the centerline of the channel across the tool vertical section, showing the tool influence zone (X).

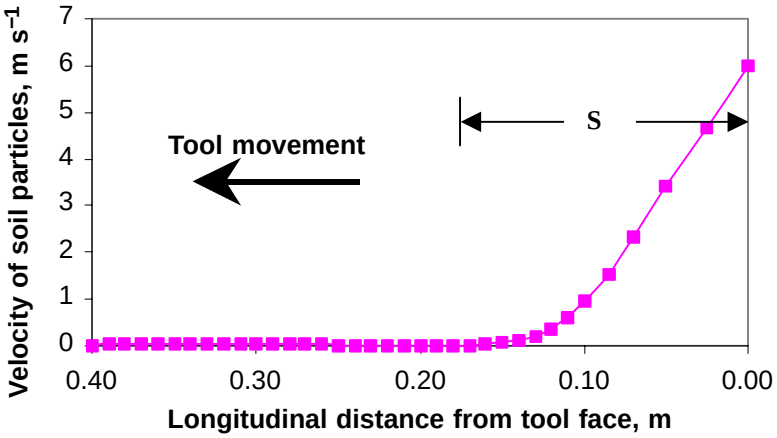

Figure 8. Soil failure front (*S*) for the moving tool.

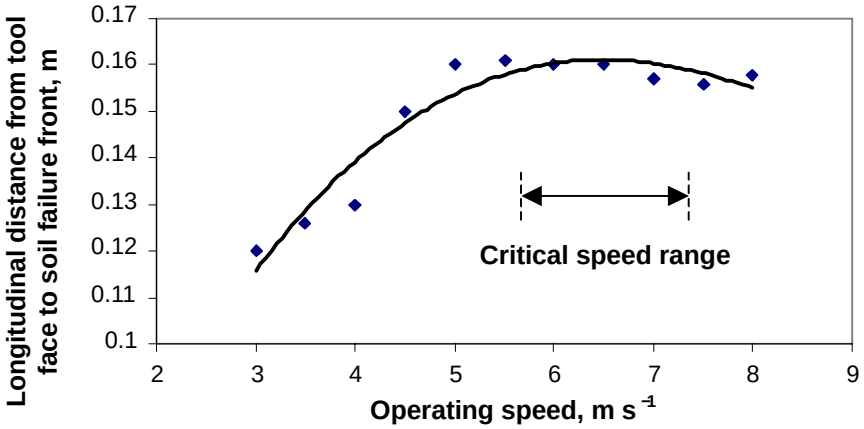

Figure 9. Relationship between soil failure front and tool velocity.

the wave propagation of the soil stress. As the tool speed increased faster than the wave of soil stress propagation, the plastic zone of soil in front of the tool decreased or even disappeared.

Validation with Published Results

Soil Failure Front

In their experimental study related to soil failure patterns, Durairaj and Balasubramanian (1997) found that for a bent leg tool with zero rake angle, the soil failure front was more pronounced at the cutting edge than that of the top soil surface. In addition, the soil failure front extended to a distance of 0.15 to 0.20 m in the alignment of the cutting edge of the tool and 0.05 to 0.10 m in the top layers of the soil. The results obtained from the CFD simulations agree closely with these published results.

Critical Speed Range

With the current simulations, the critical speed range has been found to be between 5 and 6.5 m s^{-1}, which is within the values reported by Kushwaha and Linke (1996). Investigation of draft-speed response using an artificial neural network (ANN) revealed a critical speed range of 3.5 to 6.0 ms^{-1} (Linke and Kushwaha, 1992).

Conclusion

The following conclusions were derived from the results of this study:

- Computational fluid dynamics has a significant potential in tillage tool modeling.
- The Bingham model successfully depicted soil plastic failure with respect to the yield stress.
- The longitudinal distance of the soil failure front from the tool face for a 50 mm wide tool operating at about 22 km h^{-1} was found to be about 160 mm.
- The critical speed range was found to be in the range of 18 to 23 km h^{-1}.
- The flow domain has been considered as a conduit. The results would be more realistic if the top surface were considered as a free surface.

Acknowledgements

The financial support received from the Canadian Department of National Defence, the Natural Sciences and Engineering Research Council of Canada, and the University of Saskatchewan Partnership Research Program is gratefully acknowledged.

REFERENCES

Adichi, K., and N. Yoshioka. 1973. On creeping flow of a visco-plastic fluid past a circular cylinder. *Chem. Eng. Sci.* 28(1): 215-226.

AEA Technologies. 2001. *CFX Release 4.4 User Guide*. Harwell, Didcot, U.K.: CFX International.

Azyamova, E. N. 1963. *Studies of Dynamics of Deformation of Soil*. Trudy Minsk 1:131-139. Translated by W. R. Gill. Auburn, Ala.: USDA National Tillage Machinery Laboratory.

Beris, A. N., J. A. Tsamopoulos, R. C. Armstrong, and R. A. Brown. 1985. Creeping motion of a sphere through a Bingham plastic. *J. Fluid Mech*. 158: 219-244.

Bird, R. B., G. C. Dai, and B. J. Yarusso. 1983. The rheology and flow of visco-plastic materials. *Rev. Chem. Eng.* 1: 1-70.

Chhabra, R. P., and J. F. Richardson. 1999. *Non-Newtonian Flow in the Process Industries: Fundamentals and Engineering Applications.* Oxford, U.K.: Butterworth Heinemann.

Chi, L., and R. L. Kushwaha. 1991. Three-dimensional finite element interaction between soil and simple tillage tool. *Trans. ASAE* 34(2): 361-366.

Day, P. R., and G. G. Holmgren. 1952. Microscopic change in soil structure during compression. *SSSA Proc.* 16: 73-77.

Desai, C. S., and H. V. Phan. 1980. Three-dimensional finite element analysis including material and geometric nonlinearity. In *Proc. TICOM Second International Conf. on Computational Methods in Nonlinear Mechanics*, 205-224. J. T. Oden, ed. New York, N.Y.: Elsevier North-Holland.

Durairaj, C. D., and M. Balasubramanian. 1997. A method for dynamic measurement of soil failure patterns caused by tillage tools. *Soil Tillage Res*. 41: 119-125.

Fornstrom, K. J., R. D. Brazee, and W. H. Johnson. 1970. Tillage-tool interaction with a bounded, artificial soil. *Trans. ASAE* 13(4): 409-416, 418.

Ghavami, M., J. Keller, and I. S. Dunn. 1974. Predicting soil density following irrigation. *Trans. ASAE* 17(1): 166-171.

Ghezzehei, T. A. and D. Or. 2001. Rheological properties of wet soils and clays under steady and oscillatory stresses. *SSSA J.* 65: 24-637.

Goryachkin, V. P. 1968. *Collected Works in Three Volumes.* N. D. Luchinski, eds. Translated 1972. Jerusalem, Israel: Ketter Press.

Grisso, R. D., and J. V. Perumpral. 1981. Models for predicting narrow tillage tool behavior in soil: A review and comparison. ASAE Paper No. 811535. St. Joseph, Mich.: ASAE.

Hanna, H. M., D. C. Erbach, S. J. Marley, and S. W. Melvin. 1993a. Comparison of the Goryachkin theory to soil flow on a sweep. *Trans. ASAE* 36(2): 293-299.

Hanna, H. M., S. J. Marley, D. C. Erbach, and S. W. Melvin. 1993b. Change in soil microtopography by tillage with a sweep. *Trans. ASAE* 36(2): 301-307.

Kushwaha, R. L., and C. Linke. 1996. Draft-speed relationship of simple tillage tools at high operating speeds. *Soil Tillage Res*. 39(1-2): 61-73.

Linke, C., and R. L. Kushwaha. 1992. High-speed evaluation of draft with a vertical blade. ASAE Paper No. 921019. St. Joseph, Mich.: ASAE.

Lipscomb, G. G., and M. M. Denn. 1984. Flow of Bingham fluids in complex geometries. *J. Non-Newtonian Fluid Mech.* 14: 337-346.

McKyes, E., and O. S. Ali. 1977. The cutting of soil by narrow blades. *J. Terramech.* 14(2): 43-58.

McKyes, E., and F. L. Desir. 1984. Prediction and field measurement of tillage tool draft forces and efficiency in cohesive soils. *Soil Tillage Res*. 4(5): 459-470.

McMurdie, J. L., and P. R. Day. 1958. Compression of soil by isotropic stress. *SSSA Proc.* 22: 18-22.

Olson, D. J., and J. A. Weber. 1966. Effect of speed on soil failure patterns in front of model tillage tools. *Trans. SAE* 74(4): 298-310.

Patankar, S. V. 1980. *Numerical Hear Transfer and Fluid Flow.* New York, N.Y.: Hemisphere Publishing.

Payne, P. C. J. 1956. The relationship between the mechanical properties of soil and the performance of simple cultivation implements. *J. Agric. Eng. Res*. 1(1): 23-50.

Perumpral, J. V., R. D. Grisso, and C. S. Desai. 1983. A soil-tool model based on limit equilibrium analysis. *Trans. ASAE* 26(4): 991-995.

Reece, A. R. 1965. The fundamental equations of earth-moving mechanics. In *Proc. Symp. Earth Moving Machinery*, 179 (3F): 8-14. London, U.K.: Institute of Mechanical Engineering.

Rosa, U. A. 1997. Performance of narrow tillage tools with inertial and strain rate effects. PhD diss. Saskatoon, Saskatchewan: University of Saskatchewan, Department of Agricultural and Bioresource Engineering.

Sarifat, K., and R. L. Kushwaha. 1998. Soil movement by narrow tillage tools at high speeds. Paper No. 98-409. Presented at the CSAE-SCGR Joint Conference with the Agricultural Institute of Canada, Vancouver, B.C.

Sarifat, K., and R. L. Kushwaha. 2000. Modeling soil movements by tillage tools. *Canadian Agric. Eng.* 42(4): 165-172.

Schimming, B. B., H. J. Hass, and H. C. Saxe. 1965. A comparison of the dynamic and static shear strengths of cohesion less, cohesive, and combined soils. Tech Report No. AFWL TR-65-48. South Bend, Ind.: University of Notre Dame, Department of Civil Engineering.

Söhne, W. 1960. Suiting the plow body shape to higher speeds. *National Institute of Agric. Eng. Translation* 10 (12): 51-62.

Vetrov, Y. A., and V. P. Stanevski. 1972. The investigation of the factors of speed of cutting soils. *Mining, Construction, and Highway Machines* 8: 21-26. Translated by W. R. Gill. Auburn, Ala.: USDA National Tillage Machinery Laboratory.

Vyalov, S. S. 1986. *Rheological Fundamentals of Soil Mechanics*. Amsterdam, The Netherlands: Elsevier.

White, F. M. 1999. *Fluid Mechanics*. 4th ed. WCB/McGraw Hill. Columbus, Ohio:The McGraw-Hill Companies.

Zhang, Z. X., and R. L. Kushwaha. 1999. Operating speed effect on the advancing soil failure zone in tillage operation. *Canadian Agric. Eng*. 41(2): 87-92.